

## National Transportation Library

### Section 508 and Accessibility Compliance

The National Transportation Library (NTL) both links to and collects electronic documents in a variety of formats from a variety of sources. The NTL makes every effort to ensure that the documents it collects are accessible to all persons in accordance with Section 508 of the Rehabilitation Act Amendments of 1998 (29 USC 794d), however, the NTL, as a library and digital repository, collects documents it does not create, and is not responsible for the content or form of documents created by third parties. Since June 21, 2001, all electronic documents developed, procured, maintained or used by the federal government are required to comply with the requirements of Section 508.

If you encounter problems when accessing our collection, please let us know by writing to [librarian@bts.gov](mailto:librarian@bts.gov) or by contacting us at (800) 853-1351. Telephone assistance is available 9AM to 6:30PM Eastern Time, 5 days a week (except Federal holidays). We will attempt to provide the information you need or, if possible, to help you obtain the information in an alternate format. Additionally, the NTL staff can provide assistance by reading documents, facilitate access to specialists with further technical information, and when requested, submit the documents or parts of documents for further conversion.

### Document Transcriptions

In an effort to preserve and provide access to older documents, the NTL has chosen to selectively transcribe printed documents into electronic format. This has been achieved by making an OCR (optical character recognition) scan of a printed copy. Transcriptions have been proofed and compared to the originals, but these are NOT exact copies of the official, final documents. Variations in fonts, line spacing, and other typographical elements will differ from the original. All transcribed documents are noted as "Not a True Copy."

The NTL Web site provides access to a graphical representation of certain documents. Thus, if you have any questions or comments regarding our transcription of a document's text, please contact the NTL at [librarian@bts.gov](mailto:librarian@bts.gov). If you have any comment regarding the content of a document, please contact the author and/or the original publisher.

FINAL REPORT

---

---

---

---

---

---

**Evaluation of FEM Engineering  
Parameters from Insitu Tests**

Submitted by  
F.C. Townsend  
J. Brian Anderson  
Landy Rahelison



Submitted to: **Florida Department of Transportation**

Agency ID Nos. RPWO - 14  
BC-354  
UF Contract No. 450472012

December 2001

1. Report No.  RPWO-14	2. Government Accession No.	3. Recipient's Catalog No.	
4. Title and Subtitle  Evaluation of FEM Engineering Parameters from Insitu Tests		5. Report Date December 2001	
		6. Performing Organization Code	
7. Author(s) F.C. Townsend, J. Brian Anderson, Landy Rahelison		8. Performing Organization Report No. 4910-4504-720-12	
9. Performing Organization Name and Address University of Florida Department of Civil & Coastal Engineering 124 Yon Hall / P.O. Box 116580 Gainesville, FL 32611-6580		10. Work Unit No. (TRAIS)	
		11. Contract or Grant No. BC-354	
12. Sponsoring Agency Name and Address Florida Department of Transportation  Research Management Center 605 Suwannee Street, MS 30 Tallahassee, FL 32301-8064		13. Type of Report and Period Covered Final Report August 1999-December 2001	
		14. Sponsoring Agency Code	
15. Supplementary Notes  Prepared in cooperation with the Federal Highway Administration			
16. Abstract The purpose of this study was to take a critical look at insitu test methods (SPT, CPT, DMT, and PMT) as a means for developing finite element constitutive model input parameters. The first part of the research examined insitu test derived parameters with laboratory triaxial tests at three sites: Saunder's Creek, Archer Landfill, and SW Recreation Center. The triaxial tests on these sands were used to develop baseline input parameters. These parameters were verified by simulating the triaxial tests using two finite element codes. From these comparisons, the following conclusions were drawn: (1) FEM simulations of triaxial test stress-strain curves produced excellent results. (2) The hardening models (PLAXIS – Hardening Soil and PlasFEM – Sandler Dimaggio) simulated the non-linear behavior better than the Mohr-Coulomb or Drucker-Prager models. (3) In general, $E_{50}$ triaxial test modulus values agreed with those estimated from DMT and PMT unloading tests, and (4) FEM simulations of field PMT curves using triaxial test based parameters were unsuccessful. It was necessary to increase the triaxial $E_{50}$ values by $\Omega = 1.3078e^{0.0164p_1}$ $R^2 = 0.8515$ , where $\Omega$ is the triaxial $E_{50}$ modulus multiplier and $p_1$ is the PENCEL limit pressure. The second phase of this study was to predict the deformations of a cantilevered sheet pile wall (unloading case), and the deformations of a 2-m diameter shallow footing (loading case). Conventional analyses methods were compared with the FEM using insitu test derived input parameters. Conclusions were: (1) conventional analyses (CWALSHT) under-predicted wall deformations unconservatively, while wall deflections were accurately predicted by using the Hardening Soil Model with input parameters estimated from SPT correlations and "curved matched" PMT values. (2) Fundamentally, the stress history of a soil profile, i.e., OCR or preconsolidation pressure, must be known for any settlement prediction either using conventional or finite element methods. (3) Of the conventional methods for estimating settlements (CSANDSET), only the SPT based D'Appolonia, and Peck and Bazaraa methods provided reasonable estimates of the observed settlement. (4) The conventional DMT method, which correlates OCR values, slightly overestimated measured settlements. (5) None of the insitu test derived input parameters (SPT, CPT, DMT, and PMT) coupled with FEM Mohr-Coulomb or Hardening Soil models, accurately predicted the shallow footing settlements			
17. Key Words  Finite Elements, Insitu Testing, Pressuremeter, Shallow Foundations, Sheet-Pile Walls	18. Distribution Statement  No restrictions. This document is available to the public through the National Technical Information Service, Springfield, VA, 22161		
19. Security Classif. (of this report)  Unclassified	20. Security Classif. (of this page)  Unclassified	21. No. of pages  242	22. Price

## TABLE OF CONTENTS

	<u>page</u>
LIST OF TABLES .....	vii
LIST OF FIGURES .....	xi
EXECUTIVE SUMMARY .....	xix
Project Summary .....	xix
Recommendations .....	xxii
List of Symbols .....	xxiv
INTRODUCTION .....	1
Limiting Equilibrium Theory .....	1
Mohr-Coulomb Input Parameters .....	1
Deformation Based Theory .....	2
Problem Statement .....	3
Objectives .....	3
Scope of Work .....	4
LITERATURE REVIEW .....	5
History of the Pressuremeter .....	5
Previous Work with Full-Displacement Pressuremeters .....	8
Pavement Pressuremeter .....	8
General .....	11
Apparatus .....	11
Test .....	14
Research .....	14
Roberston and Hughes Full Displacement Pressuremeter .....	15
General .....	15
Apparatus .....	15
Test .....	17
Research .....	17
Fugro Prototype Pressuremeters .....	24
General .....	24
Apparatus .....	24
Test .....	25

Research .....	25
Finite Element Software .....	31
Plaxis .....	31
PlasFEM .....	36
CONSTITUTIVE MODELING .....	39
Constitutive Models for Cohesionless Soil .....	40
Plaxis .....	40
Mohr-Coulomb .....	40
Hardening soil .....	41
PlasFEM .....	44
Drucker-Prager .....	44
Sandler-Dimaggio .....	45
Constitutive Models for Cohesive Soil .....	47
Plaxis .....	47
PlasFEM .....	48
Summary of Input Parameters .....	49
Parameter Selection .....	54
Unit Weight .....	54
Shear Strength Parameters .....	55
Drained Friction Angle .....	55
Undrained Shear Strength .....	60
Soil Stiffness Parameters .....	64
Poisson's Ratio Based on Soil Type .....	64
Modulus .....	64
Sensitivity Analysis .....	69
Plaxis parameters .....	70
PlasFEM parameters .....	71
LABORATORY AND FIELD TESTING .....	72
Testing Equipment .....	72
Triaxial Test Equipment .....	72
Field Test Equipment .....	74
PENCEL Pressuremeter .....	74
University of Florida electric cone truck .....	79
Test Sites .....	79
Florida State Road 20 Site Swift/Sanders Creek .....	80
University of Florida Southwest Recreation Center Site .....	85
Alachua County Landfill .....	93
FINITE ELEMENT SIMULATIONS .....	102
Triaxial Tests .....	102
PENCEL Pressuremeter .....	115
Discussion of the PENCEL Pressuremeter .....	115

FEM Modeling of the PENCEL Pressuremeter .....	116
MOFFITT CANCER CENTER SHEET-PILE WALL PREDICTION .....	126
Introduction .....	126
Objectives .....	126
Scope of Work .....	127
Site Description and Insitu Testing .....	127
Sheet -Pile Wall Test Section .....	138
Soil Structure Profile used in CWALSHT and FEM Modeling .....	141
Slope Inclinator Data Reduction .....	143
Input Parameters and Numerical Modeling: .....	148
Modeling and Results .....	156
CWALSHT Modeling .....	156
Finite Element Meshing and Results with Plaxis .....	158
Discussion .....	160
Influence of the Choice of Modulus and Constitutive Model .....	160
Linear Elastic Model .....	161
Comparison and Discussion of the Measured Deflection versus Predicted Deflections .....	161
Conclusions .....	166
Conclusions from finite element modeling .....	166
Conclusions concerning Input Parameters .....	167
GREEN COVE SPRINGS CIRCULAR FOOTING PREDICTION .....	169
Introduction .....	169
Objectives .....	169
Scope of the Work .....	170
Site Description and Insitu Testing .....	171
Test Footing .....	182
Equipment: .....	185
Survey Measurements .....	188
Loading Sequence .....	189
Soil-Structure Profile for the Conventional and Finite Element Modeling: .....	191
Conventional Method: .....	191
Finite Element Method .....	193
Correlations for Input Parameters .....	194
Ultimate Bearing Capacities .....	205
Results .....	205
Measured Settlements (LVDTs and Survey) .....	205
Discussion of Results .....	209
Conclusion and Recommendations .....	211
CONCLUSION .....	214
Conclusions .....	214

Recommendations ..... 216

ADDITIONAL INSITU TEST DATA ..... 217

LIST OF REFERENCES ..... 239

ACKNOWLEDGEMENTS ..... 242

## LIST OF TABLES

<u>Table</u>		<u>Page</u>
Table 1	Input Parameter for Plaxis .....	50
Table 1	Continued .....	51
Table 2	Input Parameters for PlasFEM .....	52
Table 2	Continued .....	53
Table 3	Typical Values of Unit Weight for Soil (Coduto, 1994) .....	54
Table 4	Soil Parameters (Teng, 1962, as referenced in U.S. Steel, 1971) .....	55
Table 5	Correlation Between $q_c$ and $\phi'_{tc}$ (after Meyerhof, 1956) .....	57
Table 6	Correlation Between Relative Density and Net Limit Pressure ( $P_N$ ) and Pressuremeter Modulus ( $E_O$ ) for Sands (after Briaud, 1992, Baguelin et al., (1978) .....	60
Table 7	Unconfined Compressive Strength from SPT N (Teng, 1962, as referenced in U.S. Steel, 1971) .....	61
Table 8	Correlation Between Soil Consistency and Net Limit Pressure ( $P_N$ ) and Pressuremeter Modulus ( $E_O$ ) for Clays (after Briaud, 1992) .....	63
Table 9	Summary of soil parameters from lab and insitu tests on State Road 20 Swift/Sanders Creek at the depth of tube 7 .....	85
Table 10	Summary of possible PENCEL moduli from pressuremeter a tests at State Road 20 Swift/Sanders Creek at the depth of tube 7 .....	85
Table 11	Summary of soil parameters from lab and insitu tests at the Southwest Recreation Center .....	92
Table 12	Summary of possible PENCEL moduli from pressuremeter a tests at Southwest Recreation Center .....	93
Table 13	Summary of soil parameters from lab and insitu tests at the Archer Landfill .....	101

Table 14	Summary of possible PENCEL moduli from pressuremeter a tests at the Archer Landfill .....	101
Table 15	Spreadsheet used to verify triaxial test invariants .....	104
Table 16	Summary of Sandler-Dimaggio parameters R and D from literature .....	106
Table 17	Summary of input parameters for triaxial tests .....	114
Table 18	Results of modulus iteration for research site pressuremeter curves .....	124
Table 19	Summary of cone penetration test sounding, North, at Moffitt Cancer Center ....	130
Table 19	Continued .....	131
Table 20	Summary of cone penetration test at Moffitt Cancer Center south .....	133
Table 20	Continued .....	134
Table 21	Tabular input and output from DMMWin Software, A Axis and B Axis – Casing 2 .....	143
Table 21	Continued .....	144
Table 22	Excel spreadsheet for inclinometer deflection .....	147
Table 23	CZ128 wall properties for CWALSHT and Plaxis .....	149
Table 24	Soil Properties from MCPT for CWALSHT analysis by Ardaman and Associates(Sounding C-3) .....	151
Table 25	Soil Properties from SPT Boring G-7 for CWALSHT analysis .....	152
Table 26	Soil Properties from SPT for FEM analysis with Plaxis .....	152
Table 27	Soil Properties from Soundings CPT1, PMT1 for CWALSHT .....	153
Table 28	Soil Properties for FEM analysis with Plaxis: Mohr-Coulomb Model .....	154
Table 29	Input parameters for numerical modeling with Plaxis: Hardening Soil Model ....	154
Table 30	Soil properties from PMT curve matching (Figure 123) .....	155
Table 31	Comparison of results from CWALSHT .....	157
Table 32	Comparison of results from FEM analysis with Plaxis .....	159
Table 33	Deflections of top of the wall: measured versus predicted .....	164

Table 34	Effect of modulus and Constitutive Models on top deflection .....	164
Table 35	Soil properties from CPT data reduction .....	174
Table 36	Soil properties from DMT data reduction .....	175
Table 36	Continued .....	176
Table 36	Continued .....	177
Table 36	Continued .....	178
Table 37	Compressive and unit weight tests on the concrete specimens .....	183
Table 38	Loading schedule followed at Green Cove Springs .....	190
Table 39	Input of main parameters for CSANDSET .....	193
Table 40	Properties of layers for Oweis and Schmertmann methods .....	193
Table 41	Stress History for sand by combining DMT and CPT data .....	197
Table 42	Comparison for overconsolidation ratios - OCR .....	198
Table 43	Soil properties from consolidation tests .....	198
Table 44	Properties of the Footing Concrete .....	202
Table 45	Soil properties from the different insitu tests for Plaxis (OCR = 1) .....	203
Table 46	$K_0$ and OCR values from DMT based on Kulhawy and Mayne, (1982) .....	204
Table 47	Bearing capacity estimation .....	205
Table 48	Settlements measured with LVDTs and survey versus loads .....	207
Table 49	Settlements from LVDTs versus conventional methods .....	207
Table 50	Settlements from LVDTs versus finite element analysis with Plaxis using insitu data .....	208
Table A1	Summary of cone penetration test at State Road 20 Swift/Sanders Creek .....	219
Table A1	Continued .....	220
Table A2	Summary of dilatometer test at State Road 20 Swift/Sanders Creek .....	221
Table A2	Ccontinued .....	222
Table A3	Summary of cone penetration test at Southwest Recreation Center .....	224

Table A3	Continued	225
Table A4	Summary of dilatometer test at Southwest Recreation Center	226
Table A4	Continued	227
Table A4	Continued	228
Table A4	Continued	229
Table A5	Summary of cone penetration test at Archer Landfill	232
Table A6	Summary of dilatometer test at Archer Landfill	234
Table A6	Continued	235
Table A6	Continued	236
Table A6	Continued	237

## LIST OF FIGURES

<u>Figure</u>	<u>Page</u>
Figure 1 The engineering design paradigm . . . . .	1
Figure 2 Kögler's sausage-shaped pressuremeter (Baguelin et al., 1978, reprinted, with permission, copyright Trans Tech Publications) . . . . .	5
Figure 3 A modern version of the Ménard Pressuremeter <a href="http://www.roctest.com/roctelemac/product/product/g-am_menard.html">http://www.roctest.com/roctelemac/product/product/g-am_menard.html</a> ) . . . . .	6
Figure 4 Self-boring pressuremeter sold by Cambridge Insitu ( <a href="http://www.cambridge-insitu.com/csbp_leaflet2.htm">http://www.cambridge-insitu.com/csbp_leaflet2.htm</a> ) . . . . .	7
Figure 5 The push-in pressuremeter (Reid et al., 1982, reprinted, with permission, copyright Editions Technip) . . . . .	9
Figure 6 A full displacement pressuremeter ( <a href="http://www.cambridge-insitu.com/specs/Instruments/CPM.html">http://www.cambridge-insitu.com/specs/Instruments/CPM.html</a> ) . . . . .	10
Figure 7 The pavement pressuremeter probe (Briaud and Shields, 1979, reprinted, with permission, copyright ASTM) . . . . .	12
Figure 8 The pavement pressuremeter control unit (Briaud and Shields, 1979, reprinted, with permission, copyright ASTM) . . . . .	13
Figure 9 The full displacement pressuremeter (Hughes and Robertson, 1985, reprinted, with permission, copyright NRC Research Press) . . . . .	16
Figure 10 Zone of high lateral stress around a pushed cone penetrometer (Hughes and Robertson, 1985, reprinted, with permission, copyright NRC Research Press) . . . . .	18
Figure 11 Proposed stress path followed by soil adjacent to a cone penetration test (Hughes and Robertson, 1985, reprinted, with permission, copyright NRC Research Press) . . . . .	19
Figure 12 Stress field around a pushed cone penetration tip (Hughes and Robertson, 1985, reprinted, with permission, copyright NRC Research Press) . . . . .	21

Figure 13	Stress path followed by a full displacement pressuremeter test after pushing (Hughes and Robertson 1985, reprinted, with permission, copyright NRC Research Press) .....	22
Figure 14	Comparative stress paths followed by each of the pressuremeter methods (Hughes and Robertson 1985, reprinted, with permission, copyright NRC Research Press) .....	23
Figure 15	Fugro cone pressuremeter (Withers, et al., 1986, reprinted, with permission, copyright ASTM) .....	26
Figure 16	Stress paths and stress concentrations during a cone pressuremeter test (Withers et al., 1989, reprinted, courtesy of Thomas Telford Ltd, London) .....	27
Figure 17	Cone pressuremeter calibration chamber setup at Oxford (Schnaid and Houlsby, 1992, reprinted, courtesy of Thomas Telford Ltd, London) .....	29
Figure 18	Relative density and friction angle based on calibration chamber tests (Schnaid and Houlsby, 1992, reprinted, courtesy of Thomas Telford Ltd, London) .....	30
Figure 19	View of Plaxis input interface .....	33
Figure 20	Plaxis automatic mesh generation .....	33
Figure 21	Plaxis Calculation engine window .....	35
Figure 22	Plaxis Output example .....	35
Figure 23	PlasPLOT example output .....	37
Figure 24	An embankment model in the pre-release version of PlasGEN .....	37
Figure 25	Mohr-Coulomb failure surface (Plaxis, 1998) .....	40
Figure 26	An elastic perfectly plastic stress strain curve .....	41
Figure 27	Hardening soil model with cap in p-q space (Plaxis 1998) .....	42
Figure 28	Hardening soil model with cap in principal stress space, (Plaxis 1998) .....	43
Figure 29	Drucker-Prager failure surface in invariant stress space (Pinto 1998) .....	44
Figure 30	Mohr-Coulomb and Drucker-Prager failure surfaces viewed in the $\pi$ plane .....	45
Figure 31	Sandler-Dimaggio cap model (Pinto 1998) .....	46
Figure 32	Diagram of peq-ellipse in a p-q plane .....	47
Figure 33	Yield surface of Cam Clay model in p-q space .....	49

Figure 34	Friction Angle from Overburden Pressure and SPT N (Demello, 1971, as referenced in Schmertmann, 1975) .....	55
Figure 35	Friction Angle from Overburden Pressure, Relative Density, and SPT N. (Gibbs and Holtz, 1967, as referenced in O'Neill and Murchison, 1983) .....	56
Figure 36	Friction Angle from Overburden Pressure and CPT Tip Resistance (Robertson and Campanella, 1983) .....	58
Figure 37	Cohesive Soil Shear Strength (EPRI, 1990) .....	61
Figure 38	Relationship between $q_c$ and $S_u$ (EPRI, 1990) .....	62
Figure 39	Typical Values for Poisson's Ratio for Soil and Other Materials (Bowles, 1996) .....	64
Figure 40	Typical Values for Poisson's Ratio for Soil (Bowles, 1996) .....	64
Figure 41	Typical Values of Young's Modulus for Soil (Bowles, 1996) .....	65
Figure 42	Typical Values of Young's Modulus for Soil (Coduto, 1994) .....	65
Figure 43	Normalized Young's Modulus from SPT (EPRI, 1990) .....	66
Figure 44	Constrained Modulus from CPT (Robertson and Campanella, 1983) .....	67
Figure 45	Drained Secant Young's Moduli from CPT (Robertson and Campanella, 1983) ...	68
Figure 46	Triaxial testing load frame and control board .....	73
Figure 47	Triaxial cell and data acquisition computer .....	73
Figure 48	The PENCEL Pressuremeter control unit .....	75
Figure 49	The PENCEL Pressuremeter probe .....	75
Figure 50	The PENCEL Pressuremeter probe fully assembled .....	76
Figure 51	System compliance correction for the PENCEL Pressuremeter (Briaud and Shields, 1979, reprinted, with permission, copyright ASTM) .....	77
Figure 52	PENCEL Pressuremeter curve with limit pressure and moduli denoted .....	78
Figure 53	The University of Florida electric cone truck .....	79
Figure 54	Plan view of soil exploration at State Road 20 Swift/Sanders Creek .....	81
Figure 55	Standard penetration test boring B1 at State Road 20 Swift/Sanders Creek .....	82

Figure 56	PENCEL Pressuremeter tests at State Road 20 Swift/Sanders Creek at depths 10.5-25 ft .....	83
Figure 57	PENCEL Pressuremeter tests at State Road 20 Swift/Sanders Creek at depths 35-45 ft .....	83
Figure 58	Consolidated drained triaxial test of tube 7 specimen 2 from State Road 20 Swift/Sanders Creek at depth 34 ft .....	84
Figure 59	Mohr-Coulomb envelope for consolidated drained triaxial test of tube 7 specimen 2 from State Road 20 Swift/Sanders Creek at depth 34 ft .....	84
Figure 60	Plan view of soil exploration at Southwest Recreation Center .....	86
Figure 61	Standard penetration test boring B1 at Southwest Recreation Center .....	87
Figure 62	PENCEL Pressuremeter tests at Southwest Recreation Center at depths 8-16 ft. ...	88
Figure 63	PENCEL Pressuremeter tests at Southwest Recreation Center at depths 22-30 ft .....	88
Figure 64	PENCEL Pressuremeter tests at Southwest Recreation Center at depths 34-38 ft .....	89
Figure 65	Consolidated drained triaxial test of tube 1 from Southwest Recreation Center at depth 10-12 ft .....	89
Figure 66	Mohr-Coulomb envelope for consolidated drained triaxial test from tube 1 at Southwest Recreation Center at depth 10-12 ft .....	90
Figure 67	Consolidated drained triaxial tests of tube 2 from Southwest Recreation Center at depth 14-16 ft .....	90
Figure 68	Mohr-Coulomb envelope for consolidated drained triaxial tests of tube 2 from Southwest Recreation Center at depth 14-16 ft .....	91
Figure 69	Consolidated drained triaxial tests of tube 3 from Southwest Recreation Center at depth 18-20 ft .....	91
Figure 70	Mohr-Coulomb envelope for consolidated drained triaxial tests of tube 3 from Southwest Recreation Center at depth 18-20 ft .....	92
Figure 71	Plan view sketch of soil exploration at the Alachua County Landfill in Archer, Florida .....	94
Figure 72	Standard penetration test boring B1 at Archer Landfill .....	95
Figure 73	PENCEL Pressuremeter tests at Archer Landfill at depths 5-15 ft .....	96

Figure 74	PENCEL Pressuremeter tests at Archer Landfill at depths 20-30 ft . . . . .	96
Figure 75	Consolidated drained triaxial tests of tube 1 from Archer Landfill at depth 4-6 ft . . . . .	97
Figure 76	Mohr-Coulomb envelope for consolidated drained triaxial tests of tube 1 from Archer Landfill at depth 4-6 ft . . . . .	97
Figure 77	Consolidated Drained Triaxial tests of tube 2 from Archer Landfill at depth 9-11 ft . . . . .	98
Figure 78	Mohr-Coulomb envelope for consolidated drained triaxial tests of tube 2 from Archer Landfill at depth 9-11 ft . . . . .	98
Figure 79	Consolidated drained triaxial test of tube 3 from Archer Landfill at depth 14-16 ft . . . . .	99
Figure 80	Mohr-Coulomb envelope for consolidated drained triaxial test of tube 3 from Archer Landfill at depth 14-16 ft . . . . .	99
Figure 81	Consolidated drained triaxial test of tube 4 from Archer Landfill at depth 19-21 ft . . . . .	100
Figure 82	Mohr-Coulomb envelope for consolidated drained triaxial test of tube 4 from Archer Landfill at depth 19-21 ft . . . . .	100
Figure 83	Invariant stress paths for triaxial tests at Southwest Recreation Center . . . . .	105
Figure 84	Meshes of finite elements used in Plaxis, left, and PlasFEM simulations of triaxial tests . . . . .	107
Figure 85	Simulations of triaxial test at State Road 20 tube 7 depth 34 ft . . . . .	108
Figure 86	Simulations of triaxial test at Southwest Recreation Center tube 1 depth 10-12 ft . . . . .	108
Figure 87	Simulations of triaxial test at Southwest Recreation Center tube 2 specimen 1 depth 14-16 ft . . . . .	109
Figure 88	Simulations of triaxial test at Southwest Recreation Center tube 2 specimen 2 depth 14-16 ft . . . . .	109
Figure 89	Simulations of triaxial test at Southwest Recreation Center tube 3 specimen 1 depth 18-20 ft . . . . .	110
Figure 90	Simulations of triaxial test at Southwest Recreation Center tube 3 specimen 2 depth 18-20 ft . . . . .	110
Figure 91	Simulations of triaxial test at Archer Landfill tube 1 specimen 1 depth 4-6 ft . . . .	111

Figure 92	Simulations of triaxial test at Archer Landfill tube 1 specimen 2 depth 4-6 ft . . . .	111
Figure 93	Simulations of triaxial test at Archer Landfill tube 2 specimen 1 depth 9-11 ft . . .	112
Figure 94	Simulations of triaxial test at Archer Landfill tube 2 specimen 2 depth 9-11 ft . . .	112
Figure 95	Simulations of triaxial test at Archer Landfill tube 3 depth 14-16 ft . . . . .	113
Figure 96	Simulations of triaxial test at Archer Landfill tube 4 depth 19-21 ft . . . . .	113
Figure 97	Plaxis finite element mesh for PENCEL Pressuremeter . . . . .	118
Figure 98	Simulations of PENCEL Pressuremeter test at State Road 20 depth 35 ft . . . . .	120
Figure 99	Simulations of PENCEL Pressuremeter test at Southwest Recreation Center depth 8 ft . . . . .	120
Figure 100	Simulations of PENCEL Pressuremeter test at Southwest Recreation Center depth 12 ft . . . . .	121
Figure 101	Simulations of PENCEL Pressuremeter test at Southwest Recreation Center depth of 16 ft . . . . .	121
Figure 102	Simulations of PENCEL Pressuremeter test at Archer Landfill depth 5 ft . . . . .	122
Figure 103	Simulations of PENCEL Pressuremeter test at Archer Landfill depth 10 ft . . . . .	122
Figure 104	Simulations of PENCEL Pressuremeter test at Archer Landfill depth 15 ft . . . . .	123
Figure 105	Simulations of PENCEL Pressuremeter test at Archer Landfill depth 20 ft . . . . .	123
Figure 106	Proposed function of triaxial stiffness multiplier versus limit pressure . . . . .	124
Figure 107	Plan view of the Moffitt Cancer Center: field exploration . . . . .	128
Figure 108	Cone penetration test sounding, North, at Moffitt Cancer Center . . . . .	129
Figure 109	Cone penetration test sounding, South, at Moffitt Cancer Center . . . . .	132
Figure 110	Corrected PENCEL Pressuremeter Test, North, Moffitt Cancer Center (5 – 15ft) . . . . .	135
Figure 111	Corrected PENCEL Pressuremeter Test, North, Moffitt Cancer Center (20 – 25ft) . . . . .	135
Figure 112	Corrected PENCEL Pressuremeter Test, South, Moffitt Cancer Center ( 5 – 15ft) . . . . .	136

Figure 113 Corrected PENCEL Pressuremeter Test, South, Moffitt Cancer Center (20 – 25ft) .....	136
Figure 114 Standard Penetration Test Boring G-7 at Moffitt Center .....	137
Figure 115 Typical drawing of the cantilevered sheet pile wall at Moffitt Cancer Center .....	138
Figure 116 Schematic drawing of CZ128 with the 2.5” by 2.5” ¼” box tubing .....	139
Figure 117 CZ128 pile driving (a), and inclinometer casing attached to CZ128 (b) .....	140
Figure 118 Plan view of inclinometer casings: 1, 2, 3 and CZ128 wall .....	141
Figure 119 Soil-wall profile for CWALSHT and numerical modeling analyses-Casing 2 ...	142
Figure 120 Soil-wall profile after 3-staged excavation – Casing 2 .....	142
Figure 121 Deflections in A Axis (Perpendicular to wall) and B Axis (Parallel) – Casing 2 .....	145
Figure 122 Plan view of wall deflection – Casing 2 .....	146
Figure 123 Matching Mohr-Coulomb and Hardening Soil Models with insitu PMT Curve (3.00ft) .....	155
Figure 124 Profile type for CWALSHT analysis .....	156
Figure 125 CWALSHT results: (a) deflected shape, (b) moment diagram, (c) shear diagram, (d) net pressure .....	157
Figure 126 Finite element modeling the soil-wall structure (plane strain) .....	158
Figure 127 Results from FEM with Plaxis: (a) Deformed mesh, (b) Wall Deflection(c) Moment Diagram, (d) Shear Diagram .....	159
Figure 128 Comparison of results: measured vs. predicted (MC: Mohr-Coulomb, HS: Hardening Soil) .....	162
Figure 129 Constitutive models and unload-reload moduli on Plaxis modeling .....	163
Figure 130 Insitu testing boring locations at Applied Foundation Testing Inc., site .....	171
Figure 131 Cone penetration test sounding at Green Cove Springs .....	173
Figure 132 DMT data at Green Cove Springs .....	179
Figure 133 Corrected pressuremeter curves at depths $z = 1.0\text{m}, 2.0\text{m}, 3.0\text{m}$ .....	180
Figure 134 Corrected pressuremeter curves at depths $z = 5.0\text{m}, 7.0\text{m}, 10.0\text{m}$ .....	180

Figure 135	SPT blow counts and soil description	181
Figure 136	Soil-footing profile with ground water table	182
Figure 137	Plan view of concrete footing and loaded area	182
Figure 138	Loading process using TINIUS OLSEN, model CMH 289 controller	184
Figure 139	Steel reinforced concrete footing	184
Figure 140	Footing before and after the casting of the concrete	185
Figure 141	Load cells, LVDTs, steel plates (bottom and top), and seating weight	186
Figure 142	Layout of the load cells (L.C.), LVDTs and reference beams	187
Figure 143	Data acquisition with the computer and Megadec	187
Figure 144	Data acquisition equipment used at Green Cove Springs	188
Figure 145	Survey level and ruler locations	189
Figure 146	Loading process and final load applied	190
Figure 147	Plot of the load steps versus time	191
Figure 148	Soil layers for Schmertmann and Oweis methods in CSANDSET	192
Figure 149	Overconsolidation ratio at depth 2.5ft from consolidation test, $OCR \cong 12.8$	199
Figure 150	Overconsolidation ratio at depth 3.5ft from consolidation test, $OCR \cong 5.5$	200
Figure 151	Model meshing for finite element analysis with Plaxis	201
Figure 152	Curve fitting with Plaxis (Hardening Soil Model) to determine PMT $\phi$ (depth = 1.0m)	202
Figure 153	LVDTs settlements and load versus time	206
Figure 154	Graphical representation of the settlement: predicted and measured (Plaxis: Mohr-Coulomb Model)	209
Figure A1	Cone penetration test at SR 20 Swift/Sanders Creek	218
Figure A2	Cone presentation test at Southwest Recreation Center	223
Figure A3	Grain size distributions for tubes tested from Southwest Recreation Center	230

## List of Symbols

### **General Terms**

$z$	depth
$\sigma$	Normal Stress
$\tau$	Shear Stress
$p$	Mean Normal Stress, $(\sigma_1 + \sigma_2)/2$
$q$	$(\sigma_1 - \sigma_2)/2$
$I_1$	First Invariant of Principal Stress
$J_2$	Second Invariant of Deviatoric Stress
$\phi$	Angle of Internal Friction
$\phi'$	Drained Angle of Internal Friction
$\gamma$	Total Unit Weight
$\gamma'$	Effective Unit Weight
$c$	cohesion
$s_u$	Undrained Shear Strength
$k_0$	ratio of initial horizontal stress / initial vertical stress
$\rho$	soil density
$E$	Young's Modulus
$E_{50}$	Secant Young's Modulus at 50% of failure stress from Triaxial test
$E_{25}$	Secant Young's Modulus at 25% of failure stress from Triaxial test
$\nu, \mu$	Poisson's Ratio
$N$	Standard Penetration Test blowcount
$N_{60}$	Standard Penetration Test blowcount corrected to 60% hammer efficiency
$q_c$	Cone Penetration Test Tip resistance
$E_D$	Dilatometer Modulus
$\Omega$	Tangent stiffness multiplier

### **PENCEL Pressuremeter**

$V_c$	initial volume of the pressuremeter
$V_o, p_o$	the first point on the linear portion of the pressuremeter curve
$V_f, p_f$	the final points on the linear portion of the pressuremeter curve
$E_{UR}$	Unload- Reload Modulus
$p_L$	Limit Pressure
$E_{UL}$	Final unloading modulus
$E_i$	Initial Modulus

## Plaxis Constitutive Model Terms

### *Mohr Coulomb*

$\phi$	Friction Angle
c	cohesion
$\psi$	Dilation Angle
E	Young's Modulus
$\nu$	Poisson's Ratio
$\rho$	unit weight
$K_0$	ration of initial horizontal stress / initial vertical stress

### *Hardening Soil*

$\phi$	Friction Angle
c	cohesion
$\psi$	Dilation Angle
$E_{ref}$	<u>Secant</u> stiffness in standard triaxial test at $p_{ref}$
$E_{ref}$	<u>Tangent</u> Stiffness for primary oedometer loading at $p_{ref}$
m	Power for stress level dependency of stiffness
$E_{ur}$	Unloading/reloading stiffness
$\nu_{ref}$	Poisson's Ratio for unloading-reloading
p	Reference stress for stiffness
$R_f$	Failure ratio
$\sigma_{tension}$	Tension Cutoff
$c_{increment}$	Incremental increase of cohesion with depth
$K_0^{nc}$	$\sigma'_{xx} / \sigma'_{yy}$ stress ratio in a state of normal consolidation
$\rho$	unit weight
$K_0$	ratio of initial horizontal stress / initial vertical stress
POP	Preconsolidation Pressure or
OCR	Overconsolidation Ratio

### *Soft Soil Creep*

c	cohesion
$\phi$	Friction Angle
$\psi$	Dilatancy Angle
$\kappa^*$	Modified swelling index
$\lambda^*$	Modified compression index
$\mu^*$	Modified creep index
$\rho$	unit weight
$\sigma_0$	initial vertical stress in elements
$K_0$	ration of initial horizontal stress / initial vertical stress
$K_0^{nc}$	$\sigma'_{xx} / \sigma'_{yy}$ stress ratio in a state of normal consolidation
M	Slope of the Critical State Line
$\nu_{ur}$	Poisson's ratio for unloading-reloading (default 0.15)

## EXECUTIVE SUMMARY

### Project Summary

For many years, numerical codes that use the Finite Element Method were restricted to research. Advances in computing power have now enabled these codes to be accessible to geotechnical engineers for design purposes. Soil behavior is implemented in these codes by way of constitutive models. These models were typically derived based on theoretical soil mechanics or fitted empirically to a laboratory soil test with known boundary conditions. In order to apply these constitutive models to a specific soil in question, a set of soil parameters must be passed into the code.

In the simplest case, a linear elastic model could be used where the only parameters needed are modulus and Poisson's ratio. In many cases, such a simple representation is not sufficient. Instead of a constant stiffness, the stiffness may change with changes in stress. Strains may include elastic and plastic contributions. Failure or yield surfaces may be implemented to describe soil strength, and other limits. Consequently, the accuracy of design calculations depends upon the accuracy of the characterizing soil input parameters. Considering the difficulty of obtaining high quality samples for laboratory testing, insitu testing is a viable alternative for soil characterization.

The purpose of this study was to take a critical look at insitu test methods ( SPT, CPT, DMT, and PMT) as a means for developing finite element constitutive model input

parameters. The first part of the research examined insitu test derived parameters with laboratory triaxial tests at three sites: Saunder's Creek, Niceville, Florida; Archer Landfill, Archer, Florida; and SW Recreation Center, Gainesville Florida. The triaxial tests on these sands were used to develop baseline input parameters. These parameters were verified by simulating the triaxial tests using two finite element codes. From these comparisons, the following conclusions were drawn:

1. A input parameter sensitivity analysis of the FEM models shows that  $\phi$  is the most sensitive parameter.  $E_{50}$ ,  $E_{\text{oad}}$ , and  $m$  had little effect on modeling the stress-strain curve from a triaxial test.
2. FEM simulations of triaxial test stress-strain curves produced excellent results. The hardening models ( PLAXIS – Hardening Soil and PlasFEM – Sandler Dimaggio) simulated the non-linear behavior better than the Mohr-Coulomb or Drucker-Prager models.
3. In general, triaxial test  $\phi$  values were much lower that those estimated from CPT and DMT tests, but slightly higher than those estimated from SPT tests.
4. In general,  $E_{50}$  triaxial test modulus values agreed with those estimated from DMT and PMT unloading tests.
5. FEM simulations of field PMT curves using triaxial test based parameters were unsuccessful. It was necessary to increase the triaxial  $E_{50}$  values by  $\Omega = 1.3078e^{0.0164p_1} R^2 = 0.8515$ , where  $\Omega$  is the triaxial  $E_{50}$  modulus multiplier and  $p_1$  is the PENCEL limit pressure.

Tempered by these findings, the second phase of this study was to predict the deformations of a cantilevered sheet pile wall (unloading case). Conventional analyses

methods were compared with FEM using insitu test derived input parameters.

Correlations were used for SPT, and CPT parameters, while “curve matching” was used to obtain the PMT parameters. Deflections of the wall were measured during excavation and compared with finite element predictions of the wall deflections with depth. From these comparisons the following conclusions are drawn:

6. For the sheet-pile wall, conventional analyses ( CWALSHT) using parameters from SPT, CPT, and PMT under-predicted wall deformations unconservatively.
7. The FEM Hardening Soil Model more accurately predicted sheet-pile wall deflections than the Mohr-Coulomb Model. This is due to the Hardening Soil Model using a stiffer unload modulus.
8. Even at very small deflections (less than 25mm), the Linear Elastic FEM Model unconservatively underpredicts wall deflections.
9. Wall deflections were accurately predicted using the Hardening Soil Model with input parameters estimated from SPT correlations and “curved matched” PMT values. CPT based parameters under-prediction wall deformations due to too high  $\phi$  value estimates.

The third phase of this study was to predict the deformations of a 2-m diameter shallow footing (loading case). Conventional analyses methods were compared with FEM using insitu test derived input parameters. Correlations were used for SPT, CPT and DMT derived parameters, while “curve matching” was used to obtain the PMT parameters. Footing deflections were measured during loading and compared with finite element predictions. From these comparisons the following conclusions are drawn:

10. Fundamentally, the stress history of a soil profile, i.e., OCR or preconsolidation pressure, must be known for any settlement prediction either using conventional or finite element methods.
11. Surprisingly, of the conventional methods for estimating settlements (CSANDSET), only the SPT based D'Appolonia, and Peck and Bazaraa methods provided reasonable estimates of the observed settlement.
12. The conventional DMT method, which correlates a OCR values slightly overestimated measured settlements.
13. None of the insitu test derived input parameters (SPT, CPT, DMT, and PMT) coupled with FEM Mohr-Coulomb or Hardening Soil models, accurately predicted the shallow footing settlements.

#### Recommendations

Fundamentally, the FEM constitutive models require knowledge of the insitu state of stress (OCR, preconsolidation stress, or  $K_0$ ), and pore pressure. Unless an accurate estimate of these values is known, design predictions will be limited. For design problems involving driven structural elements (piles, sheet-piles) the state of stress due to driving is unknown. However, inserted insitu devices (CPT, DMT, and PMT) perhaps create similar stress states and thus lead to better predictions. It is our opinion that FEM analyses for this boundary value problem are superior to conventional analyses, and the hardening soil model is recommended. For settlement design problems, insertion of the insitu probe alters the stress state. Consequently, only the DMT provides accurate estimations of OCR and is recommended. For settlements, conventional methods are as accurate as FEM.

As a first approximation for conventional or FEM input parameters, the correlations listed in Chapter 3 are recommended. Alternatively, “curve matching” PMT results can provide valid input parameters.

## CHAPTER 1 INTRODUCTION

Geotechnical engineering design traditionally uses the paradigm shown below in figure 1 for design:

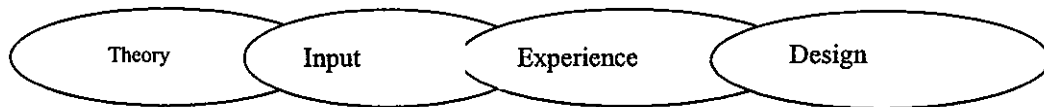


Figure 1 The engineering design paradigm.

### Limiting Equilibrium Theory

As engineers we tend to be quantitative using applied physics. Consequently, we tend to express ourselves mathematically to solve design problems. Historically, our theories are limiting equilibrium based (no fail - fail), and soil is deemed as being a frictional material. Thus Mohr-Coulomb theory is used to express behavior, and soil deforms (slides) along finite "failure planes". Using this combination of "Mohr-Coulomb" frictional behavior and "failure planes", limiting equilibrium of forces can be solved via normal forces (including pore water pressures - effective stresses) and shearing forces. Examples are: bearing capacity, slope stability, and earth pressures.

### Mohr-Coulomb Input Parameters

To solve mathematically Mohr Coulomb theory we need input parameters of: unit weight ( $\gamma$ ) friction angle ( $\phi$ ) and cohesion ( $c$ ). To obtain these parameters the common laboratory tests are: direct shear, and triaxial tests.

## Deformation Based Theory

If we choose to move from a limiting equilibrium theory to a deformation based elastic theory, then the input parameters become; normal and shear stresses, and various moduli; i.e., Young's modulus (E), Shear modulus (G), bulk modulus (K), and Poisson's ratio ( $\nu$ ). If we invoke permanent deformations (plasticity) then we need to separate elastic from plastic deformations via yield surfaces, flow rules, and hardening laws. These require knowledge of preconsolidation stresses and void ratio – effective stress relationships. To obtain these parameters, the triaxial and consolidation tests are commonly used.

Limitations: Unfortunately, laboratory testing requires obtaining high quality undisturbed samples from the field, which are subsequently transported back to the laboratory, carefully trimmed, and subsequently placed into the testing device. Backpressures for saturation to measure pore pressures (undrained tests) or volume change (drained tests) are applied, and the sample consolidated prior to shearing.

If one now considers that Florida consists of mostly sands with a very high water table, undisturbed sampling and laboratory testing become quite difficult/impossible. In addition, most design problems (retaining walls, deep foundations) would require many samples from a variety of depths. Consequently, in Florida, insitu tests are very popular for procuring soil parameters; among these are SPT, CPT, DMT, and PMT.

In addition to the problem of obtaining the soil properties, selection of the FEM constitutive model requires consideration. Fundamental to all models is knowledge of the insitu stress magnitude and drainage conditions (drained vs. undrained). For linear and non-linear elastic models, the initial modulus depends upon the confining stress. In

addition to drainage and initial stress conditions, for plasticity models, the degree of overconsolidation (OCR) is required. Faced with these requirements and as many as 3-12 input parameters, and utilizing conventional insitu tests (SPT, CPT, DMT, and PMT) it is apparent that some soil properties must be estimated. For example, SPT and CPT tests fail the soil by penetration and thus at best can be used for correlations. DMT only provides 1mm of deformation vs. stress. The PMT is the only test providing a stress deformation relationship. Accordingly, it maybe necessary to use “matching techniques”, whereby soil parameters would be systematically modified until a test result is matched with FEM predictions.

#### Problem Statement

The age-old dilemma for geotechnical engineers when analyzing design issues is, “What are the properties of the soil?” From the above discussion, there are three primary issues. First, the classical laboratory tests by which most constitutive models are calibrated often are not performed during geotechnical investigations on soils in Florida. Second, the common insitu method that is used, the Standard Penetration Test, provides little information for the engineer who wishes to extrapolate a constitutive relationship. Third, FEM constitutive models may require from 3-12 input parameters, and a knowledge of the initial stress state.

#### Objectives

Based upon the aforementioned problems, the objectives of this research proposal are: (1) to examine FEM computer programs with respect to their applicability for geotechnical design problems, (2) to evaluate insitu testing techniques (SPT, CPT, DMT,

and PMT) and corresponding data reduction to characterize Florida soils, and (3) to evaluate FEM capabilities, for predicting observed field case histories.

### Scope of Work

This project consists of two primary phases; Dr. Brian Anderson's dissertation on using the PENCEL pressuremeter and triaxial tests in FEM and Landy Rahelison's dissertation covering case histories modeled with FEM and insitu tests.

#### 1) Anderson

- a. Literature search and discussion of constitutive models
- b. Field and laboratory testing
  - i. Florida state road 20 at Swift/Sanders Creek
  - ii. University of Florida Southwest Recreation Center
  - iii. Alachua County Landfill-Archer
- c. Finite element modeling with Plaxis and PlasFEM
  - i. Triaxial Tests
  - ii. PENCEL Pressuremeter Tests

#### 2) Rahelison

- a. Comparison of FEM and Conventional solutions to geotechnical problems.
- b. Prediction of sheet pile wall deformation (unloading case) at the University of South Florida Moffitt Cancer Center
- c. Prediction of circular footing settlement (loading case) at Green Cove Springs Florida

## CHAPTER 2 LITERATURE REVIEW

This section consists of two parts. First, the history of the pressuremeter is examined, with a focus on previous research and development of full displacement probes. The latter portion of this section introduces the finite element codes utilized in this research.

### History of the Pressuremeter

Kögler, a German, developed the first pressuremeter and used it to determine soil properties somewhere around 1930. His pressuremeter was a single cell, long, and hollow device, which he inflated with gas. The results of this early pressuremeter were often difficult to interpret, and its development was hampered by technological difficulties (Baguelin et al., 1978). Figure 2 shows Kögler's pressuremeter.

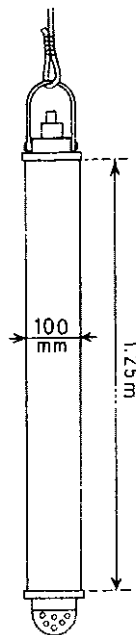


Figure 2 Kögler's sausage-shaped pressuremeter (Baguelin et al., 1978, reprinted, with permission, copyright Trans Tech Publications)

While working as a density inspector for a new airport runway near Paris, Louis Ménard pondered why he was measuring the density of the soil rather than the strength and deformation properties. As an answer to his dilemma, Ménard developed the modern soil pressuremeter in 1954 working on his university final year project. This apparatus was a tri-cell design with two gas-filled guard cells and a central water-filled measuring cell. Ménard continued his work under Peck at the University of Illinois for his Masters degree, “An Apparatus for Measuring the Strength of Soils in Place.” By 1957, Ménard had opened the Center d’Etudes Ménard where he produced pressuremeters for practicing engineers. Figure 3 shows a modern Ménard Pressuremeter marketed by Rocctest, Inc.

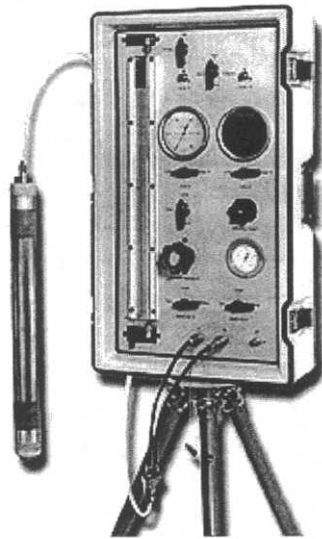


Figure 3 A modern version of the Ménard Pressuremeter ([http://www.roctest.com/roctelemac/product/product/g-am\\_menard.html](http://www.roctest.com/roctelemac/product/product/g-am_menard.html))

Although the pressuremeter seemed a radical departure from traditional geotechnical tests, there were inherent problems with the device. Many believed that the stresses induced or reduced by drilling the borehole were significant. These stresses were further complicated by the general quality of drilling. If the hole were too large, the

pressuremeter would possibly not inflate enough to develop a full pressuremeter curve. On the other hand, if the hole was too small, the insertion of the probe would disturb the borehole and therefore diminish the quality of the test data.

In an attempt to rectify these drilling issues, engineers at the Saint Briec Laboratory of the Ponts et Chaussées (LPC) in France developed the first self-boring pressuremeter. As the name implies, this pressuremeter inserts itself into the borehole as the borehole is being drilled. The premise behind the new device was to prevent movement of the borehole wall after drilling, and therefore prevent any changes in stress. A similar device was developed at Cambridge and is sold by Cambridge Insitu called the Camkometer (Figure 4). Data from this pressuremeter proved to be radically different than that of the Ménard. While the self-boring pressuremeter may have seemed to be the panacea to PMT problems, it suffered from more of its own. These new probes were extremely complex and required a great deal of experience and maintenance to operate.

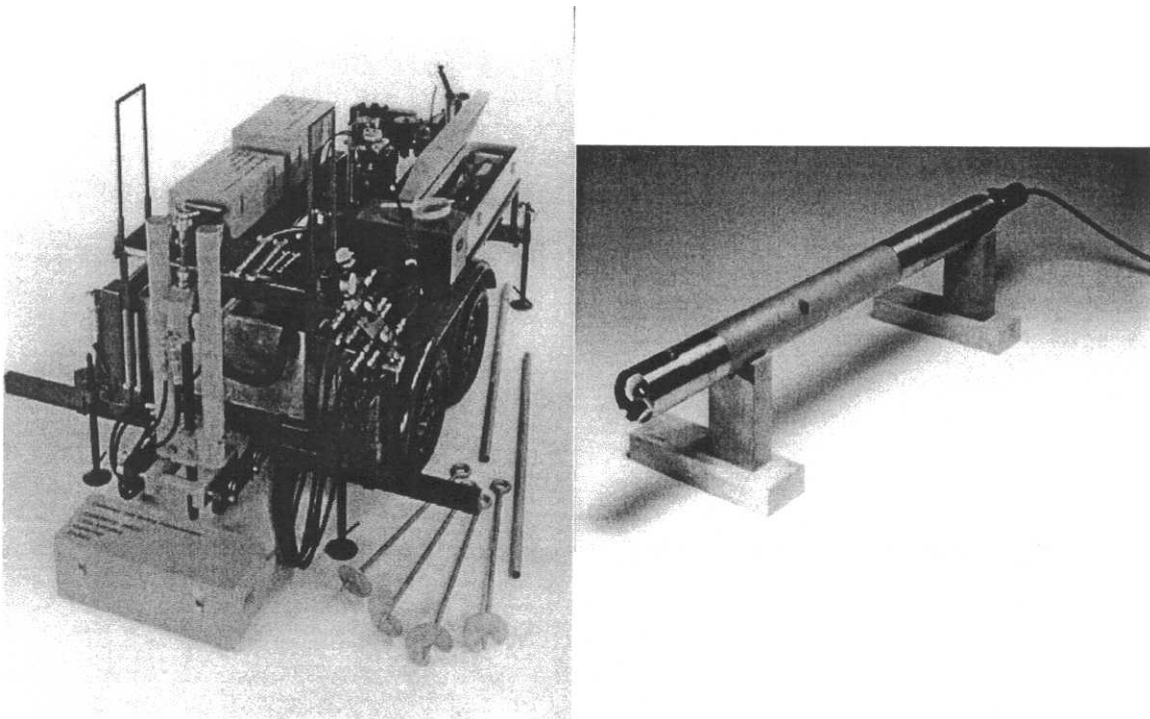


Figure 4 Self-boring pressuremeter sold by Cambridge Insitu ([http://www.cambridge-insitu.com/csbp\\_leaflet2.htm](http://www.cambridge-insitu.com/csbp_leaflet2.htm))

Also to address the problems with drilled pressuremeters, Reid et al.,(1982) and Fyffe et al.,(1985) developed a push-in type of pressuremeter. Shown in Figure 5, this new probe was developed primarily for use in the characterization of soils for offshore drilling structures. This new pressuremeter is hollow much like a Shelby tube. Soil is displaced into the probe during pushing, thus eliminating the cutting system. Unfortunately, the probe has to be extracted after every test to clean out the displaced soil.

A more recent development in pressuremeter technology is the full displacement or cone pressuremeter. This probe is pushed, as a cone penetration test, and then inflated as a traditional pressuremeter. This method eliminates the problems associated with drilling and the complexity of the self-boring equipment. Full displacement probes have been researched at the University of British Columbia, the University of Ottawa, and Oxford University. A commercially available full displacement type of pressuremeter is shown in Figure 6.

#### Previous Work with Full-Displacement Pressuremeters

As mentioned in the introduction, the full displacement type pressuremeter was the focus of this research. There have been three significant studies into this type of pressuremeter since the late 1970s.

#### Pavement Pressuremeter

The first group to develop such a probe was Briaud and Shields (1979). Their pressuremeter was developed primarily for the pavement industry to test the granular base and subbase layers and cohesive and granular subgrades. Transport Canada funded research into alternative methods of determining stiffness of pavement systems for airport runways. Current practice of the time included nondestructive tests such as

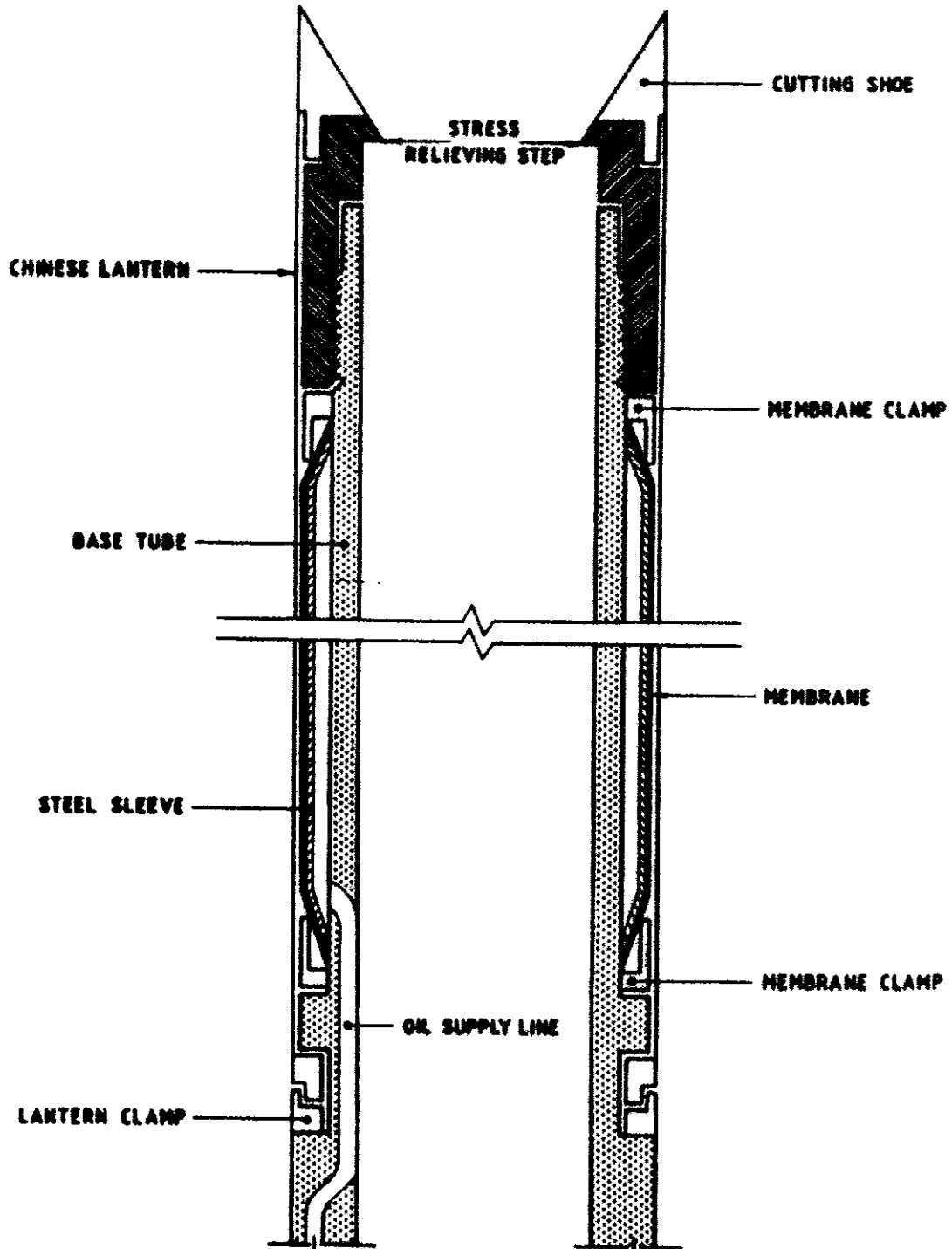


Figure 5 The push-in pressuremeter (Reid et al., 1982, reprinted, with permission, copyright Editions Technip)



Figure 6 A full displacement pressuremeter (<http://www.cambridge-insitu.com/specs/Instruments/CPM.html>)

Benkelman beam, dynaflect, and impulse tests that provided a “bulk” stiffness for the entire pavement system, rather than specific layers. Other tests were destructive in nature, (including CBR and plate bearing) were expensive, and often required significant patching. Lab tests that, were destructive in nature, suffered the typical lab problems of sample disturbance, small scale, and cost.

### General

The pavement pressuremeter was developed as a rugged, inexpensive, portable apparatus for the direct evaluation of the deformation characteristics of the pavement and subgrade layers. A traditional Ménard type of probe could not be used in the case of pavement design. The magnitude of the loads and depths of influence due to traffic loading are very different to that of a shallow foundation. Since the depth of influence was much smaller, a cone penetration test tip sized monocellular probe with a singular hydraulic tubing used. The shortened length of the probe facilitated a reasonable amount of measurements within the relatively shallow zone of influence. Strain control was chosen to allow for better definition of the elastic portion of the curve since stiffness is the important measurement. Additionally, strain control also simplified the equipment and facilitated cyclic testing.

### Apparatus

The pavement pressuremeter works by way of a hand-wheel pump that forces water through the tubing to the probe. The pressure in the water increases as the membrane is pushed into the soil. Pressure is read on a gauge while the volume change is monitored by the displacement of a column of red kerosene in a graduated tube. After the probe is fully inflated, reversing the direction of the hand-wheel easily deflates it.

The probe consists of three parts. The first part, the body, is a 500 mm (19.7 in) long and 25 mm (0.98 in) diameter pipe threaded at both ends. It has grooves for O-Rings at both ends to facilitate sealing of the membrane and two holes to allow water to pass through the pipe wall during inflation.

The membrane is a rubber tube, 430 mm (16.9 in) long. This portion of the probe expands when filled with water and is in essence the measuring cell. A Chinese Lantern of metal strips is glued to the outside to protect the membrane. Strips included, the membrane has an outside diameter of 31 mm (1.22 in). A sheathed membrane should last for 100 to 200 tests. Figure 7 shows a schematic of the probe.

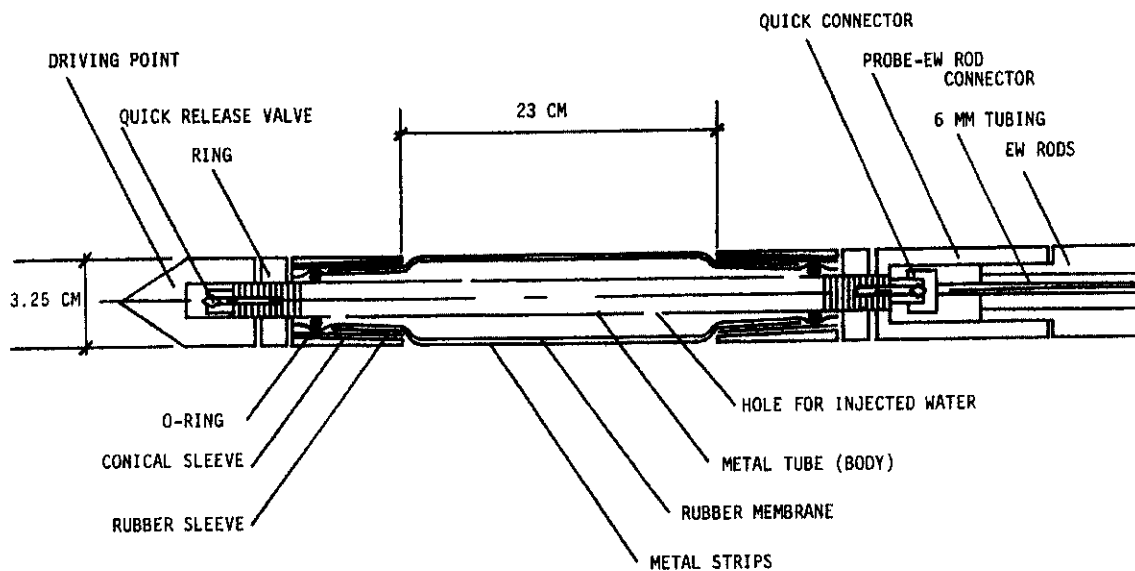


Figure 7 The pavement pressuremeter probe (Briaud and Shields, 1979, reprinted, with permission, copyright ASTM)

To restrict the movement of the membrane on the body and seal the system so that no air enters the membrane, rubber sleeves and conical metal sleeves are forced over the membrane at the ends of the body. Two metal nuts are screwed on until the length of the membrane between the sleeves is 230 mm (9.1 in).

A control unit, shown schematically in Figure 8, provides pressurization for the pavement pressuremeter. Pressure is applied to a column of water using a hand pump. The pressure in the system is displayed on a pressure gauge. Two Plexiglas tubes and three Plexiglas containers hold the fluid pumped into the probe, and the volume change is read by graduations on the Plexiglas tubes. The control unit is contained in a plywood box with dimensions 1200 mm x 600 mm x 300 mm (47.2 in x 23.6 in x 11.8 in). The probe, tubing, rods, and other accessories are also stored in the box. The box weighs 50 kg (112 lb).

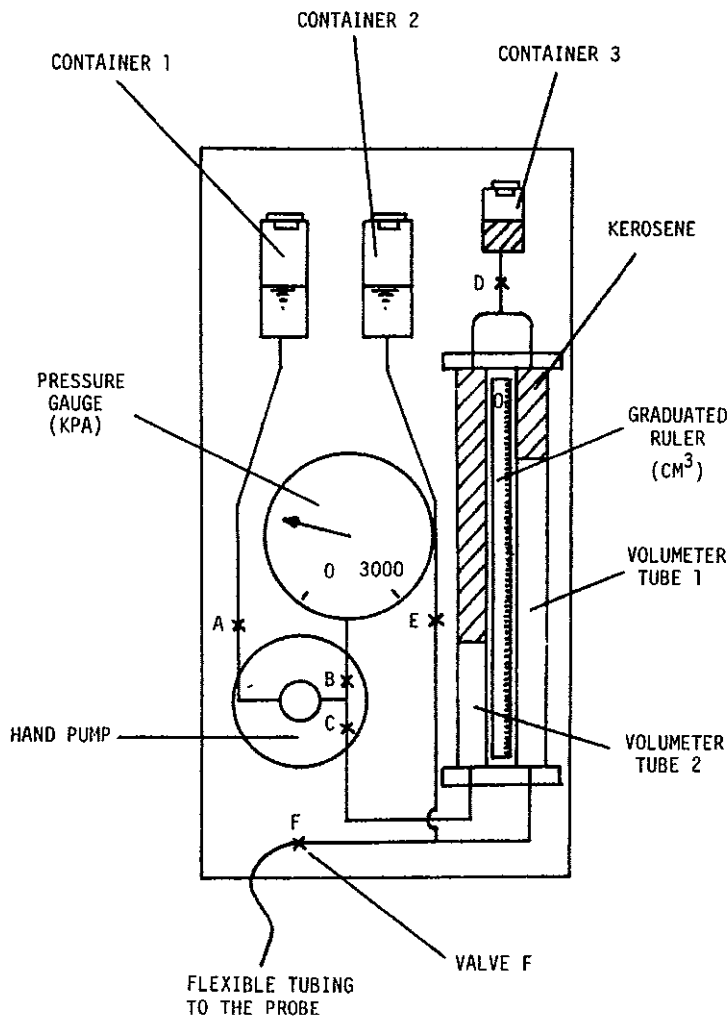


Figure 8 The pavement pressuremeter control unit (Briaud and Shields, 1979, reprinted, with permission, copyright ASTM)

## Test

To test a pavement and its subgrade with a pavement pressuremeter, first a hole is drilled through the pavement to a depth of 2000 mm (78.7 in). The probe is inserted through the 35 mm (1.38 in) hole and tests are performed every 300 mm (11.8 in). Preparation of the hole takes on the order of 2 to 10 minutes while each test (inflation of the membrane) takes around 6 to 7 minutes. A single hole could be logged with 6 tests in about one hour.

## Research

The literature only contains two cases where the pavement pressuremeter was used in research. The first case (Briaud and Shields, 1981a) investigates whether there is a critical depth for measuring stiffness by the pressuremeter similar to the critical depth for the development of pile capacity in sand. Briaud and Shields performed 66 tests in prepared sand and 38 tests in natural clay. Triaxial tests were performed on specimens of similarly prepared sands as well as Shelby tube specimens of the clay. Vane shear tests were also performed in the natural clay layer. The increase in stiffness of the sand with depth as measured by the pavement pressuremeter was attributed to that due to increase in horizontal stress with depth. In clay, the variation in pressuremeter modulus coincided with the variation in vane shear strengths with depth. The authors conclude that the proximity of the ground surface had little to no effect on the small strain deformation around the probe. As a corollary, the assumption of small strain is valid; therefore, the same mathematical technique can be used to obtain stiffness from a shallow test as from a deep test.

The second research study (Briaud and Shields, 1981b) performed with the pavement pressuremeter was more along the lines of pavement evaluation. The primary

findings were that the pavement pressuremeter tests compare well with McLeod plate load tests.

### Robertson and Hughes Full Displacement Pressuremeter

#### General

The second study into the full displacement pressuremeter was conducted at the University of British Columbia (Hughes and Robertson, 1985). As mentioned earlier, the pressuremeter had already been the subject of much research. Standard practices were developed for the Ménard probe to account for the difficulty of hole preparation. Design rules were established for use of pressuremeter parameters much like design rules based on standard penetration tests in the United States. The self-boring pressuremeter was developed to overcome the installation problems of the Ménard probe, but brought along an entire new set of problems including the complexity of equipment as well as the total cost. It was proposed if a pressuremeter probe was pushed into the ground before inflation, that a quantifiable amount of soil disturbance would occur. This disturbance would be operator independent, since pushing would be identical to the well established CPT procedure, as well as repeatable.

#### Apparatus

Instead of developing a new tool, an existing tool was modified for the job. The full-displacement pressuremeter used during this study was a 76 mm diameter (45.4 cm<sup>2</sup> area) self-boring pressuremeter with the cutting shoe removed and a solid 60° cone tip fitted in place of the cutting shoe. Lateral deformations were measured electronically with feeler gauges. The center of the pressuremeter membrane was located about 380 mm (14.9 in) behind the cone. A diagram of the full displacement pressuremeter is shown in Figure 9.

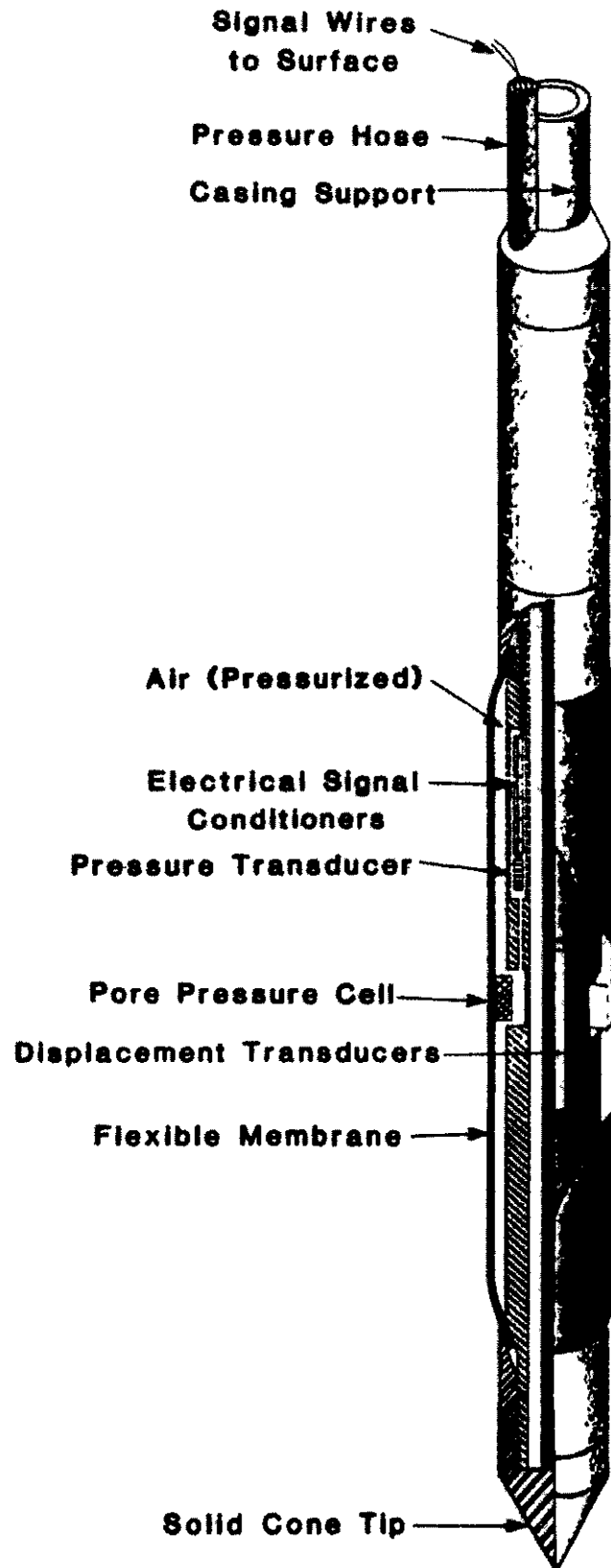


Figure 9 The full displacement pressuremeter (Hughes and Robertson, 1985, reprinted, with permission, copyright NRC Research Press)

## Test

Because no method for this test was established, the published procedure is merely summarized. For these full-displacement pressuremeter tests, the tool was pushed to depth using the UBC research vehicle, which has a 200 kN pushing capacity. The pressuremeter was pushed at the standard 2 cm/s rate used in cone penetration testing. The pushing force on the rods and probe was monitored with a load cell. Tests were performed by expanding the membrane with small increments of gas pressure. The displacement of the membrane at the feeler gauges was logged continuously.

## Research

Robertson proposes that in contrast to the self-boring and push-in pressuremeters, a full displacement probe would cause a quantifiable amount of disturbance that could be considered analytically. Thus, the boundary conditions would be much better defined or well known unlike the predrilled and self boring pressuremeters.

Since a full displacement pressuremeter is much like a CPT when inserted, this study starts with the considerations of the stress condition around a cone penetrometer. Hughes and Robertson conclude that the ratio of the lateral sleeve stress to the tip stress of a penetrometer pushed into sand at, for this example, a depth of 6m, to be 1:70 or somewhere close to a two orders of magnitude difference. As the tip passes the element, the ratio of stresses decreases rapidly. When the element of soil is adjacent to the friction sleeve, the lateral stresses are most likely similar to the insitu lateral stress. This phenomenon is shown in Figure 10. For loose to medium sands, the average lateral stress at the friction sleeve is very close to the insitu horizontal stress, but for dense sands at shallow depths, the lateral stresses are higher than the initial horizontal stress.

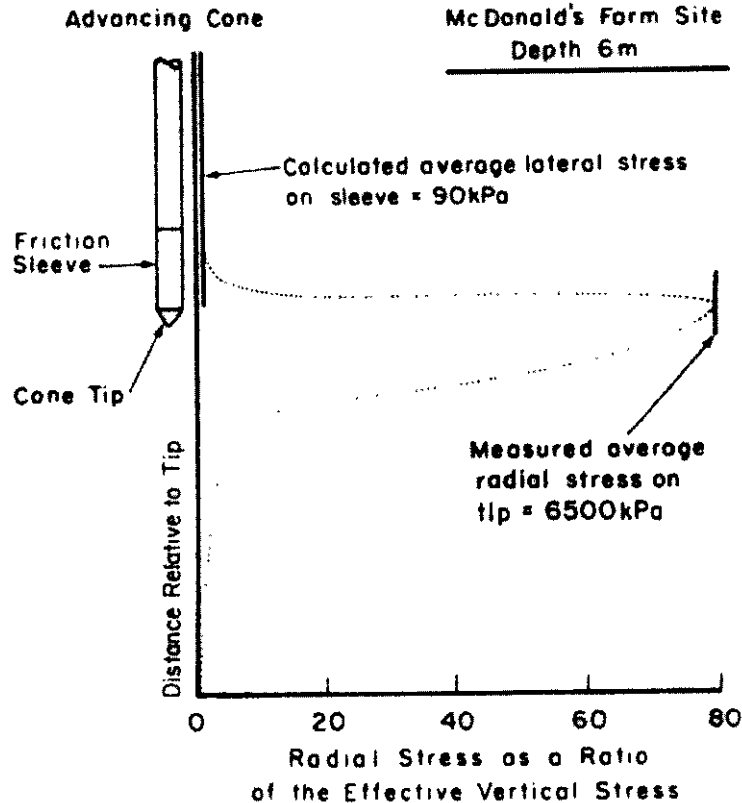


Figure 10 Zone of high lateral stress around a pushed cone penetrometer (Hughes and Robertson, 1985, reprinted, with permission, copyright NRC Research Press)

The penetrated sand has already experienced a complex stress path. Robertson and Hughes have idealized this stress path in Figure 11. With the starting point A representing the insitu state of stress, the stress path immediately moves toward the failure surface upon the approach of the cone. During penetration of the cone, the stress path moves along the failure surface until the tip begins to move past the point in question. At some point, C, the stresses will begin to diminish and likely reach the opposite failure surface, then finally settling back to something close to the original state of stress, but now there is a stress history. Points located some distance from the probe will, obviously, not feel the same magnitude of stress as those closer. But it is not likely that their final stress state will be the same as the points on the boundary. There is likely

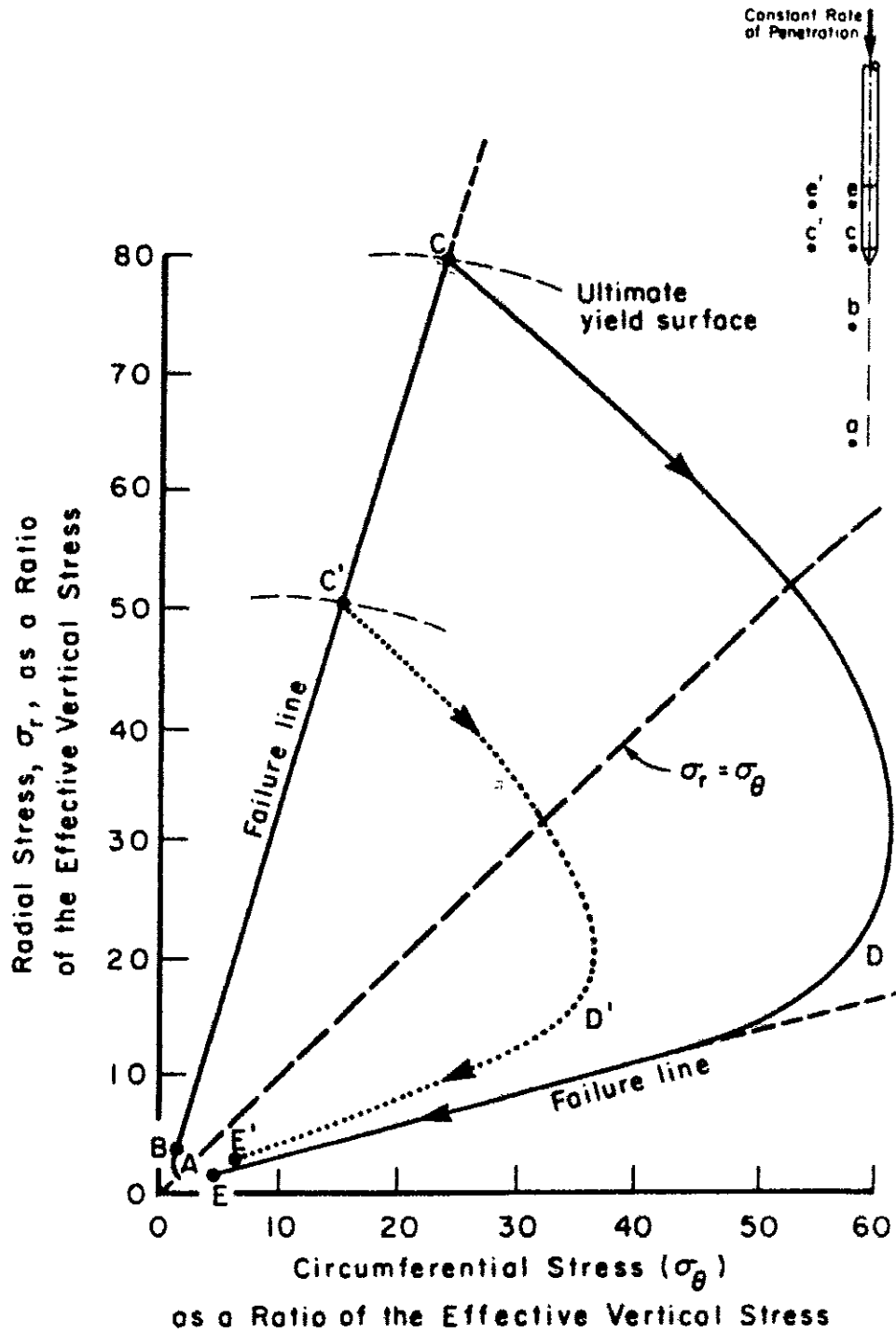


Figure 11 Proposed stress path followed by soil adjacent to a cone penetration test (Hughes and Robertson, 1985, reprinted, with permission, copyright NRC Research Press)

a zone of high residual stress some distance from the probe probably due to arching effects. Figure 12 shows the level of radial and circumferential (hoop) stresses when point C is at the cone and point E is somewhere past the cone, most likely in the position of the friction sleeve. The stresses at point E have reduced, but a residual zone exists at some radius from the probe.

Since the full displacement pressuremeter membrane is often a short distance behind the cone tip, the stress distribution around the pressuremeter will not be uniform and would vary with radial distance from the probe. Additionally, the failure surface may have shifted inwards due to the enormous (1:70) stress reduction and the fact that the soil has failed.

Depending on the radial distance of a soil element from the pressuremeter membrane, the initial stress could fall anywhere on the curve AE'E in the lower part of Figure 13. Loading from any of these points would begin as linear elastic until the stress path reaches the first yield surface. Then the loading will continue non-linearly until the failure condition is reached. Due to the high stresses already experienced by the soil, the yield and failure surfaces could be very high. Figure 13 shows an idealization of the pressuremeter curve that results from a full-displacement test and the non-linear elastic yielding nature of sand as the stress path passes through progressive yield surfaces.

To put it all together, the stress paths for an element of soil adjacent to the membrane of a traditional Ménard pressuremeter, a self-boring pressuremeter, and a full displacement pressuremeter are shown together on the left-hand side of Figure 14. The corresponding pressuremeter expansion curves are shown on the right-hand side of the figure. The primary difference among the figures is the initial stresses induced by the method by which the pressuremeter was advanced to depth. In the case of the prebored

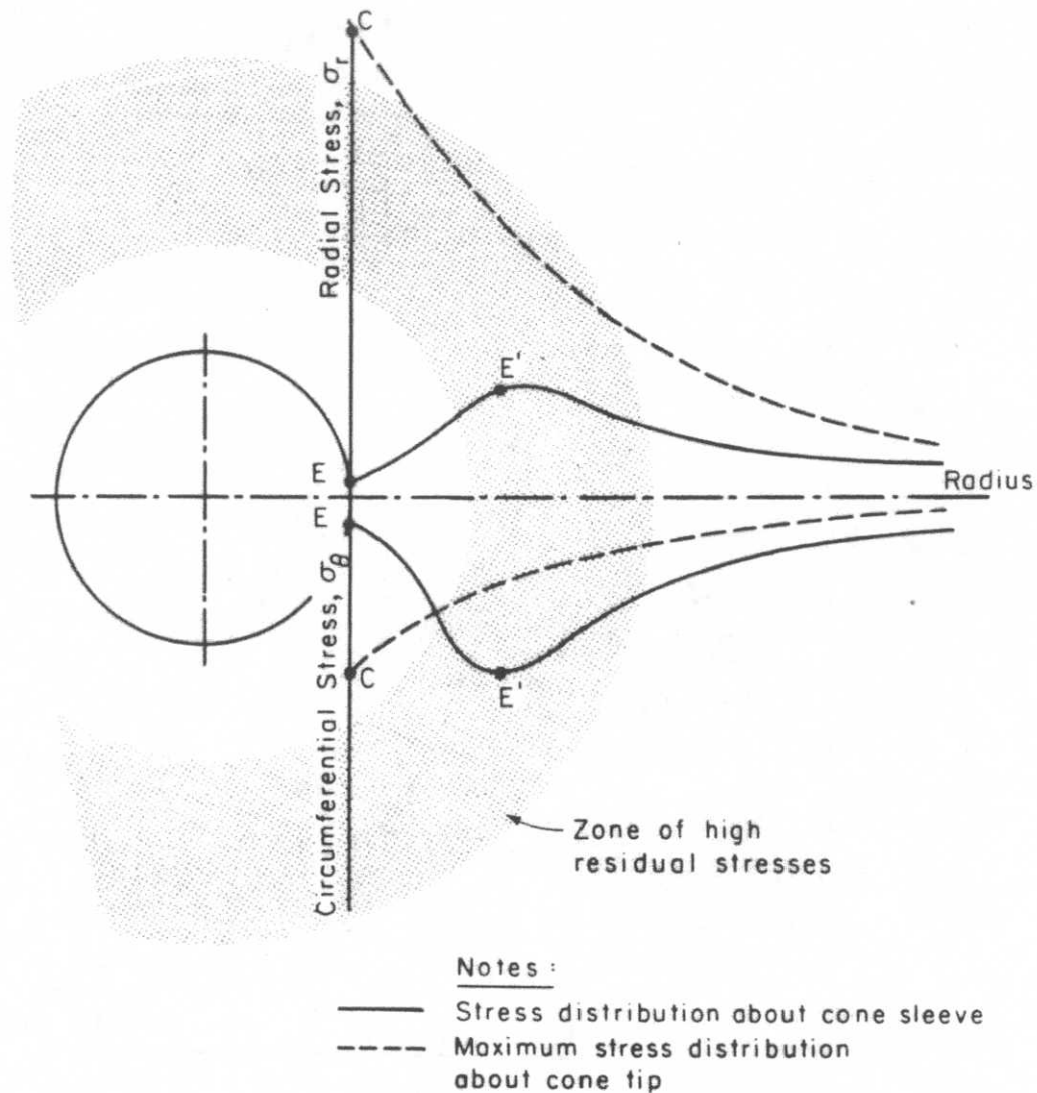


Figure 12 Stress field around a pushed cone penetration tip (Hughes and Robertson, 1985, reprinted, with permission, copyright NRC Research Press)

probe, some amount of unloading occurs, but to what extent? Is it repeatable? With both the self-boring and full displacement probes, the amount of displacement is known and repeatable, thus the initial condition is better known. Regardless of the method, the unload-reload cycle should be similar for all tests.

The last part of this study included a small field program to compare/contrast the full displacement pressuremeter with its self-boring equivalent. With respect to the lift

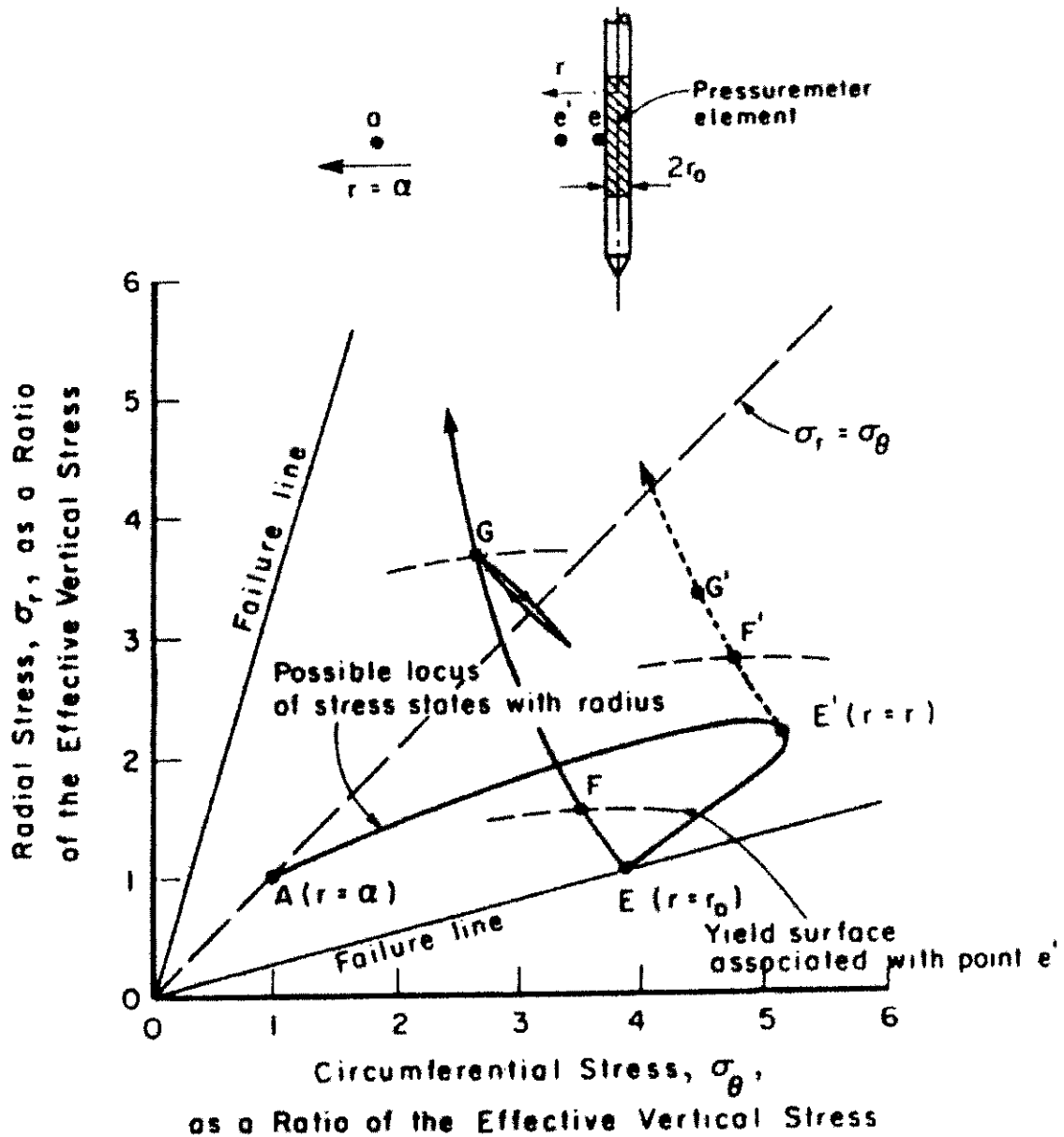


Figure 13 Stress path followed by a full displacement pressuremeter test after pushing (Hughes and Robertson 1985, reprinted, with permission, copyright NRC Research Press)

off pressures, although there was a good deal of scatter from both pressuremeters, the results seem to center somewhere around the assumed initial horizontal stress. Friction angles estimated based on the self-boring tests were reasonable. Application of the same method to determine friction angle in with the full displacement were incorrect, likely due to the very different stress paths the soil experiences *before* each test is run. And

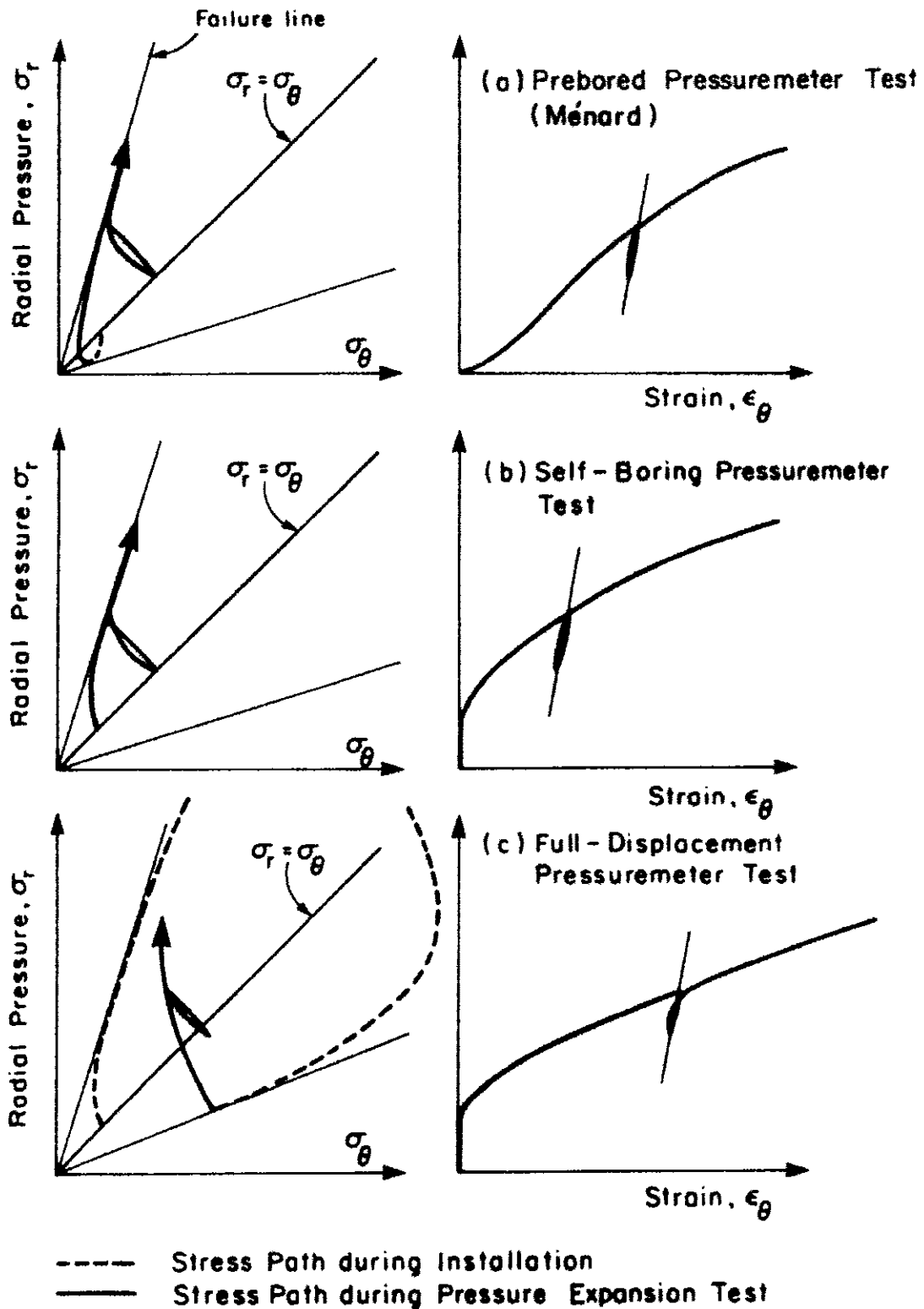


Figure 14 Comparative stress paths followed by each of the pressuremeter methods (Hughes and Robertson 1985, reprinted, with permission, copyright NRC Research Press)

finally, as expected, shear moduli based on unload/reload loops from both were very similar.

### Fugro Prototype Pressuremeters

#### General

By far the most investigated full displacement pressuremeters have been those produced in conjunction with Fugro. Work with this family of probes was conducted in house at Fugro, University of British Columbia, and at Oxford University. The first description of the cone pressuremeter appeared in work by Withers (Withers et al., 1986). The impetus for the development of this pressuremeter was primarily offshore testing. Pressuremeters on the market at the time were not suitable for all soil types and strengths. In addition, the tools were not robust enough to be used in such extreme conditions and often times needed precoring due to high embedment forces. As with the other probes discussed, the benefit of this tool would be an accurate measure of shear modulus without the unpredictable effects of stress relaxation and operator dependency. With that in mind, Fugro, set out to develop a commercial grade full displacement pressuremeter. Since this pressuremeter was intended for use with CPT equipment, it was thus called the cone pressuremeter.

#### Apparatus

The cone pressuremeter was constructed to the same diameter as a standard 15 cm<sup>2</sup> ( 2.33 in<sup>2</sup>) cone penetrometer. The volume measurement system included a Chinese lantern, internal membrane, and feeler gauges for measuring deformation changes. The membrane length is 450 mm (17.9 in) and the distance between the center of the membrane and the cone is 930 mm (36.6in). Circumferential strain is measured at the midpoint of the membrane at 3 locations 120° apart. The maximum probe pressure is 10

MPa (1450 psi) and the radial strain capacity is 50%. The prototype probe is inflated with nitrogen gas, with the production offshore model to be inflated with oil. Behind the pressuremeter is a module that amplifies the pressuremeter signals. CPT signals pass through on separate connections. Figure 15 shows the prototype Fugro cone pressuremeter.

### Test

Little detail was given as to the method of testing followed for the cone pressuremeter. Like the pavement pressuremeter, the cone pressuremeter test is strain controlled. Since this tool is used in conjunction with a traditional CPT, the probe is pushed to depth using a standard CPT rig. Tests are performed by inflating the monocellular probe with high pressure gas at carefully strain controlled intervals.

### Research

The first study of the prototype Fugro cone pressuremeter was conducted between the University of British Columbia and Fugro Holland (Withers et al., 1989). Twenty-five tests were performed at the McDonalds farm site as well as an additional six at Fugro's test site in Leidschendam, Holland. Being the first examination of the new pressuremeter, the authors went to great analytical length to use the test results to predict the friction angle or undrained strength. It was necessary to quantify the states of stress induced by the pressuremeter, so the authors presented a revised view of the stress path of soil around the pressuremeter probe. The stress paths and stress concentrations around a pushed and inflated probe are shown in Figure 16. Cylindrical and spherical cavity expansion and contraction models were attempted, but most over predicted the strength. On the other hand, as with the previously discussed probes, they found that the shear modulus compared very well with self-boring pressuremeter tests in the same place.

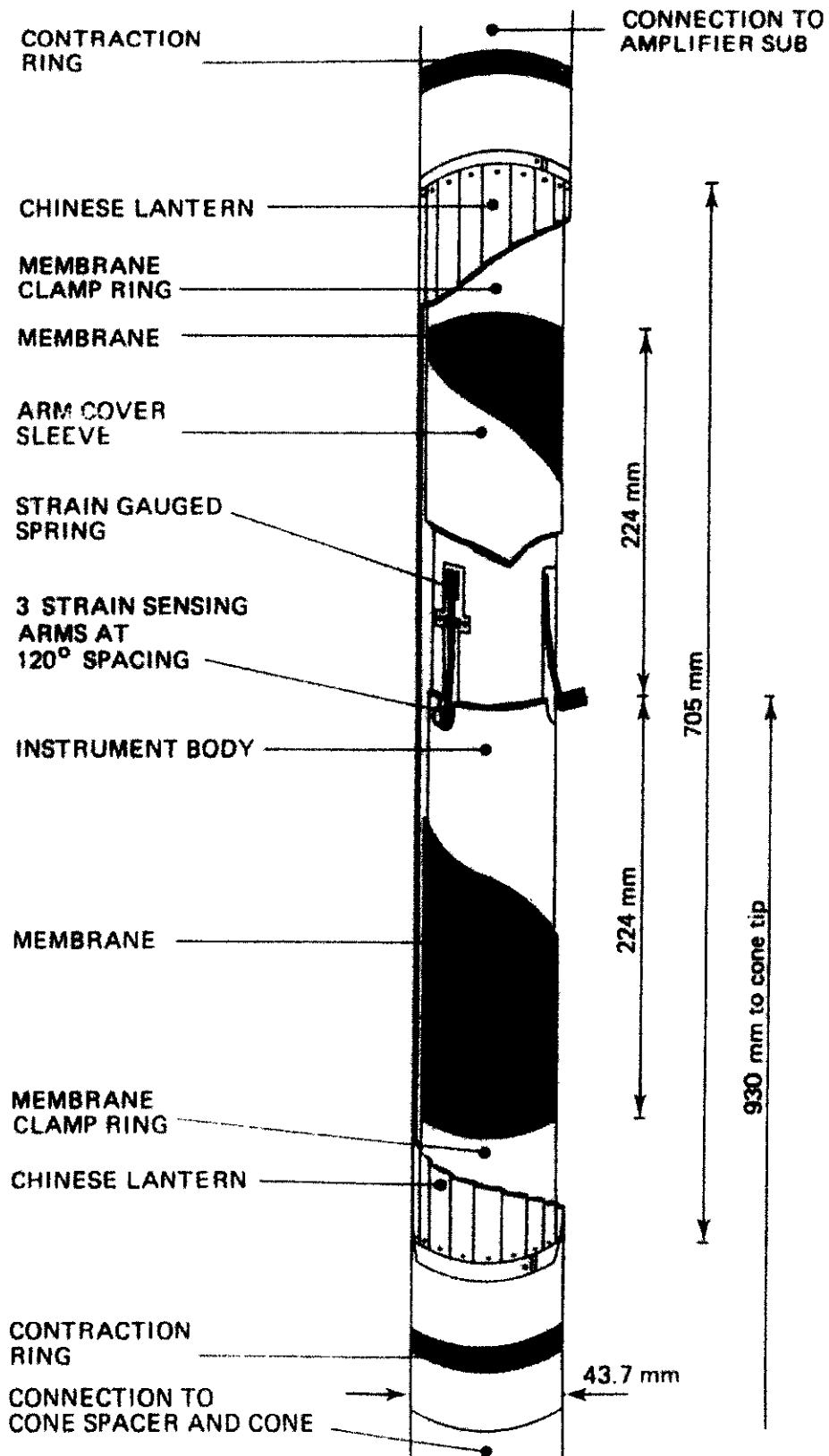


Figure 15 Fugro cone pressuremeter (Withers, et al., 1986, reprinted, with permission, copyright ASTM)

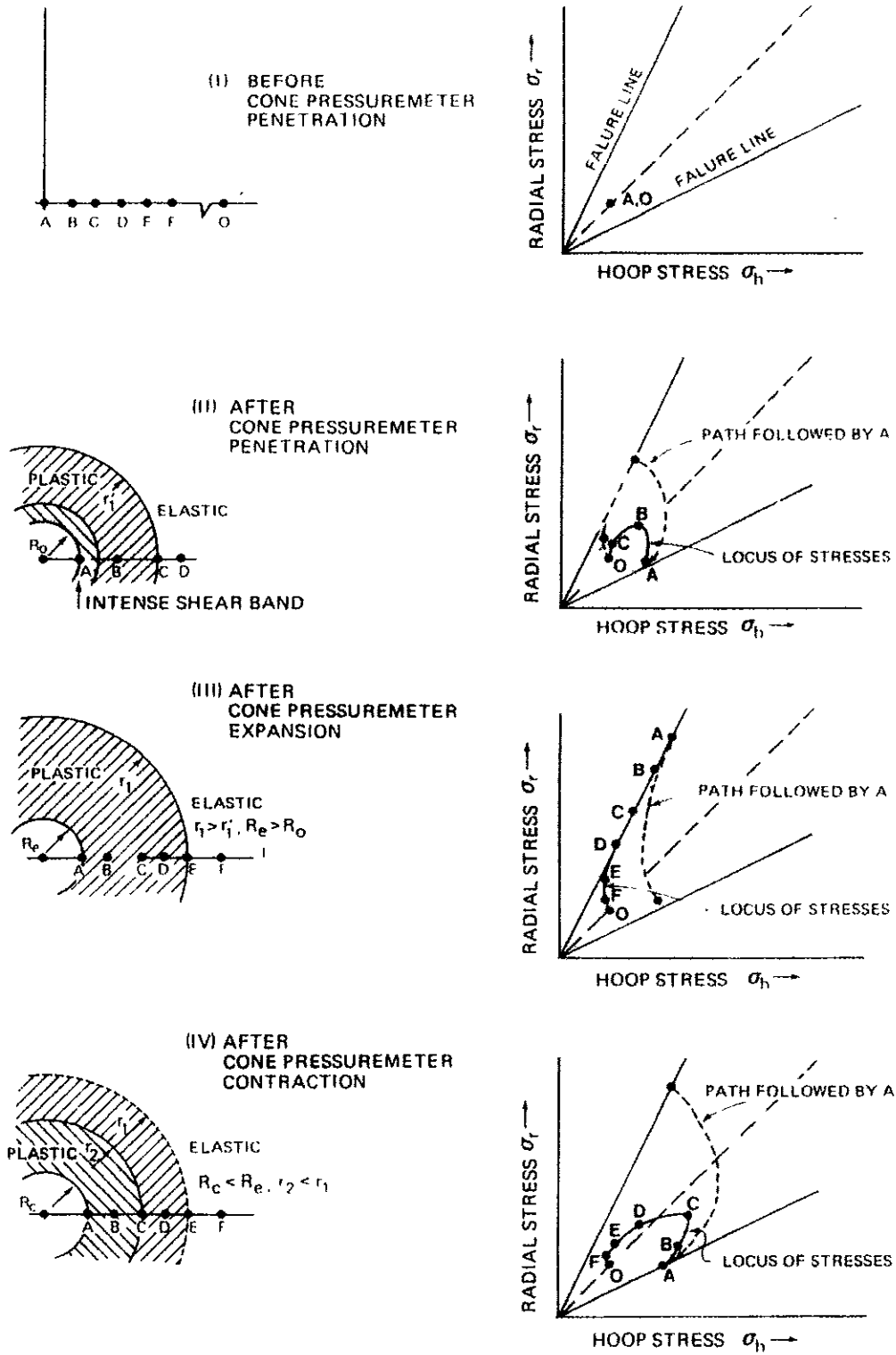


Figure 16 Stress paths and stress concentrations during a cone pressuremeter test (Withers et al., 1989, reprinted, courtesy of Thomas Telford Ltd, London)

The most recent, and perhaps most extensive, research with the cone pressuremeter has been by Guy Houlsby and his students at Oxford University. For their studies, Fugro constructed two additional smaller scale pressuremeters. One probe was a  $10 \text{ cm}^2$  ( $1.55 \text{ in}^2$ ) version that included a volumetric measurement system in addition to feeler gauges. The other tool was a  $5 \text{ cm}^2$  ( $0.775 \text{ in}^2$ ) version. Due to size limitations, deformations were only monitored volumetrically.

An early attempt to model the cone pressuremeter using FEM was done by Houlsby and Yu (1990). The soil was represented by the Mohr-Coulomb constitutive model with two-noded elements with nonlinear displacement functions to create a simple cavity expansion mesh to create a right cylindrical model. Limit pressures calculated agreed well with those measured during calibration chamber tests. A second method was used to estimate friction angle using the plastic unloading slope. This yielded poor results.

The research project at Oxford was primarily undertaken to calibrate the cone pressuremeter much like the cone penetrometer and flat dilatometer were previously. During the course of the study, it was determined that the size of the calibration chamber had a significant effect on the results (Schnaid and Houlsby, 1991). Although there was only one chamber (Figure 17) used in the experiment, there were visible trends in limit pressure, stiffness, and inferred friction angle in relation to the ratio of chamber to probe diameter. Size effects seem to become more prominent as soil density increases.

Knowing the limitations of the chamber, a program consisting of 34 cone pressuremeter tests was performed in the calibration chamber (Schnaid and Houlsby, 1992). The  $10 \text{ cm}^2$  probe was used as the primary testing tool with which 21 tests were completed. There were an additional 5 tests with the  $15 \text{ cm}^2$  tool and 8 with the  $5 \text{ cm}^2$ .

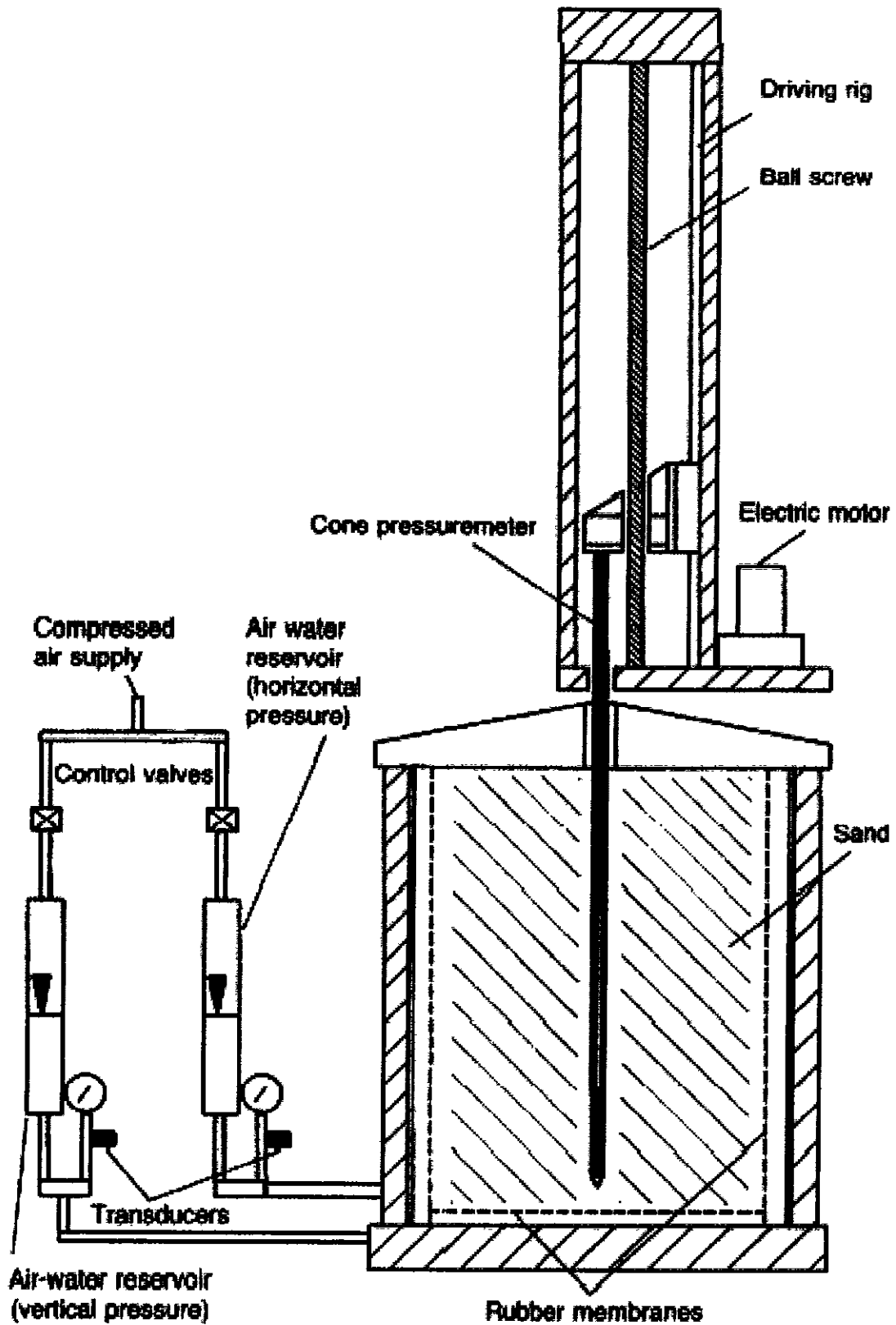


Figure 17 Cone pressuremeter calibration chamber setup at Oxford (Schnaid and Houlby, 1992, reprinted, courtesy of Thomas Telford Ltd, London)

Since tests with the cone pressuremeter have shown that the cone resistance and limit pressure depend primarily on the effective horizontal stress and not the vertical stress, the testing program varied such parameters as the density,  $K_0$ , vertical and horizontal stress.

Analysis of the calibration chamber tests showed almost unique correlations between  $q_c$  and  $\sigma_h'$  and  $\psi_l$  and  $\sigma_h'$ . In light of these findings, the authors define a term called the cone resistance-limit pressure ratio.

$$\text{Cone resistance-limit pressure ratio} = \frac{(q_c - \sigma_h')}{(\psi_l - \sigma_h')}$$

where  $q_c$  is tip resistance,  $\psi_l$  is the limit pressure, and  $\sigma_h'$  is, of course, the horizontal effective stress. Based on this ratio, the friction angle and relative density can be estimated.

$$\phi = 1.45 \frac{(q_c - \sigma_h')}{(\psi_l - \sigma_h')} + 26.5$$

$$R_d = 9.0 \frac{(q_c - \sigma_h')}{(\psi_l - \sigma_h')} - 30$$

This is shown graphically in Figure 18.

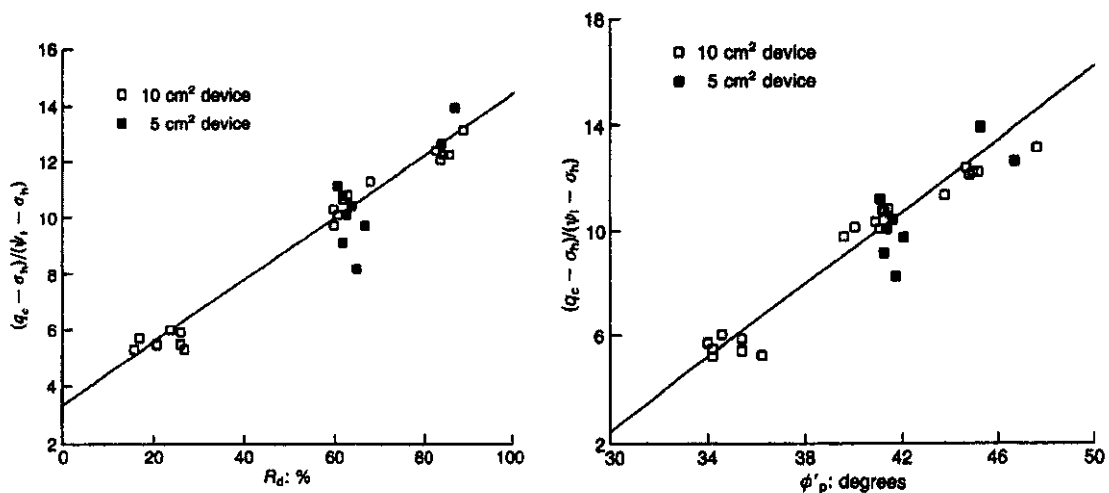


Figure 18 Relative density and friction angle based on calibration chamber tests (Schnaid and Houlsby, 1992, reprinted, courtesy of Thomas Telford Ltd, London)

The last portion of the published research concerned the interpretation of shear moduli (Houlsby and Schnaid, 1994). Unload-reload loops from the calibration tests were analyzed. One of the primary findings was that there was no appreciable difference in the use of feeler gauge measurements or volumetric measurements when calculating the shear modulus. Furthermore, it was discovered that calculating the modulus using the two external points of a loop, the apexes, systematically produced a higher value for modulus than performing a least squares regression of all points in the loop.

Houlsby and Schnaid (1994) used a method proposed by Fahey and Jewel (1990) for calibration of the Fugro pressuremeter shear modulus for system compliance. The membrane stiffness correction is carried out as before. On the other hand, the volume loss correction is applied differently. Instead of just inflating the probe in a steel pipe and noting the volume, unload-reload loops were performed at ascending increments of cell pressure. These loops were used to derive the unload-reload shear modulus for the system. The shear modulus of the soil could then be estimated by first correcting the raw curve for membrane stiffness and hydrostatic pressure only. Then, the unload-reload shear modulus is calculated at the desired point on the curve. Next, the unload-reload shear modulus of the system is calculated. Finally, the unload-reload shear modulus of the soil can be determined using this equation:

$$\frac{1}{G_{corrected}} = \frac{1}{G_{measured}} - \frac{1}{G_{system}}$$

### Finite Element Software

#### Plaxis

Two finite element codes were used in the course of this research. The first code, Plaxis, was chosen due to its commercial availability and ease of use. Development of

Plaxis began in 1987 at the Technological University of Delft (Plaxis, 1998). Initially, the code was developed to analyze river embankments over soft soils of Dutch lowlands. With further development, Plaxis has been extended for use in most geotechnical problems. Version 7.2 is capable of modeling static plane strain or two-dimensional axisymmetric problems using 6 or 15 node triangular soil elements. In addition, special elements are available for modeling tunnels, beams, anchors, geotextiles, and soil-structure interfaces. Plaxis utilizes several constitutive models for soils including linear elastic, Mohr-Coulomb, soft soil (clay), and hardening soil (hyperbolic sand).

The true advantage to using Plaxis lies in its user friendliness. The input pre-processor and output post-processor are completely functional. Inputting the problem geometry is done easily with cad-like drawing tools. Material properties and boundary conditions are easily assigned using dialogue boxes and a simple mouse click or drag and drop. Figure 19 shows the Plaxis pre-processor window.

Once the geometry, material properties, and boundary conditions are set, the next step is mesh generation. Choosing the mesh generation tool in Plaxis will fill each of the delineated polygon areas of the model with triangular finite elements. The elements will be placed in the mesh such that nodal points will correspond with cluster interfaces, boundary conditions, and external loads. It is also possible to degrade the entire mesh or refine the mesh around individual features such as nodes, lines, or clusters of elements. An example showing a complex mesh of finite elements is shown in Figure 20.

After the mesh generation is complete, the next step in the problem is to define initial conditions. Plaxis has implemented a module that allows for the specification of initial pore pressure and flow conditions, staged construction steps, and initial linear

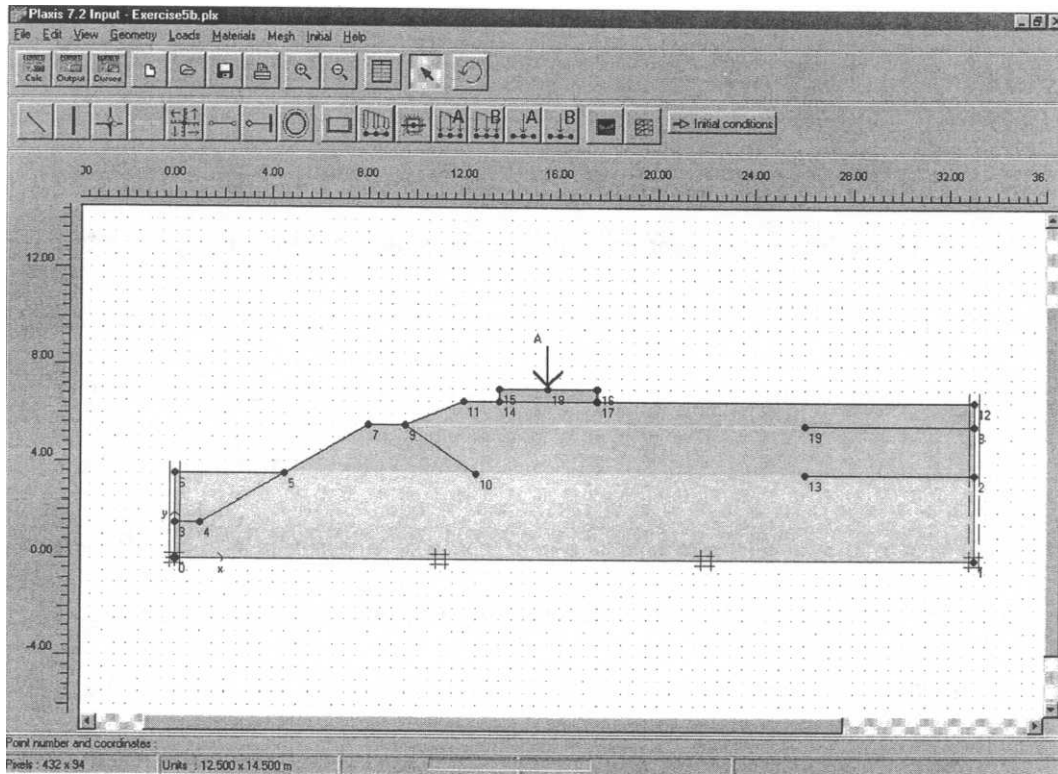


Figure 19 View of Plaxis input interface

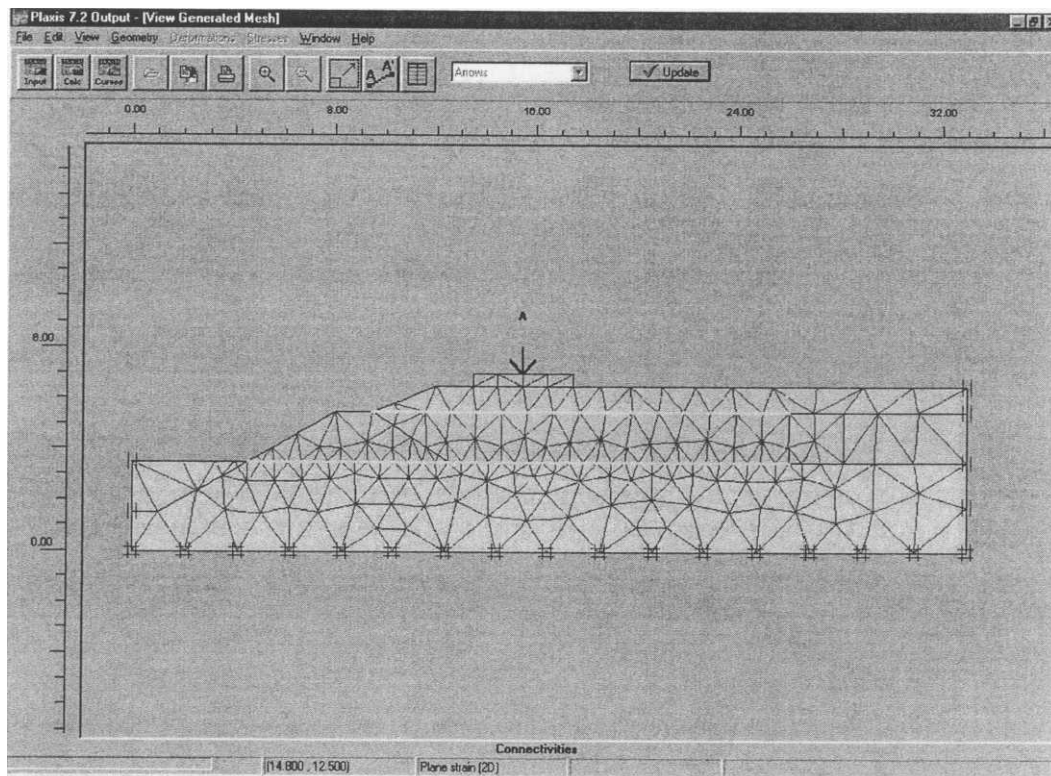


Figure 20 Plaxis automatic mesh generation

elastic stress calculations. Again, all of the options are easily input with dialogue boxes and mouse clicks.

The main engine portion of the code is referred to as Plaxis Calculations. This module allows the user to set up multiple chronological loading, excavation, or consolidation events. If the problem is a simple loading, then the user would simply enter the load multiplier and the program would automatically step the load up to calculate the deformations. For fill/excavation problems, the loading events can be edited graphically by again clicking on and/or off clusters of elements. There is a time interval input for use in consolidation analyses. Finally, the user is encouraged by the engine to select a “watch point” that will be monitored during the calculation. The movement and force at this point are monitored so the user can get visual feedback on the progress of the analysis. Figure 21 shows the main engine window with time stepping and load multipliers.

The output of a Plaxis analysis can be viewed with one of two output post-processors. The first is called Plaxis Output. This program reads the output stresses and deformations from the analysis and plots the results over the original mesh for a single loading event. The data can be plotted as contours, shadings, or vectors. Plaxis Output also has scaling, zooming, and printing capabilities. An example plot of vector displacements can be seen in Figure 22.

The second post-processor is called Plaxis Curves. This program allows for the plotting of monitored variables through the entire analysis. For example, one might choose the toe point of a dam, or the top of a retaining wall. The movement of that point can be plotted against the loading multiplier imposed on the model. Pore pressure in a consolidation model can be plotted against time for such a point. Additionally, stress

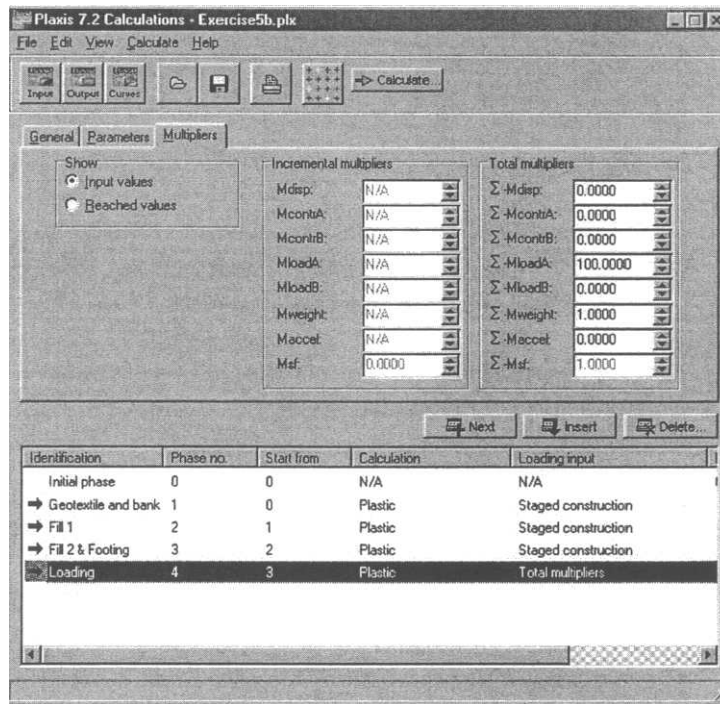


Figure 21 Plaxis Calculation engine window

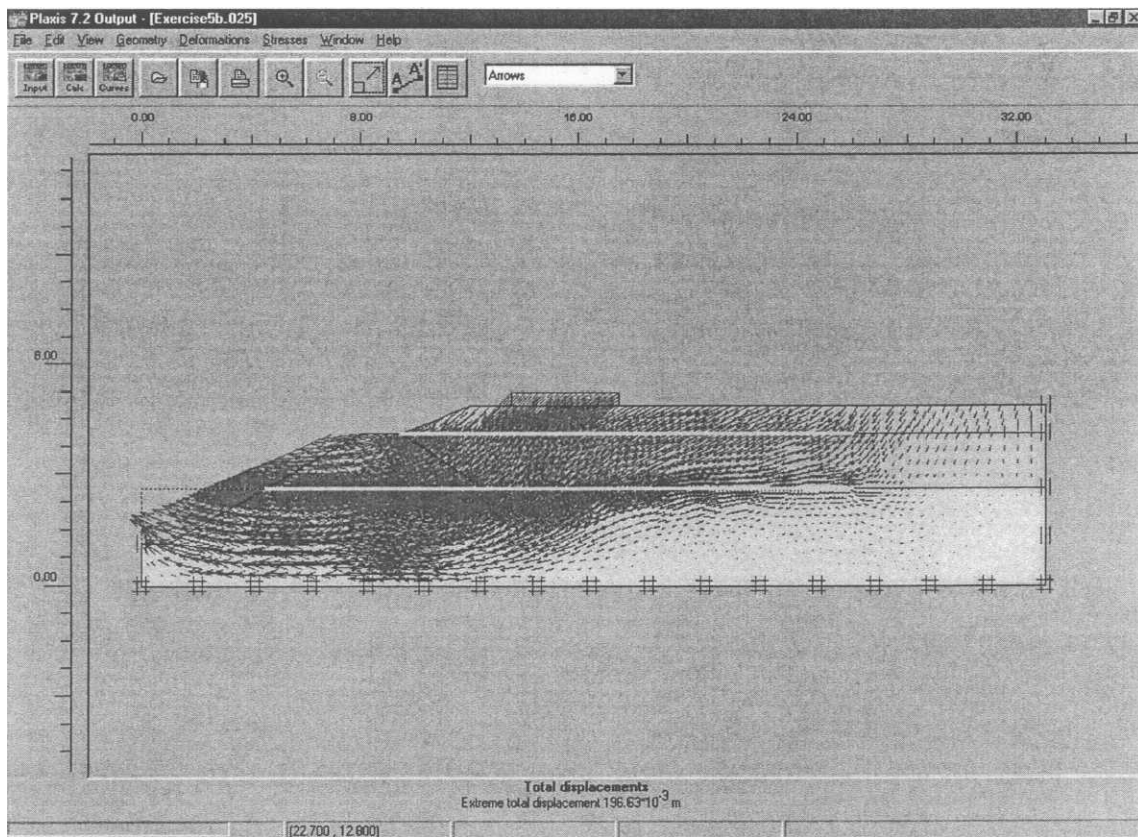


Figure 22 Plaxis Output example

strain points can be chosen, and a plot of the stress and strain at that gauss point can be plotted.

### PlasFEM

PlasFEM (Pinto, 1998) was the second finite element code used in this research. It is currently under development at the University of Florida by Dr. Michael McVay. The program is well suited to handle most geotechnical problems and is capable of dynamic analysis of dry or saturated soil in 1D, 2D or 3D with elements ranging from simple 2 node truss elements to 27 node bricks. Being primarily a research tool, the code is extremely versatile. The user can impose very complex loading conditions, initial stresses, and boundary conditions. Constitutive models available include: linear elastic, Drucker-Prager, Sandler-Dimaggio, Cam Clay and Modified Cam Clay, viscoplasticity, and a Mohr-Coulomb interface formulation.

Stresses and deformations can be visualized with the post-processor called PlasPLOT. In a similar manner to Plaxis Output, the stresses and deformations data can be represented by different levels of shading. The deformed mesh can also be plotted with or without a magnification factor. As with Plaxis Output, the resulting plots can be scaled, zoomed or printed. Figure 23 shows an example PlasPLOT session showing four screens with undeformed mesh, vertical effective stress, pore pressures, and deformed mesh.

A pre-processor for PlasFEM called PlasGEN is under development by the University of Florida Geotechnical Numerical Group. Figure 24 shows a sample of the current development version of PlasGEN. Features of this new module will include cad-like geometry definition and an automatic mesh generator. Loading events will be defined in the pre-processor, and material properties and boundary conditions will be

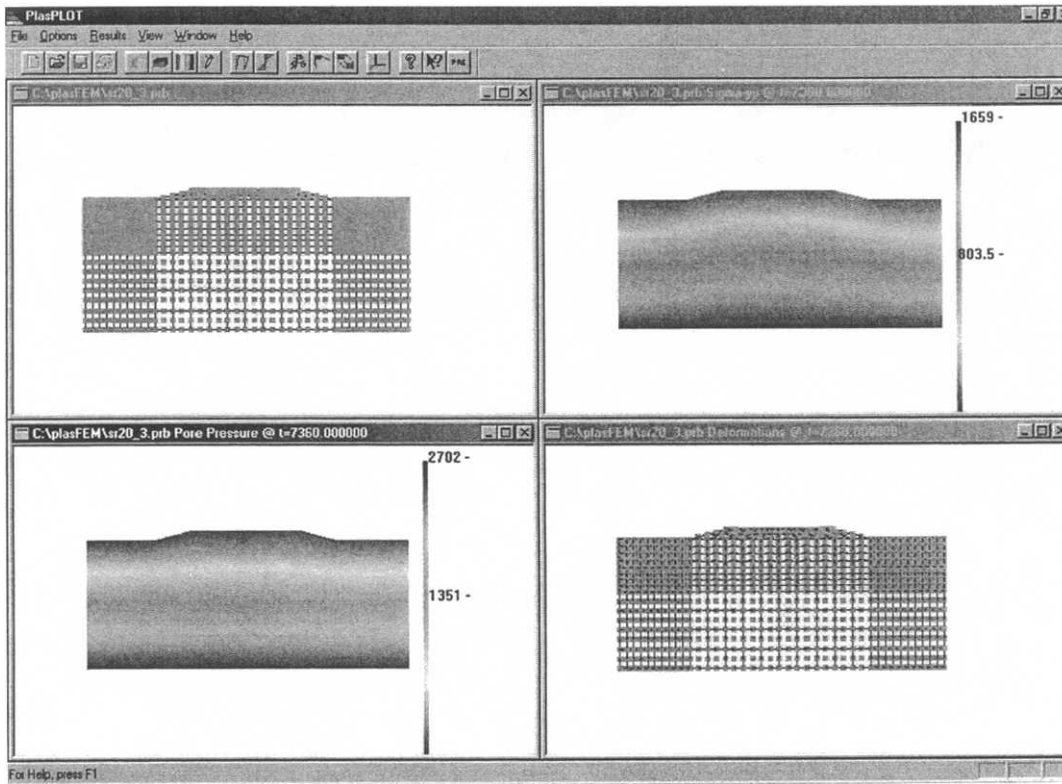


Figure 23 PlasPLOT example output

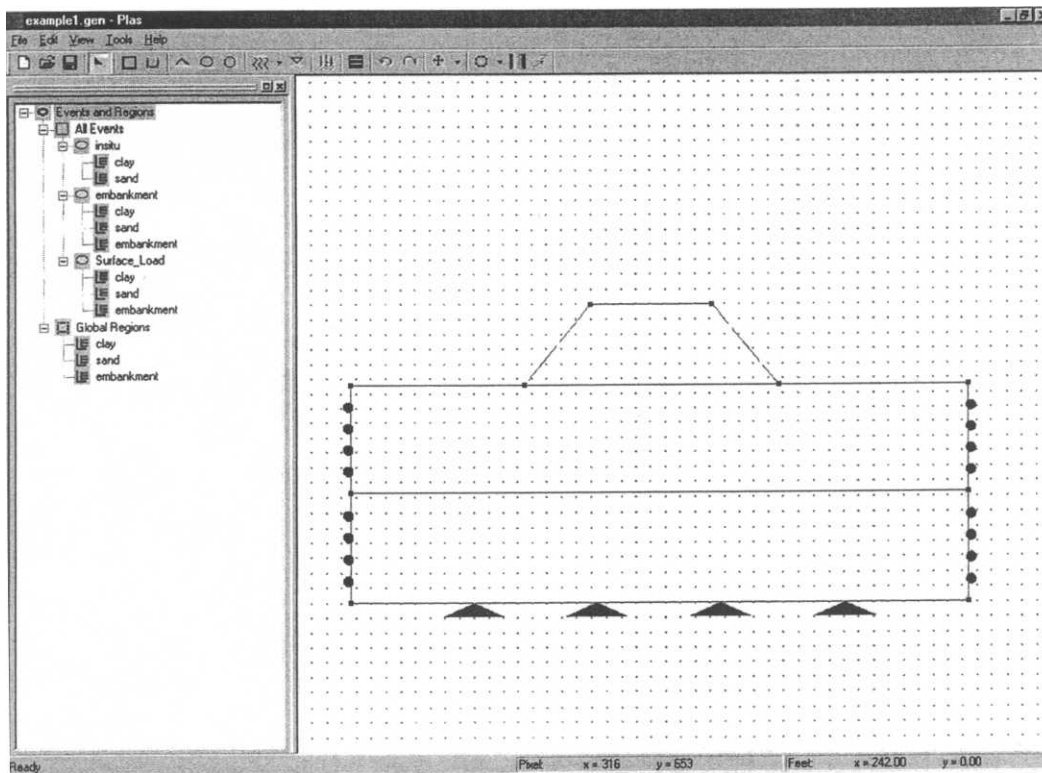


Figure 24 An embankment model in the pre-release version of PlasGEN

specific to loading events, not global to the problem. Until PlasGEN's full capabilities are realized, PlasFEM input files must be prepared by hand in ASCII format. Meshes can easily be implemented on a spreadsheet, but small alterations of a complex problem often require a complete remeshing.

## CHAPTER 3 CONSTITUTIVE MODELING

Finite element programs allow the user to determine stresses or deformations in a soil continuum that is subject to events such as external loadings, prescribed displacements, or cuts and fills. Therefore, the relationship between stress and strain is of the utmost importance to the program. In the simplest case, it could be said that there is a linear relationship between stress and strain. This is known as Hooke's Law.

$$\sigma = E\varepsilon$$

This relationship is ideal, and may work for some materials, but soils do not often follow this model. Soil is heterogeneous, exhibits non-linear stress strain behavior, has a strength limit, and is sensitive to water moving through its pores. Therefore such a simple representation is not sufficient.

With that in mind, many researchers have attempted to emulate the behavior of soil by way of constitutive models. So, instead of the simple "E" in Hooke's Law, more complex mathematical formulations have been developed. Now instead of a constant stiffness, the stiffness may change as the sample is strained in shear or hydrostatically. In order to track these changes and impose limits such as failure surfaces or yield surfaces, a convenient representation for stresses is necessary.

It is worth noting at this juncture that all finite element programs contain a basic linear-elastic model. This model is often an appropriate choice for preliminary analyses or cases where very little soil information is available, whether the material is cohesive or cohesionless.

## Constitutive Models for Cohesionless Soil

Although both of the finite element codes contain many constitutive models, specific models are more appropriate for sandy soils. The following is a brief discussion of the models that were used in this research.

### Plaxis

Plaxis contains two constitutive models that are appropriate for cohesionless soils.

### Mohr-Coulomb

By far the most familiar is the Mohr-Coulomb model (Plaxis, 1998). This relationship is the same that is used in common everyday soil mechanics, just expanded to three dimensions. Figure 25 shows the Mohr-Coulomb failure surface in principal stress space.

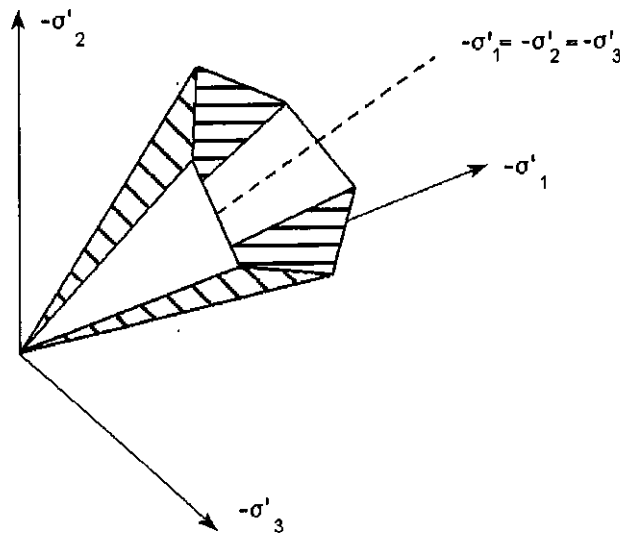


Figure 25 Mohr-Coulomb failure surface (Plaxis, 1998)

The failure surface, in this case, is directional, meaning that it depends on the type of loading (i.e. triaxial compression, triaxial extension, etc.). The equations for the failure surface are the following:

$$f_1 = \frac{1}{2}|\sigma_2' - \sigma_3'| + \frac{1}{2}(\sigma_2' + \sigma_3') \sin \phi - c \cos \phi \leq 0$$

$$f_2 = \frac{1}{2}|\sigma_3' - \sigma_1'| + \frac{1}{2}(\sigma_3' + \sigma_1') \sin \phi - c \cos \phi \leq 0$$

$$f_3 = \frac{1}{2}|\sigma_1' - \sigma_2'| + \frac{1}{2}(\sigma_1' + \sigma_2') \sin \phi - c \cos \phi \leq 0$$

After the stresses exceed these limits, the material will yield in a perfectly plastic manner as idealized in Figure 26.

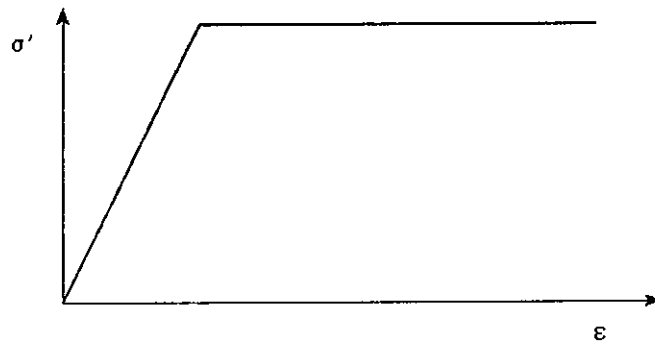


Figure 26 An elastic perfectly plastic stress strain curve

The basic parameters necessary to define the Mohr-Coulomb model are the following:

#### Failure Surface

$\phi$	Friction Angle
$c$	cohesion
$\psi$	Dilation Angle

#### Stiffness

$E$	Young's Modulus
$\nu$	Poisson's Ratio

#### Initial Stresses

$\rho$	unit weight
$K_0$	ratio of initial horizontal stress / initial vertical stress

#### Hardening soil

Although it would seemingly be easy to assume that soil behaves as in the Mohr-Coulomb model, sands are often more complex. A triaxial test on sand will likely not

appear as the elastic perfectly plastic curve in Figure 26. More likely, during shear, the stiffness of the sand specimen will decrease. In order to emulate this behavior, the hardening soil model has been implemented in Plaxis. The hardening soil (Plaxis, 1998) model utilizes the same failure surface as the Mohr-Coulomb. A hyperbolic function provides the relationship between the vertical strain and deviatoric stress. As with the Mohr-Coulomb model, when the state of stress reaches the failure surface, perfectly plastic strains occur.

In addition to the hyperbolic stress strain relationship, the hardening soil model includes a hardening cap. When a cohesionless material is loaded in isotropic compression, the material will likely not continually strain elastically as the Mohr-Coulomb model would imply. In fact, plastic volumetric strains will occur. In order to describe these strains, a hardening cap was formulated. Figures 27 and 28 show the hardening soil model with its cap in both p-q and principal stress space.

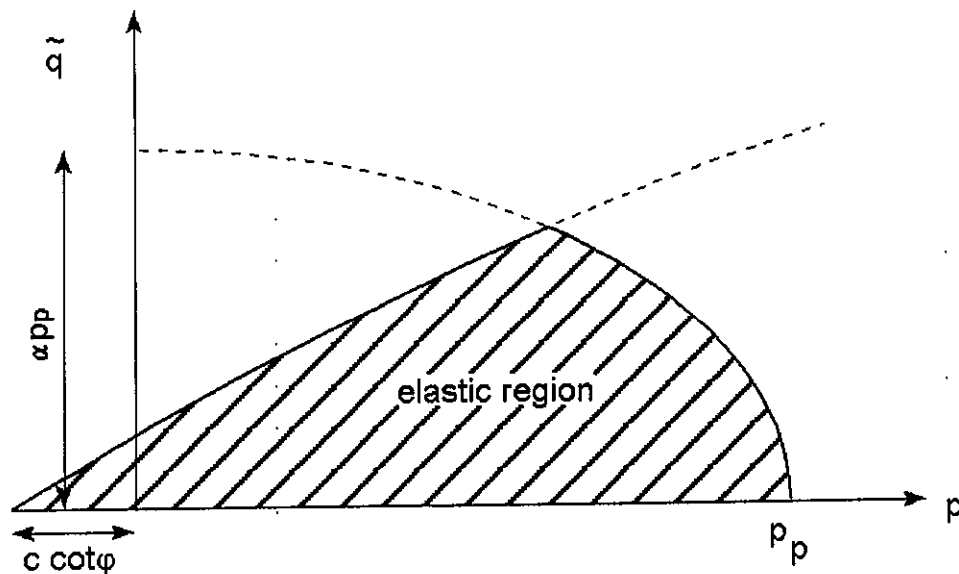


Figure 27 Hardening soil model with cap in p-q space (Plaxis 1998)

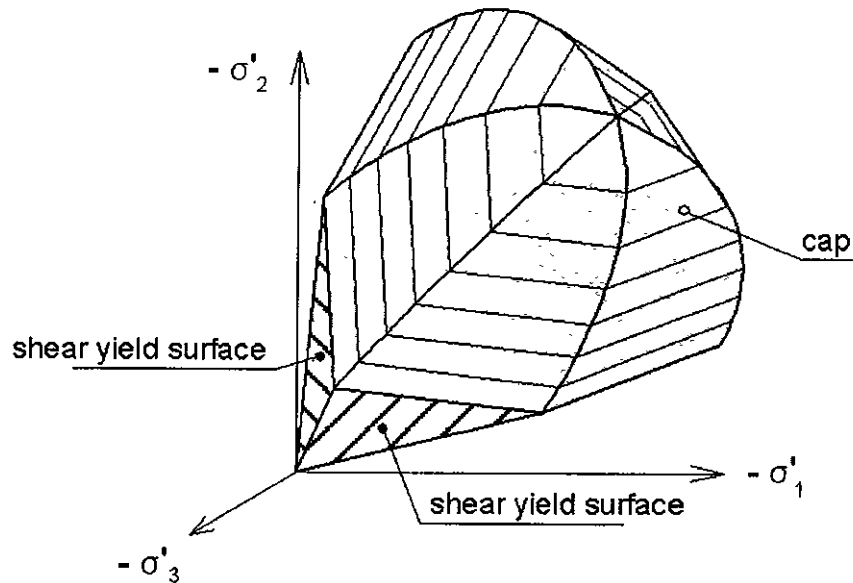


Figure 28 Hardening soil model with cap in principal stress space, (Plaxis 1998)

The basic parameters for the hardening soil model are as follows:

Failure Surface remains the same as before:

- $\phi$  Friction Angle
- $c$  cohesion
- $\psi$  Dilation Angle

Hyperbolic Stiffness Parameters

- $E_{50}^{ref}$  **Secant** stiffness in standard triaxial test at  $p_{ref}$
- $E_{oed}^{ref}$  **Tangent** Stiffness for primary oedometer loading at  $p_{ref}$
- $m$  Power for stress level dependency of stiffness
- $E_{ur}^{ref}$  Unloading/reloading stiffness
- $\nu_{ur}$  Poisson's Ratio for unloading-reloading
- $p^{ref}$  Reference Stress for stiffness
- $R_f$  Failure ratio
- $\sigma_{tension}$  Tension Cutoff
- $c_{increment}$  Incremental increase of cohesion with depth
- $K_0^{nc}$   $\sigma'_{xx} / \sigma'_{yy}$  stress ratio in a state of normal consolidation

Initial Stresses as before

- $\rho$  unit weight
- $K_0$  ratio of initial horizontal stress / initial vertical stress

POP Preconsolidation Pressure or  
OCR Overconsolidation Ratio

## PlasFEM

Similar to Plaxis, PlasFEM contains two constitutive models that can be used to represent sand.

### Drucker-Prager

The Drucker-Prager (1952) model is very similar to the Mohr-Coulomb model employed by Plaxis. The stresses are limited by a simple two parameter failure surface. Underneath, any strains are elastic. If the stresses reach the failure surface, shown in Figure 29, any further strains will be perfectly plastic.

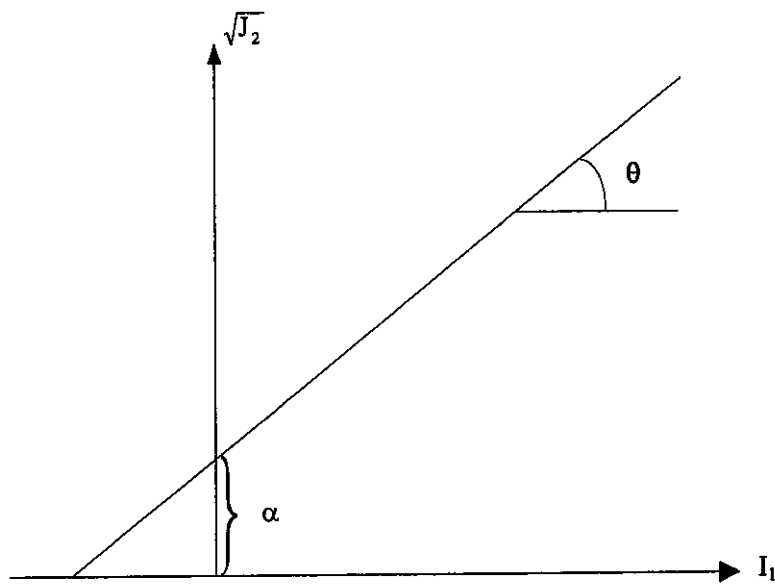


Figure 29 Drucker-Prager failure surface in invariant stress space (Pinto 1998)

The Drucker-Prager failure surface is a cone centered around the hydrostatic axis in invariant stress space. It can be expressed by the equation:

$$f = \sqrt{J_2} - \alpha - I_1 \theta = 0$$

This relationship differs from the Mohr-Coulomb in that it is not dependent on the type of loading. Figure 30 shows both models plotted in principal stress space oriented to the  $\pi$  plane.

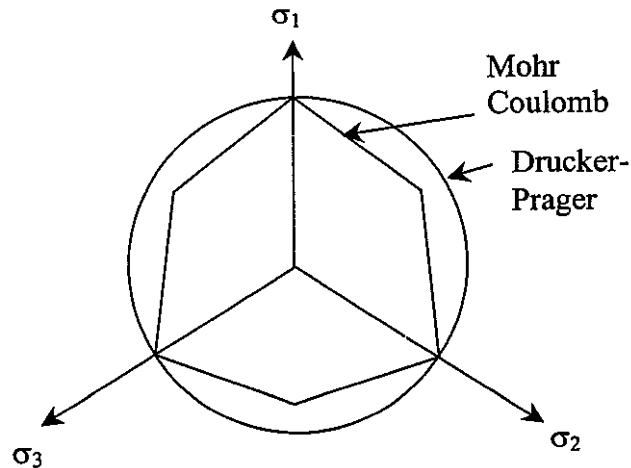


Figure 30 Mohr-Coulomb and Drucker-Prager failure surfaces viewed in the  $\pi$  plane

The parameters for the Drucker-Prager model are listed below:

#### Failure Surface

- $\alpha$  strength intercept (similar to cohesion)
- $\theta$  strength parameter (similar to friction angle)

#### Stiffness Parameters:

- $E$  Young's Modulus
- $\nu$  Poisson's Ratio

#### Initial Stresses

- $\rho$  unit weight
- $\sigma_0$  initial vertical stress in elements
- $K_0$  ratio of initial horizontal stress / initial vertical stress

#### Sandler-Dimaggio

Just as in Plaxis, PlasFEM includes a model for cohesionless materials that includes a hardening cap. The Sandler-Dimaggio (1971) model contains a failure surface that is an advanced curved version of the Drucker-Prager, as well as a hardening cap.

Unlike the hardening soil model, strains remain linear elastic until the stresses reach the failure surface or yielding cap. Figure 31 shows the Sandler-Dimaggio constitutive model.

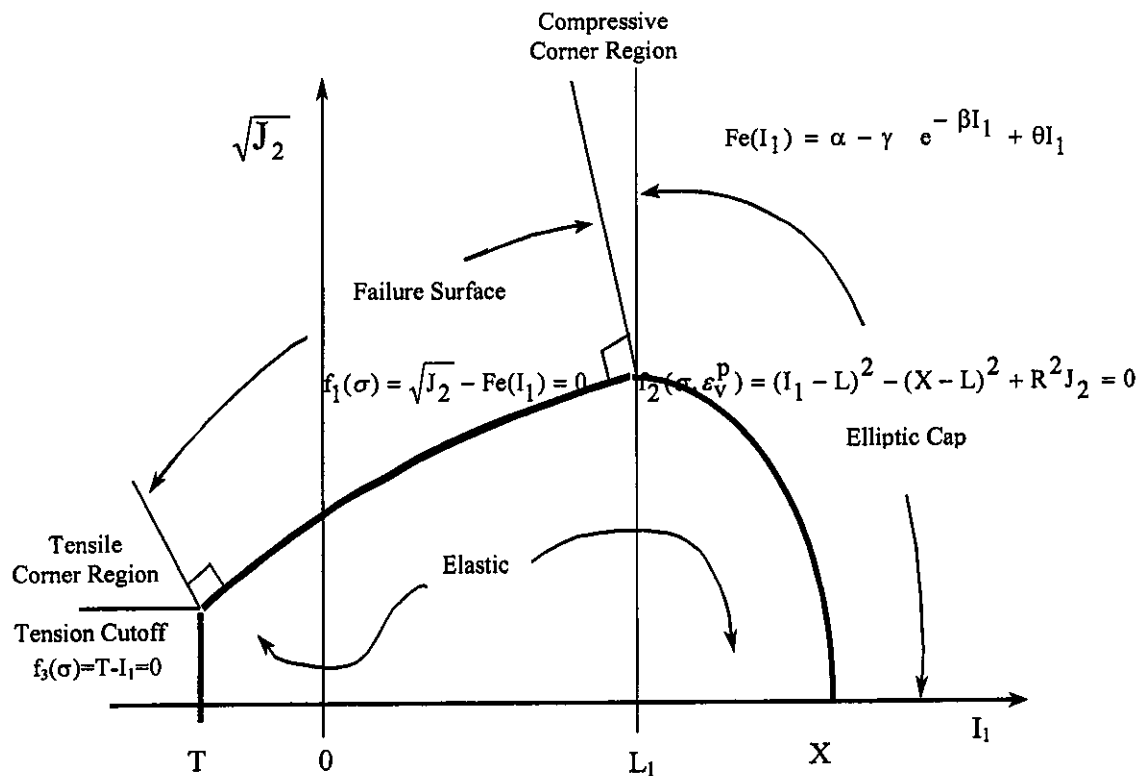


Figure 31 Sandler-Dimaggio cap model (Pinto 1998)

The parameters necessary to defined the Sandler-Dimaggio model are the following:

#### Failure Surface

- $\alpha$  strength intercept (similar to cohesion)
- $\theta$  strength parameter (similar to friction angle)
- $\gamma$  strength parameter (curvature)
- $\beta$  strength parameter (curvature)
- T tension cutoff stress

#### Stiffness

- E Initial Young's Modulus
- $\nu$  Poisson's Ratio

### Hardening Cap

X0 preconsolidation pressure

W cap parameter ( $\epsilon_v^p$  max)

R cap parameter (ellipticity)

D cap parameter (hardening)

### Initial Stresses

$\rho$  unit weight

$\sigma_0$  initial vertical stress in elements

$K_0$  ratio of initial horizontal stress initial vertical stress

## Constitutive Models for Cohesive Soil

In addition to the models for cohesionless soil, there are appropriate models in both programs for cohesive soils. In the case of both Plaxis and PlasFEM, the appropriate models are based partly or wholly on the original Cam Clay model developed by Roscoe and Burland (1968).

### Plaxis

The soft soil model is used in Plaxis. Figure 32 shows the soft soil model yield surface.

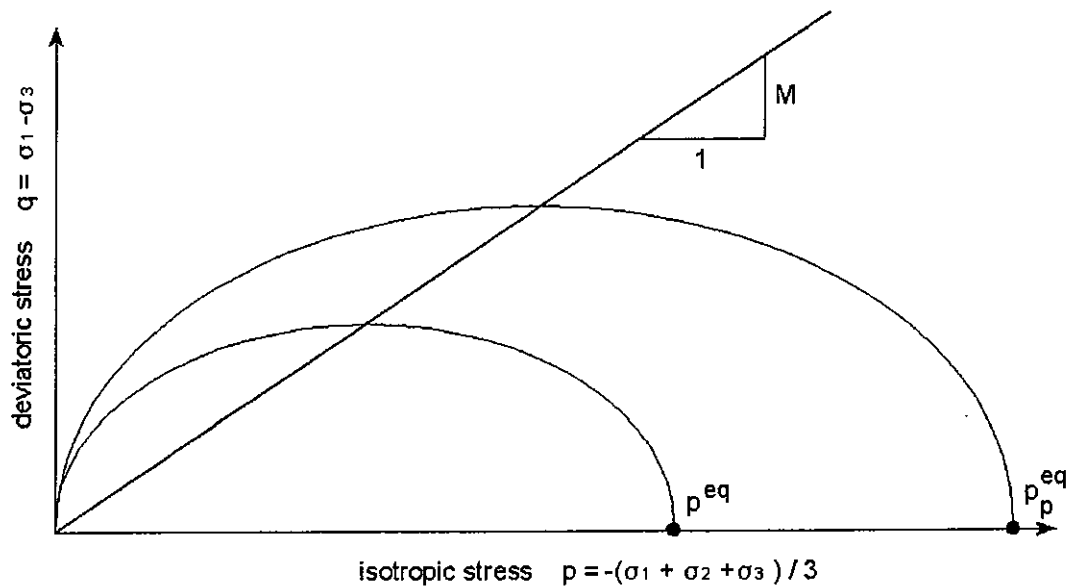


Figure 32 Diagram of  $p^{eq}$ -ellipse in a p-q-plane

The model is defined using multiple soil parameters. As with all Plaxis models, there is a Mohr-Coulomb failure surface. The stiffness and plasticity parameters are then defined similar to those used in the Cam Clay formulation. The parameters are:

Failure surface:

- c Cohesion
- $\varphi$  Friction angle
- $\psi$  Dilatancy angle

Basic stiffness parameters:

- $\kappa^*$  Modified swelling index
- $\lambda^*$  Modified compression index
- $\mu^*$  Modified creep index

Initial Stresses

- $\rho$  unit weight
- $\sigma_0$  initial vertical stress in elements
- $K_0$  ratio of initial horizontal stress / initial vertical stress

Advanced parameters

- $K_0^{nc}$   $\sigma'_{xx} / \sigma'_{yy}$  stress ratio in a state of normal consolidation
- M Slope of the Critical State Line
- $v_{ur}$  Poisson's ratio for unloading-reloading (default 0.15)

### PlasFEM

The Cam Clay model is coded into PlasFEM. While somewhat similar to the soft soil model in Plaxis, the following are the parameters necessary to define the model:

Stiffness and Plasticity

- K bulk modulus
- $\nu$  Poisson's Ratio
- $e_0$  Initial Void Ratio
- M critical state slope
- $\kappa$  recompression / swell index
- $\lambda$  compression index
- $p_{c0}$  preconsolidation pressure

Initial Stresses

- $\rho$  unit weight
- $\sigma_0$  initial vertical stress in elements

$k_0$  ratio of initial horizontal stress initial vertical stress

Figure 33 shows the Cam Clay yield surface in p-q space. Notice the similarity to the Soft Soil model from Plaxis.

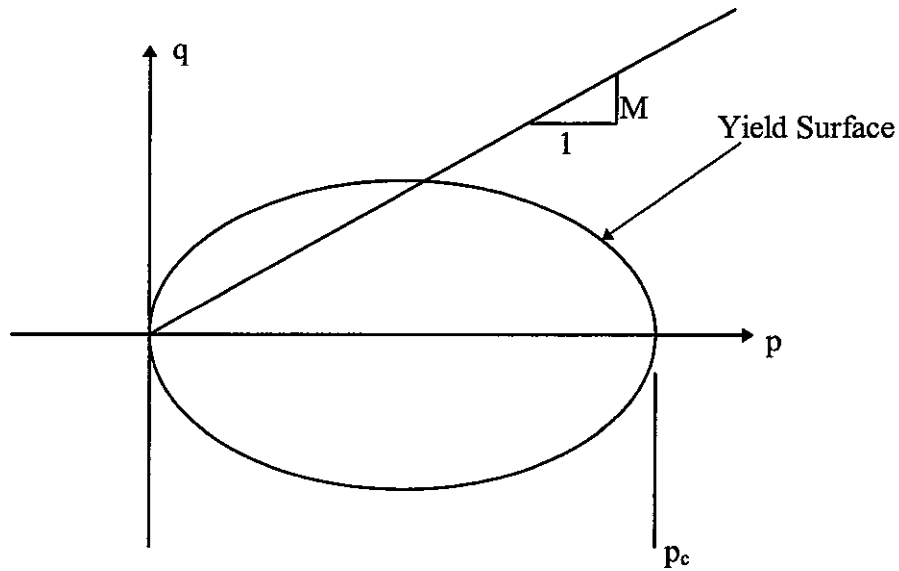


Figure 33 Yield surface of Cam Clay model in p-q space

### Summary of Input Parameters

The following tables are summaries of the input parameters for both programs. The raw units for each quantity are listed as a brief summary of each parameter. The status column denotes where/how numerical values of these parameters can be found/determined. In some cases, the exact equations are given whereby the parameter could be calculated. Typical values are also listed where available. Table 1 shows the parameters for Plaxis while Table 2 contains those for PlasFEM.

Table 1 Input Parameters for Plaxis

Linear Elastic	Units	Explanation	Status
E	(F/L <sup>2</sup> )	Linear elastic stiffness Young's Modulus	lab, Multiple Correlations from Literature
Poissons	(-)	Poisson's Ratio	Usually 0.2 to 0.4 for soil
k <sub>0</sub>	(-)	Earth Pressure at Rest	1 - sin φ
ρ	(F/L <sup>3</sup> )	unit weight	typical (90-120) pcf
Mohr Coulomb	Units	Explanation	Status
E	( F/L <sup>2</sup> )	Linear elastic stiffness Young's Modulus	lab, Multiple Correlations from Literature
Poissons	(-)	Poisson's Ratio	Usually 0.2 to 0.4 for soil
c	(F/L <sup>2</sup> )	Cohesion	lab, Multiple Correlations from Literature
φ	(°)	Friction Angle	lab, Multiple Correlations from Literature
ψ	(°)	Dilatency Angle	typically φ - 30
E <sub>increment</sub>	(F/L <sup>2</sup> /L)	Increment for increasing Modulus with depth	user defined
C <sub>increment</sub>	(F/L <sup>2</sup> /L)	Increment for increasing cohesion with depth	user defined
k <sub>0</sub> or	(-)	Earth Pressure at Rest	1 - sin φ
ρ	(F/L <sup>3</sup> )	unit weight	typical (90-120) pcf
Hardening Soil Model	Units	Explanation	Status
E <sub>50</sub> <sup>ref</sup>	(F/L <sup>2</sup> )	Primary Loading Modulus under Reference Stress	lab, Multiple Correlations from Literature
E <sub>ur</sub> <sup>ref</sup>	(F/L <sup>2</sup> )	Unload/Reload Modulus under Reference Stress	lab =4*E <sub>50</sub>
E <sub>oed</sub> <sup>ref</sup>	(F/L <sup>2</sup> )	1-D Compression Modulus	lab =E <sub>50</sub>
ν <sub>r</sub>	(-)	Unload/Reload Poisson's Ratio	Usually 0.2 to 0.4 for soil
p <sup>ref</sup>	(F/L <sup>2</sup> )	Reference Traxial Cell Confining Pressure	lab reference number
m	(-)	Stress dependency exponent	assumed
c	(F/L <sup>2</sup> )	Cohesion	lab, Multiple Correlations from Literature
φ	(°)	Friction Angle	lab, Multiple Correlations from Literature
ψ	(°)	Dilatency Angle	typically φ - 30
K <sub>0</sub> <sup>nc</sup>	(-)	At rest lateral stress for NC	1 - sin φ
σ <sub>tension</sub>	(F/L <sup>2</sup> )	Tensile Strength	0 or small value for stability
R <sub>f</sub>	(-)	Failure Ratio	lab test (0.9 good estimate)
C <sub>increment</sub>	(F/L <sup>2</sup> /L)	Increment for increasing cohesion with depth	user defined

Table 1 Continued

Hardening Soil Model		Units	Explanation	Status
$k_0$		(-)	Earth Pressure at Rest	$1 - \sin \phi$
PCP or		(F/L <sup>2</sup> )	Preconsolidation Pressure	lab test
OCR		(-)	Overconsolidation Ratio	lab test
$\rho$		(F/L <sup>3</sup> )	unit weight	typical (90-120 pcf)

Soft Soil	(Creep)	Units	Explanation	Status
$\lambda^*$		(-)	Modified Compression Index	From lab test <sup>†</sup>
$\kappa^*$		(-)	Modified Swelling Index	From lab test <sup>†</sup>
$\mu^*$		(-)	Modified Creep Index	From lab test <sup>†</sup>
c		(F/L <sup>2</sup> )	Cohesion	lab, Multiple Correlations from Literature
$\phi$		( <sup>o</sup> )	Friction Angle	lab, Multiple Correlations from Literature
$\psi$		( <sup>o</sup> )	Dilatency Angle	typically $\phi - 30$
M		(-)	critical state slope	calculate <sup>‡</sup>
$K_0^{nc}$		(-)	At rest lateral stress for NC	$1 - \sin \phi$
$\nu_r$		(-)	Unload/Reload Poisson's Ratio	Usually 0.2 to 0.4 for soil
$k_0$		(-)	Earth Pressure at Rest	$1 - \sin \phi$
PCP or		(F/L <sup>2</sup> )	Preconsolidation Pressure	lab test
OCR		(-)	Overconsolidation Ratio	lab test
$\rho$		(F/L <sup>3</sup> )	unit weight	typical (90-120 pcf)

$$† \quad \lambda^* = \frac{C_c}{2.3(1+e)} \quad \kappa^* \approx \frac{3}{2.3} \frac{1-\nu_{ur}}{1+\nu_{ur}} \frac{C_r}{1+e} \quad \mu^* = \frac{C_\alpha}{2.3(1+e)}$$

$$‡ \quad M = 3 \sqrt{\frac{(1 - K_0^{NC})^2}{(1 + 2K_0^{NC})^2} + \frac{(1 - K_0^{NC})(1 - 2\nu_{ur})(\lambda^*/\kappa^* - 1)}{(1 + 2K_0^{NC})(1 - 2\nu_{ur})\lambda^*/\kappa^* - (1 - K_0^{NC})(1 + \nu_{ur})}}$$

$$M = \frac{6 \sin \phi_{cv}}{3 \sin \phi_{cv}}$$

Table 2 Input Parameters for PlasFEM

Linear Elastic	Units	Explanation	Status
E	(F/L <sup>2</sup> )	modulus of elasticity	lab, Multiple Correlations from Literature
nu	(-)	poisson's ratio	Usually 0.2 to 0.4 for
area	(L <sup>2</sup> )	cross section area (for truss elements)	measured
row	(F/L <sup>3</sup> )	unit weight	typical (90-120 pcf)
sig0	(F/L <sup>2</sup> )	initial vertical stress in elements	row * z or other specified
k0	(-)	ratio of initial horizontal stress / initial vertical stress	1 - sin $\phi$
Drucker-Prager	Units	Explanation	Status
E	(F/L <sup>2</sup> )	modulus of elasticity	lab, Multiple Correlations from Literature
nu	(-)	Poisson's ratio	Usually 0.2 to 0.4 for soil
$\alpha$	(F/L <sup>2</sup> )	strength parameter (intercept on $\sqrt{J}$ axis)	similar to c <sup>†</sup>
$\theta$	(-)	strength parameter (slope of the yield surface)	similar to $\phi$ <sup>†</sup>
row	(F/L <sup>3</sup> )	unit weight	typical (90-120 pcf)
sig0	(F/L <sup>2</sup> )	initial vertical stress in elements	row * z or other specified
k0	(-)	ratio of initial horizontal stress / initial vertical stress	1 - sin $\phi$
Sandler-Dimaggio	Units	Explanation	Status
E	(F/L <sup>2</sup> )	modulus of elasticity	lab, Multiple Correlations from Literature
nu	(-)	poisson's ratio	Usually 0.2 to 0.4 for soil
alpha	(F/L <sup>2</sup> )	strength parameter (intercept on $\sqrt{J}$ axis)	similar to c <sup>†</sup>
theta	(-)	strength parameter (slope of the yield surface)	similar to $\phi$ <sup>†</sup>
gamma	(-)	strength parameter (curvature or envelope)	assume 0 for most cases
beta	(-)	strength parameter (curvature or envelope)	assume 0 for most cases
X0	(F/L <sup>2</sup> )	preconsolidation pressure	lab/field test
T	(F/L <sup>2</sup> )	tension cutoff stress	0 for soil, but use small number for stability
W	(in./in.)	cap parameter (max volumetric plastic strain)	From DRAINED Triaxial Test
R	(-)	cap parameter (Ellipticity ratio)	From literature <sup>†</sup>
D	(L <sup>2</sup> /F)	cap parameter (hardening)	From literature <sup>†</sup>
row	(F/L <sup>3</sup> )	unit weight	typical (90-120 pcf)
sig0	(F/L <sup>2</sup> )	initial stress in elements	row * z or other specified
k0	(-)	ratio of initial horizontal stress / initial vertical stress	1 - sin $\phi$

Table 2 Continued

Cam-Clay	Units	Explanation	Status
rK	(F/L <sup>2</sup> )	bulk modulus	lab, Correlations from Literature
nu	(-)	poisson's ratio	Usually 0.2 to 0.4 for soil
e <sub>0</sub>	(-)	initial void ratio	calculate
M	(-)	critical state slope	calculate**
rkappa	(-)	recompression / swell index	From Consolidation Test***
rlambda	(-)	compression index	From Consolidation Test***
p <sub>co</sub>	(F/L <sup>2</sup> )	preconsolidation pressure	From Consolidation Test
row	(F/L <sup>3</sup> )	unit weight	typical (90-120 pcf)
sig0	(F/L <sup>2</sup> )	initial stress in elements	row * z or other specified
k0	(-)	ratio of initial horizontal stress / initial vertical stress	1 - sin φ

$$\dagger \quad \alpha = \frac{6c \cos \phi}{\sqrt{3}(3 - \sin \phi)} \quad \theta = \frac{2 \sin \phi}{\sqrt{3}(3 - \sin \phi)}$$

Source	R (--)	D (in <sup>2</sup> /lb)
Sandler and Dimaggio (1971)	2.5	0.00067
Sandler et al.(1976)	4.3	0.002
Voyiadjis et al. (1990)	4.4	0.000514
Pinto (1998)	4.33	0.000977

$$\varepsilon_v^p = W(1 - \exp(-DX))$$

and  
D\*Xo < 0.5

$$** \quad M = \frac{6 \sin \phi}{3 - \sin \phi}$$

$$*** \quad \lambda^* = \frac{C_c}{2.3} \quad \kappa^* \approx \frac{3}{2.3} \frac{1 - v_{ur}}{1 + v_{ur}} C_r$$

### Parameter Selection

A good place to start with many of aforementioned soil parameters is correlation.

The literature contains many tried and true relationships for shear strength and deformation properties from insitu tests.

### Unit Weight

Table 3 Typical Values of Unit Weight for Soil (Coduto, 1994)

Soil Type (See Table 3.4)	Typical Unit Weight, $\gamma$			
	Above Groundwater Table		Below Groundwater Table	
	(lb/ft <sup>3</sup> )	(kN/m <sup>3</sup> )	(lb/ft <sup>3</sup> )	(kN/m <sup>3</sup> )
GP — Poorly graded gravel	110 - 130	17.5 - 20.5	125 - 140	19.5 - 22.0
GW — Well graded gravel	110 - 140	17.5 - 22.0	125 - 150	19.5 - 23.5
GM — Silty gravel	100 - 130	16.0 - 20.5	125 - 140	19.5 - 22.0
GC — Clayey gravel	100 - 130	16.0 - 20.5	125 - 140	19.5 - 22.0
SP — Poorly graded sand	95 - 125	15.0 - 19.5	120 - 135	19.0 - 21.0
SW — Well graded sand	95 - 135	15.0 - 21.0	120 - 145	19.0 - 23.0
SM — Silty sand	80 - 135	12.5 - 21.0	110 - 140	17.5 - 22.0
SC — Clayey sand	85 - 130	13.5 - 20.5	110 - 135	17.5 - 21.0
ML — Low plasticity silt	75 - 110	11.5 - 17.5	80 - 130	12.5 - 20.5
MH — High plasticity silt	75 - 110	11.5 - 17.5	75 - 130	11.5 - 20.5
CL — Low plasticity clay	80 - 110	12.5 - 17.5	75 - 130	11.5 - 20.5
CH — High plasticity clay	80 - 110	12.5 - 17.5	70 - 125	11.0 - 19.5

## Shear Strength Parameters

### Drained Friction Angle

#### Drained Friction Angle from SPT Blowcount

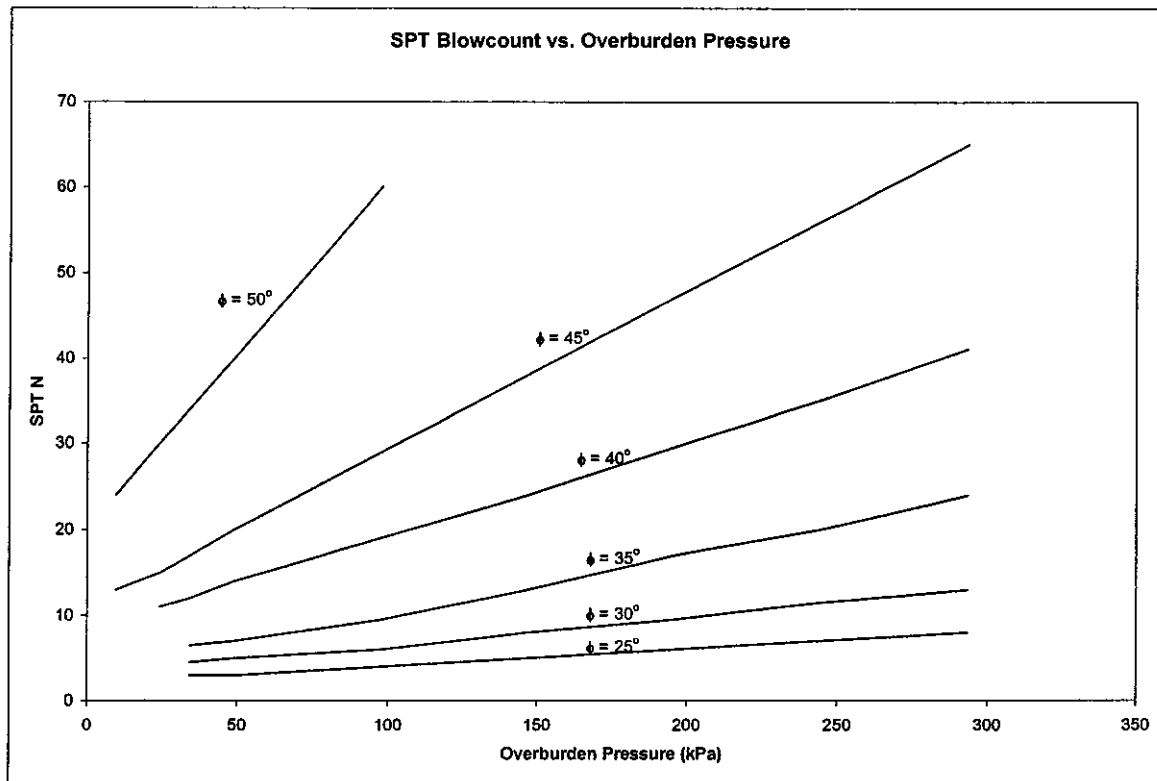


Figure 34 Friction Angle from Overburden Pressure and SPT N (Demello, 1971, as referenced in Schmertmann, 1975).

Table 4 Soil Parameters (Teng, 1962, as referenced in U.S. Steel, 1971)

Compactness	Very Loose	Loose	Medium	Dense	Very Dense
Relative Density %	0 to 15	15 to 35	35 to 65	65 to 85	85 to 100
Blows/30cm, N	0 to 4	4 to 10	10 to 30	30 to 50	50+
φ, degrees	28	28 to 30	30 to 36	36 to 41	41+

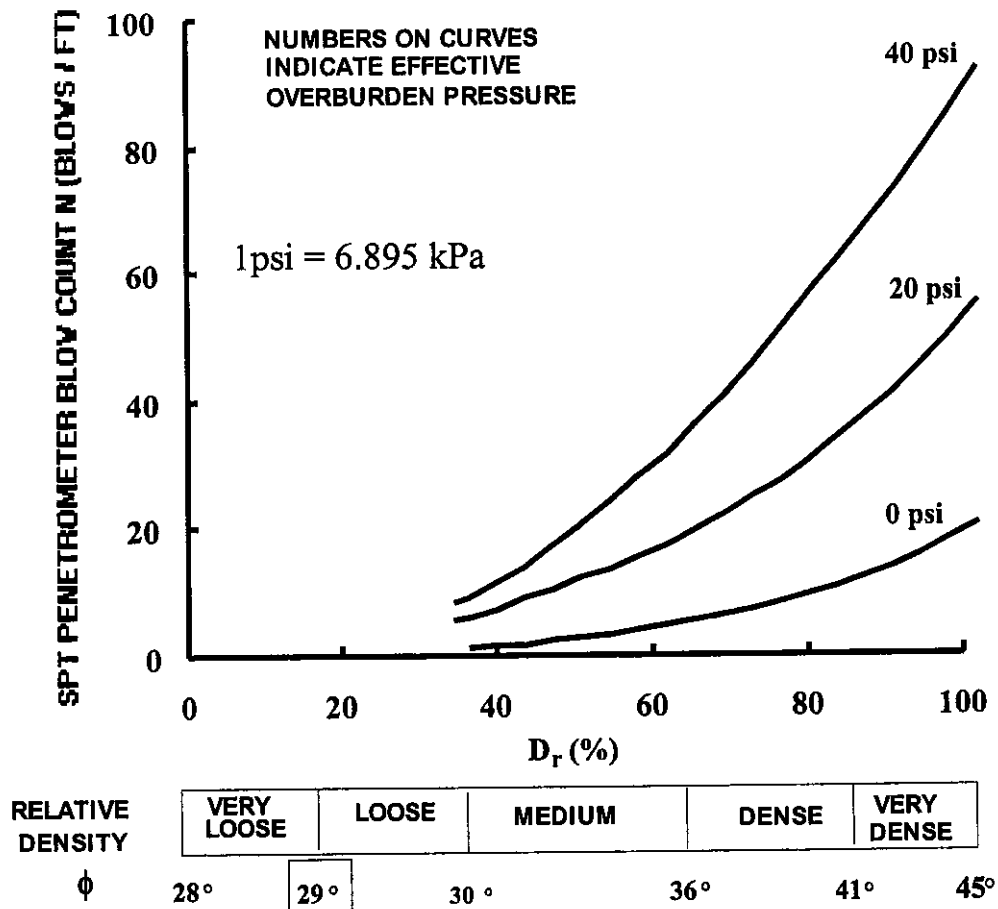


Figure 35 Friction Angle from Overburden Pressure, Relative Density, and SPT N. (Gibbs) and Holtz, 1967, as referenced in O'Neil and Murchison, 1983)

Schmertmann (1975, as referenced in EPRI, 1990) correlated  $N$  and  $\phi'_{tc}$  as a function of stress level. It is approximated as follows:

$$\phi'_{tc} = \tan^{-1} [N / (12.2 + 20.3 \sigma'_{vo} / Pa)]^{0.34}$$

$N$  = Uncorrected SPT blow-count

$\sigma_{vo}$  = Effective Overburden Stress

$Pa$  = Atmospheric pressure (100 kPa)

Not to be used at very shallow depths, less than 1 or 2 m (3.3 to 6.6 ft).

Another estimation of  $\phi$  can be made using the following equation obtained from Peck, Hanson, and Thornburn (Peck et. al, 1974) using uncorrected N-values.

$$\phi = 53.881 - 27.6034 * e^{-0.0147 * N}$$

#### Drained Friction Angle from Cone Penetration Tests

Equation from Muhs and Weiss (Muhs and Weiss 1971, as referenced in Schmertmann, 1975)

$$N_{\gamma} = \frac{q_c (kpa)}{80}; \quad N_{\gamma} \rightarrow \phi \text{ from bearing capacity theory}$$

Equation from DeBeer (Debeer 1974, as referenced in Schmertmann, 1975)

$$q_c = 1.3 p_0' \tan\left(\frac{\pi}{4} + \frac{\phi}{2}\right) e^{(\pi \tan \phi)}; \quad p_0' = \text{overburden stress}$$

Equation from Kulhawy and Mayne (1980, as referenced in EPRI, 1990)

$$\phi_{tc} = 17.6 + 11.0 \log[(q_c / Pa) / (\sigma_{VO} / Pa)^{0.5}]$$

Equation from Masood and Mitchell (1993)

$$\phi_{tc} = 30.8[\log(f_s / \sigma_{VO}) + 1.261]; \quad f_s = \text{unit sleeve friction}$$

Table 5 Correlation Between  $q_c$  and  $\phi_{tc}$  (after Meyerhof, 1956).

q <sub>c</sub> verses $\phi_{tc}$		
Normalized ConeTip Resistance, q <sub>c</sub> /Pa	Relative Density	Approximate $\phi'_{tc}$ (Deg)
<20	Very Loose	<30
20 to 40	Loose	30 to 35
40 to 120	Medium	35 to 40
120 to 200	Dense	40 to 45
>200	Very Dense	>45

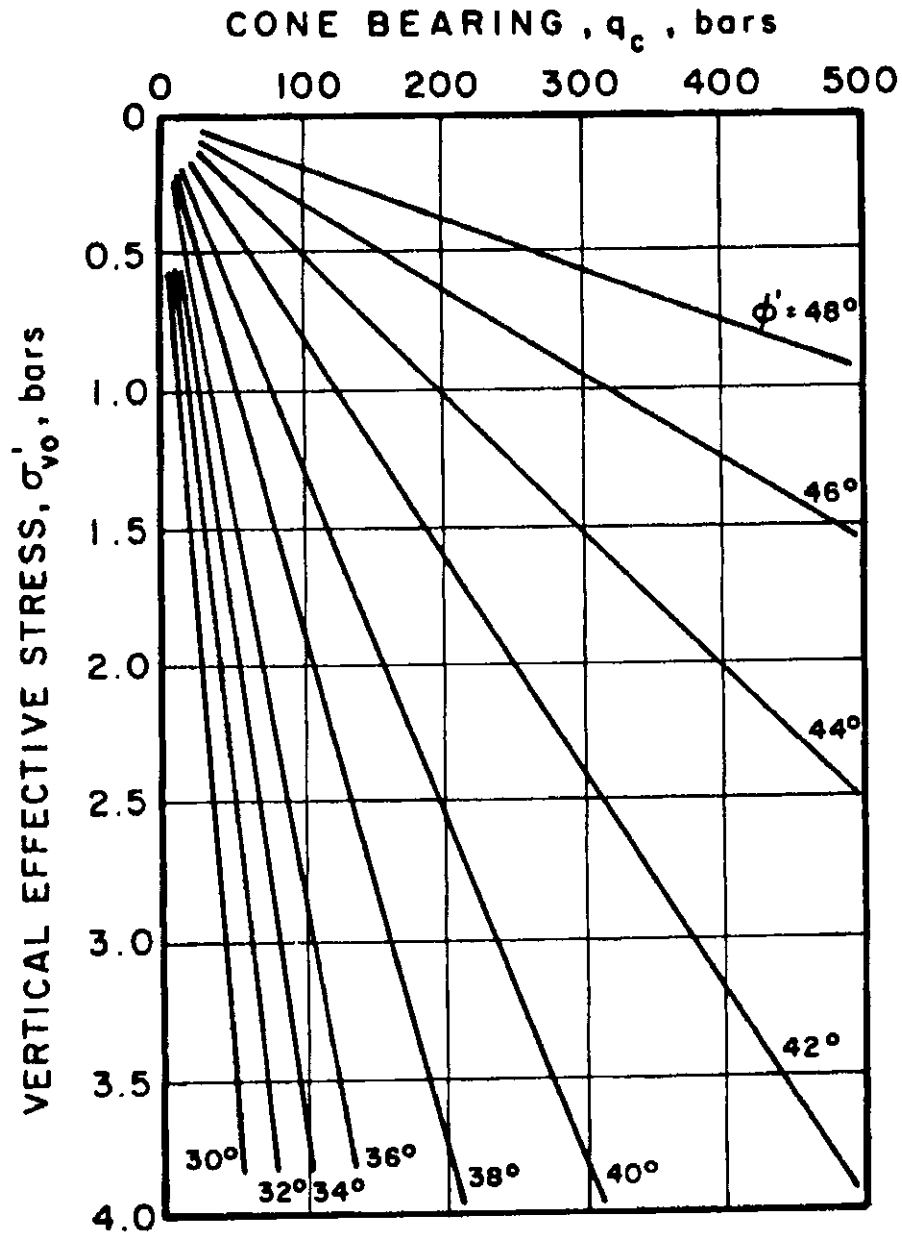


Figure 36 Friction Angle from Overburden Pressure and CPT Tip Resistance (Robertson and Campanella, 1983)

### Drained Friction Angle from Dilatometer Tests

Schmertmann (1982, as referenced in Schmertmann, 1988) proposed this procedure for obtaining friction angle from DMT:

$$\tan(\phi'_{ps}/2) = [THRUST - (\pi/4) \times RODIAM^2 \times U_o \times 1.019 - (DMAREA + (\pi/4) \times DFRIC^2 - B \times DFRIC) \times q_f + RODWT \times (ZS + 2)] / F_H$$

where

$\phi'_{ps}$  = Drained friction angle of the soil –plane strain

THRUST = Insertion thrust (kg)

RODIAM =Drill rod diameter (cm)

U<sub>o</sub> = Pore water pressure prior to insertion of the dilatometer (bars)

DMAREA = Bearing area of the dilatometer (12.9 or 14.4 cm<sup>2</sup>)

B = Thickness of the dilatometer (1.37 or 1.5 cm)

DFRIC = Diameter of the friction reducer (cm)

q<sub>f</sub> = Durgunoglu and Mitchell bearing capacity (kg/cm<sup>2</sup>)

RODWT = Drill rod weight per unit length (kg/m)

ZS = Test depth (m)

F<sub>H</sub> = Horizontal force normal to the dilatometer blade, (P<sub>o</sub>-U<sub>o</sub>) x Blade area (355cm<sup>2</sup>) x 1.019.

Marchetti (1997, as referenced in Mayne and Martin, 1998) presented two correlations based upon the DMT horizontal stress index, K<sub>D</sub>, as:

$$\phi' = 28^\circ + \frac{\log K_D}{0.0685} - \frac{(\log K_D)^2}{0.476}$$

The second correlation is:

$$\phi' = 31^\circ + \frac{1}{\frac{0.236}{K_D} + 0.066}$$

Robertson and Campanella (1991, as referenced in EPRI, 1990)

$$\phi' = 37.3 \left[ \frac{K_D - 0.8}{K_D + 0.8} \right]^{0.082} \quad \text{where DMT material index, } Id, > 3.3$$

### Drained Friction Angle from Pressuremeter Tests

Centre d'Etudes Menard (1970, as referenced in EPRI, 1990).

$$P_N = 250x(2)^{\frac{\phi'-24}{4}}$$

Briaud (1992) and Baguelin et al. (1978)

Table 6 Correlation Between Relative Density and Net Limit Pressure (PN) and Pressuremeter Modulus (EO) for Sands (after Briaud, 1992, Baguelin et al., 1978).

SAND					
Relative Density	Very Loose	Loose	Medium	Dense	Very Dense
Dr	0-15%	15-35%	35-65%	65-85%	85-100%
P <sub>N</sub> (kpa)	0-200	200-500	500-1500	1500-2500	>250
E <sub>O</sub> (kpa)	0-1400	1400-3500	3500-12000	12000-22500	>22500

### Undrained Shear Strength

The literature gives some relationships for unconfined compressive strength based on SPT. Both programs require undrained shear strength, which is half of the unconfined compressive strength. The following are correlations for undrained shear strength or unconfined compressive strength from insitu tests:

### Undrained Shear Strength from Standard Penetration Tests

Table 7 Unconfined Compressive Strength from SPT N (Teng, 1962, as referenced in U.S. Steel, 1971)

Consistency	Very Soft	Soft	Medium	Stiff	Very Stiff	Hard
$q_u$ , kPa	0 to 25	25 to 50	50 to 100	100 to 200	200 to 400	400+
Blows/30cm, N	0 to 2	2 to 4	4 to 8	8 to 16	16 to 32	32+

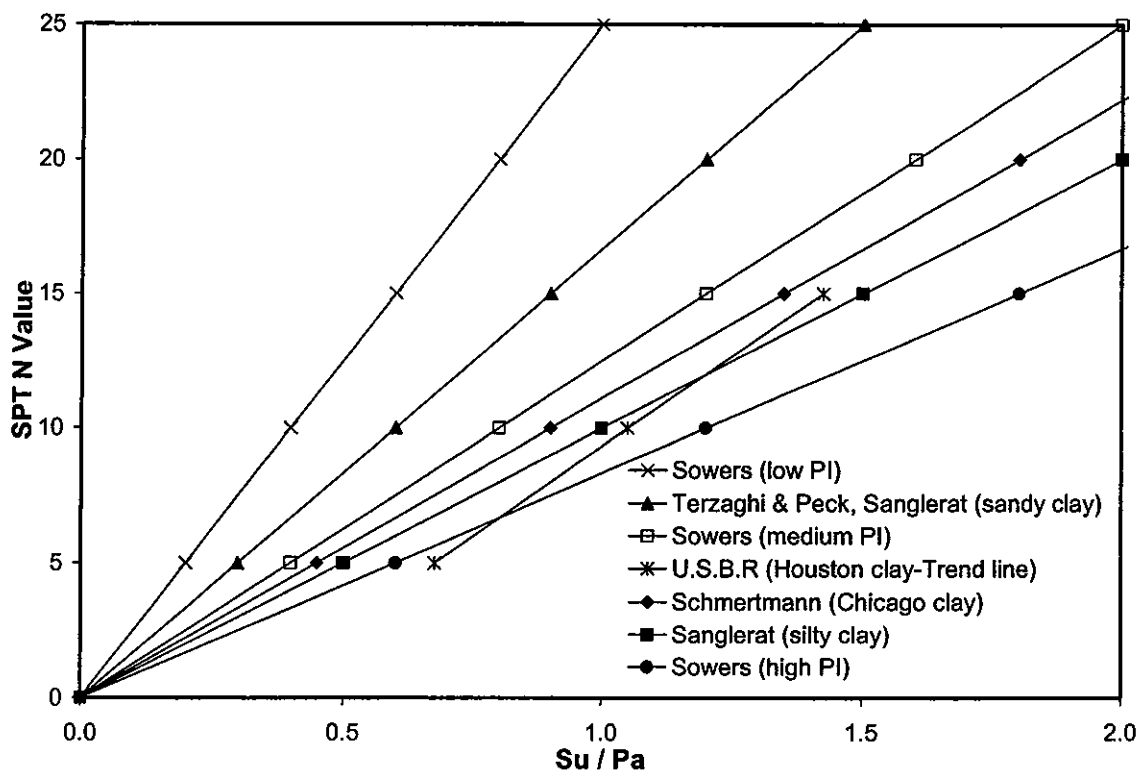


Figure 37 Cohesive Soil Shear Strength (EPRI, 1990)

### Undrained Shear Strength from Cone Penetration Tests

Equation from bearing capacity theory (Bowles, 1988):

$$q_c = c_u * N_{kk} + \sigma_{vo}' \quad 10 < N_{kk} < 20 ; N_{kk} = \text{cone factor}$$

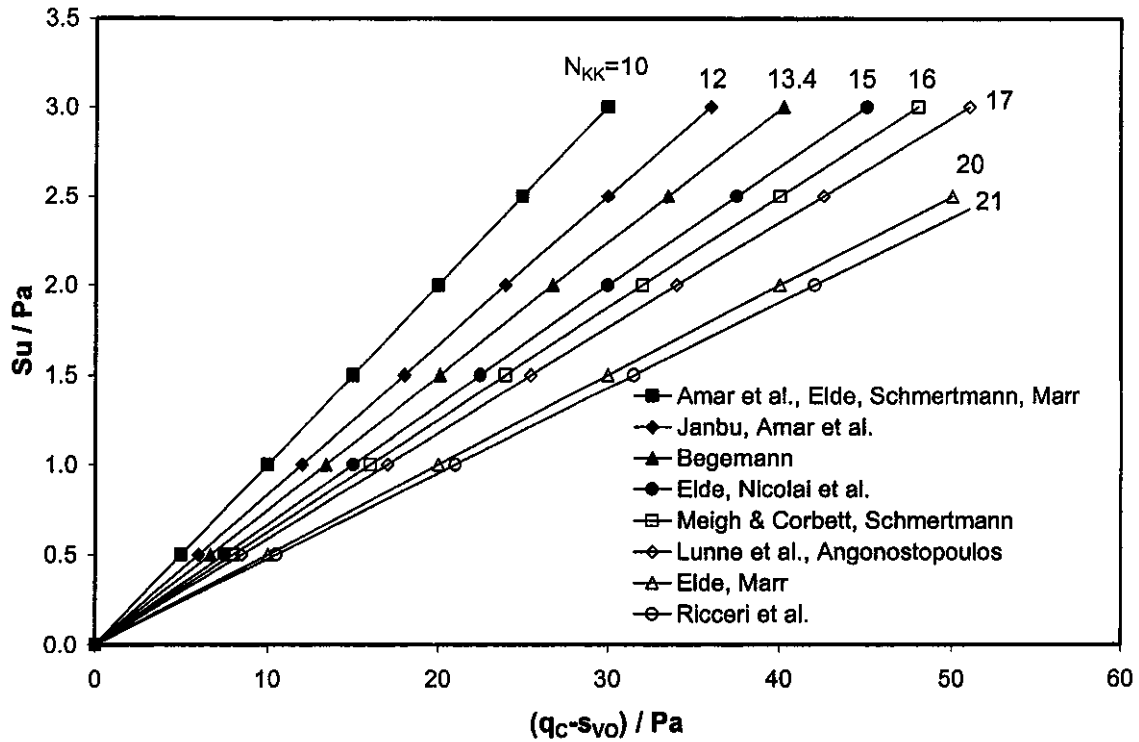


Figure 38 Relationship between  $q_c$  and  $S_u$  (EPRI, 1990)

### Undrained Shear Strength from DMT Results

Marchetti (1980) suggested:

$$S_U / \sigma'_{VO} = 0.22(0.5K_D)^{1.25}; \text{ where } K_D \text{ is the DMT horizontal stress index}$$

Schmertmann (1988):

$$S_U = (P_o - U_o) / (8t_0l_0); \text{ where } P_o \text{ and } U_o = \text{overburden stress and pore pressure, respectively.}$$

### Undrained Shear Strength from PMT Results

Baguelin et al. (1978)

$$S_U = (P_L - P_O) / N_P$$

$P_L$  = PMT limit stress,  $P_O$  = PMT total horizontal stress,  $N_p = 1 + \ln(E_{PMT}/3S_u)$ ,  
and  $E_{PMT}$  = PMT modulus. Typical values of  $N_p$  range from 5 to 12, with an  
average of 8.5.

Briaud (1992) for pre-bored PMT

$$S_U = \frac{P_N}{\beta}$$

where  $\beta$  is a constant dependent on the ratio of the shear modulus  $G$  over the  
undrained shear strength  $S_u$  for the soil. A  $\beta$  value of 7.5 is typically used.  $P_N$  is  
the net limit pressure.

Briaud (1992) for pre-bored PMT

$$\frac{S_U}{P_a} = \left[ \frac{P_N}{P_a} \right]^{0.75}$$

where  $P_a$  is equal to the atmospheric pressure.

Table 8 Correlation Between Soil Consistency and Net Limit Pressure ( $P_N$ ) and  
Pressuremeter Modulus ( $E_O$ ) for Clays (after Briaud, 1992).

CLAY					
Soil Consistency	Soft	Medium	Stiff	Very Stiff	Hard
$P_N$ (kpa)	0-200	200-400	400-800	800-1600	>1600
$E_O$ (kpa)	0-2500	2500-5000	5000-12000	12000-25000	>25000

## Soil Stiffness Parameters

### Poisson's Ratio Based on Soil Type

**Values or value ranges for Poisson's ratio  $\mu$**

Type of soil	$\mu$
Clay, saturated	0.4–0.5
Clay, unsaturated	0.1–0.3
Sandy clay	0.2–0.3
Silt	0.3–0.35
Sand, gravelly sand commonly used	– 0.1–1.00 0.3–0.4
Rock	0.1–0.4 (depends somewhat on type of rock)
Loess	0.1–0.3
Ice	0.36
Concrete	0.15
Steel	0.33

Figure 39 Typical Values for Poisson's Ratio for Soil and Other Materials (Bowles, 1996)

$\mu$	Soil type
0.4–0.5	Most clay soils
0.45–0.50	Saturated clay soils
0.3–0.4	Cohesionless—medium and dense
0.2–0.35	Cohesionless—loose to medium

Figure 40 Typical Values for Poisson's Ratio for Soil (Bowles, 1996)

## Modulus

Bowles presents a list of general values for modulus based on soil type.

Soil	$E_s$ , MPa
Clay	
Very soft	2–15
Soft	5–25
Medium	15–50
Hard	50–100
Sandy	25–250
Glacial till	
Loose	10–150
Dense	150–720
Very dense	500–1440
Loess	15–60
Sand	
Silty	5–20
Loose	10–25
Dense	50–81
Sand and gravel	
Loose	50–150
Dense	100–200
Shale	150–5000
Silt	2–20

Figure 41 Typical Values of Young's Modulus for Soil (Bowles, 1996)

Soil or Rock Type and Condition	Modulus of Elasticity, $E$	
	(lb/ft <sup>2</sup> )	(kPa)
Undrained Condition (Also see Equation 7.10)		
Soft Clay	30,000 - 200,000	1,500 - 10,000
Medium clay	100,000 - 1,000,000	5,000 - 50,000
Stiff clay	300,000 - 1,500,000	15,000 - 75,000
Drained Condition		
Soft clay	5,000 - 30,000	250 - 1,500
Medium clay	10,000 - 70,000	500 - 3,500
Stiff clay	25,000 - 400,000	1,200 - 20,000
Loose sand	200,000 - 500,000	10,000 - 25,000
Medium dense sand	400,000 - 1,200,000	20,000 - 60,000
Dense sand	1,000,000-2,000,000	50,000 - 100,000
Sandstone	$1.4 \times 10^8$ - $4.0 \times 10^8$	7,000,000 - 20,000,000
Granite	$5.0 \times 10^8$ - $1.0 \times 10^9$	25,000,000 - 50,000,000
Steel	$4.2 \times 10^9$	200,000,000

Figure 42 Typical Values of Young's Modulus for Soil (Coduto, 1994)

### Modulus from Standard Penetration Tests

SPT FloridaPier Manual (1996)

$$\text{Clean NC sand} \quad G(kPa) = \frac{479.2 * N_{60}}{(1 + \nu)}$$

$$\text{Clean OC sand} \quad G(kPa) = \frac{717.1 * N_{60}}{(1 + \nu)}$$

$$\text{Sand with fines} \quad G(kPa) = \frac{237.9 * N_{60}}{(1 + \nu)}$$

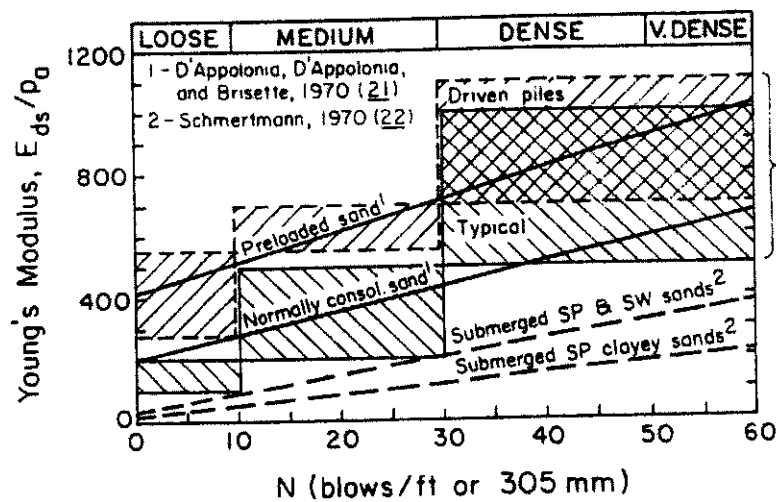


Figure 43 Normalized Young's Modulus from SPT (EPRI, 1990)

### Modulus from Cone Penetration Tests

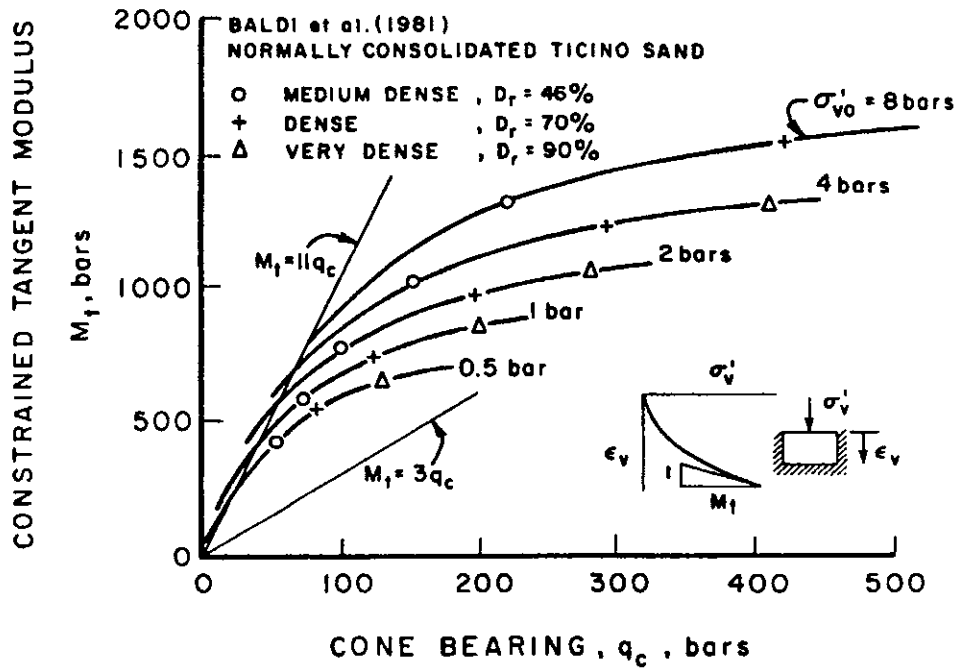


Figure 44 Constrained Modulus from CPT (Robertson and Campanella, 1983)

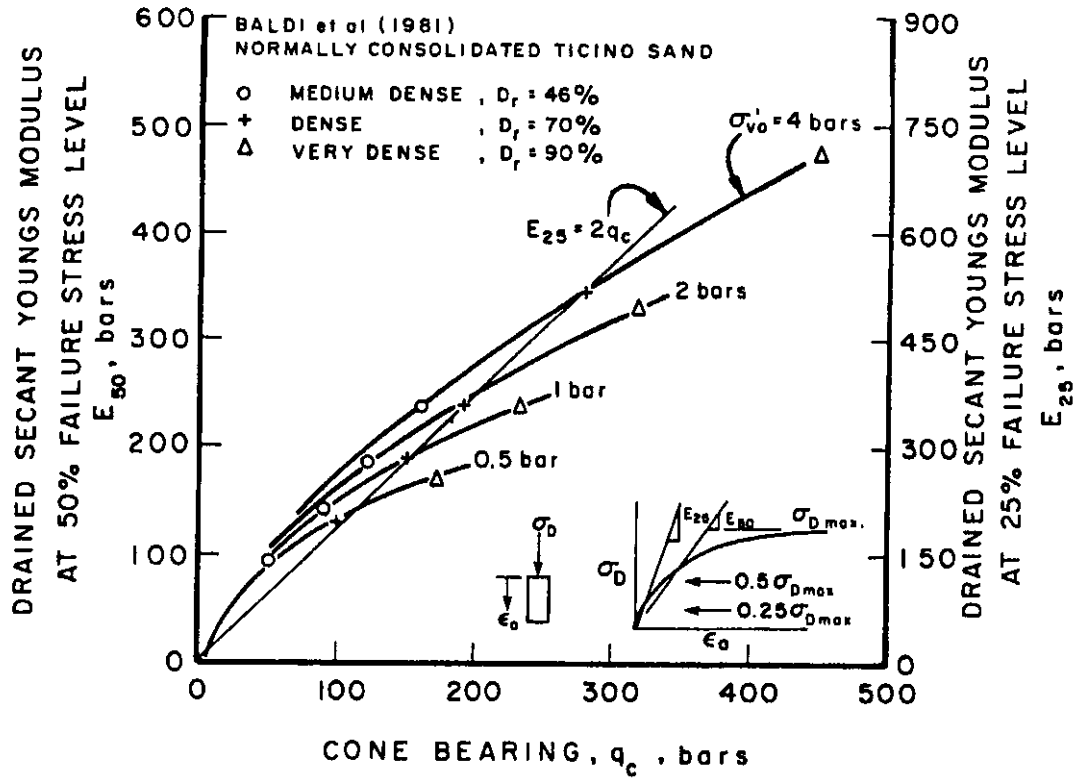


Figure 45 Drained Secant Young's Moduli from CPT (Robertson and Campanella, 1983)

### Modulus from Dilatometer Tests

$$M \text{ (constrained modulus)} = R_M E_D \text{ (bars)}$$

where:

$$\begin{aligned} \text{if } I_D \leq 0.6 & \quad R_M = 0.14 + 2.36 \log K_D \\ \text{if } 0.6 < I_D < 3.0 & \quad R_M = R_{M,0} + (2.5 - R_{M,0}) \log K_D \\ & \quad \text{with } R_{M,0} = 0.14 + 0.15 (I_D - 0.6) \\ \text{if } I_D > 3.0 & \quad R_M = 0.50 + 2.00 \log K_D \\ \text{if } K_D > 10 & \quad R_M = 0.32 + 2.18 \log K_D \end{aligned}$$

Convert constrained modulus to Young's Modulus:

$$\text{drained: } E' = M \frac{(1 + \mu')(1 - 2\mu')}{(1 - \mu')}$$

$$\text{undrained: } E_u = M \frac{(1 + \mu_u)(1 - 2\mu')}{(1 - \mu')}$$

In sands  $E_D \approx E_{25}$

### Modulus from Pressuremeter Tests

$$E = 2(1 + \mu) \left( V_c + \frac{V_o + V_f}{2} \right) \left( \frac{p_f - p_o}{v_f - v_o} \right)$$

where:

- $V_c$  uninflated volume of the probe
- $V_o$  initial volume
- $V_f$  final volume
- $p_o$  initial pressure
- $p_f$  final pressure

### Sensitivity Analysis

A sensitivity analysis was performed using the primary parameters for Plaxis hardening soil and PlasFEM Sandler-Dimaggio. A single triaxial test, Archer Landfill Tube 1 Specimen 2, was used as the control case for each. Each parameter was first varied by -50%, -25%, -10%, -5%, +5%, +10%, +25%, and +50% of their given value. Less sensitive parameters were given extra intervals of  $\div 10$  and  $\times 10$ . In some cases, a reasonable range could be discerned for the variable through experience. Other variables have been far less studied and no true range was known. Thus, the above variation was used arbitrarily.

Since the simulation resulted in a set of numbers, triaxial test curve, rather than a single value, it was not possible to look at a single figure to determine statistical significance or variability. Instead, the results of the sensitivity analysis were examined qualitatively.

### Plaxis parameters

Since the hardening soil model contained the same basic parameters as the Mohr-Coulomb, the sensitivity was examined for hardening soil only. The results are summarized as follows:

- $\phi$  Natural range 25 to 45° for sand. Most sensitive parameter. Limited maximum value of deviatoric stress. Small variations ~5% resulted in substantial differences.
- $E_{50}$  This value naturally varied by orders of magnitude. Plaxis parameter checking will not allow for certain combinations of  $E_{50}$ ,  $E_{oed}$  and  $\phi$  to occur, thus the arbitrary range was used. Small percentage variations had little effect on the results while, variation in the ~50% range had an appreciable effect.
- $E_{oed}$  When varied in the arbitrary range, exhibited little effect on results. Low sensitivity.
- $m$  This parameter is ~0.5 for sands and 1.0 for clays. Variation of this parameter had little effect.
- $\psi$  Natural range not very well established. In the case of this research was found to be close to 1.5°. Regardless, it is often very difficult to discern and calculate. Caused little variation when varied between 1 and 8°.

### PlasFEMparameters

As with the Plaxis parameters, the Sandler-Dimaggio model contains the basic parameters from the Drucker-Prager. The sensitivity was examined for the Sandler-Dimaggio only.

- $\theta$  Similar to  $\phi$  from above, the simulation was very sensitive to small changes in this parameter. When calculated based on a normal range of  $\phi$ ,  $\theta$  ranges from 0.189 to 0.356.
- E Model was insensitive to small changes on E, but was sensitive to order of magnitude changes.
- $\mu$  Model was insensitive to changes in  $\mu$  between 0 and 0.5.
- X0 Arbitrary variation affected the initial yielding of the model, but the results varied little on the whole.
- W Small changes reflected small changes in the total strain. Model was very sensitive to order of magnitude changes.
- R Small variations in R had little effect. Large percentage variations affected strain amounts.
- D Order of magnitude variations had a large effect on this parameter while the model was less sensitive to small variations.

## CHAPTER 4 LABORATORY AND FIELD TESTING

Parallel laboratory and field tests were conducted as the experimental phase of the research. This chapter looks at the methods and equipment used in the tests as well as the test locations and data from the tests.

### Testing Equipment

#### Triaxial Test Equipment

A new triaxial testing system was assembled for this research. The system is composed of a loading frame, pressure/volume control board, testing chamber, and data acquisition. The control panel is a three independent burette system built by Trautwein Soil Testing Equipment. The test cell, also manufactured by Trautwein, is a three piece design with dual ports for the top and bottom of the sample. A Humboldt Triscan 50 load frame was purchased for this testing. It is fully software controlled and features a LCD and keypad interface. Instrumentation includes an Omegadyne Load Cell, an Omegadyne Pore Pressure Transducer with internal amplifier, and a Macro Sensors linear voltage displacement transducer. All of these devices are powered by Omega power supplies.

The data acquisition system is based on a 16 channel DAQPad<sup>TM</sup>-MIO-16XE-50 made by National Instruments. The DAQPad is connected to a Pentium 233 PC through a parallel port interface. Figure 46 shows the control panel and loading frame. A close-up of the triaxial cell and the data acquisition computer are shown in Figure 47.

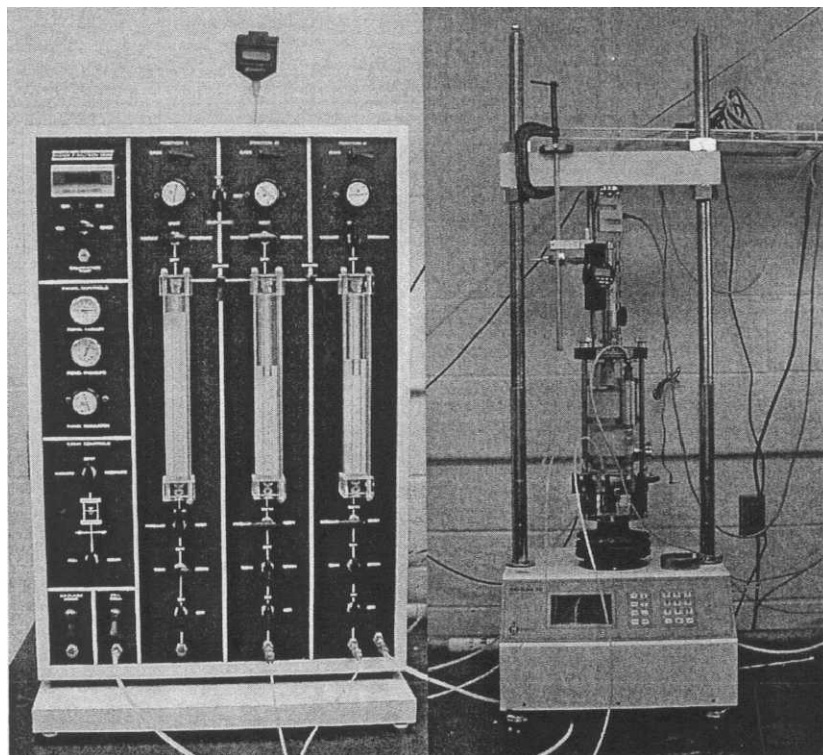


Figure 46 Triaxial testing load frame and control board

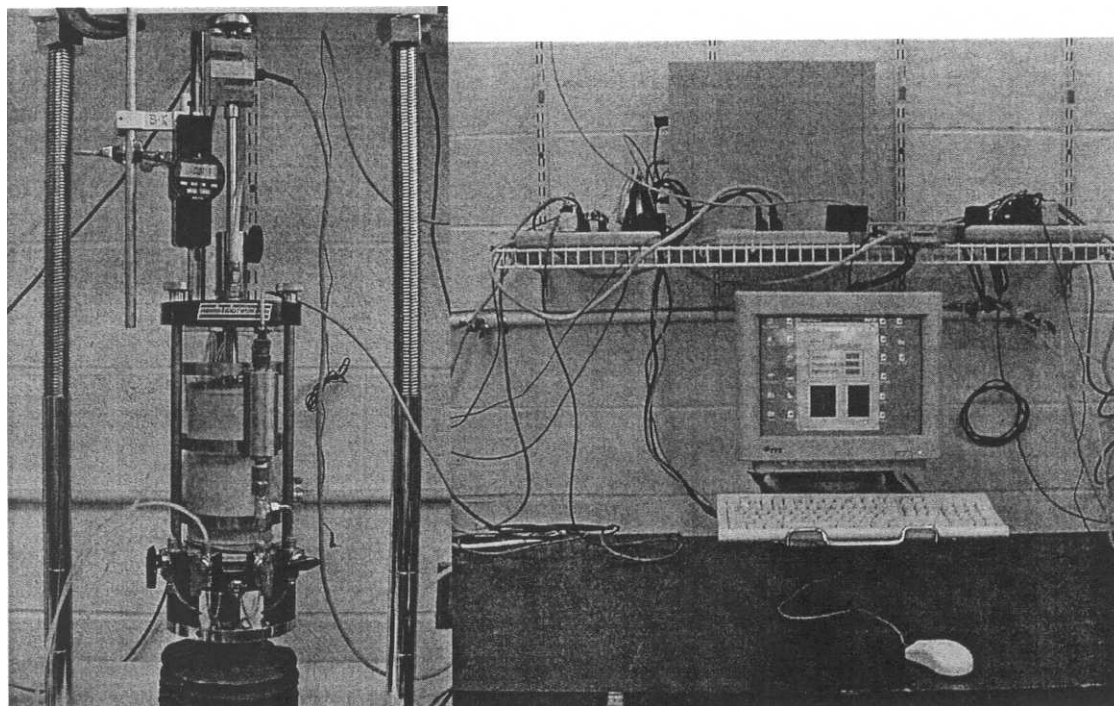


Figure 47 Triaxial cell and data acquisition computer

Field specimens were collected in accordance with ASTM D1587. All of the triaxial tests conducted for this research were consolidated and drained. ASTM D4767 was followed with provision for cohesionless free draining soil.

### Field Test Equipment

Several insitu tests were conducted for this research. Although the primary focus of this study was the PENCEL Pressuremeter, standard penetration tests, cone penetration tests, and dilatometer tests were conducted at each of the sites as well. The following discussion describes the PENCEL Pressuremeter and the penetration rig necessary to advance it.

The standard penetration test and the cone penetration tests are covered by ASTM standards D1586 and D3441, respectively. The dilatometer test currently has no accepted ASTM standard, but the tests were performed in accordance with the proposed ASTM standard suggested by Schmertmann (1986).

### PENCEL Pressuremeter

The testing device used in this study was the PENCEL model pressuremeter. This is more or less the commercial version of the pavement pressuremeter developed by Briaud and Shields (1979). Roctest, Inc. manufactures the unit in Canada and markets it worldwide.

The control unit, shown in Figure 48, has been modernized. A volume calibrated screw piston has replaced the graduated Plexiglas tube with kerosene. The unit is lightweight and easily transportable. The monocellular tubing was carried on from the original model. Swagelok™ quick connects are used to, theoretically, allow for the unit, line, and probe to be presaturated in the lab and then disconnected for easy transport.

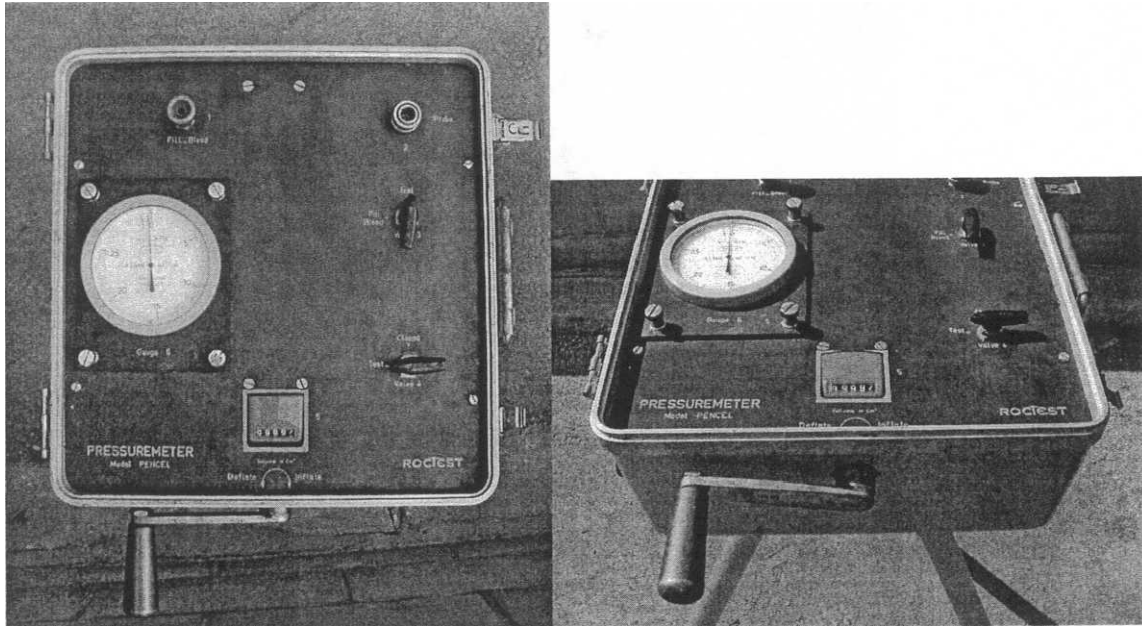


Figure 48 The PENCEL Pressuremeter control unit

The probe has undergone a slight modification where, instead of O-rings, metal protrusions now create the seal between the membrane and the body. Figure 49 shows both an assembled probe with its drive point and friction reducer and a disassembled probe with the retaining nuts and brass rings. An assembled PENCEL Pressuremeter system is shown in Figure 50.

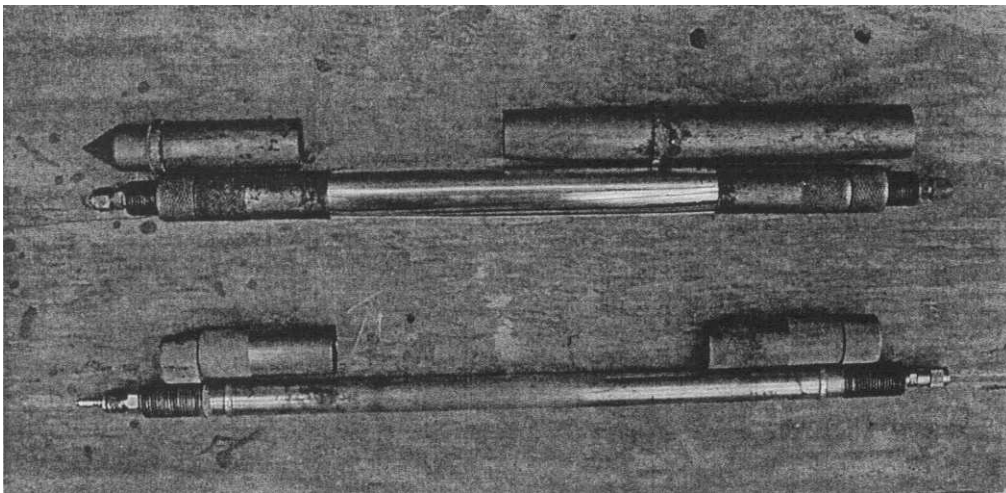


Figure 49 The PENCEL Pressuremeter probe

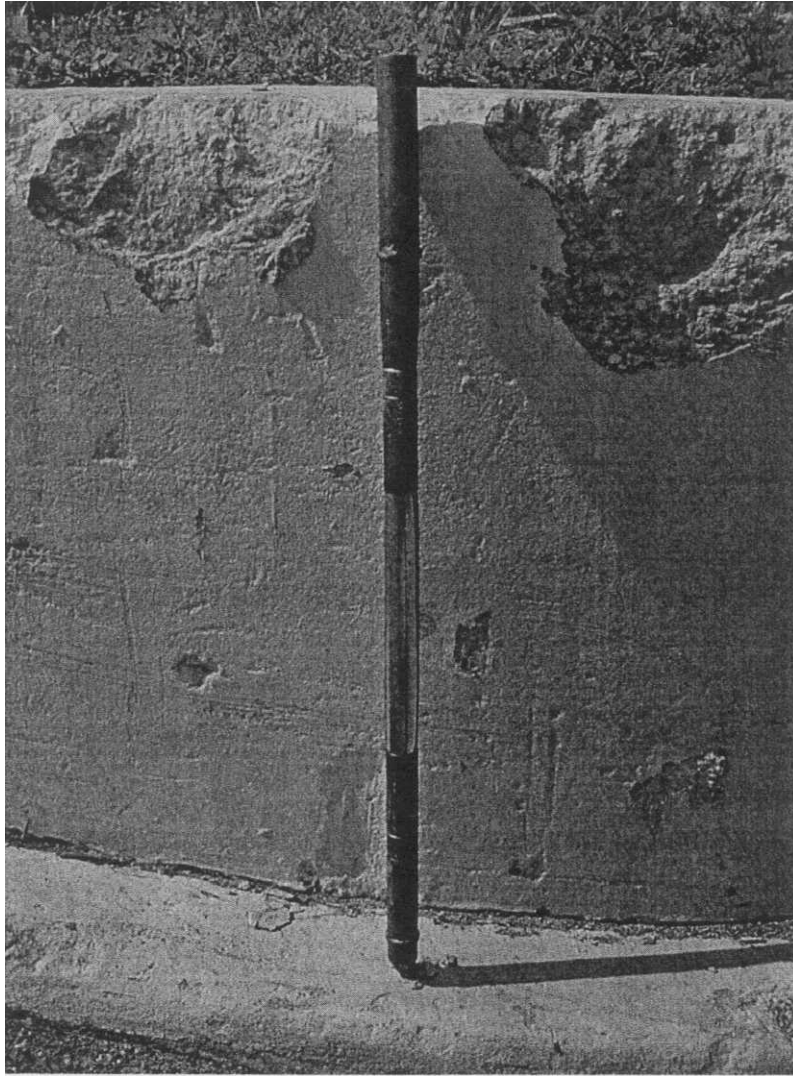


Figure 50 The PENCEL Pressuremeter probe fully assembled

No ASTM standard exists for the PENCEL Pressuremeter test. Instead, the test and calibration methods are based on the manual published by Briaud and Shields (1979). Calibration of the system is conducted in three steps. First, the free air correction is determined by inflating the probe in air, with no obstruction, at the same elevation as the pressure gauge. The second calibration is the system compliance or volume loss correction. The probe is inserted into a steel tube and inflated. Since there is an annular space between the probe and the tube, some correction will need to be made to the

compliance curve so that it can be used to correct the PENCEL volumes without over correction. A third curve is generated by detaching the probe and injecting volume into the control unit and tubing. The latter two corrections are combined to develop the compliance correction. This construction is shown in Figure 51.

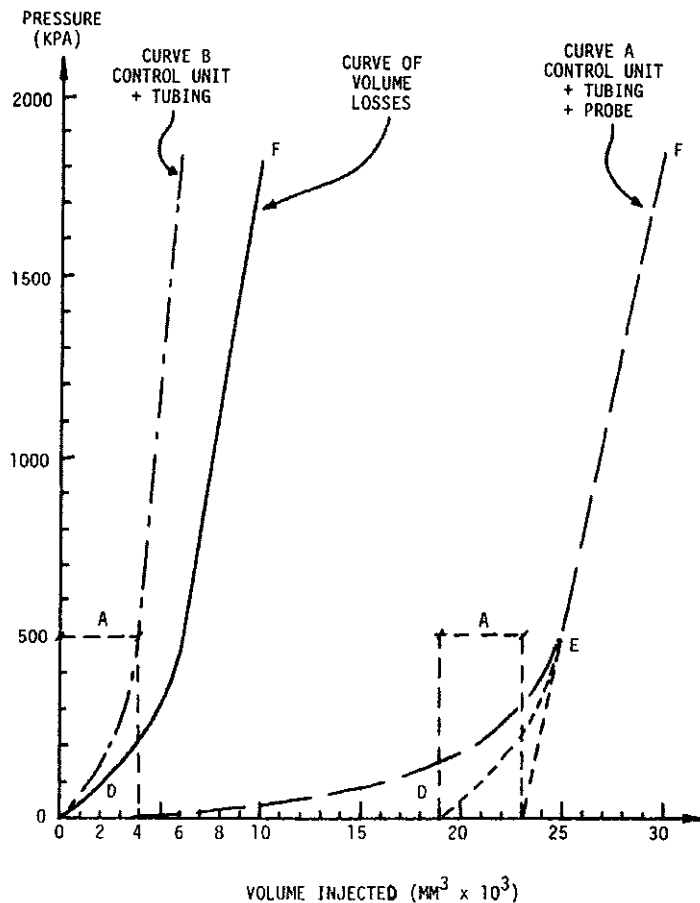


Figure 51 System compliance correction for the PENCEL Pressuremeter (Briaud and Shields, 1979, reprinted, with permission, copyright ASTM)

As with other pressuremeters, the parameters determined are the limit pressure and pressuremeter modulus. The PENCEL limit pressure is defined as the pressure required to double the probe volume, or more simply the maximum pressure during the test. On the other hand, the modulus could come from many portions of the

pressuremeter curve. Due to probe insertion, the initial modulus,  $E_i$ , may not be that reliable. Other portions of the PENCEL curve that could be used for calculating stiffness are an unload-reload loop, if available, and the final unload portion of the test. These moduli are referred to as  $E_{UR}$  and  $E_{UL}$ , respectively. Figure 52 shows these moduli and the limit pressure on an arbitrary pressuremeter test.

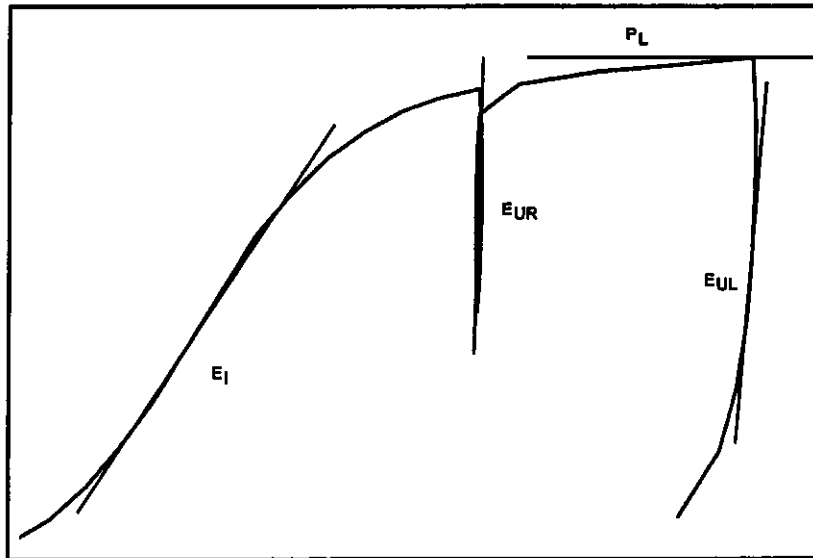


Figure 52 PENCEL Pressuremeter curve with limit pressure and moduli denoted

Calculation of the PENCEL Pressuremeter modulus is identical to the Ménard method:

$$E_{PMT} = 2(1 + \mu) \left[ V_c + \frac{V_o + V_f}{2} \right] \left[ \frac{p_f - p_o}{V_f - V_o} \right]$$

Where:

$\mu$  is Poisson's Ratio

$V_c$  is the initial volume of the pressuremeter

$V_o$  and  $p_o$  are the first point on the linear portion of the pressuremeter curve

$V_f$  and  $p_f$  are the final points on the linear portion of the pressuremeter curve

### University of Florida electric cone truck

All of the insitu tests performed by the University of Florida were done utilizing the electric cone penetration testing vehicle, shown in Figure 53. As the name implies, the primary use of this vehicle is for cone penetration testing. The truck was purchased with matching funds from the National Science Foundation and the University of Florida College of Engineering (Davidson and Bloomquist, 1986). Fortunately, other penetration type testing devices have been adapted for use with this equipment including, for this research, the PENCEL Pressuremeter. Other devices include the dilatometer, BAT groundwater system and piston sampler.

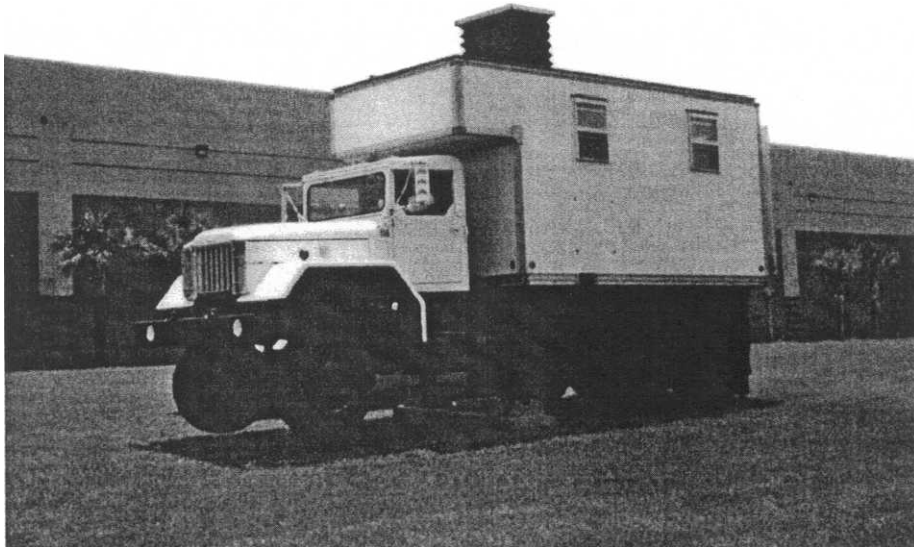


Figure 53 The University of Florida electric cone truck

### Test Sites

Three research tests sites were established where field tests were performed and laboratory samples were collected for analysis.

### Florida State Road 20 Site Swift/Sanders Creek

The first specimen tested was collected at State Road 20 Swift/Sanders Creek near Niceville, Florida. Maintenance problems helped establish this site as a research location. Differential settlements were occurring around a heavily trafficked five-lane bridge. Compressible soils on either side of the bridge were causing the approaches to settle while the bridge maintained level. The FDOT district asked UF to look at the problem, and then predict what future settlements would occur if different remedial measures were taken.

FDOT characterized the site by three standard penetration tests and over 50 cone penetration tests. Since the project was going to be modeled using a finite element program, the UF Geotechnical Numerical Group desired some stiffness values for the soil at the site, particularly layers that had not been tested in the lab (i.e. not Shelby tube sampled).

The University of Florida provided support to FDOT to conduct PENCEL Pressuremeter and dilatometer tests on the east (STA 381+00) and west (STA 380+25) sides of the bridge at Swift/Sanders Creek. Of the collected data, a single pressuremeter test overlapped with the Shelby tubes collected. A consolidated drained triaxial test was performed on sand from Tube 7 at the Florida Department of Transportation State Materials Office. Figure 54 shows the location of the field borings and soundings. Stratigraphy based on standard penetration tests is shown in Figure 55. The corrected PENCEL Pressuremeter curves from 5 depths are shown in Figures 56 and 57. Finally a triaxial test is detailed in Figures 58 and 59. Additional insitu test data can be found in the appendix.

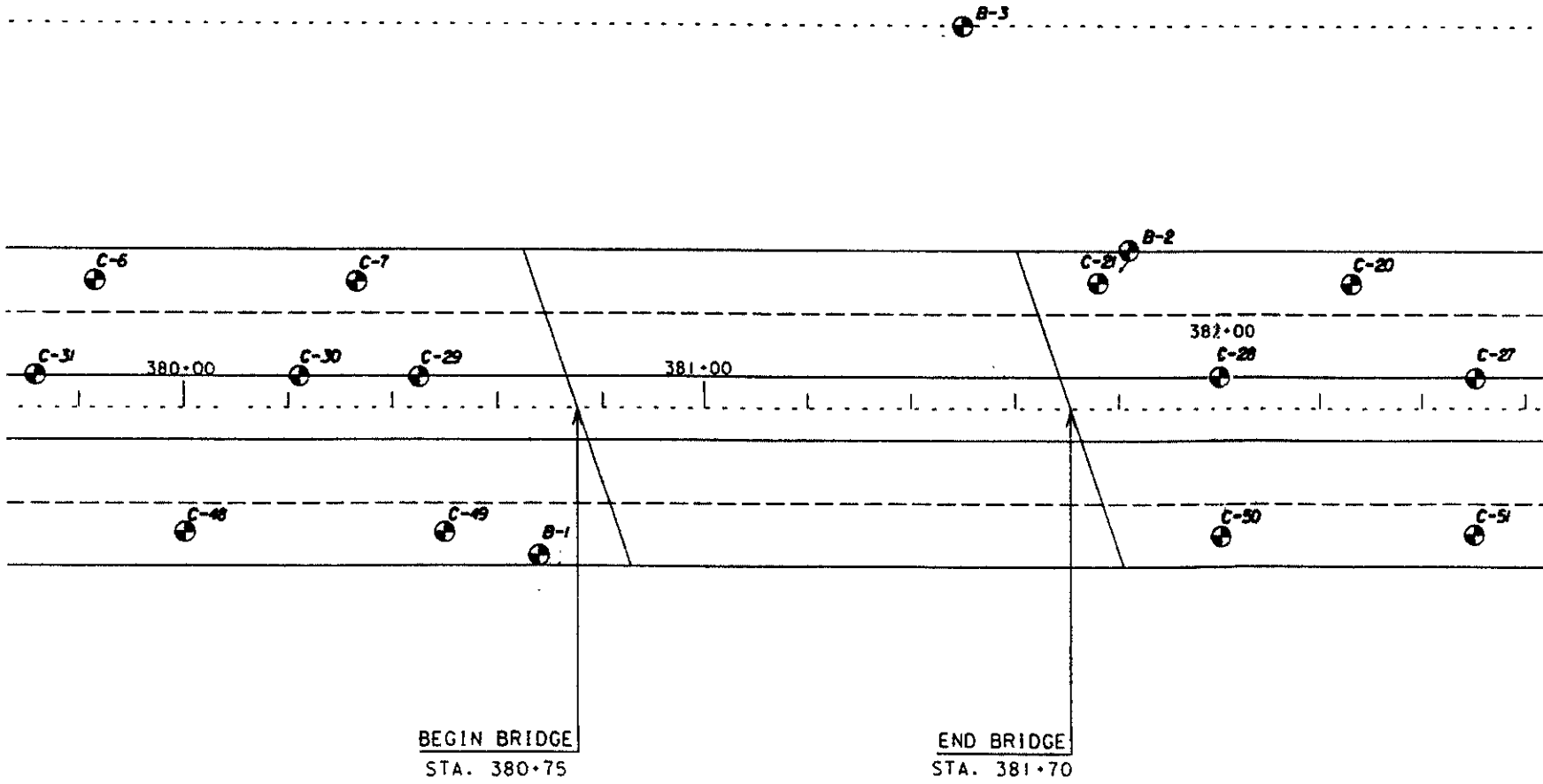


Figure 54 Plan view of soil exploration at State Road 20 Swift/Sanders Creek



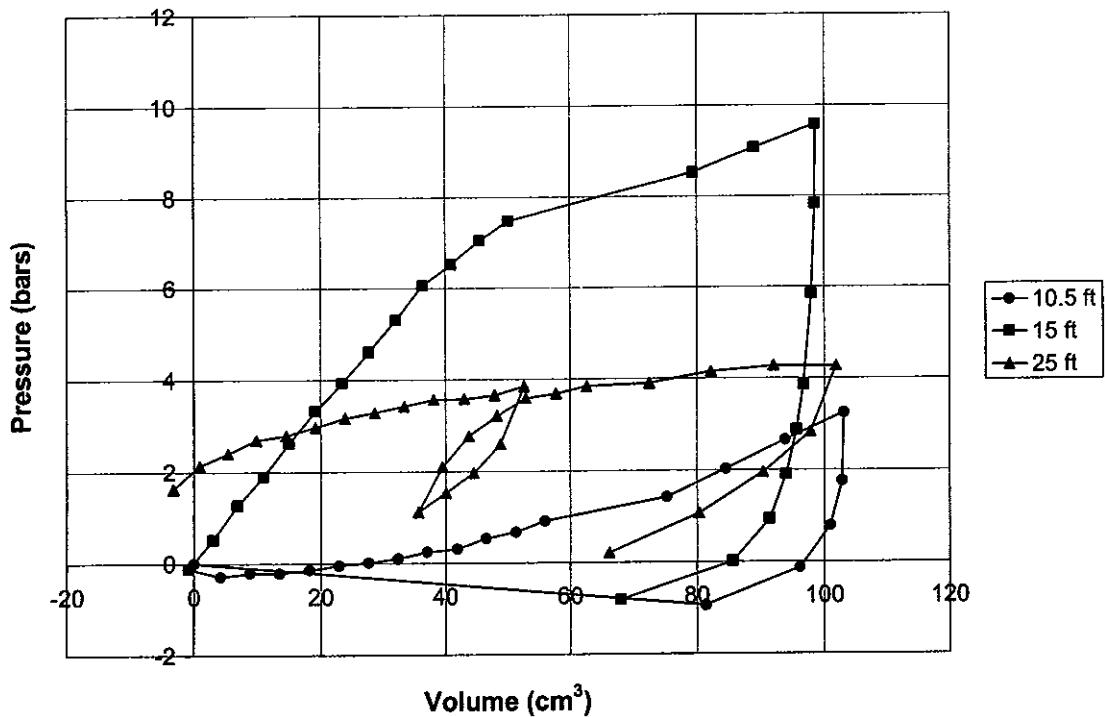


Figure 56 PENCIL Pressuremeter tests at State Road 20 Swift/Sanders Creek at depths 10.5-25 ft

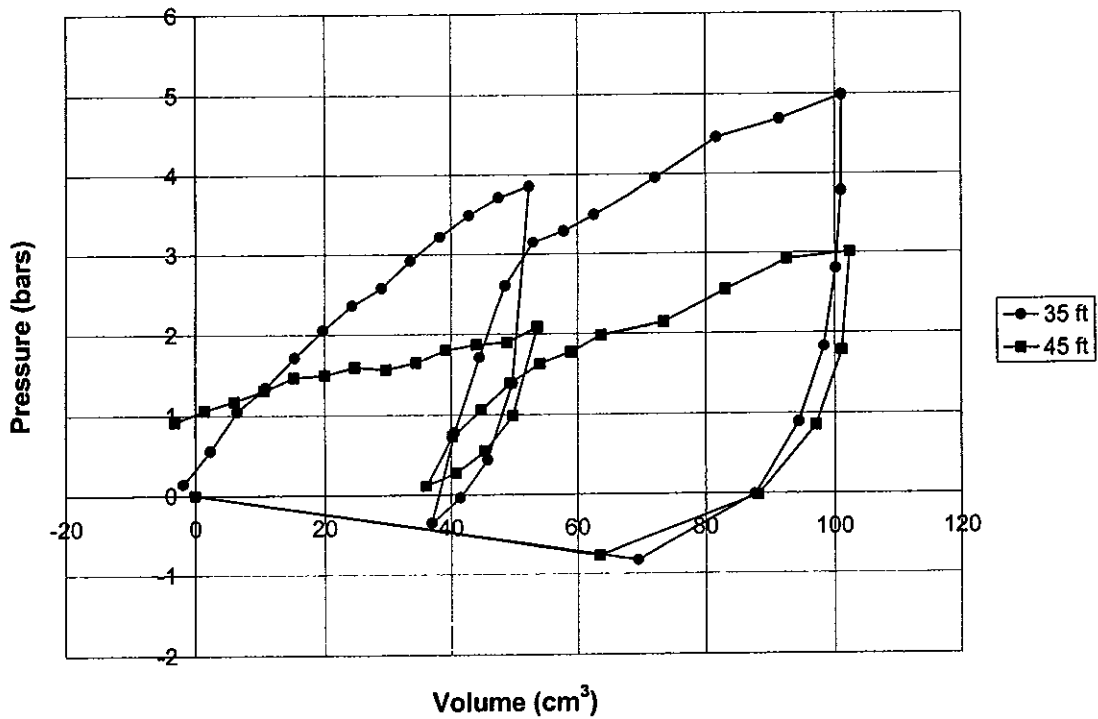


Figure 57 PENCIL Pressuremeter tests at State Road 20 Swift/Sanders Creek at depths 35-45 ft

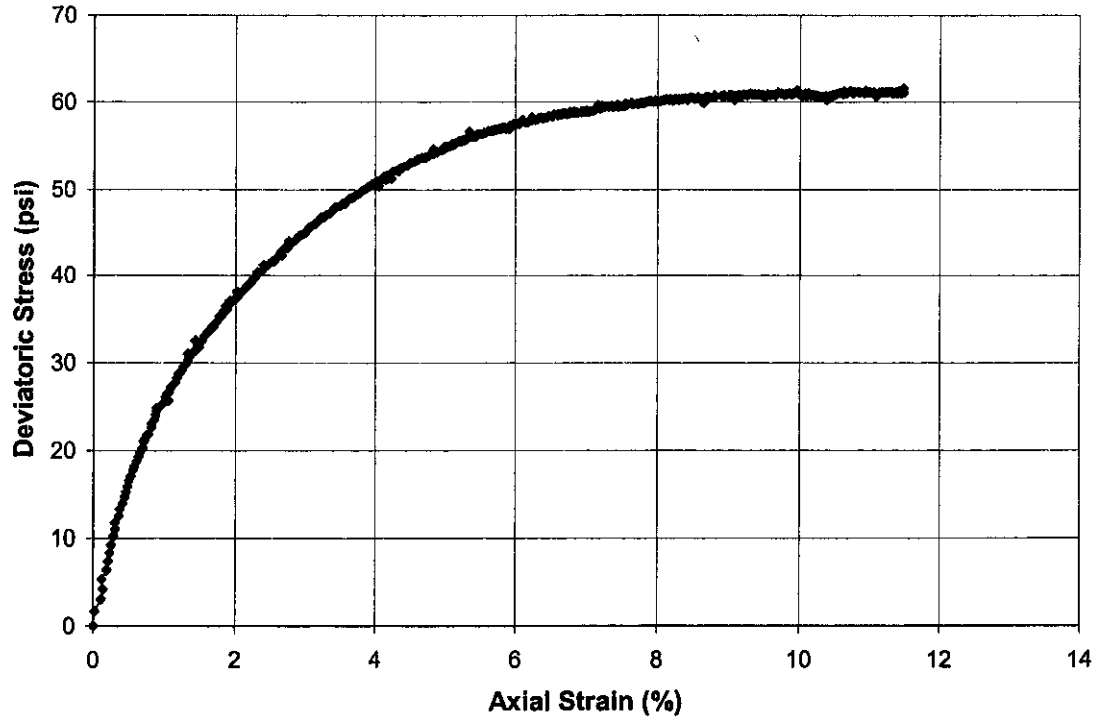


Figure 58 Consolidated drained triaxial test of tube 7 specimen 2 from State Road 20 Swift/Sanders Creek at depth 34 ft

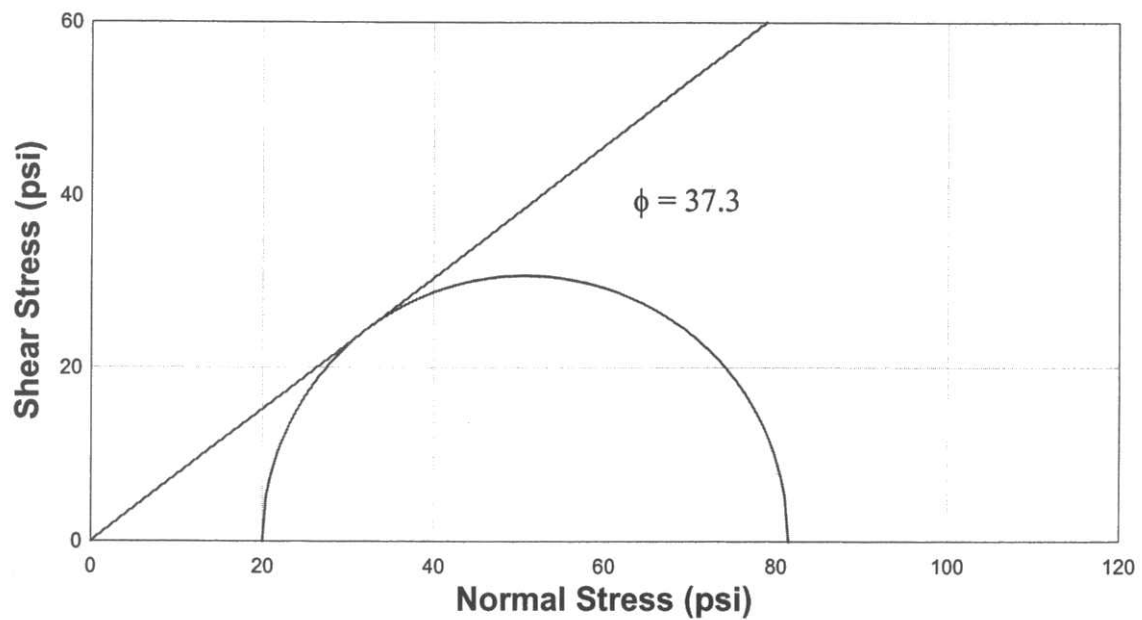


Figure 59 Mohr-Coulomb envelope for consolidated drained triaxial test of tube 7 specimen 2 from State Road 20 Swift/Sanders Creek at depth 34 ft

Soil parameters from the depth of Tube 7 are shown in Table 9. All of the possible values for PENCEL Pressuremeter modulus are shown in Table 10.

Table 9 Summary of soil parameters from lab and insitu tests on State Road 20 Swift/Sanders Creek at the depth of tube 7

Tube Depth (ft.)	$\phi$ TRIAX (°)	$E_{50}$ TRIAX (psi)	N (blows)	qc (psi)	$\phi$ CPT (°)	$\phi$ DMT (°)	$K_o$ DMT (-)	E DMT (psi)	M DMT (psi)	Limit Pressure (psi)	E PMT (psi)
34.0	37.3	2300.0	6.0	486.4	32.0	36.0	0.61	2436.0	3422.0	72.2	3726.5

Table 10 Summary of possible PENCEL moduli from pressuremeter a tests at State Road 20 Swift/Sanders Creek at the depth of tube 7

Tube Depth (ft)	$E_i$ PMT (psi)	EUR apexes PMT (psi)	EUR Secant PMT (psi)	MAX E UL Secant PMT (psi)	MIN E UL Secant PMT (psi)	MAX EUL Tangent PMT (psi)	MIN EUL Tangent PMT (psi)
34.0	556.1	2069.7	(--)	186528.0	1964.8	186528.0	1191.9

#### University of Florida Southwest Recreation Center Site

Five consolidated drained triaxial tests were conducted on material collected for the Southwest Recreation Center site on the University of Florida Campus. Boring logs were secured from the initial construction of (Universal Testing) and the current addition to (Law/Gibb Engineering) the Southwest Recreation Center. After reviewing borings from the site, and due to the existence of shallow sand layers, the site was chosen. Cone penetration tests and a dilatometer test were conducted by the UF Geotechnical insitu class. Universal Testing donated the time and labor for the collection of eight Shelby tubes. Finally, two PENCEL Pressuremeter tests were conducted at the site as the construction project began in the fall of 2000.

Due to time elapsed between the collection of Shelby tubes at this site and triaxial tests, a complication arose. The moisture contained in the soil caused corrosion of the tube walls thereby locking the soil inside. The specimens were often difficult to extract, resulting in lost and disturbed samples. It should be duly noted that all of the specimens from this site might suffer from preloading and disturbance. Therefore, after testing material from the first three tubes, the remaining five tubes were abandoned. A total of five consolidated drained triaxial tests were conducted on material from the three viable tubes.

The locations of the standard penetration test borings are shown in Figure 60. All of the tests were performed in the vicinity of B12. The log of standard penetration test B12 is shown in Figure 61. Corrected PENCEL Pressuremeter results are included as Figures 62 through 64. Lastly, triaxial tests are shown in Figures 65 through 70. Additional insitu test data can be found in the appendix.

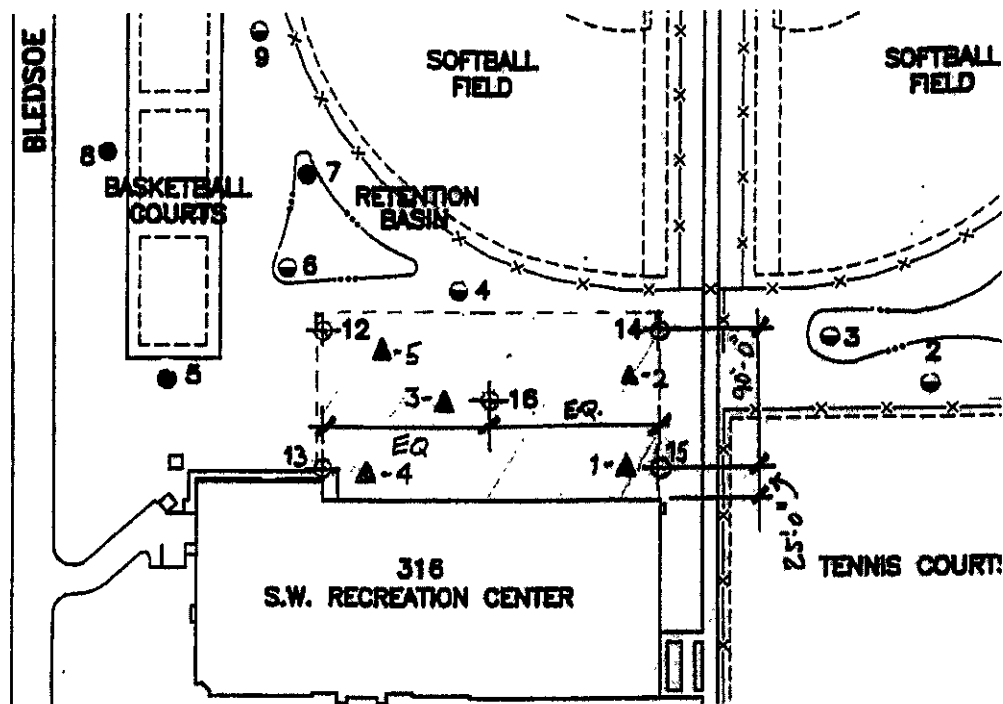


Figure 60 Plan view of soil exploration at Southwest Recreation Center

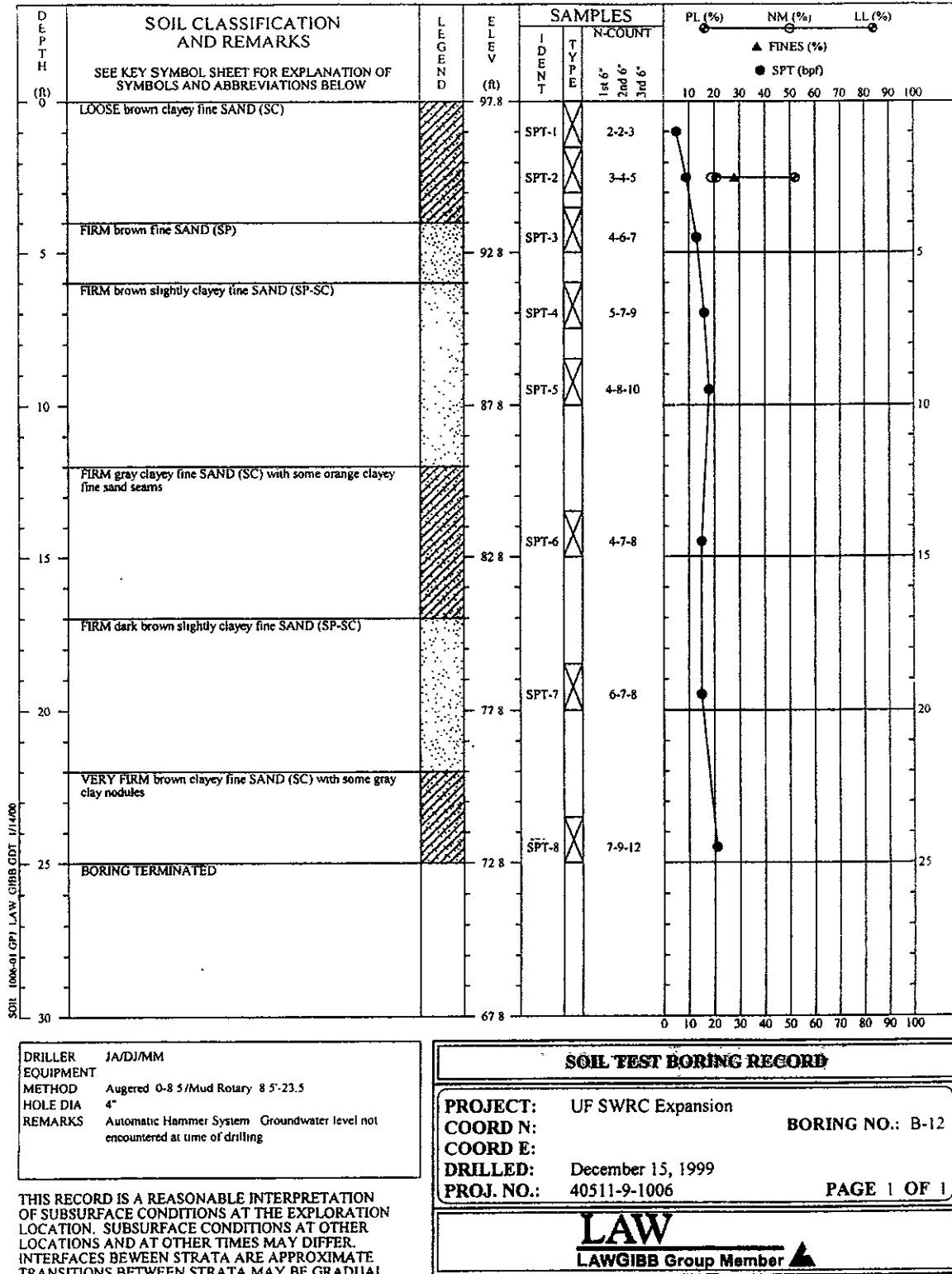


Figure 61 Standard penetration test boring B1 at Southwest Recreation Center

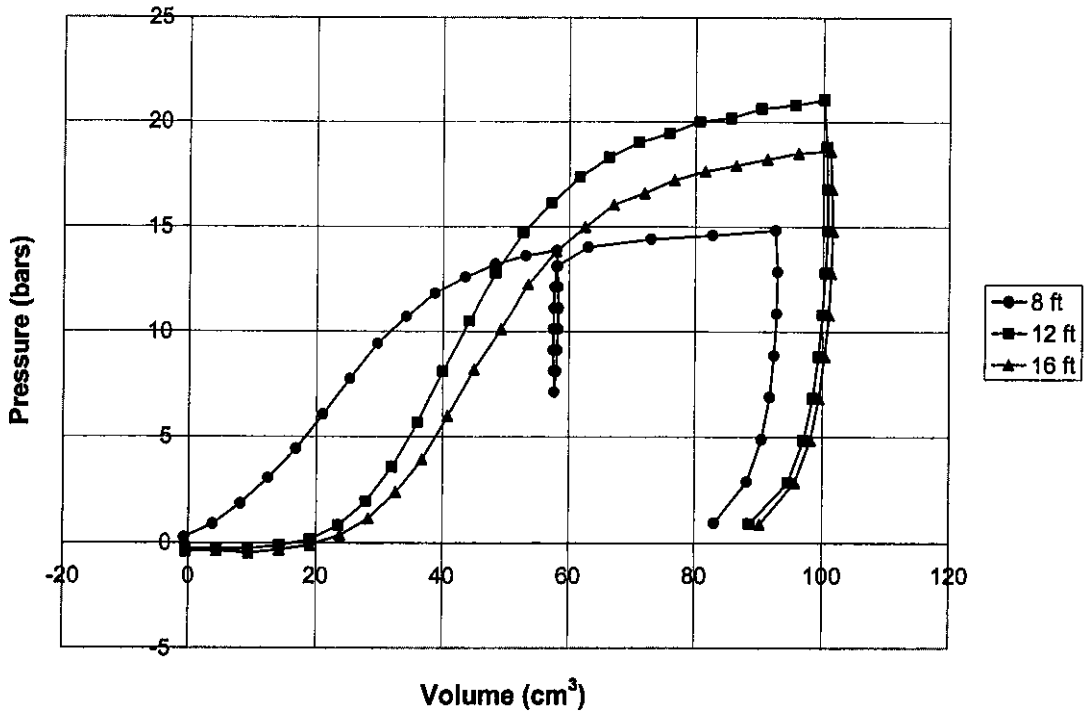


Figure 62 PENCEL Pressuremeter tests at Southwest Recreation Center at depths 8-16 ft

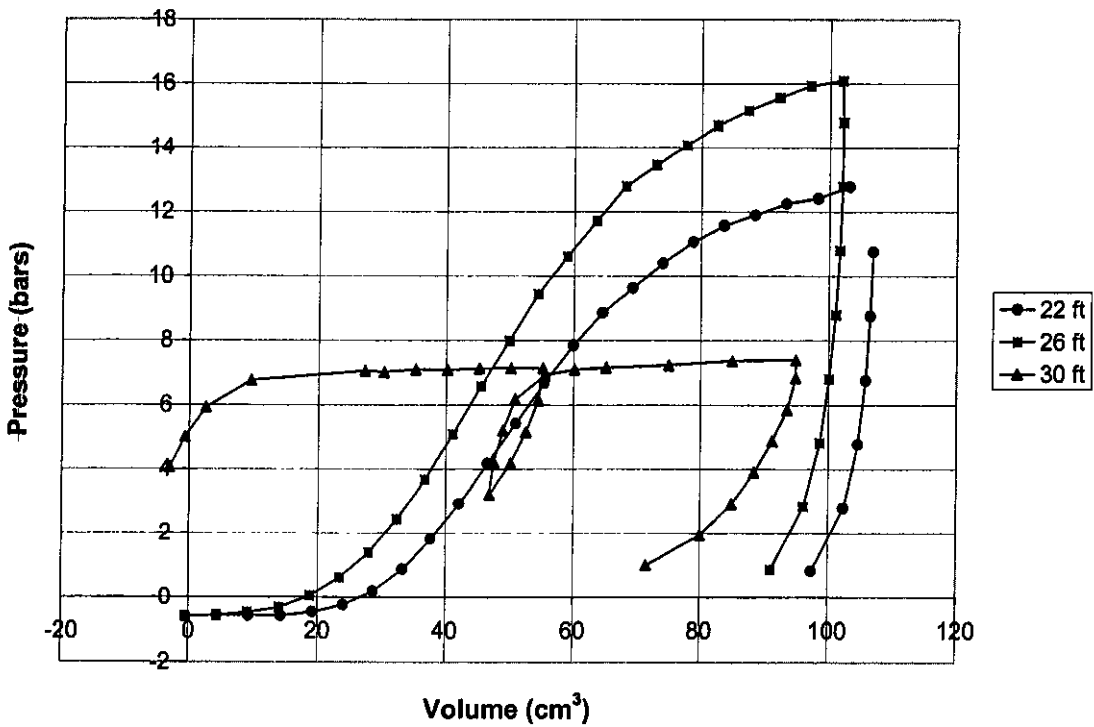


Figure 63 PENCEL Pressuremeter tests at Southwest Recreation Center at depths 22-30 ft

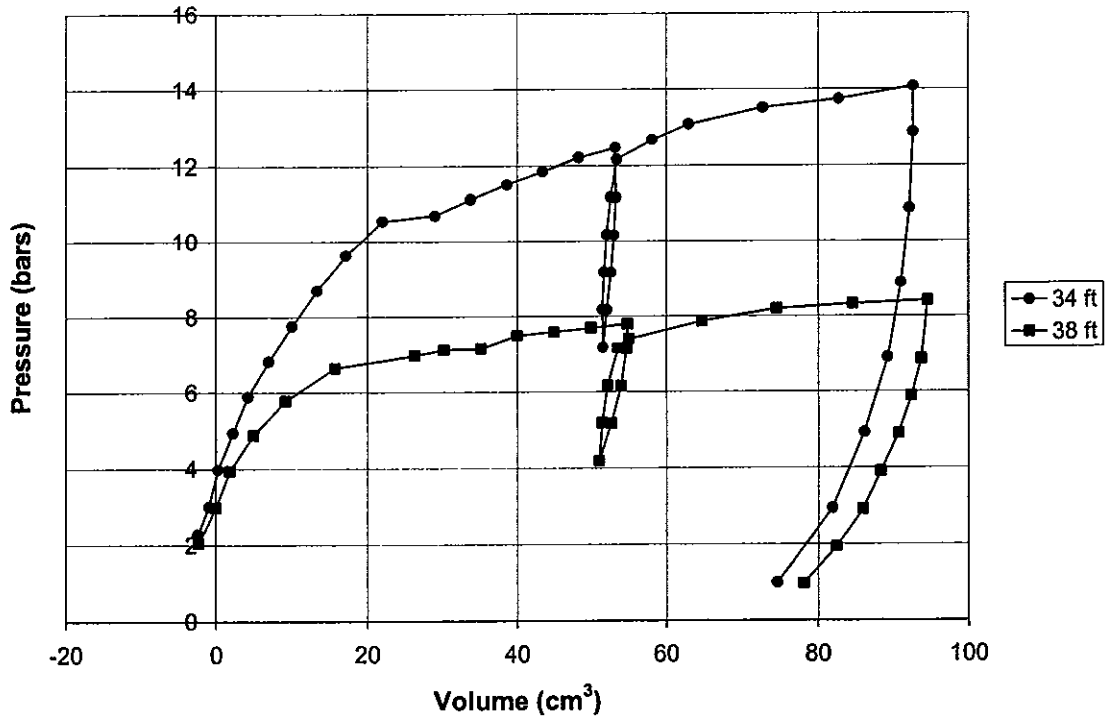


Figure 64 PENCEL Pressuremeter tests at Southwest Recreation Center at depths 34-38 ft

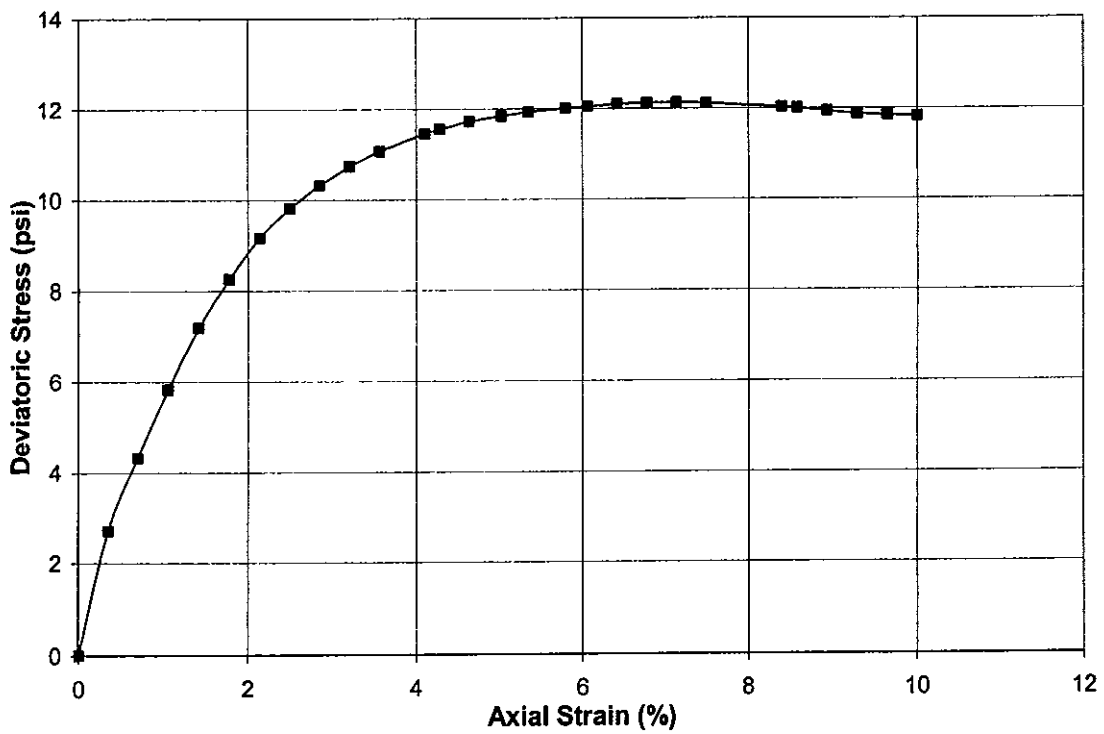


Figure 65 Consolidated drained triaxial test of tube 1 from Southwest Recreation Center at depth 10-12 ft

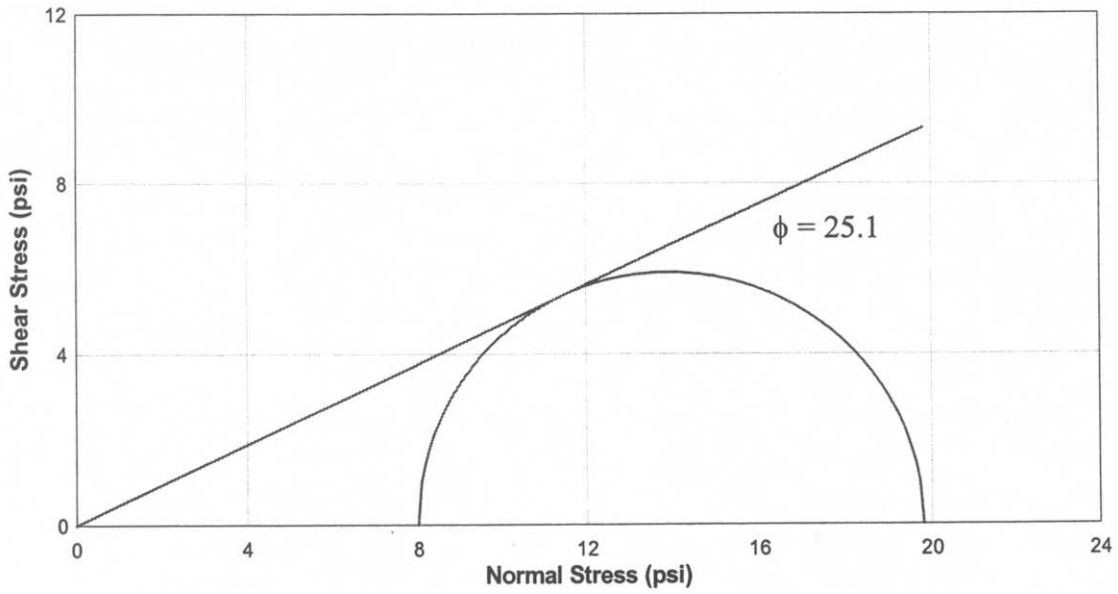


Figure 66 Mohr-Coulomb envelope for consolidated drained triaxial test from tube 1 at Southwest Recreation Center at depth 10-12 ft

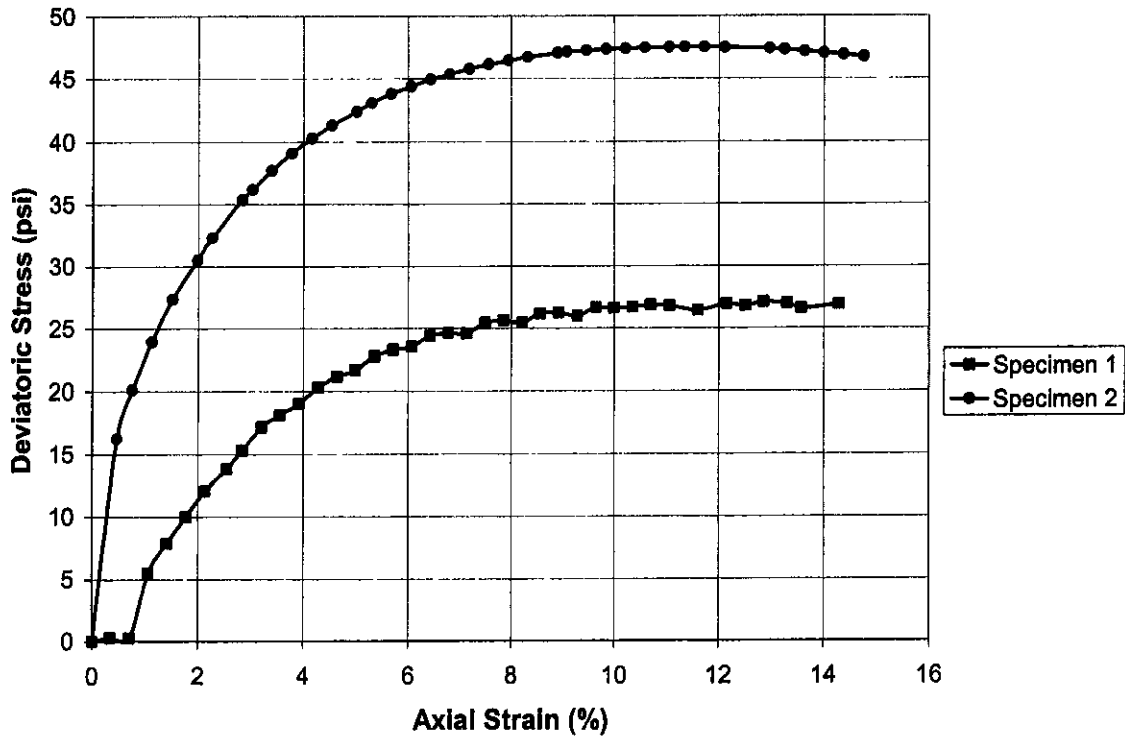


Figure 67 Consolidated drained triaxial tests of tube 2 from Southwest Recreation Center at depth 14-16 ft

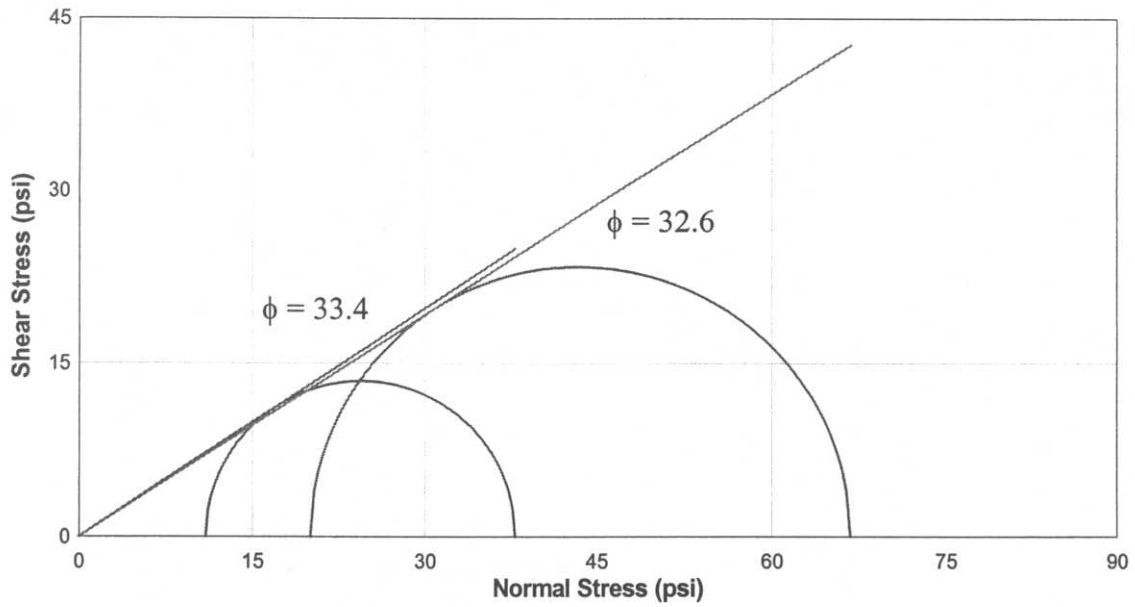


Figure 68 Mohr-Coulomb envelope for consolidated drained triaxial tests of tube 2 from Southwest Recreation Center at depth 14-16 ft

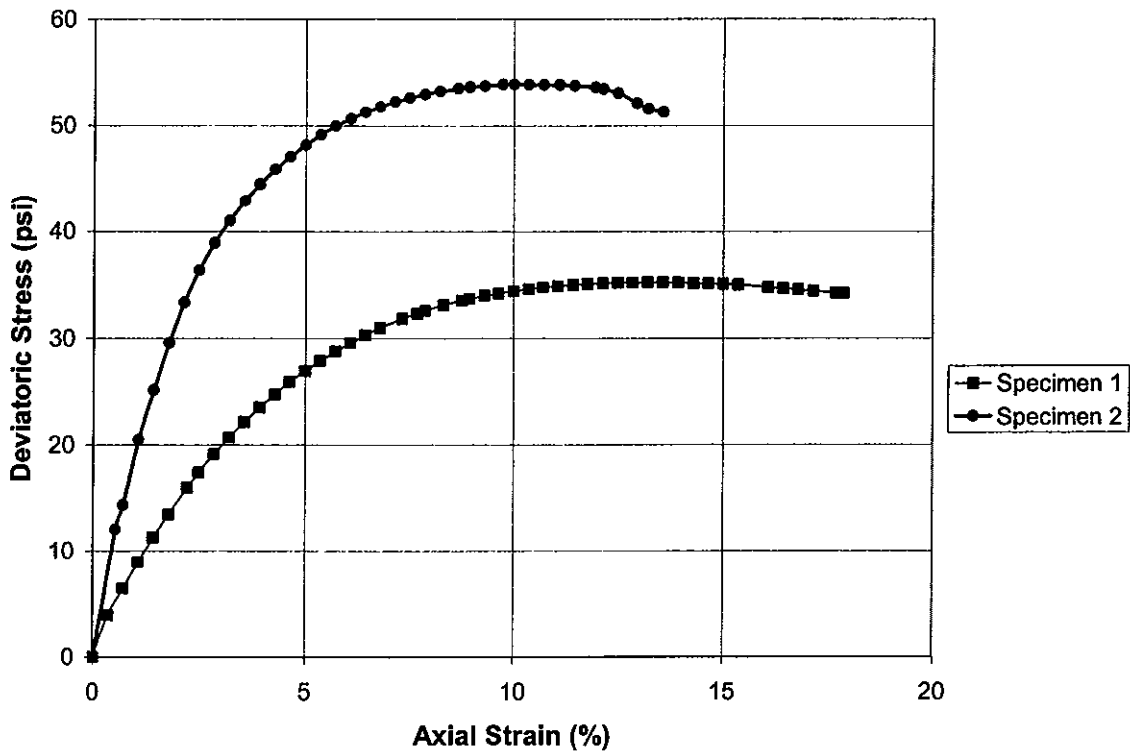


Figure 69 Consolidated drained triaxial tests of tube 3 from Southwest Recreation Center at depth 18-20 ft

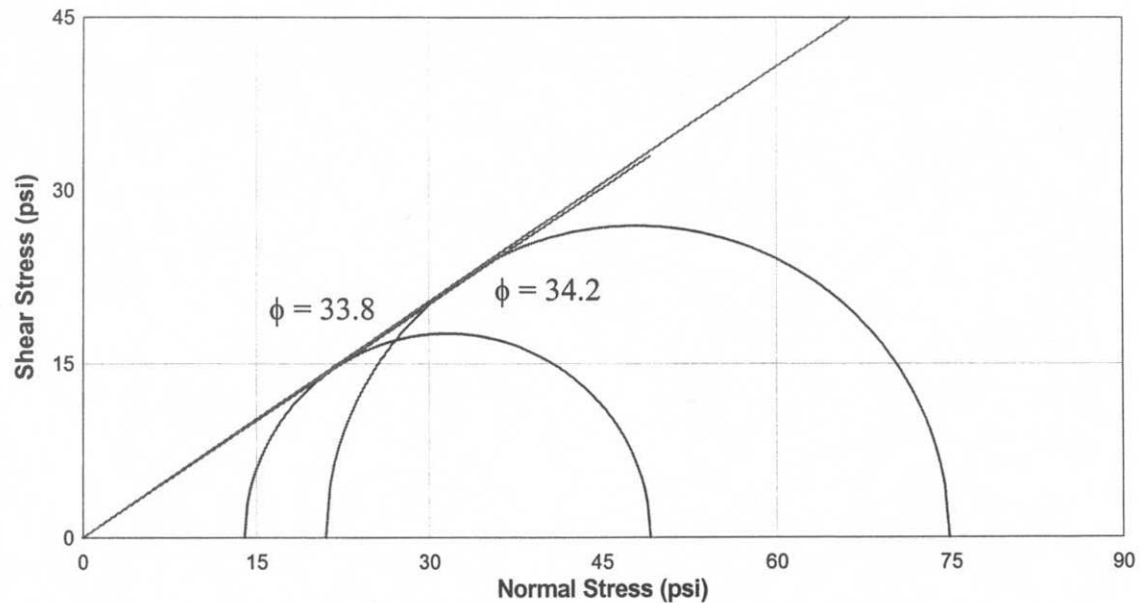


Figure 70 Mohr-Coulomb envelope for consolidated drained triaxial tests of tube 3 from Southwest Recreation Center at depth 18-20 ft

Soil parameters corresponding to the depths where Shelby tube samples were tested are shown in Table 11. All of the possible values for PENCEL Pressuremeter moduli are shown in Table 12.

Table 11 Summary of soil parameters from lab and insitu tests at the Southwest Recreation Center

Tube Depth (ft.)	$\phi$ TRIAX (°)	$E_{50}$ TRIAX (psi)	N (blows)	$q_c$ (psi)	$\phi$ CPT (°)	$\phi$ DMT (°)	$K_o$ DMT (-)	E DMT (psi)	M DMT (psi)	Limit Pressure (psi)	E PMT (psi)
11.0	25.1	540.0	16.0	1830.4	45.0	44.0	2.59	11136.0	36221.0	214.6	42093.5
15.0	34.5 33.3	830.0 2000.0	18.0	839.8	41.0	41.0	3.55	9715.0	34075.0	305.2	44080.0
19.0	33.8 34.2	700.0 1800.0	15.0	686.0	39.0	46.0	2.06	11455.0	35844.0	269.7	48879.5

Table 12 Summary of possible PENCEL moduli from pressuremeter a tests at Southwest Recreation Center

Tube Depth (ft)	Ei PMT (psi)	EUR apexes PMT (psi)	EUR Secant PMT (psi)	MAX E UL Secant PMT (psi)	MIN E UL Secant PMT (psi)	MAX EUL Tangent PMT (psi)	MIN EUL Tangent PMT (psi)
11.0	3190.0	160051.0	(--)	421065.5	4988.0	181308.0	4096.3
15.0	4925.7	(--)	(--)	919050.6	19436.8	70380.1	3540.9
19.0	4471.8	(--)	(--)	594268.0	18188.8	103074.7	3951.3

### Alachua County Landfill

To complete the laboratory testing, a third set of Shelby tubes was collected at the Alachua County Landfill in Archer, Florida. This site was chosen for accessibility. For several years the Archer Landfill has allowed the University of Florida to conduct research on their grounds. Furthermore, the landfill staff provided a location where there was at least forty feet of sand overlying limerock.

With this site secured, CPT tests were conducted to verify the stratigraphy. Once again, Universal Testing donated time to collect 4 Shelby tubes at the site and perform 4 Standard Penetration Tests. The fourth tube, from depth 19 to 20 ft, had poor take and may have been disturbed by the drilling crew during collection. The final tests to be completed at the site were PENCEL Pressuremeter and dilatometer soundings.

Knowing that the material contained in tubes from this location was fairly clean sand, we realized that extraction might compromise the materials. Therefore, the decision was made to cut the tubes to test length, and then freeze them for at least 48 hours before extraction and trimming. This method worked extremely well. The average 3 percent moisture provided enough virtual cohesion when frozen to allow for extraction

and trimming as well as placement of the specimen in the triaxial chamber. Six specimens were tested from these four tubes.

A sketch of the approximate location of all borings and soundings is shown in Figure 71. The field boring log for the standard penetration test performed at the site is included as Figure 72. Figures 73 and 74 show the corrected PENCEL Pressuremeter curves. Finally, the six triaxial tests performed on the Archer Landfill sands are shown in Figures 75 through 82. Additional insitu test data can be found in the appendix.

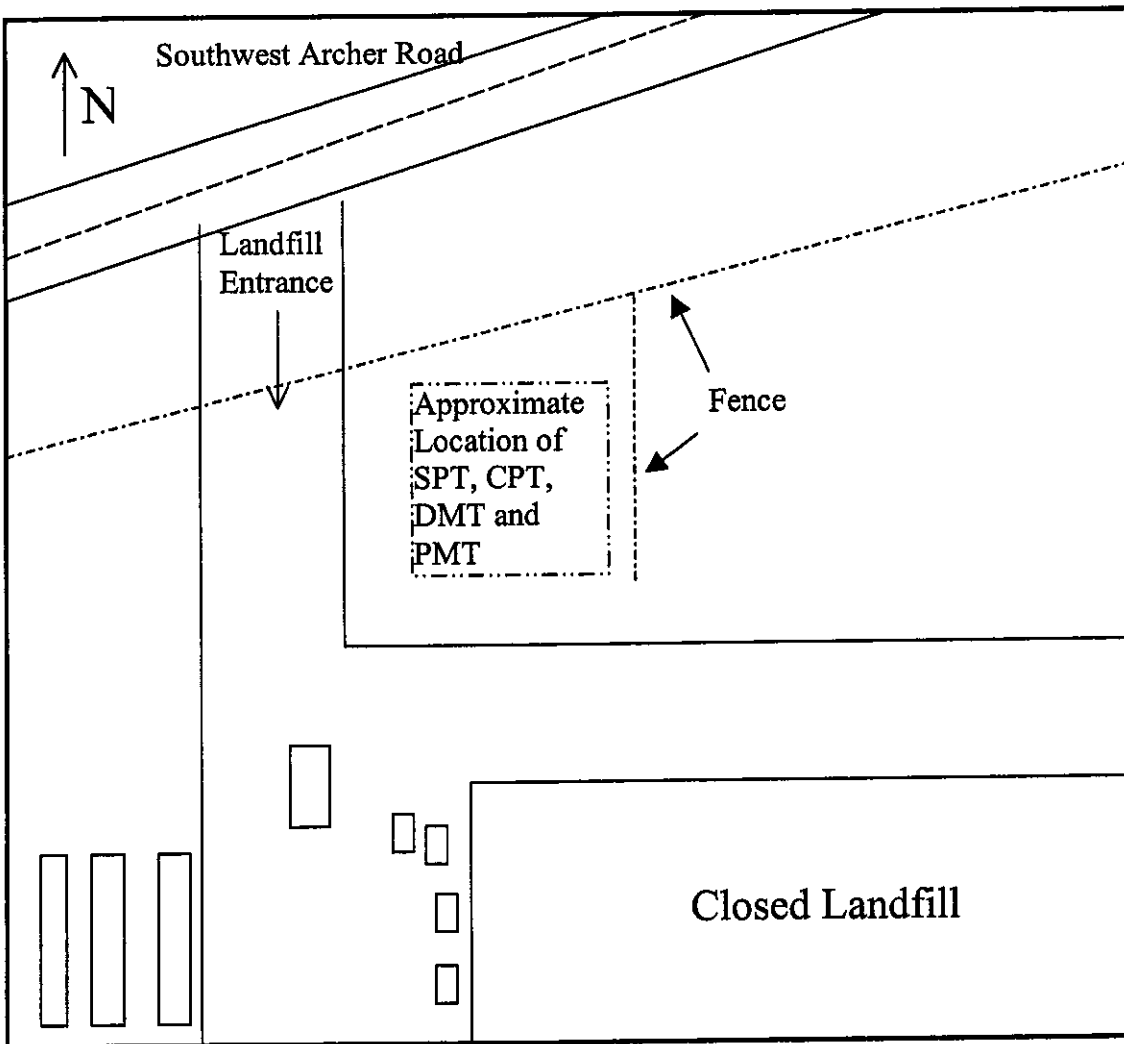


Figure 71 Plan view sketch of soil exploration at the Alachua County Landfill in Archer, Florida

FIELD LOG OF BORING										B-1	
PROJECT: Archer Landfill					CLIENT: U of F			W.O. NUMBER: 502		DATE STARTED: 10/25/00	
DRILLED BY:					RIG:			ELEVATION (DATUM):		TOTAL DEPTH: 22.5'	
					SURFACE CONDITIONS:					WATER DEPTH:	
										DATE:	
										TIME:	
SAMPLE TYPE	SAMPLE NUMBER	SET #	2 IN	3 IN	N VALUE	SAMPLE RECOV.	DEPTH (FT.)	LOG	CLASSIFICATION OF MATERIAL	REMARKS	
							1		tan fine sand		
							2				
							3				
							4				
							5		Shelby Tube #1	spooned 6-7.5'	
1	1	1	1	2			6		t.f.s.		
							7				
							8				
							9		shelby tube #2		
							10			spooned 11-12.5'	
2	1	2	3				11		t.f.s.		
							12				
							13				
							14				
							15		shelby tube #3		
3	2	2	3				16		t.f.s.	spooned 16-17.5'	
							17				
							18				
							19				
							20		shelby tube #4		
4	2	4	7				21		t.f.s.	spooned 21-22.5'	
							22				
							23				
							24				
							25				
							26				
							27				
							28				
							29				
							30				
							31				
							32				

6/1/88 - Universal Engineering Sciences

Figure 72 Standard penetration test boring B1 at Archer Landfill

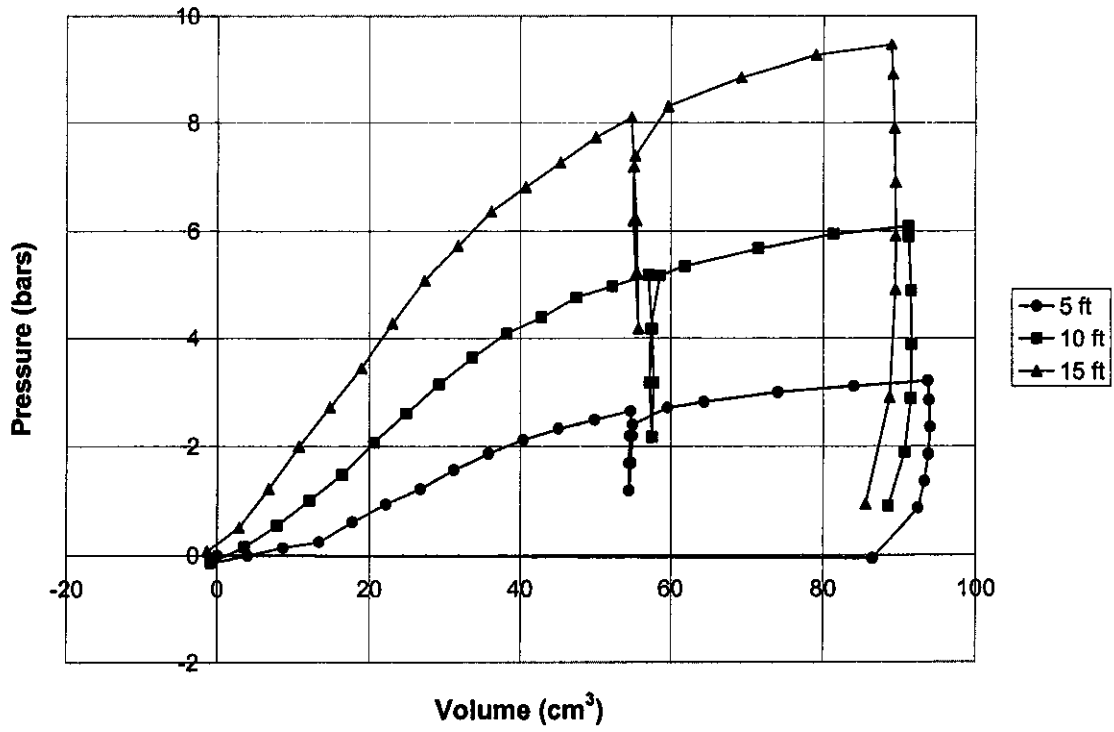


Figure 73 PENCIL Pressuremeter tests at Archer Landfill at depths 5-15 ft

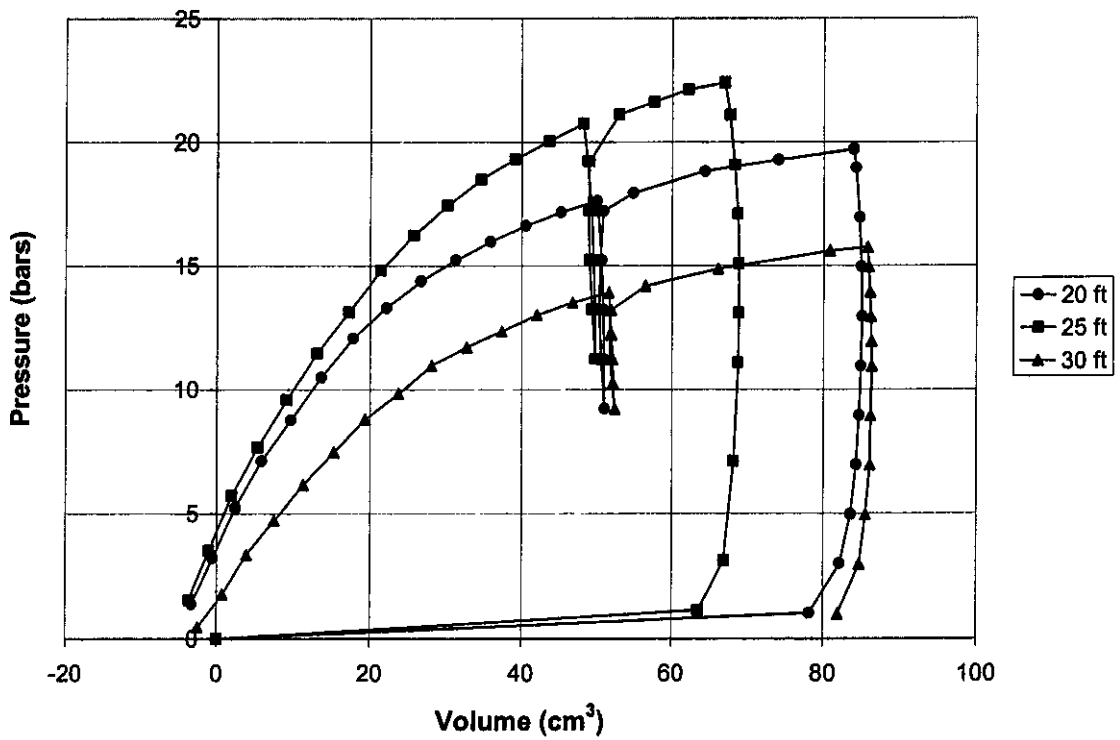


Figure 74 PENCIL Pressuremeter tests at Archer Landfill at depths 20-30 ft

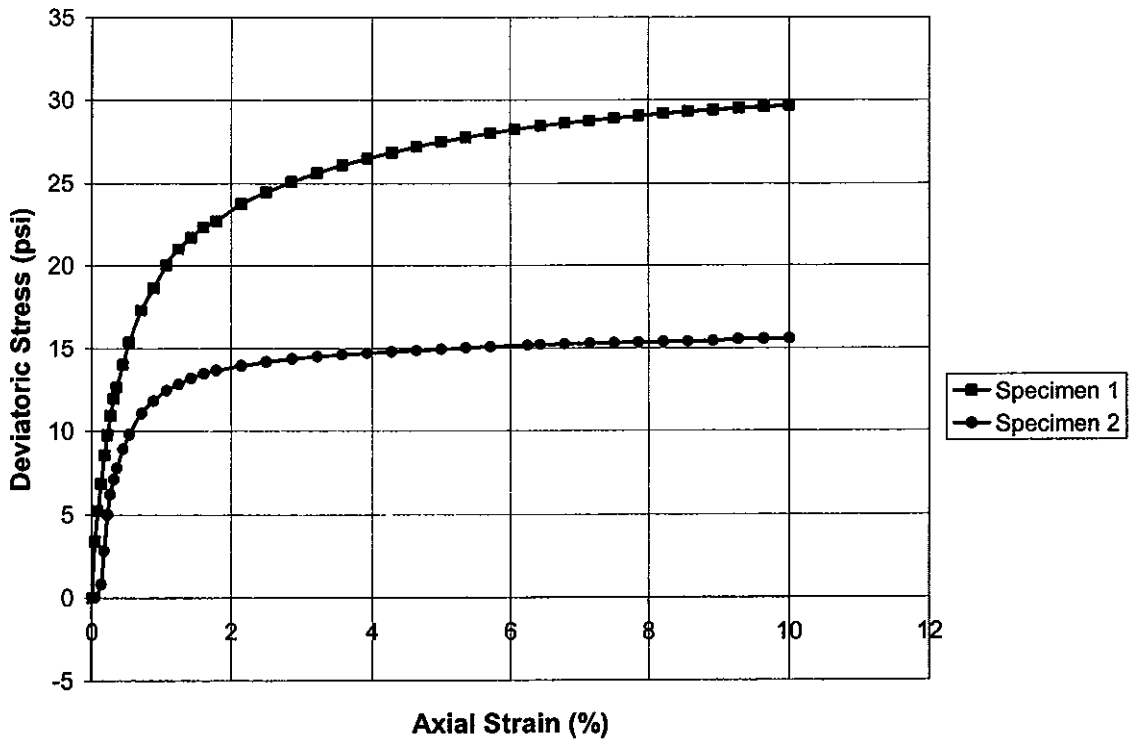


Figure 75 Consolidated drained triaxial tests of tube 1 from Archer Landfill at depth 4-6 ft

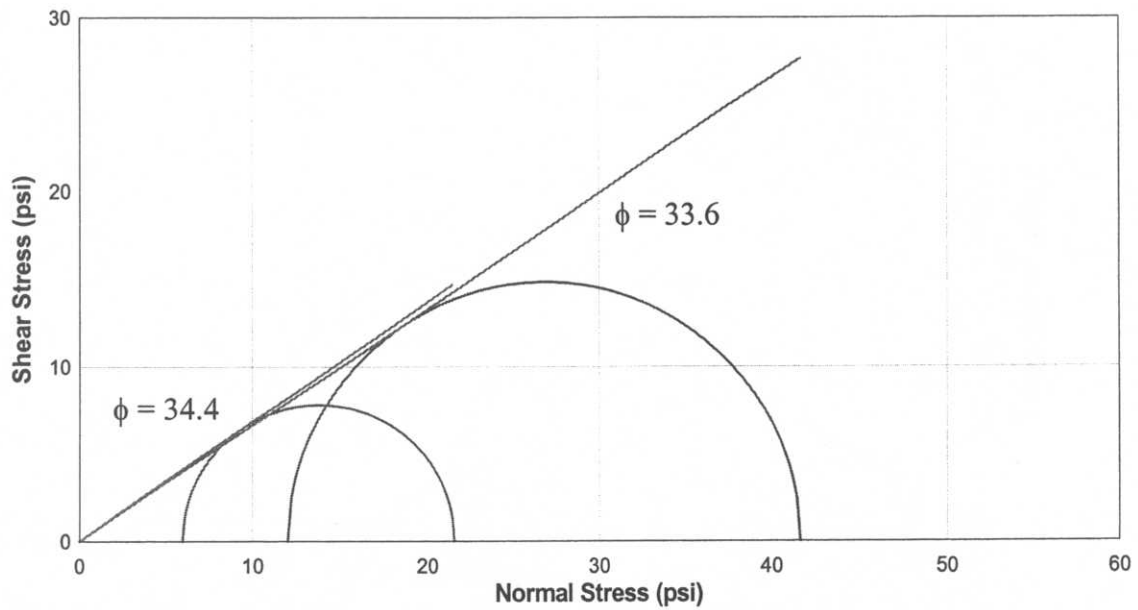


Figure 76 Mohr-Coulomb envelope for consolidated drained triaxial tests of tube 1 from Archer Landfill at depth 4-6 ft

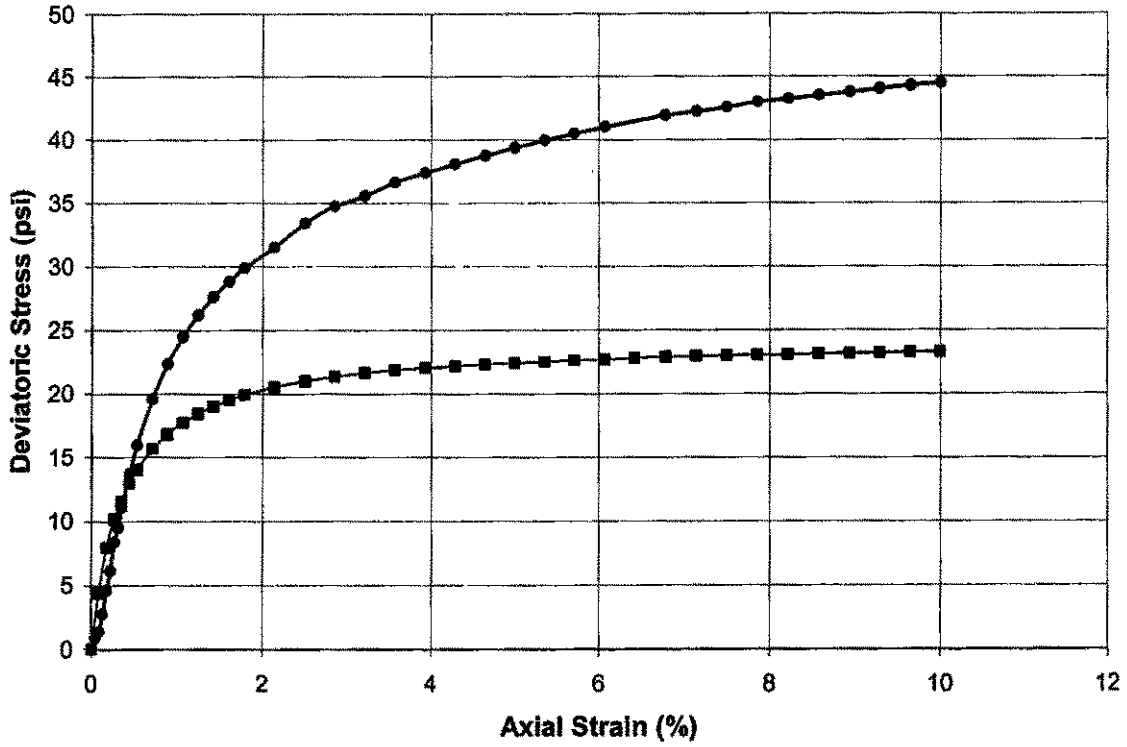


Figure 77 Consolidated Drained Triaxial tests of tube 2 from Archer Landfill at depth 9-11 ft

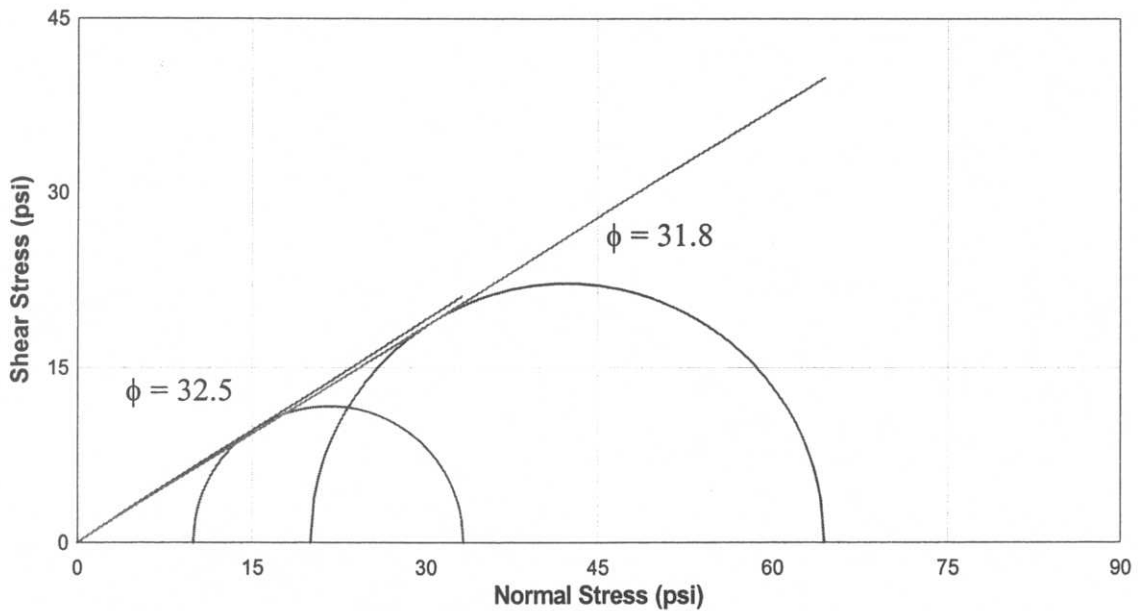


Figure 78 Mohr-Coulomb envelope for consolidated drained triaxial tests of tube 2 from Archer Landfill at depth 9-11 ft

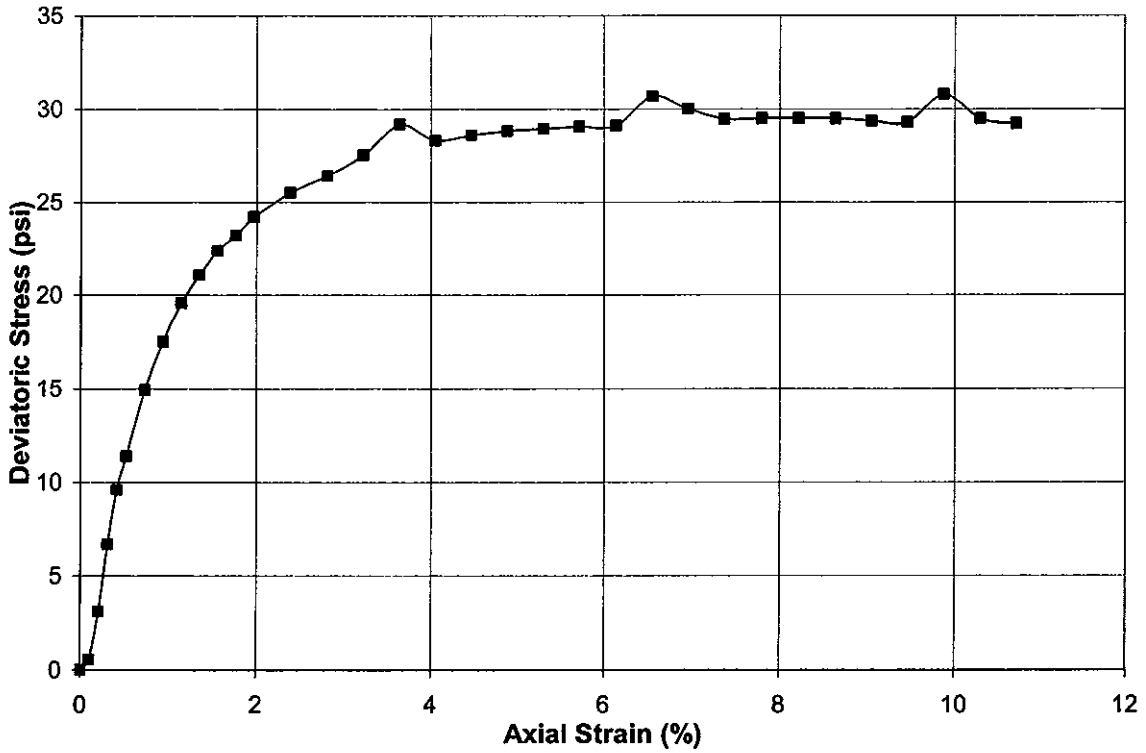


Figure 79 Consolidated drained triaxial test of tube 3 from Archer Landfill at depth 14-16 ft

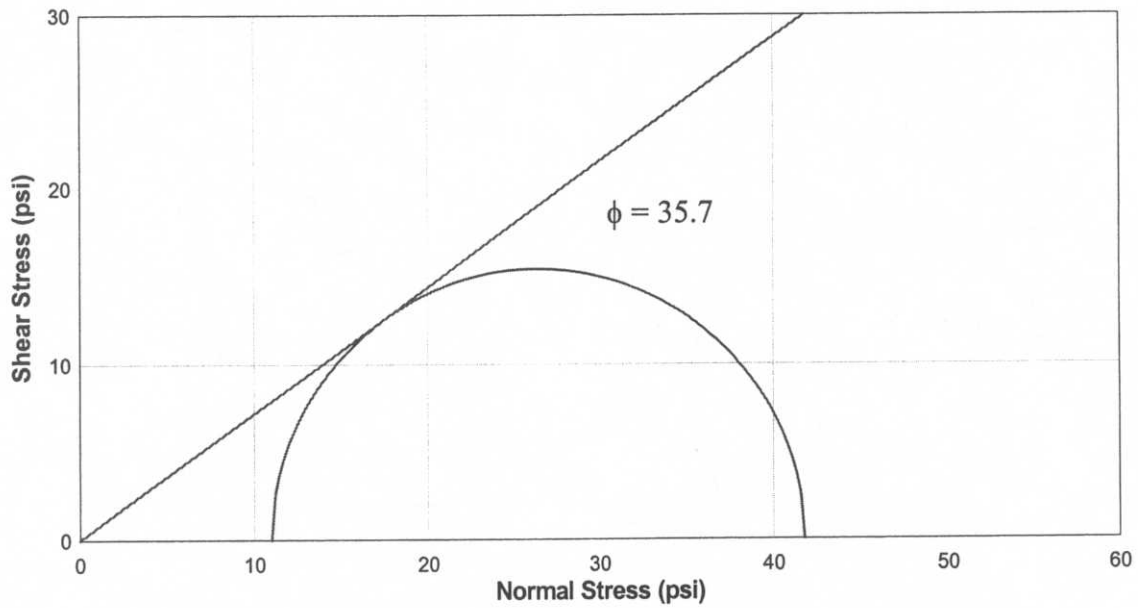


Figure 80 Mohr-Coulomb envelope for consolidated drained triaxial test of tube 3 from Archer Landfill at depth 14-16 ft

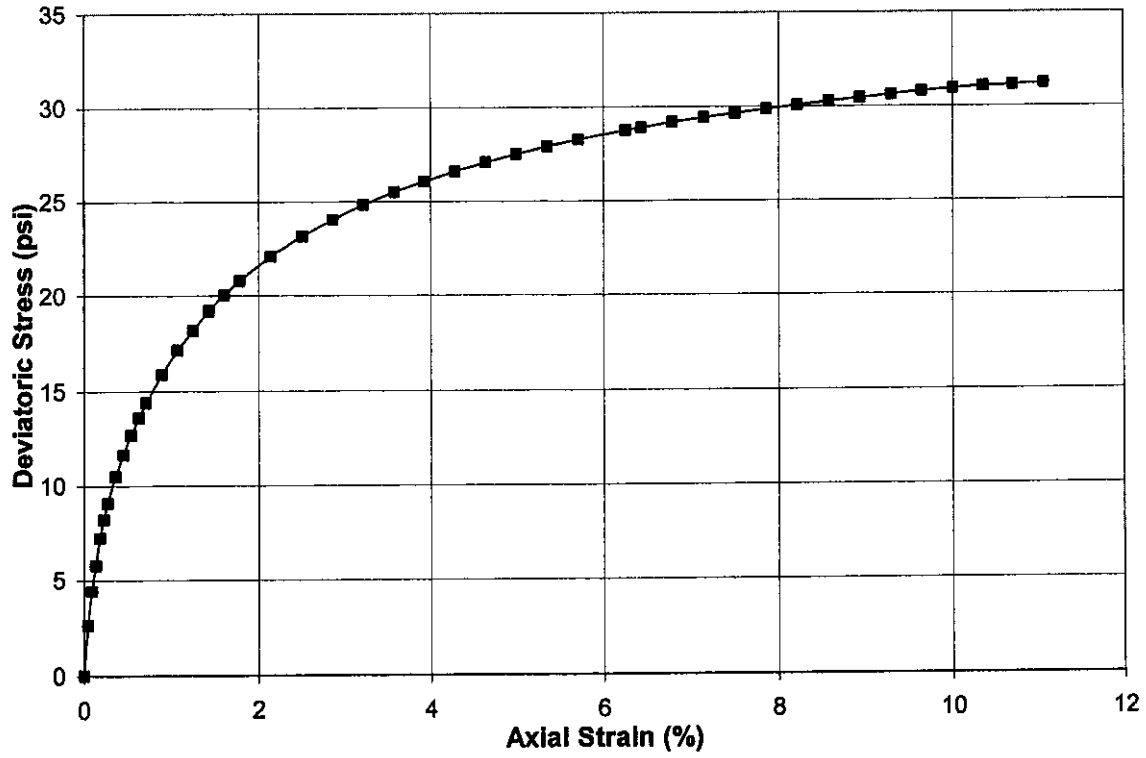


Figure 81 Consolidated drained triaxial test of tube 4 from Archer Landfill at depth 19-21 ft

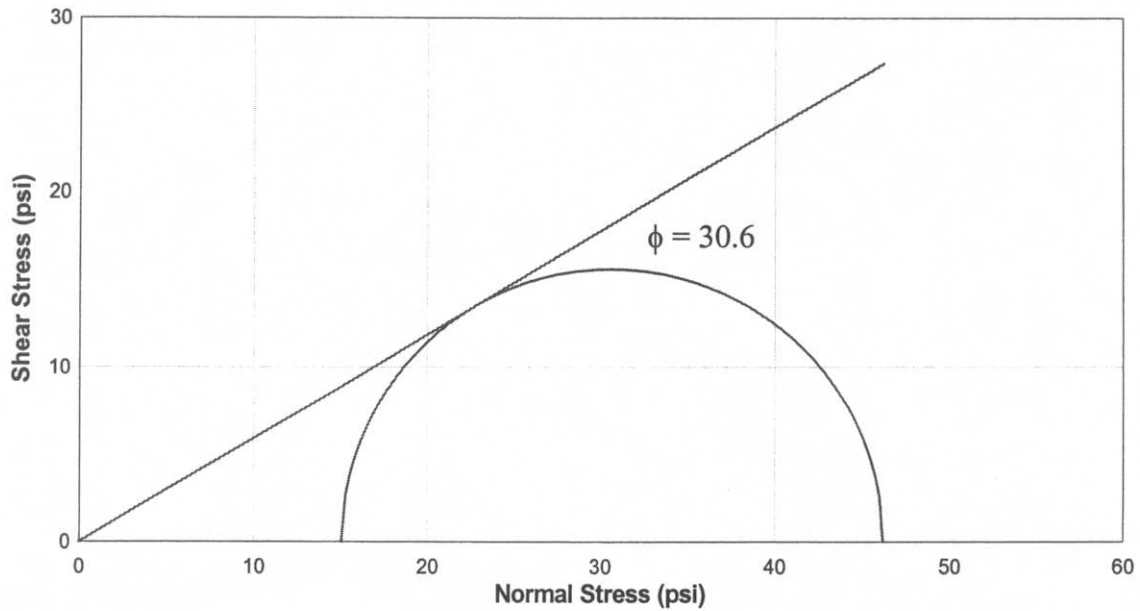


Figure 82 Mohr-Coulomb envelope for consolidated drained triaxial test of tube 4 from Archer Landfill at depth 19-21 ft

Soil parameters corresponding to the depths where Shelby tube samples were tested are shown in Table 13. All of the possible values for PENCEL Pressuremeter moduli are shown in Table 14.

Table 13 Summary of soil parameters from lab and insitu tests at the Archer Landfill

Tube Depth (ft.)	$\phi$ TRIAX (°)	$E_{50}$ TRIAX (psi)	N (blows)	qc (psi)	$\phi$ CPT (°)	$\phi$ DMT (°)	$K_o$ DMT (-)	E DMT (psi)	M DMT (psi)	Limit Pressure (psi)	E PMT (psi)
5.0	33.6 34.4	2863.0 2172.0	3.0	293.0	39.0	47.0	0.34	1508.0	3697.5	46.4	14601.5
10.0	31.8 32.5	2498.0 3217.0	5.0	488.8	39.0	45.6	0.12	1870.5	2189.5	88.2	23200.0
15.0	35.7	2041.0	5.0	838.3	39.0	44.6	0.17	2827.5	3262.5	137.2	42572.0
20.0	30.6	1775.0	11.0	1360.5	41.0	44.1	0.20	3987.5	4553.0	285.7	71006.5

Table 14 Summary of possible PENCEL moduli from pressuremeter a tests at the Archer Landfill

Tube Depth (ft.)	$E_i$ PMT (psi)	EUR apexes PMT (psi)	EUR Secant PMT (psi)	MAX E UL Secant PMT (psi)	MIN E UL Secant PMT (psi)	MAX EUL Tangent PMT (psi)	MIN EUL Tangent PMT (psi)
5.0	591.0	24567.4	356241.8	44877.5	4857.5	23040.5	1696.5
10.0	1074.5	27558.7	399591.0	93612.0	21634.0	93365.5	5031.5
15.0	1539.9	(--)	(--)	411205.5	24223.7	2000652.0	6706.3
20.0	3719.3	(--)	(--)	112824.5	18707.9	137837.0	5302.7

## CHAPTER 5 FINITE ELEMENT SIMULATIONS

### Triaxial Tests

As a starting point for the determination of soil properties based on the pressuremeter, a well-defined problem was tackled. The triaxial test is a tried and true method of determining stiffness and strength properties of soil. Many geotechnical theories are calibrated to the Mohr-Coulomb failure criterion that the triaxial test is often used to define. Furthermore, many of the constitutive relationships were derived based on and/or calibrated to the triaxial test. In addition, the triaxial boundary conditions are easy to impose. This makes finite element mesh generation simple.

Every attempt was made to perform the triaxial tests at the same effective stress as existed in the original soil profile. As typically done, the effective confining pressure and the maximum deviatoric stresses were used to construct Mohr's Circles for the tests. The effective friction angle was determined based on these circles. There was no apparent cohesion observed during any of the tests, but a small value was used for numerical stability. Since the stress strain curve for sand is hyperbolic rather than linear, a modulus value was not so readily apparent. Therefore the  $E_{50}$  value was used. This is the secant modulus between the origin and the point on the stress strain curve corresponding to 50% of the maximum deviatoric load.

Since PlasFEM parameters were not necessarily so obvious, several assumptions, equalities and omissions were made. In the Drucker-Prager model,  $\alpha$  was

assumed to be a very small value corresponding to the arbitrary cohesion. The slope of the failure envelope was calculated using an equation derived by Pinto (1998):

$$\theta = \frac{2 \sin \phi}{\sqrt{3}(3 - \sin \phi)}$$

which corresponds to the triaxial compression stress path. Plotting the invariant stress paths and imposing the Drucker-Prager failure surface easily verified this relationship. Table 15 and Figure 83 show the spreadsheet and plot of a triaxial test in invariant stress space. The invariants in this case are  $I_1 = \sigma_1 + 2 \sigma_3$  and  $\sqrt{J_2}$  which is defined by  $(\sigma_1 - \sigma_3)/\sqrt{3}$ . Originally, the  $E_{50}$  stiffness was used for the simulations, the same for the Plaxis model. It was quickly noted that  $E_{50}$  was too soft. Through iteration, it was determined that  $1.5 * E_{50}$  would be a sufficient modulus.

As mentioned previously, the hardening soil model utilizes a hyperbolic model for stress and strain under the failure surface and a hardening cap. Some advanced parameters are needed to define this portion of the relationship. The one-dimensional stiffness,  $E_{oed}$ , was safely assumed to be identical to  $E_{50}$ . This follows the recommendation of the Plaxis authors. Stress level dependency is controlled by the parameter in which for sandy soils is typically 0.5. The unload-reload stiffness was calculated as  $4 * E_{50}$ . The triaxial confining stress was chosen as  $p_{ref}$ . Failure ratio, which helps define the asymptote to which the stress strain curve converges, was always 0.9. Finally, there was no tension cutoff. The hardening part of the model uses no additional parameters. The cap is merely located by the initial stress and its shape is controlled by previously defined quantities.

The Sandler-Dimaggio model contains a curved failure surface that can be

Table 15 Spreadsheet used to verify triaxial test invariants

Point	STRESS TENSOR									I <sub>1</sub>	HYDROSTATIC TENSOR			DEVIATORIC STRESS TENSOR														
	T <sub>11</sub>	T <sub>12</sub>	T <sub>13</sub>	T <sub>21</sub>	T <sub>22</sub>	T <sub>23</sub>	T <sub>31</sub>	T <sub>32</sub>	T <sub>33</sub>		P <sub>11</sub>	P <sub>22</sub>	P <sub>33</sub>	S <sub>11</sub>	S <sub>12</sub>	S <sub>13</sub>	S <sub>21</sub>	S <sub>22</sub>	S <sub>23</sub>	S <sub>31</sub>	S <sub>32</sub>	S <sub>33</sub>	J2	(J2) <sup>1/2</sup>				
1	8.0				8.0				8.0	24.0	8.0	8.0	8.0	0.0	0	0	0	0.0	0	0	0	0.0	0	0	0	0.0	0.0	0.0
2	10.7				8.0				8.0	26.7	8.9	8.9	8.9	1.8	0	0	0	-0.9	0	0	0	-0.9	0	0	0	-0.9	2.4	1.6
3	12.3				8.0				8.0	28.3	9.4	9.4	9.4	2.9	0	0	0	-1.4	0	0	0	-1.4	0	0	0	-1.4	6.2	2.5
4	13.8				8.0				8.0	29.8	9.9	9.9	9.9	3.9	0	0	0	-1.9	0	0	0	-1.9	0	0	0	-1.9	11.3	3.4
5	15.2				8.0				8.0	31.2	10.4	10.4	10.4	4.8	0	0	0	-2.4	0	0	0	-2.4	0	0	0	-2.4	17.2	4.1
6	16.3				8.0				8.0	32.3	10.8	10.8	10.8	5.5	0	0	0	-2.8	0	0	0	-2.8	0	0	0	-2.8	22.7	4.8
7	17.2				8.0				8.0	33.2	11.1	11.1	11.1	6.1	0	0	0	-3.1	0	0	0	-3.1	0	0	0	-3.1	28.0	5.3
8	17.8				8.0				8.0	33.8	11.3	11.3	11.3	6.5	0	0	0	-3.3	0	0	0	-3.3	0	0	0	-3.3	32.1	5.7
9	18.3				8.0				8.0	34.3	11.4	11.4	11.4	6.9	0	0	0	-3.4	0	0	0	-3.4	0	0	0	-3.4	35.4	6.0
10	18.7				8.0				8.0	34.7	11.6	11.6	11.6	7.2	0	0	0	-3.6	0	0	0	-3.6	0	0	0	-3.6	38.4	6.2
11	19.1				8.0				8.0	35.1	11.7	11.7	11.7	7.4	0	0	0	-3.7	0	0	0	-3.7	0	0	0	-3.7	40.8	6.4
12	19.4				8.0				8.0	35.4	11.8	11.8	11.8	7.6	0	0	0	-3.8	0	0	0	-3.8	0	0	0	-3.8	43.7	6.6
13	19.5				8.0				8.0	35.5	11.8	11.8	11.8	7.7	0	0	0	-3.8	0	0	0	-3.8	0	0	0	-3.8	44.4	6.7
14	19.7				8.0				8.0	35.7	11.9	11.9	11.9	7.8	0	0	0	-3.9	0	0	0	-3.9	0	0	0	-3.9	45.7	6.8
15	19.8				8.0				8.0	35.8	11.9	11.9	11.9	7.9	0	0	0	-3.9	0	0	0	-3.9	0	0	0	-3.9	46.7	6.8
16	19.9				8.0				8.0	35.9	12.0	12.0	12.0	7.9	0	0	0	-4.0	0	0	0	-4.0	0	0	0	-4.0	47.4	6.9
17	20.0				8.0				8.0	36.0	12.0	12.0	12.0	8.0	0	0	0	-4.0	0	0	0	-4.0	0	0	0	-4.0	48.0	6.9
18	20.0				8.0				8.0	36.0	12.0	12.0	12.0	8.0	0	0	0	-4.0	0	0	0	-4.0	0	0	0	-4.0	48.3	7.0
19	20.1				8.0				8.0	36.1	12.0	12.0	12.0	8.1	0	0	0	-4.0	0	0	0	-4.0	0	0	0	-4.0	48.8	7.0
20	20.1				8.0				8.0	36.1	12.0	12.0	12.0	8.1	0	0	0	-4.0	0	0	0	-4.0	0	0	0	-4.0	48.9	7.0
21	20.1				8.0				8.0	36.1	12.0	12.0	12.0	8.1	0	0	0	-4.0	0	0	0	-4.0	0	0	0	-4.0	49.0	7.0
22	20.1				8.0				8.0	36.1	12.0	12.0	12.0	8.1	0	0	0	-4.0	0	0	0	-4.0	0	0	0	-4.0	48.9	7.0
23	20.0				8.0				8.0	36.0	12.0	12.0	12.0	8.0	0	0	0	-4.0	0	0	0	-4.0	0	0	0	-4.0	48.2	6.9
24	20.0				8.0				8.0	36.0	12.0	12.0	12.0	8.0	0	0	0	-4.0	0	0	0	-4.0	0	0	0	-4.0	48.0	6.9
25	19.9				8.0				8.0	35.9	12.0	12.0	12.0	8.0	0	0	0	-4.0	0	0	0	-4.0	0	0	0	-4.0	47.5	6.9
26	19.9				8.0				8.0	35.9	12.0	12.0	12.0	7.9	0	0	0	-4.0	0	0	0	-4.0	0	0	0	-4.0	46.9	6.9
27	19.8				8.0				8.0	35.8	11.9	11.9	11.9	7.9	0	0	0	-3.9	0	0	0	-3.9	0	0	0	-3.9	46.7	6.8
28	19.8				8.0				8.0	35.8	11.9	11.9	11.9	7.9	0	0	0	-3.9	0	0	0	-3.9	0	0	0	-3.9	46.5	6.8

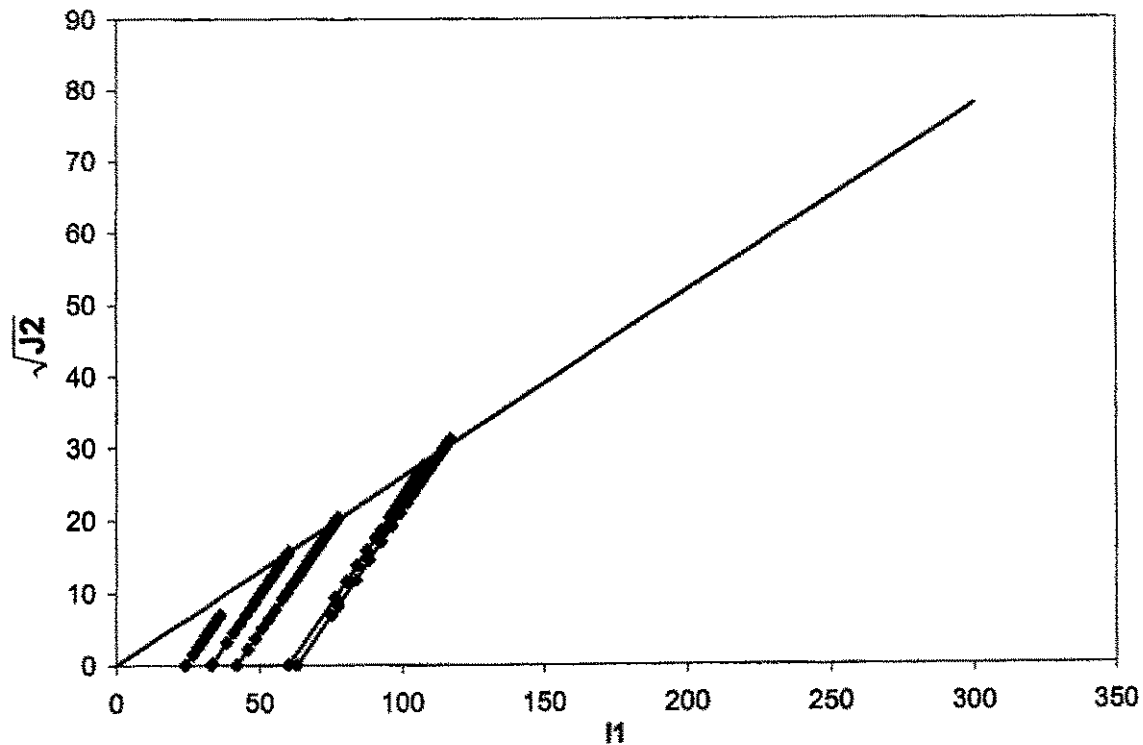


Figure 83 Invariant stress paths for triaxial tests at Southwest Recreation Center

reduced to that of the Drucker-Prager. Thus, for simplicity, the parameters  $\beta$  and  $\gamma$  are null. In addition to the failure surface and stiffness values, the Sandler-Dimaggio model requires input for the definition of a cap. Two of the parameters in the hardening law were actual measurable quantities. The preconsolidation pressure  $X_0$  was unique to each test. It was determined in conjunction with short iterations and by plotting the failure surface and stress path then superimposing the cap. The second parameter was  $W$ , the maximum volumetric plastic strain. This value could be estimated based on the volumetric data from the triaxial tests, but little confidence was associated with this number due to its extremely small magnitude and the difficulties in measurement.

The final two parameters for the model are R and D. R is the curvature of the hardening cap. This defines the relationship between volumetric plastic and shear strains. The quantity D is multiplied by the preconsolidation pressure  $X_0$  to determine the rate at which the strains develop. With very little to go on, the author chose to look to the literature for guidance for R and D. Table 16 shows R and D values found in the literature. For ease and lack of a better system, the values of W, R, and D were fixed for all tests at 0.01, 4.5, and 0.0057 after brief iteration.

Table 16 Summary of Sandler-Dimaggio parameters R and D from literature

Source	R (--)	D (in <sup>2</sup> /lb)
Sandler and Dimaggio (1971)	2.5	0.00067
Sandler et al. (1976)	4.3	0.002
Voyiadjis et al. (1990)	4.4	0.000514
Pinto (1998)	4.33	0.000977

Each of the twelve triaxial tests was simulated in both Plaxis and PlasFEM. Since all of the tests were conducted in sand, the appropriate constitutive models were chosen. In Plaxis, the Mohr-Coulomb and more advanced hardening soil models were used. In PlasFEM the Drucker-Prager and Sandler-Dimaggio models were used. The finite element meshes used from both programs are shown in Figure 84. The results of the finite element models of the triaxial tests are shown in Figures 85 through 96. Finally, parameters determined for all of the triaxial tests are shown in Table 17.

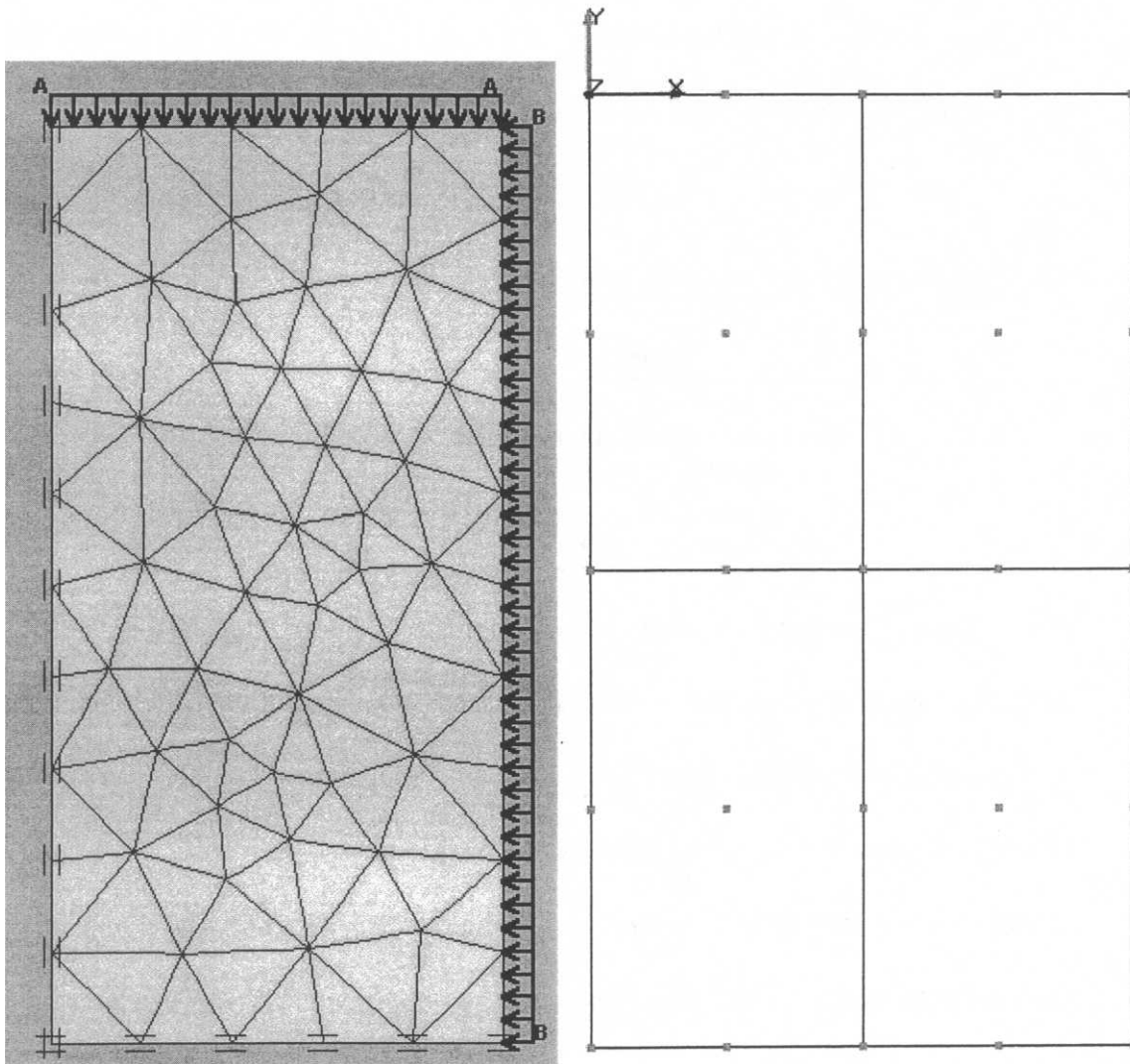


Figure 84 Meshes of finite elements used in Plaxis, left, and PlasFEM simulations of triaxial tests

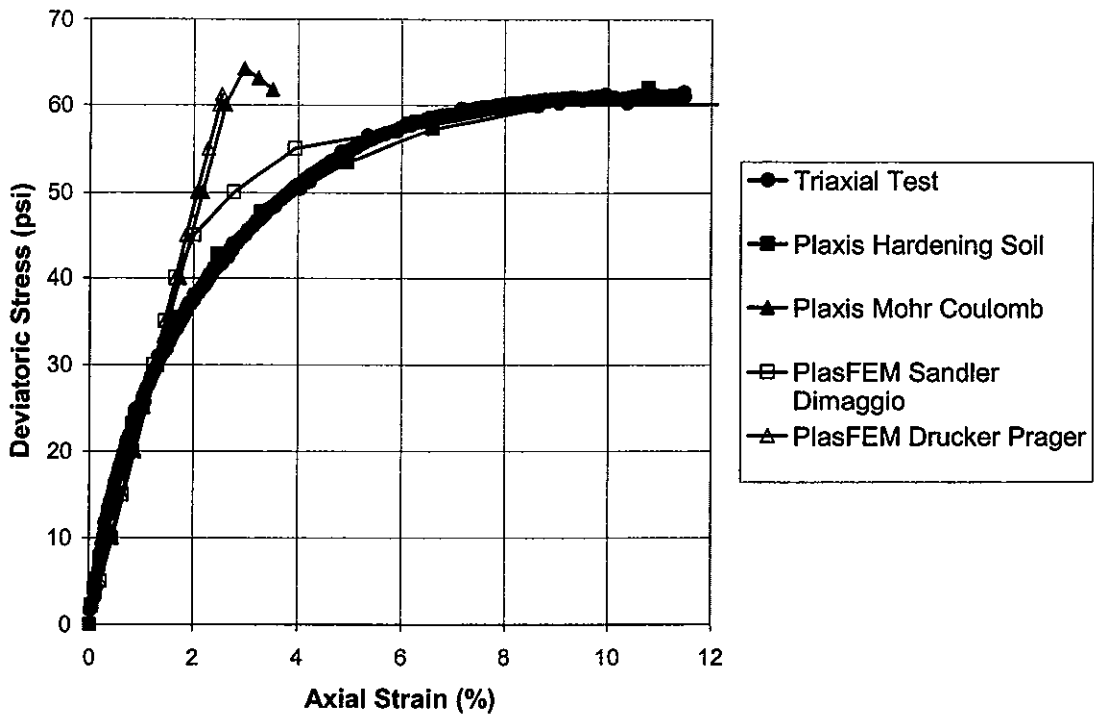


Figure 85 Simulations of triaxial test at State Road 20 tube 7 depth 34 ft

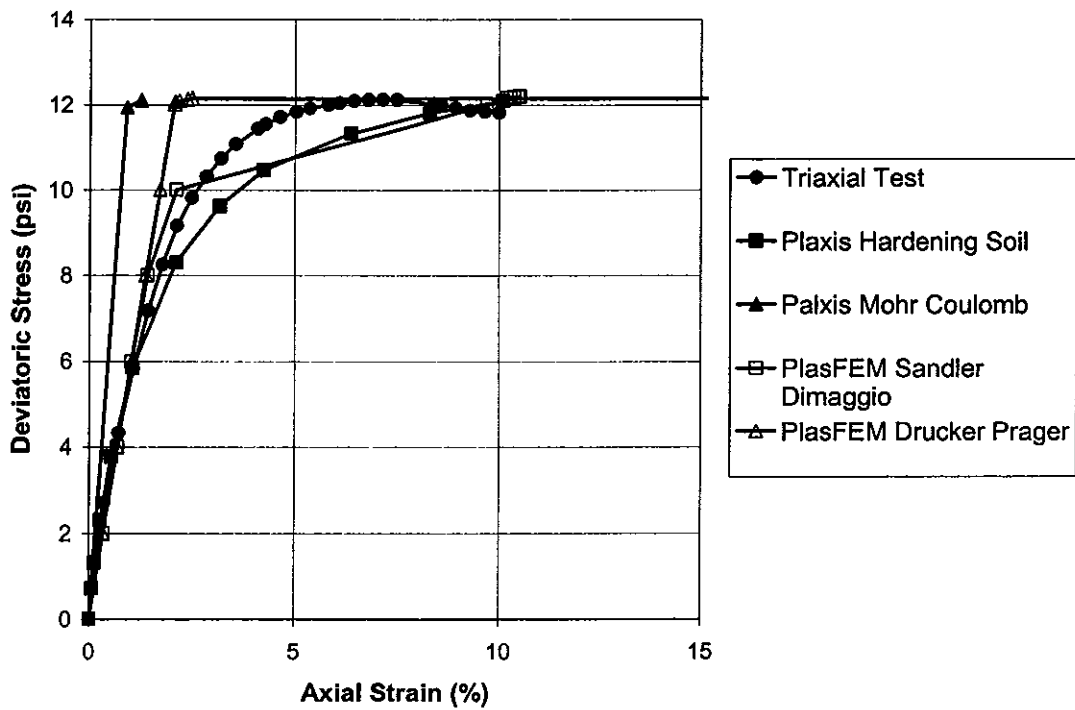


Figure 86 Simulations of triaxial test at Southwest Recreation Center tube 1 depth 10-12 ft

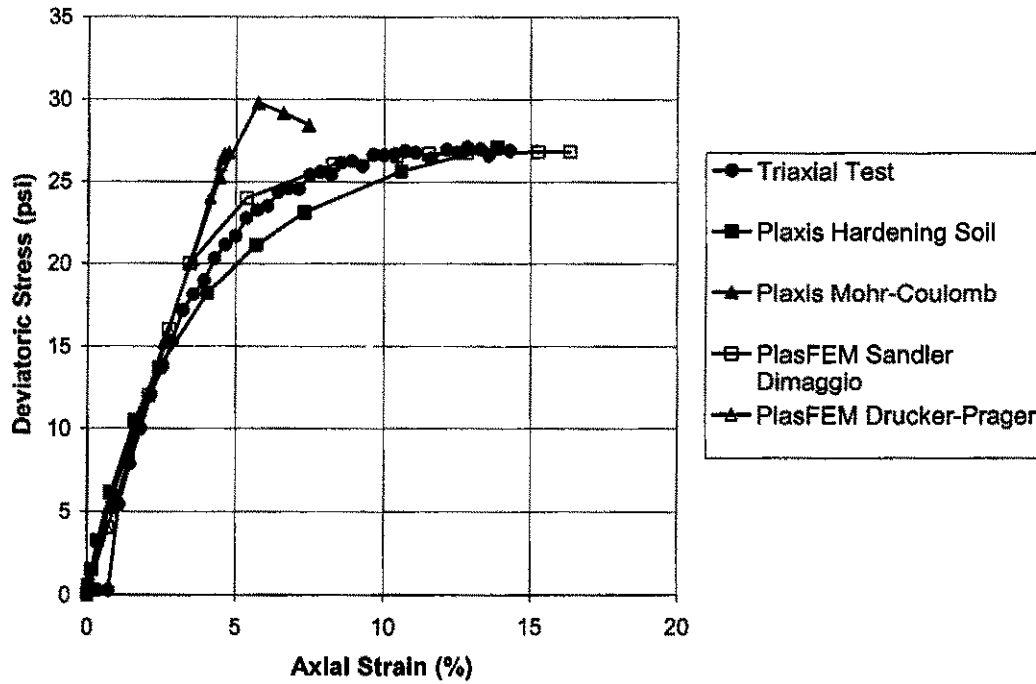


Figure 87 Simulations of triaxial test at Southwest Recreation Center tube 2 specimen 1 depth 14-16 ft

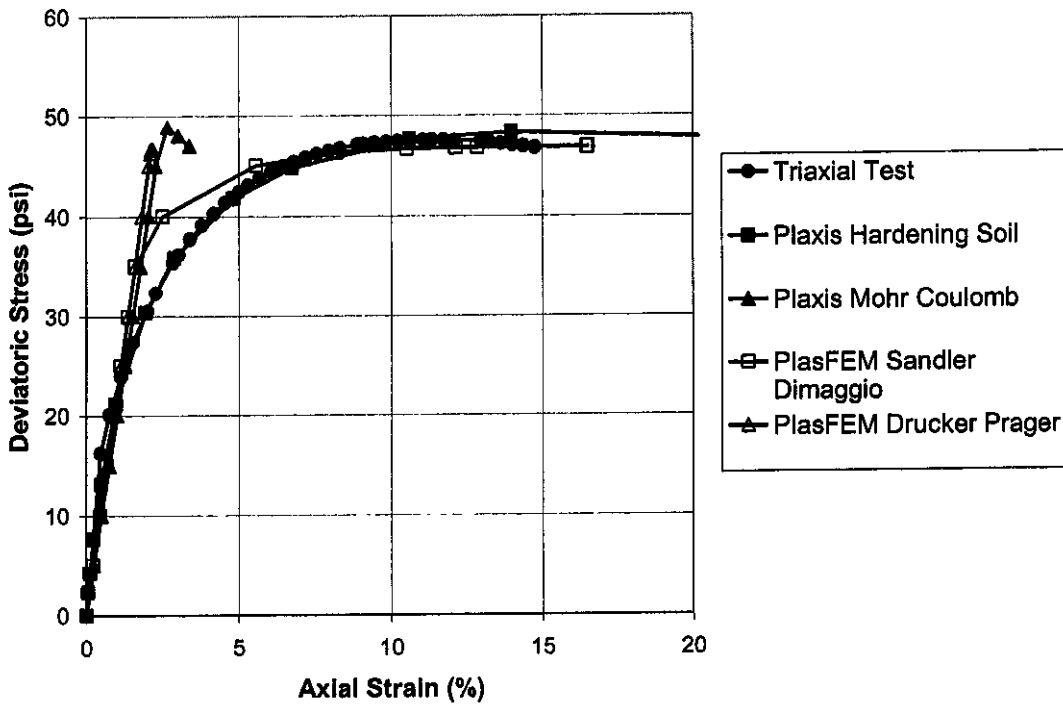


Figure 88 Simulations of triaxial test at Southwest Recreation Center tube 2 specimen 2 depth 14-16 ft

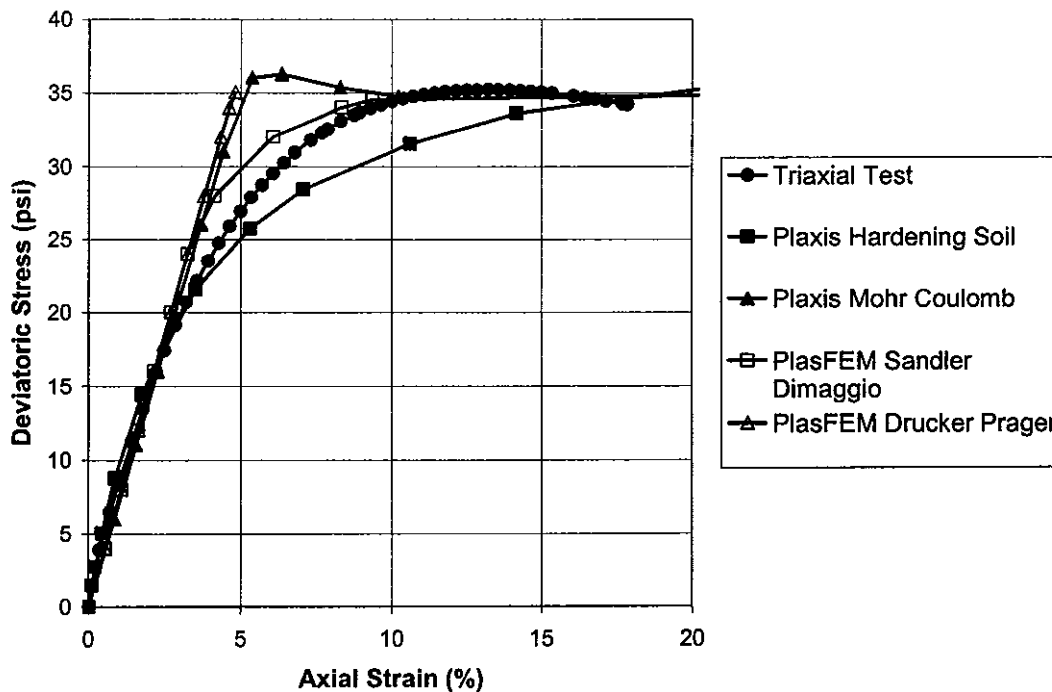


Figure 89 Simulations of triaxial test at Southwest Recreation Center tube 3 specimen 1 depth 18-20 ft

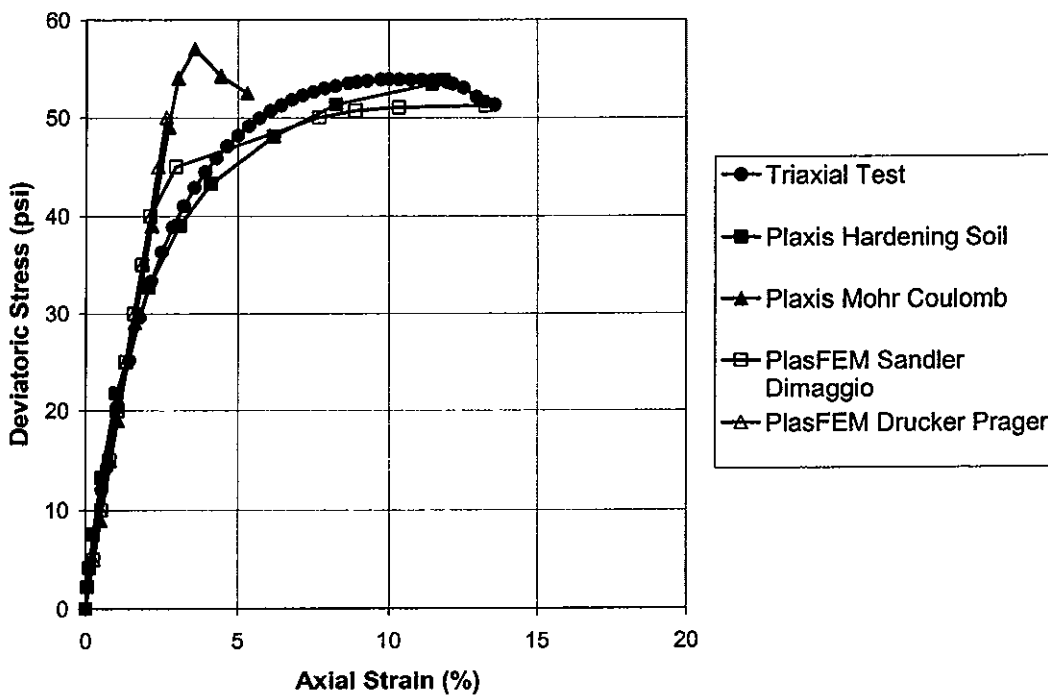


Figure 90 Simulations of triaxial test at Southwest Recreation Center tube 3 specimen 2 depth 18-20 ft

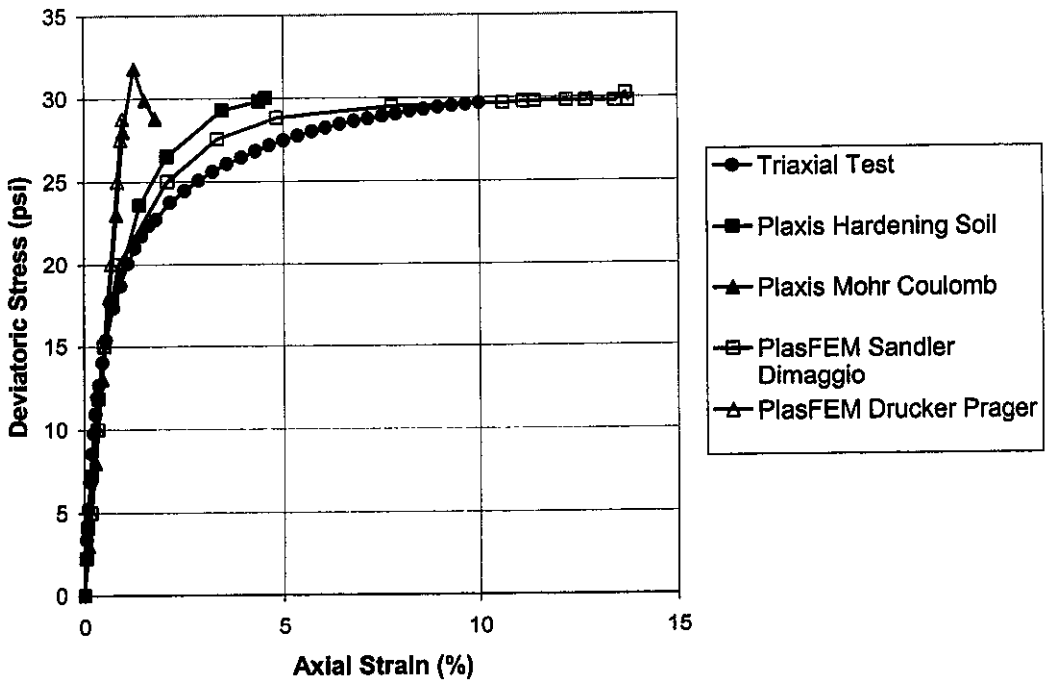


Figure 91 Simulations of triaxial test at Archer Landfill tube 1 specimen 1 depth 4-6 ft

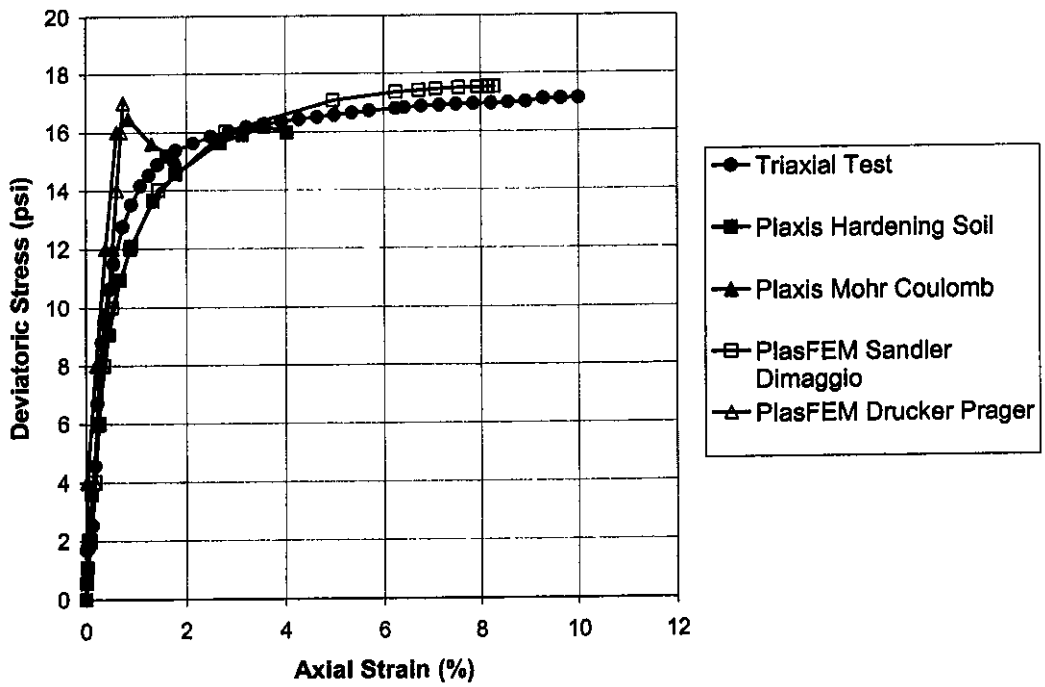


Figure 92 Simulations of triaxial test at Archer Landfill tube 1 specimen 2 depth 4-6 ft

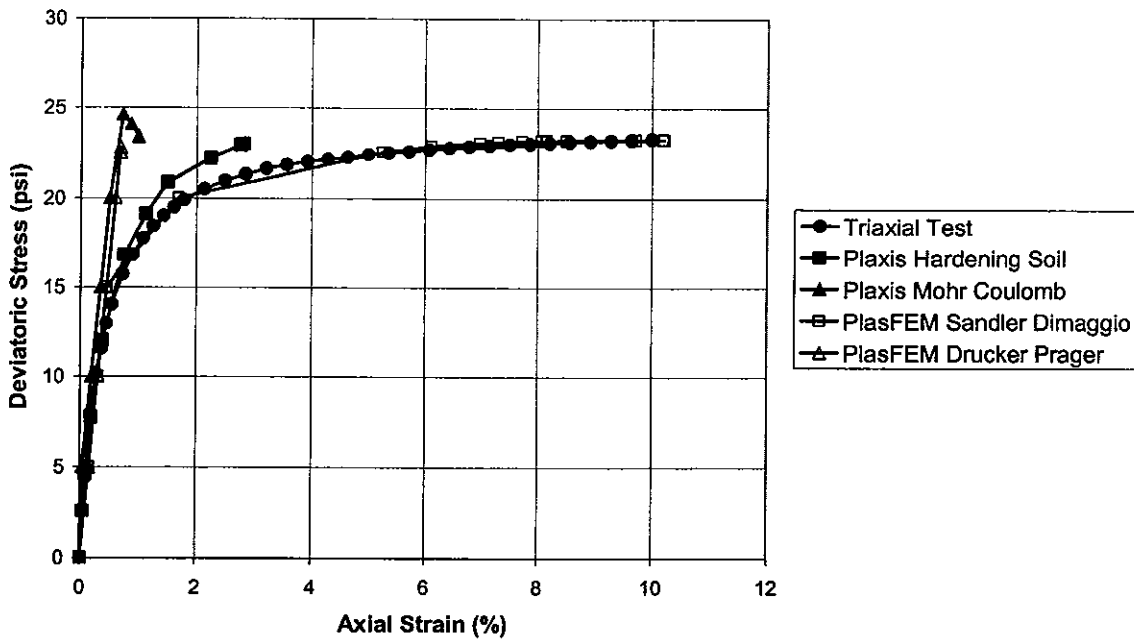


Figure 93 Simulations of triaxial test at Archer Landfill tube 2 specimen 1 depth 9-11 ft

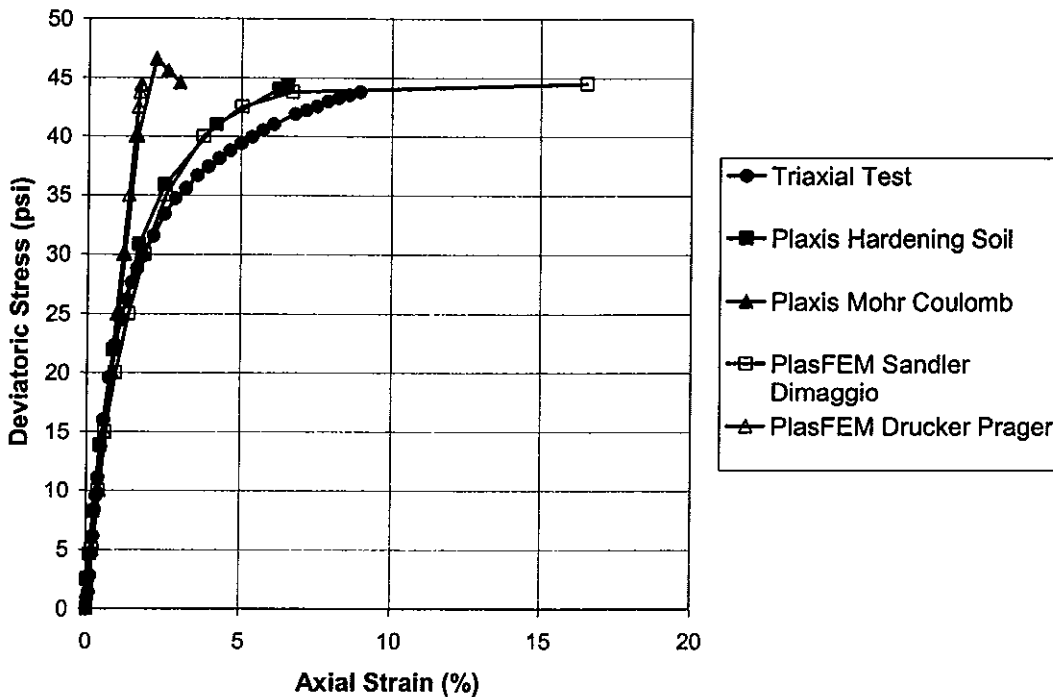


Figure 94 Simulations of triaxial test at Archer Landfill tube 2 specimen 2 depth 9-11 ft

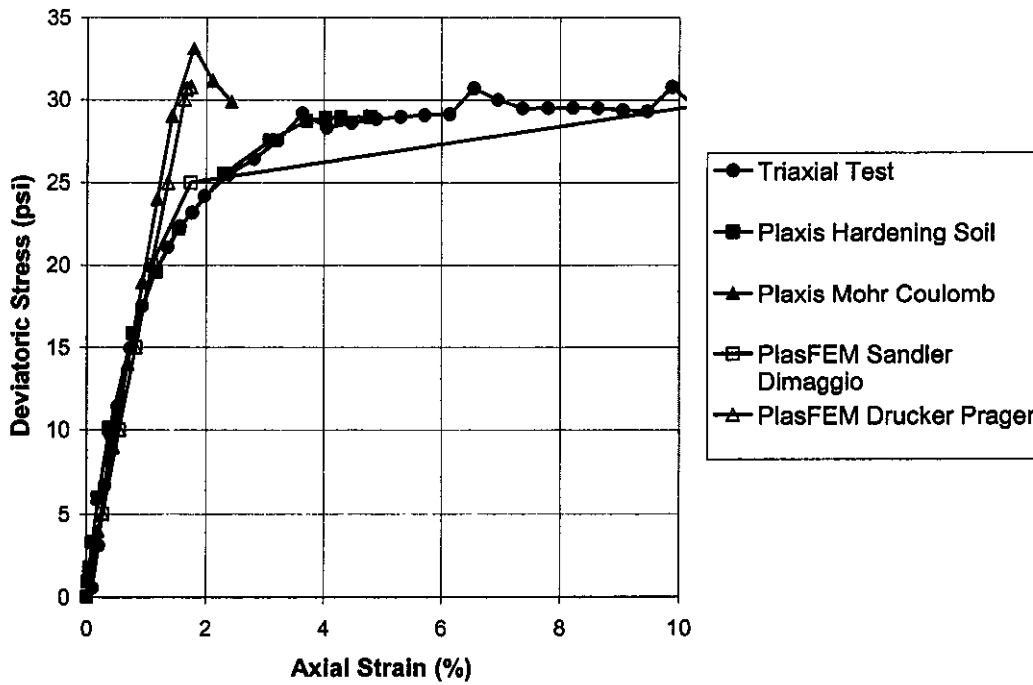


Figure 95 Simulations of triaxial test at Archer Landfill tube 3 depth 14-16 ft

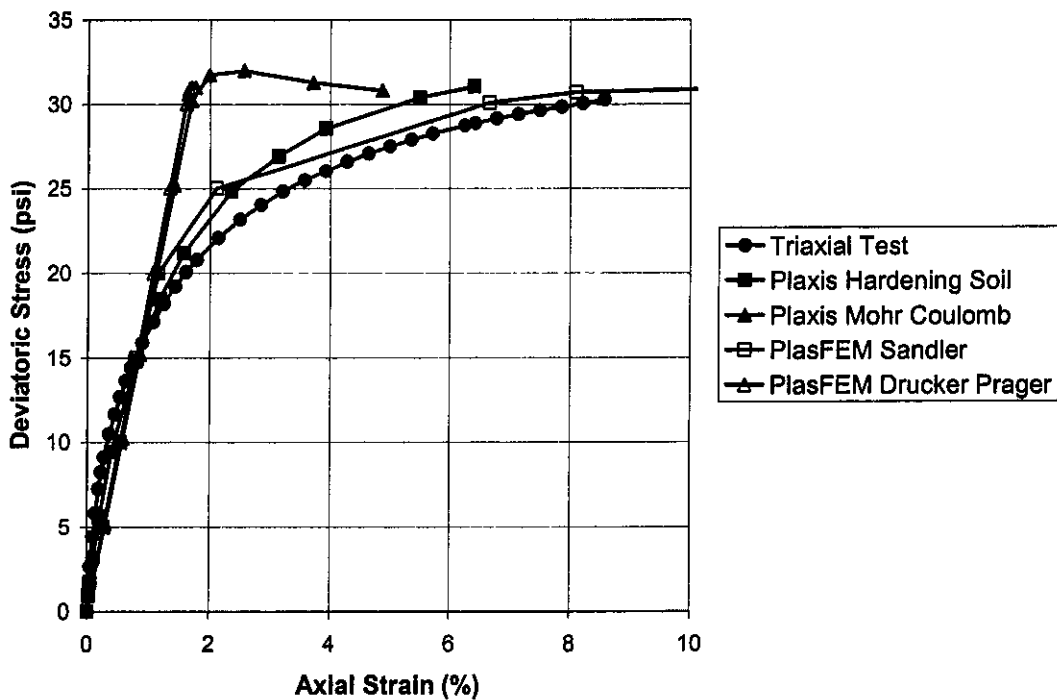


Figure 96 Simulations of triaxial test at Archer Landfill tube 4 depth 19-21 ft

Table 17 Summary of input parameters for triaxial test

Parameter	Units	SR20	SWREC	SWREC	SWREC	SWREC	SWREC	ARCH	ARCH	ARCH	ARCH	ARCH	ARCH
		T7S2	T1S3	T2S1	T2S2	T3S1	T3S2	T1S1	T1S2	T2S1	T2S2	T3S1	T4S1
Depth	(ft)	34	11	15	15	19	19	5	5	10	10	15	20
$E_{50}$	(psi)	2300	540	540	2100	700	1800	2900	2200	3220	2500	2040	1775
$E_{OED}$	(psi)	2300	540	540	2100	700	1800	2900	2200	3220	2500	2040	1775
m	(--)	0.5	0.5	0.5	0.5	0.5	0.5	0.5	0.5	0.5	0.5	0.5	0.5
c	(psi)	0	0	0	0	0	0	0	0	0	0	0	0
$\phi$	(°)	37.3	25.1	33.4	32.6	33.8	34.2	33.6	34.4	32.5	31.8	35.7	30.6
$\psi$	(°)	1.5	1.5	1.5	1.45	1.45	1.45	1.33	1.25	1.3	1.25	1.45	1.22
$\sigma_3$	(psi)	20	8	11	20	14	21	12	6	10	20	11	15
$\sigma_{dmax}$	(psi)	61.1	12.1	27	47.5	35.2	53.8	29.6	15.5	23.2	44.4	29.2	31.2
E	(psi)	3450.000	830.000	830.000	3150.000	1050.000	2700.000	4350.000	3300.000	4830.000	3750.000	3060.000	2662.000
$\theta$	(--)	0.292	0.195	0.259	0.253	0.263	0.266	0.261	0.285	0.252	0.246	0.279	0.236
X0	(psi)	200.000	45.000	100.000	175.000	125.000	200.000	85.000	45.000	80.000	130.000	80.000	100.000
W	(--)	0.01	0.01	0.01	0.01	0.01	0.01	0.01	0.01	0.01	0.01	0.01	0.01
R	(--)	4.5	4.5	4.5	4.5	4.5	4.5	4.5	4.5	4.5	4.5	4.5	4.5
D	(in <sup>2</sup> /lb)	0.0057	0.0057	0.0057	0.0057	0.0057	0.0057	0.0057	0.0057	0.0057	0.0057	0.0057	0.0057

Plaxis

PlasFEM

PENCEL PressuremeterDiscussion of the PENCEL Pressuremeter

Early in the research it was intended to use the pressuremeter parameters measured directly from the test for use in FEM modeling. Although it is recommended that the linear portion of an unload-reload cycle be used for calculation of stiffness, this quantity may often not be available. The stress and volume level at which an unload-reload loop is taken can affect the limit pressure. Therefore, there were some instances where an unload-reload loop was impractical because the test pressure failed to approach a limiting asymptote.

It should also be noted that many eccentricities have been noticed when using the PENCEL Pressuremeter in sands. Most notably are the extremely high values of modulus. During an unload-reload cycle, the volume change is minuscule when compared to the change in pressure. Slight anomalies in the pressuremeter calibration or poor resolution of measurement can have a large effect on the results. Most notably though is the occurrence of negative moduli in high pressure tests. The volume and pressure corrections obviously increase with higher pressures. Thus, when small volume increments cause high pressure changes, the pressure decrease due to system compliance might be greater than that due to the unloading. This in effect may invalidate the use of an unload-reload modulus. Houlsby and Schnaid (1994) noted these errors in volume correction during their calibration chamber studies with volume measuring and feeler gauged probes. Often times the system compliance of the probe was greater than the increment resulting in erroneous values for stiffness. Nonetheless, the PENCEL

Pressuremeter was carefully calibrated and operated in accordance with the published manual.

Noting the problem with the method of calibrating the PENCEL recommended by Roctest, Inc., Houlsby and Schanid's (1994) alternative was attempted. Application of this method to several of the PENCEL Pressuremeter tests again yielded erroneously high or negative shear moduli.

The data acquisition system employed by the Fugro device is capable of detecting variations of 0.001% cavity strain or 0.0002 min (0.00000787 in.). Assuming cylindrical cavity expansion, the volume change with this small increment would be 0.005 cm<sup>3</sup>. The total amplitude of the unload-reload loops conducted by Houlsby and Schnaid (1994) were 0.1 to 0.2 % which corresponds to 0.74 cm<sup>3</sup>.

The resolution of the volume measuring device for the PENCEL Pressuremeter is about 0.05 cm<sup>3</sup>. This is an order of magnitude higher than the Fugro. The current pressure gauge has increments of 0.25 bars (25 kPa). Observations down to 0.05 bars (5 kPa) can be made but depend on experience and may not be so reliable.

It is the opinion of the author that the resolution of the current PENCEL Pressuremeter prevents it from being a tool by which the shear modulus of sand could be easily and consistently estimated.

#### FEM Modeling of the PENCEL Pressuremeter

The mesh of finite elements used in the simulation was the result of several trial and error attempts to best match the boundary conditions of the problem. There were two primary issues. First, the initial stresses at the depth of the test must be modeled, thus the entire profile from the surface to just below the probe was included. The second issue was the boundary between the probe and the soil. Since the PENCEL is pushed like a

CPT, there is no hole where elements could be cut. When trial meshes were created with an open borehole, the soil failed under initial stresses (collapsing borehole) and this really did not represent the problem in any effect. A final mesh was adopted that included soil to represent the rods and pressuremeter in the borehole. Hughes and Robertson (1985) suggest that the stresses around the PENCEL probe would be close to the undisturbed  $K_0$  state. This would insure the correct initial stresses. Interface elements are used between the elements that represent the pressuremeter and the soil elements, to allow the soil to be pushed away. The pressuremeter inflation is simulated by application of a horizontal traction across a series of elements. Figure 97 shows the mesh with details about the elements and load.

Two groups of loading steps are used in the simulation. First, Plaxis calculates the initial vertical stresses based on elastic theory and the horizontal stresses are estimated by Jaky's equation. The next loading steps increase the pressuremeter load incrementally up to the PENCEL limit pressure.

In order to compare Plaxis to the pressuremeter, an assumption was made. The displacement of the pressuremeter membrane is read as the injected volume in the case of the PENCEL Pressuremeter. The finite element simulations are more or less two-dimensional, thus the movement of membrane is calculated as length. Therefore, the assumption was that the pressuremeter expanded cylindrically, and that the radial displacement at the center of the membrane,  $\Delta r$ , could be approximated by:

$$\Delta r = \sqrt{\frac{V_0 + \Delta V}{\pi h}} - r_0$$

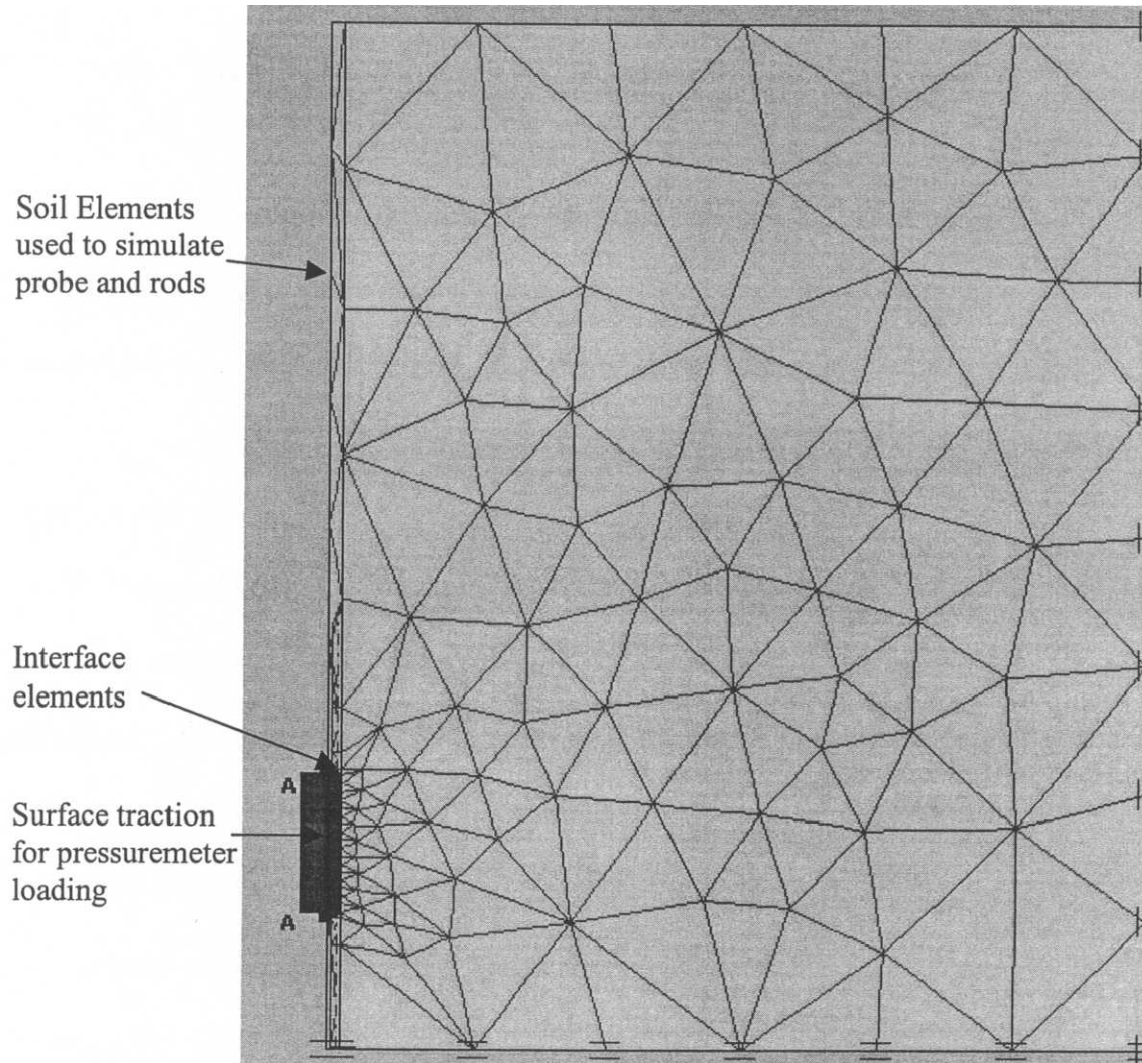


Figure 97 Plaxis finite element mesh for PENCEL Pressuremeter

where

- $V_0$  is the initial volume of the probe
- $\Delta V$  is the instantaneous volume injected into the probe
- $h$  is the initial length of the membrane
- $r_0$  is the initial radius at the center of the membrane

It is understood that this is an approximation, but without an alternative means of measuring the radial displacement, it is the best method.

A first baseline ran was made for each pressuremeter test. This baseline included a Mohr-Coulomb and hardening soil analysis, which in every case yielded almost identical results. Unfortunately, these analyses greatly under predicted the deformations. Several ideas were considered as a remedy to this problem. The first was to overconsolidate the soil, as empirically suggested by Hughes and Robertson (1985). This would in effect push the hardening cap out far away from the initial stresses. This alteration proved to have little effect on the result. A second consideration was to increase the friction angle. As with the overconsolidation, the increased friction angle had little effect, except when unrealistically large values of  $\phi$  were used. The final experiment was to increase the value of modulus. The Mohr-Coulomb constitutive model was used in this case with a reasonable friction angle estimated based on the cone penetration test. The results of all of the Plaxis simulations are shown in Figures 98 through 105. The difference between the baseline predictions and those made with the increased  $E_{50}$  is clearly visible. PlasFEM was not used in the PENCEL Pressuremeter portion of the analysis due to the lack of a stable working pre-processor.

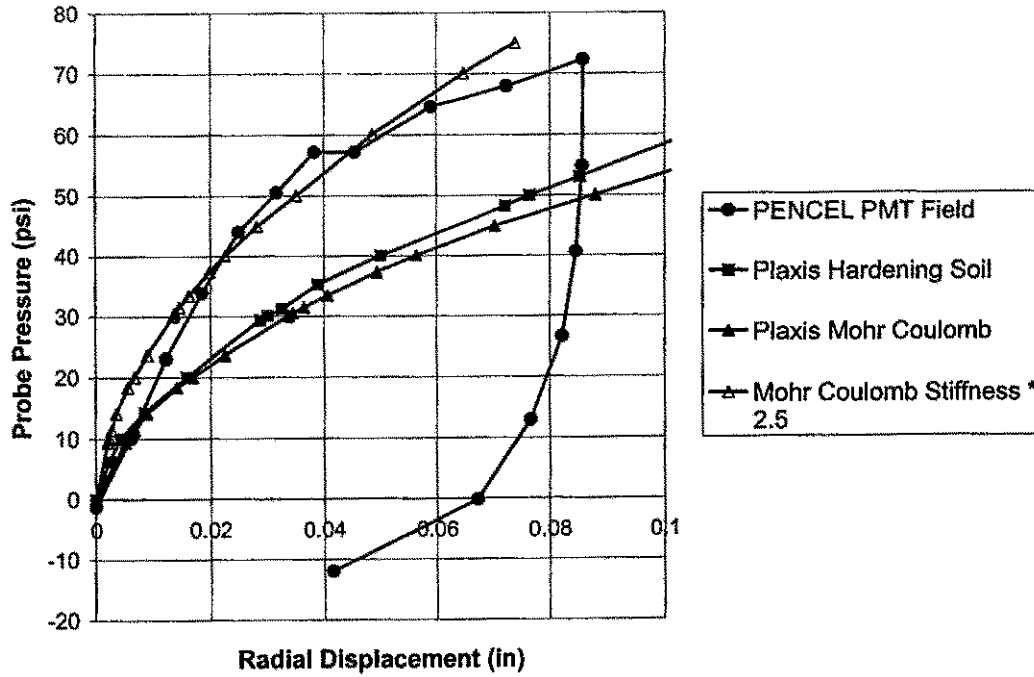


Figure 98 Simulations of PENCEL Pressuremeter test at State Road 20 depth 35 ft

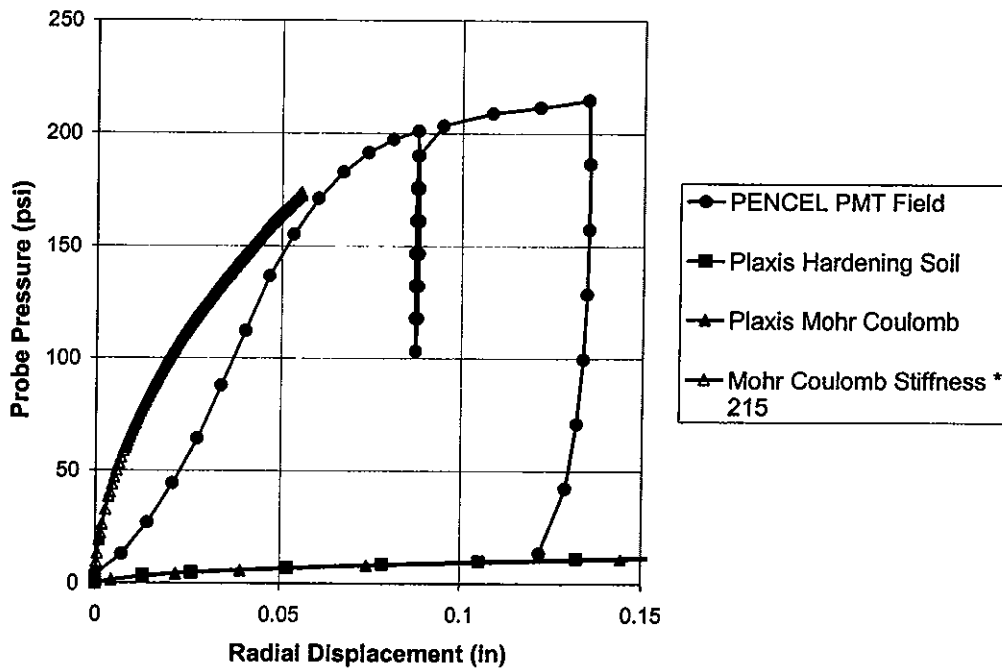


Figure 99 Simulations of PENCEL Pressuremeter test at Southwest Recreation Center depth 8 ft

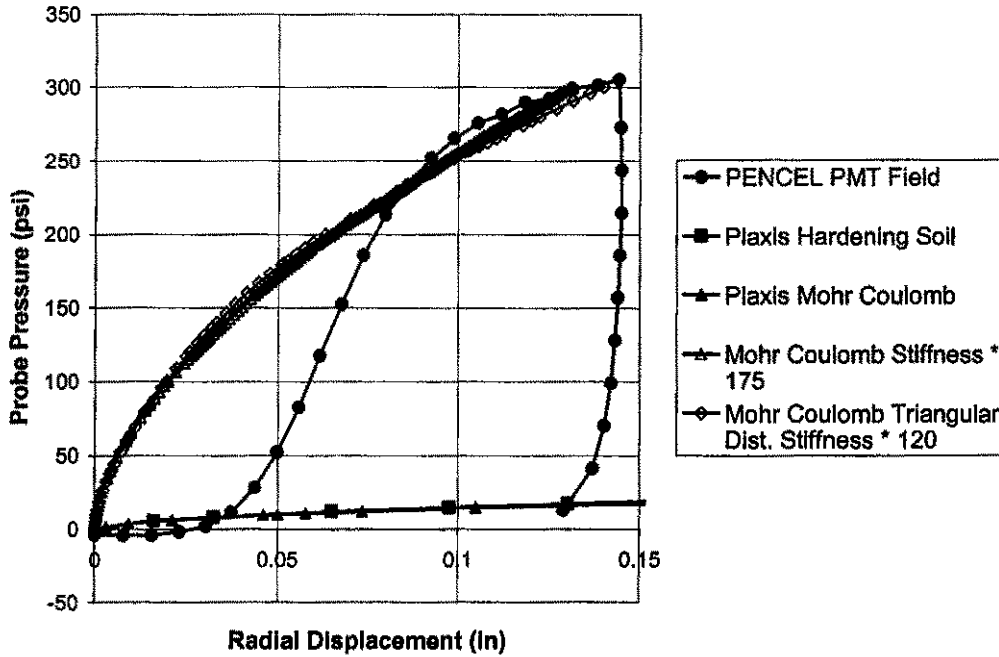


Figure 100 Simulations of PENCEL Pressuremeter test at Southwest Recreation Center depth 12 ft

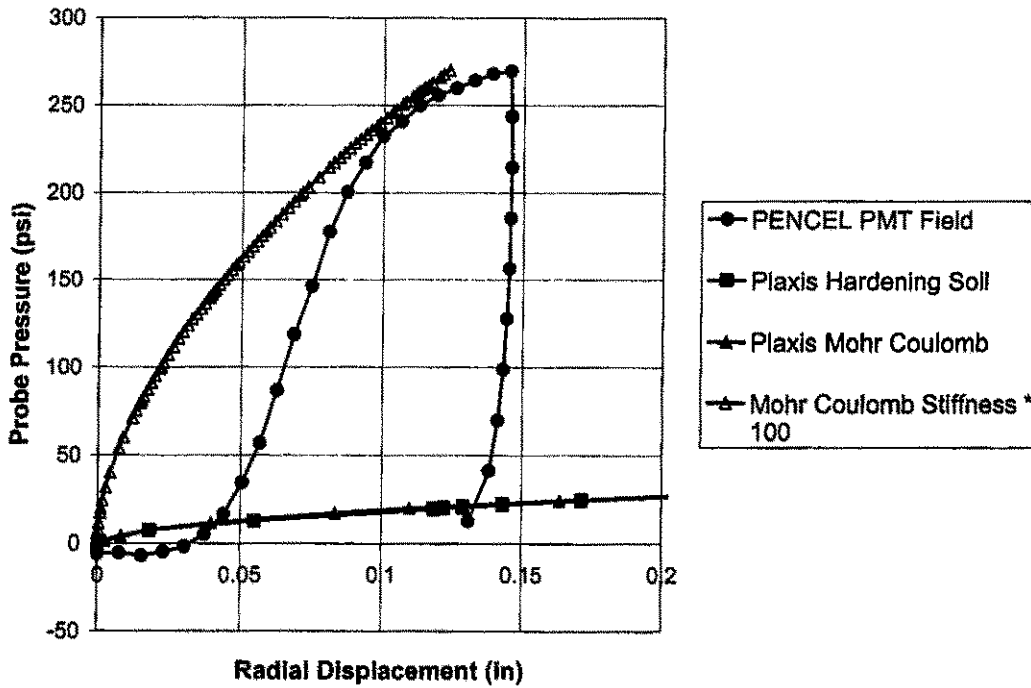


Figure 101 Simulations of PENCEL Pressuremeter test at Southwest Recreation Center depth 16 ft

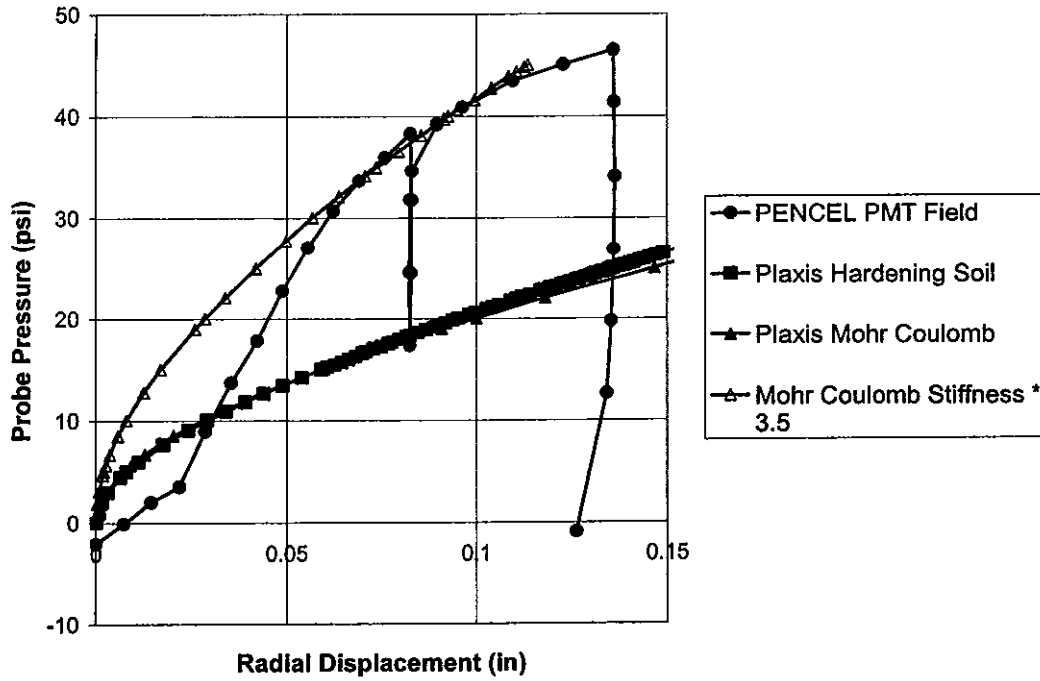


Figure 102 Simulations of PENCEL Pressuremeter test at Archer Landfill depth 5 ft

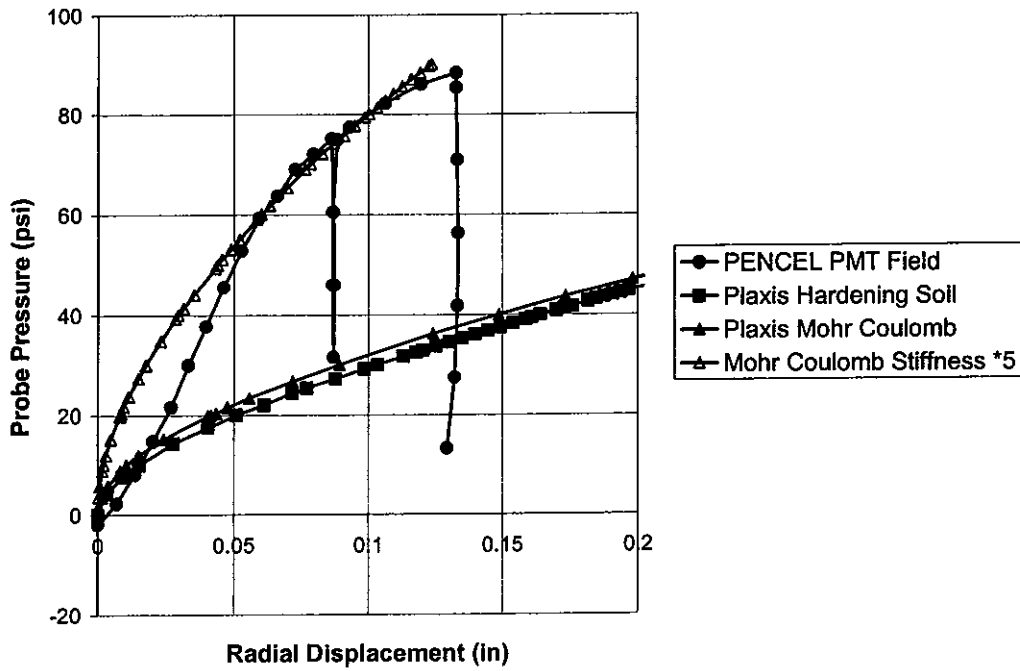


Figure 103 Simulations of PENCEL Pressuremeter test at Archer Landfill depth 10 ft

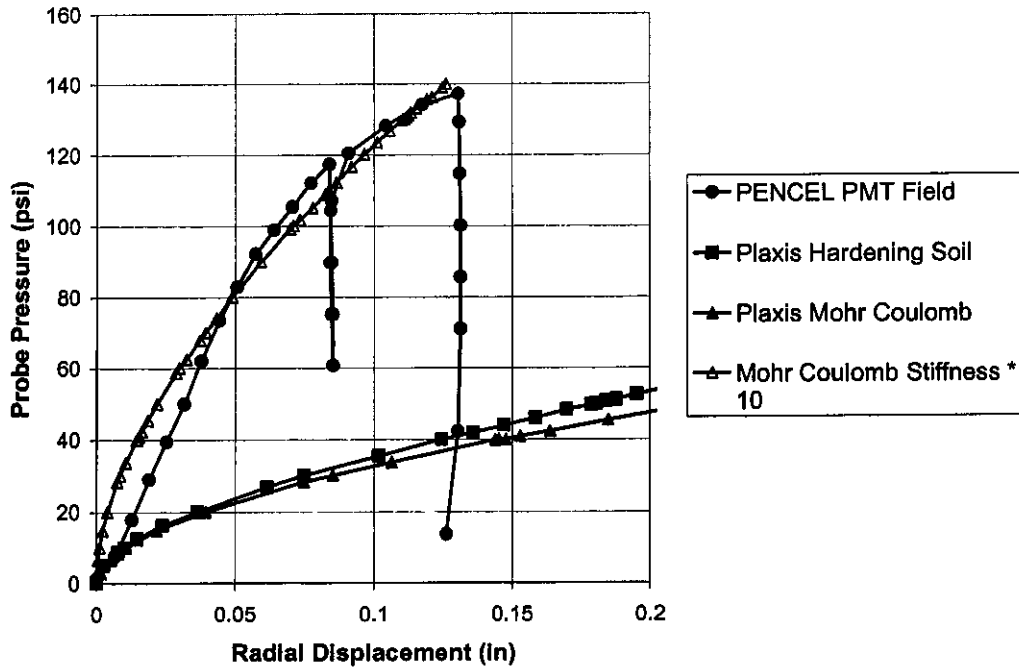


Figure 104 Simulations of PENCEL Pressuremeter test at Archer Landfill depth 15 ft

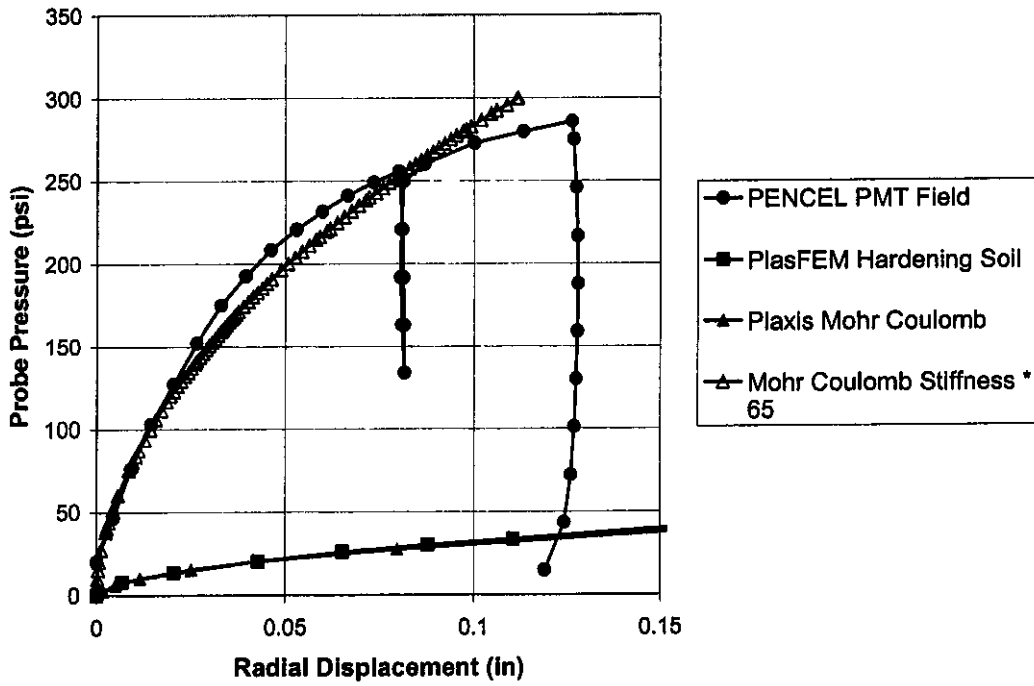


Figure 105 Simulations of PENCEL Pressuremeter test at Archer Landfill depth 20 ft

Table 18 shows the results of the pressuremeter simulations in Plaxis. It was found that increasing the triaxial  $E_{50}$  modulus by a factor of anywhere from 3.5 to 215 would produce curve matching agreement. A trend line was established for the stiffness multiplier as a function of limit pressure. An exponential function was

Table 18 Results of modulus iteration for research site pressuremeter curves

Site	Depth (feet)	Limit Pressure (psi)	Multiplier (-)	Triax E50 (psi)	EPMT (psi)
ALF	5	46.4	3.5	2172	7602
ALF	10	88.2	5	2498	12490
ALF	15	137.2	10	2041	20410
ALF	20	285	65	1775	115375
SR20	34	72.2	2.5	2300	5750
SWREC	8	214	215	540	116100
SWREC	12	305	175	830	145250
SWREC	16	269	100	700	70000

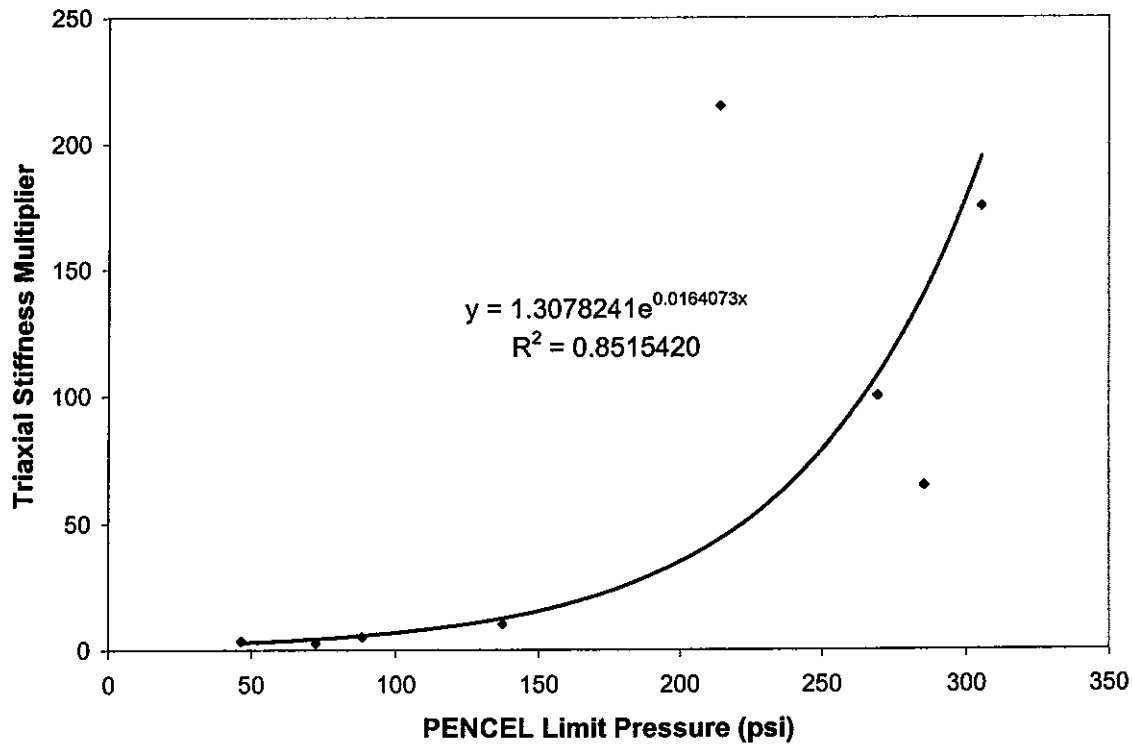


Figure 106 Proposed function of triaxial stiffness multiplier versus limit pressure

determined to be the best fit for the data:

$$\Omega = 1.3078e^{0.0164p_l}$$

$$R^2 = 0.8515$$

Where  $\Omega$  is the triaxial  $E_{50}$  modulus multiplier and  $p_l$  is the PENCEL limit pressure. The plot of the stiffness multiplier against limit pressure is shown in Figure 106.

## CHAPTER 6 MOFFITT CANCER CENTER SHEET-PILE WALL PREDICTION

### Introduction

Prediction of structural deflections (piles, footings, sheet pile walls, etc. . . ) in geotechnical problems is a better way to understand the relationship between the real field performance and theoretical prediction. In this chapter, the deflection of a sheet pile wall is studied. The site is located at the University of South Florida, Tampa.

Funding from the settlement of the State of Florida with the Tobacco companies financed a new research Tower as an addition to the Moffitt Cancer Center, which is part of the College of Medicine, University of South Florida. Excavations were necessary for the construction of the Tower and an adjacent parking garage. Temporary shoring for these excavations was to be provided by cantilevered sheet pile walls. The Moffitt Foundation, overseeing the project, agreed to allow the University of Florida to perform soil exploration tests at the site for the future wall.

### Objectives

The insitu tests by the University of Florida were performed to model the field performance, that is the deformation, of the sheet pile wall based upon the data collected from: SPT, CPT and the Cone Pressuremeter Test (PMT PENCEL type). Subsequently, comparisons and interpretations of the theoretical predictions with the field actual deflection are undertaken.

### Scope of Work

In order to accomplish the objectives mentioned above, the following tasks have been included in this project:

1. collect the data from the SPT, CPT and PMT insitu test and identify the input parameters for a conventional method of analyses (CWALSHT) and numerical FEM modeling,
2. analyze the sheet-pile using the CWALSHT program as a conventional method and the finite element code Plaxis for numerical FEM modeling,
3. instrument the sheet pile wall with Slope Inclinometer Casings at 3 locations using 2.5" by 2.5" ¼" steel box tubing,
4. measure the actual deformation of the sheet pile wall before and after the excavation,
5. compare the inclinometer measured deflections with the theoretically predicted deflections.

### Site Description and Insitu Testing

There was very little soil data for the area where the wall is to be installed, thus the University of Florida conducted CPT and PENCEL Pressuremeter Tests at two locations along the wall. As indicated in Figure 107, the wall is to be constructed near the southwest corner of the plane view in the area labeled INACCESSIBLE.

The University of Florida Cone Truck was used to conduct the CPT and the PENCEL PMT testing, the contractor Law Gibb Group Member had already performed SPT borings. Data obtained from these insitu tests are presented in Figure 108 to Figure 114 and Table 19 and Table 20.

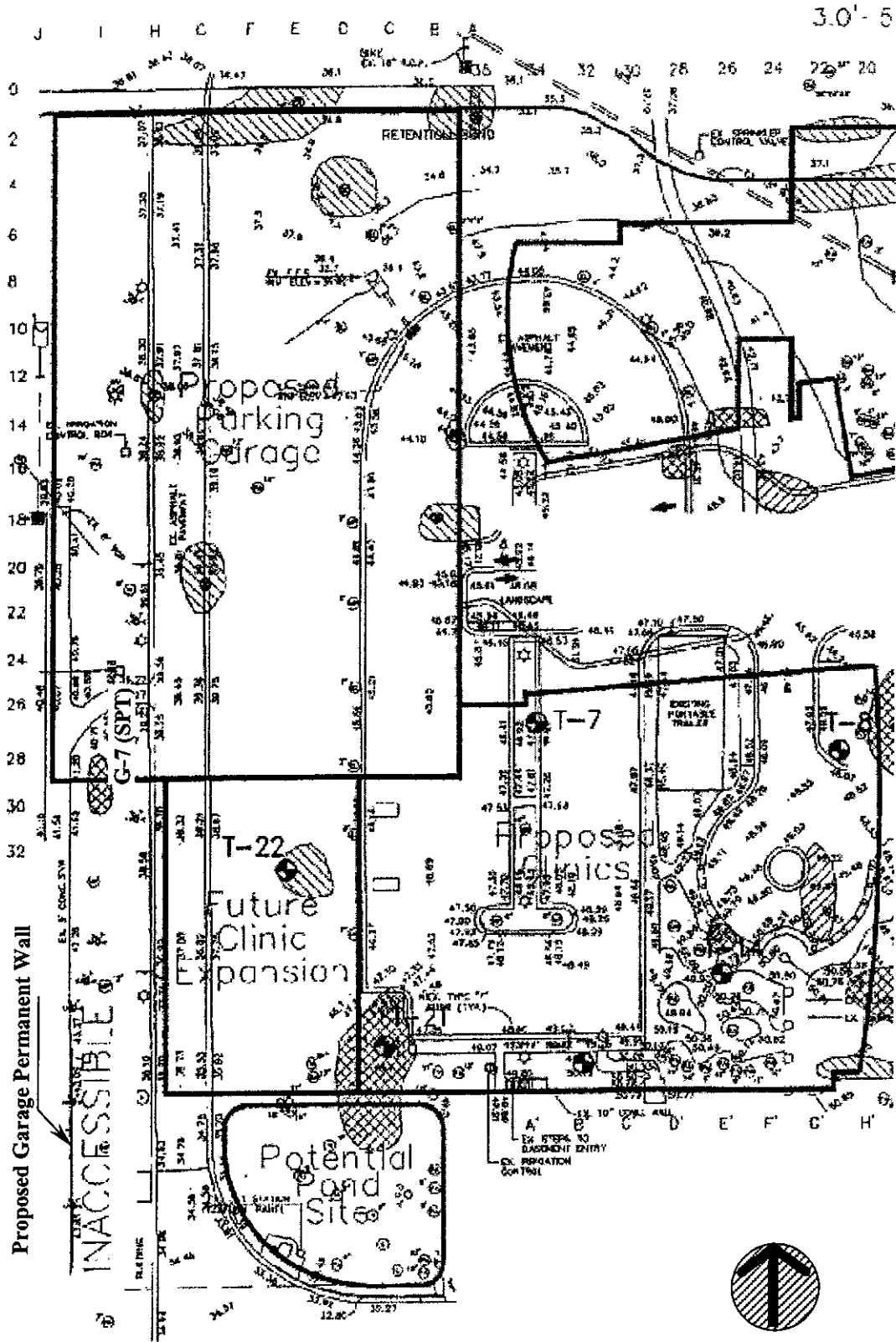


Figure107 Plan view of the Moffitt Cancer Center: field exploration

University of Florida	
Operator : JBA/LR/HM	CPT Date : 12-04-00 13:56
Sounding : swreg1 Pg 1 / 1	Location : Moffitt Center
Cone Used : 156	Job No. : MF1

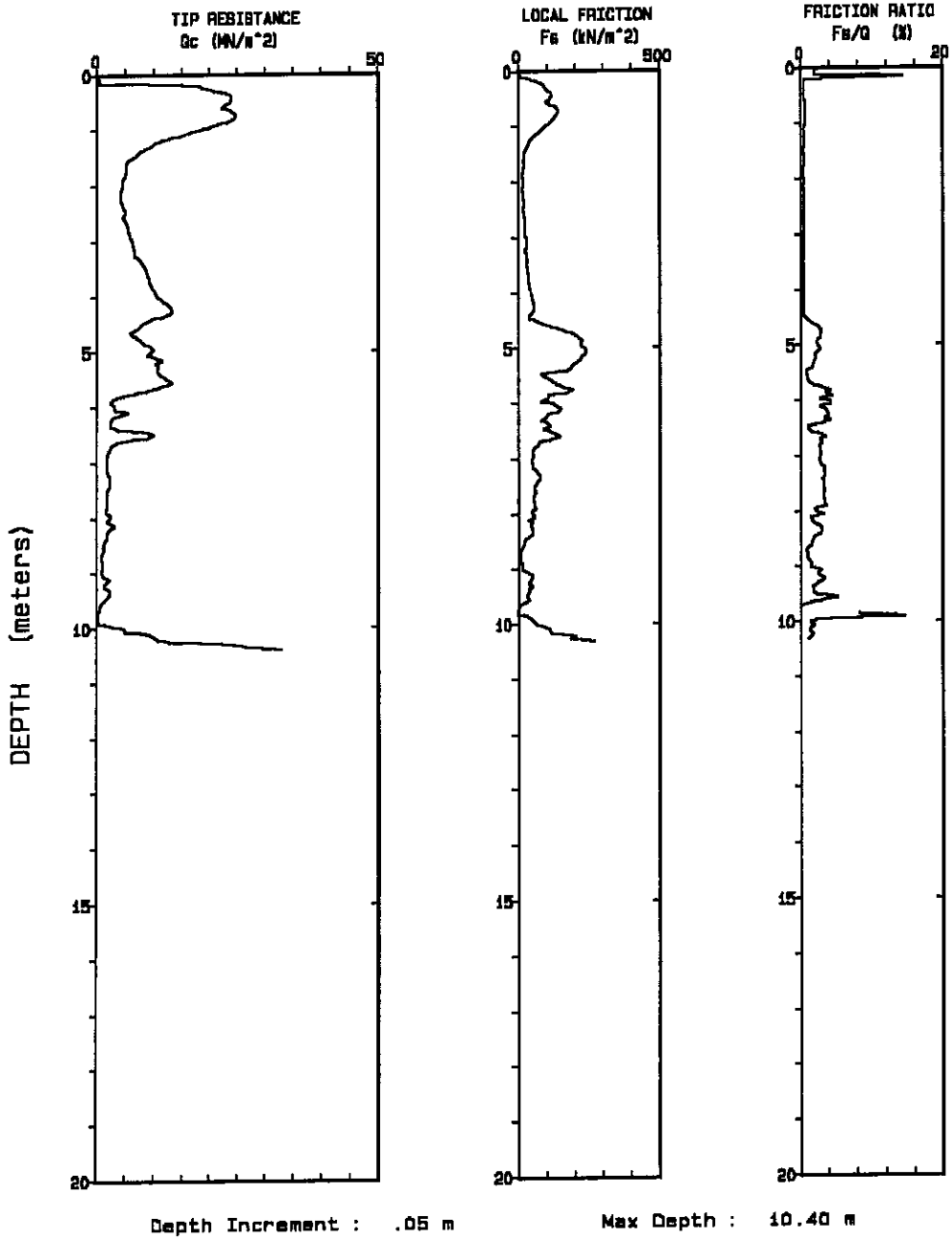


Figure 108 Cone penetration test sounding, North, at Moffitt Cancer Center



Table 19 Continued

University of Florida

Operator :JBA/LR/HM  
 On Site Loc:Moffitt Center  
 Job No. :MF1  
 Tot. Unit Wt. (avg) : 18 kN/m<sup>3</sup>

CPT Date :12-04-00 13:56  
 Cone Used :156  
 Water table (meters) : 4.1

DEPTH (meters)	DEPTH (feet)	Qc (avg) (MN/m <sup>2</sup> )	Fs (avg) (kN/m <sup>2</sup> )	Rf (avg) (%)	SIGV' (bar)	SOIL BEHAVIOUR TYPE	Eq - Dr (%)	PHI deg.	SPT N	Su bar
7.25	23.79	1.92	56.20	2.92	0.99	clayey silt to silty clay	UNDFND	UNDFD	10	1.7
7.50	24.61	2.15	68.64	3.19	1.01	clayey silt to silty clay	UNDFND	UNDFD	11	2.0
7.75	25.43	1.82	57.80	3.17	1.03	clayey silt to silty clay	UNDFND	UNDFD	9	1.6
8.00	26.25	1.98	56.52	2.85	1.05	clayey silt to silty clay	UNDFND	UNDFD	10	1.8
8.25	27.07	2.36	48.12	2.04	1.07	sandy silt to clayey silt	UNDFND	UNDFD	9	2.2
8.50	27.89	1.48	37.48	2.53	1.09	clayey silt to silty clay	UNDFND	UNDFD	7	1.3
8.75	28.71	1.01	11.92	1.18	1.11	clayey silt to silty clay	UNDFND	UNDFD	5	.8
9.00	29.53	1.03	12.14	1.17	1.13	clayey silt to silty clay	UNDFND	UNDFD	5	.8
9.25	30.35	1.55	43.32	2.80	1.15	clayey silt to silty clay	UNDFND	UNDFD	8	1.3
9.50	31.17	1.97	37.88	1.92	1.17	sandy silt to clayey silt	UNDFND	UNDFD	8	1.8
9.75	31.99	0.53	12.18	2.28	1.19	silty clay to clay	UNDFND	UNDFD	4	.3
10.00	32.81	1.72	39.98	2.32	1.21	clayey silt to silty clay	UNDFND	UNDFD	9	1.5
10.25	33.63	9.56	144.02	1.51	1.23	silty sand to sandy silt	60-70	38-40	32	UNDEFINED

Dr - All sands (Jamiolkowski et al. 1985)

PHI - Robertson and Campanella 1983

Su: Nk= 10

\*\*\*\* Note: For interpretation purposes the PLOTTED CPT PROFILE should be used with the TABULATED OUTPUT from CPTINTR1 (v 3.04) \*\*\*\*

University of Florida	
Operator : JBA/LR/HM	CPT Date : 12-04-00 14:42
Sounding : swreg3 Pg 1 / 1	Location : Moffitt Center
Cone Used : 156	Job No. : MF2

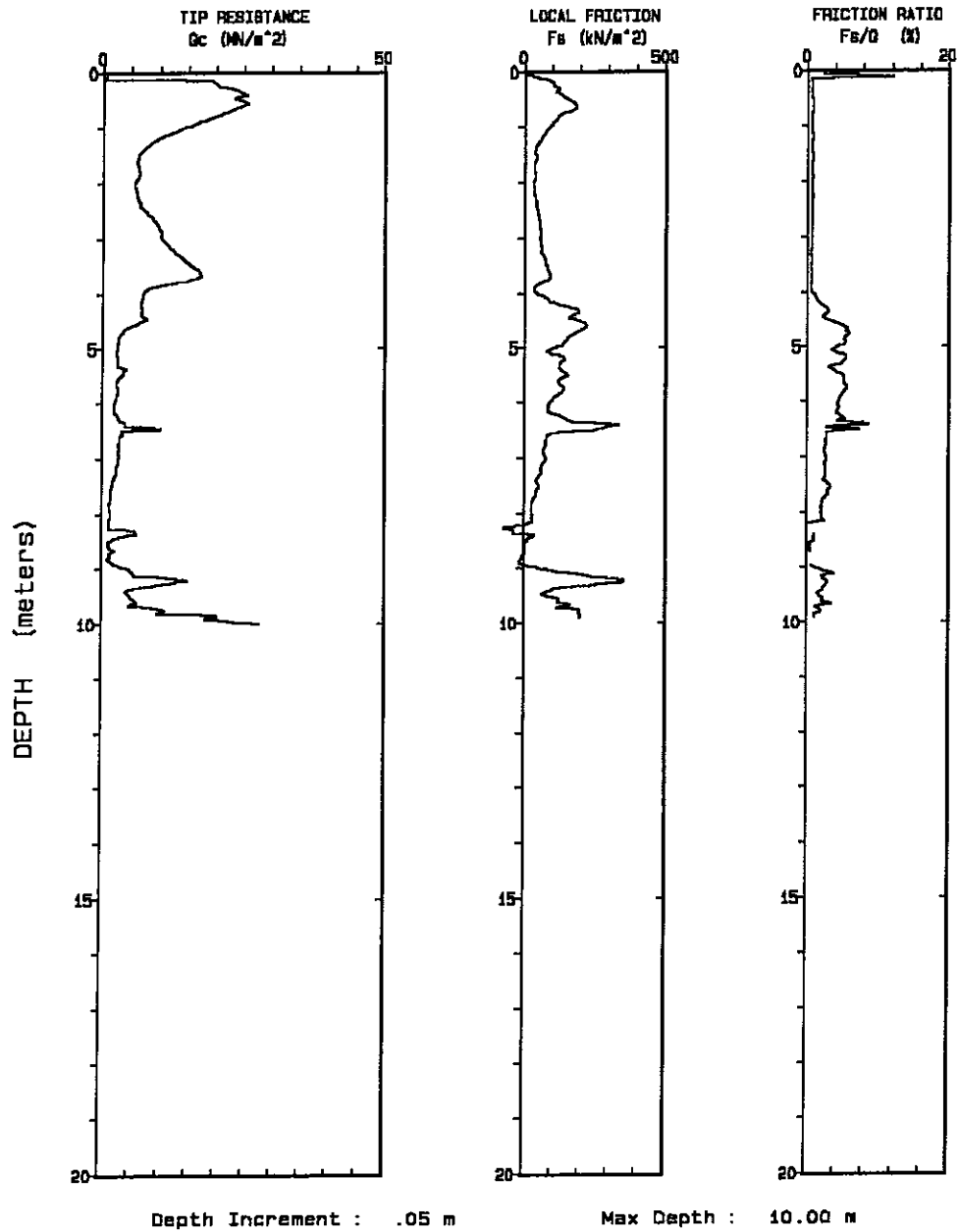


Figure 109 Cone penetration test sounding, South, at Moffitt Cancer Center



Table 20 Continued

University of Florida

Operator :JBA/LR/HM                      CPT Date :12-04-00 14:42  
 On Site Loc:Moffitt Center              Cone Used :156  
 Job No. :MF2                                Water table (meters) : 4.1  
 Tot. Unit Wt. (Avg) : 18 kN/m<sup>3</sup>

DEPTH	Qc (avg)	Fs (avg)	Rf (avg)	SIGV'	SOIL BEHAVIOUR TYPE	Eq - Dr	PHI	SPT	Su	
(meters)	(feet)	(MN/m <sup>2</sup> )	(kN/m <sup>2</sup> )	(%)	(bar)	(%)	deg.	N	bar	
7.25	23.79	2.50	64.82	2.59	0.99	clayey silt to silty clay	UNDFND	UNDFD	12	2.3
7.50	24.61	1.91	50.76	2.65	1.01	clayey silt to silty clay	UNDFND	UNDFD	10	1.7
7.75	25.43	1.50	42.48	2.83	1.03	clayey silt to silty clay	UNDFND	UNDFD	7	1.3
8.00	26.25	1.39	28.54	2.05	1.05	clayey silt to silty clay	UNDFND	UNDFD	7	1.2
8.25	27.07	1.36	5.44	0.40	1.07	sandy silt to clayey silt	UNDFND	UNDFD	5	1.2
8.50	27.89	3.74	-1.68	-0.04	1.09	undefined	UNDFND	UNDFD	UDF	UNDEFINED
8.75	28.71	1.49	3.08	0.21	1.11	sandy silt to clayey silt	UNDFND	UNDFD	6	1.3
9.00	29.53	2.55	9.12	0.36	1.13	silty sand to sandy silt	<40	32-34	8	UNDEFINED
9.25	30.35	9.90	255.26	2.58	1.15	sandy silt to clayey silt	UNDFND	UNDFD	40	9.7
9.50	31.17	5.46	119.36	2.19	1.17	sandy silt to clayey silt	UNDFND	UNDFD	22	5.2
9.75	31.99	7.46	147.90	1.98	1.19	silty sand to sandy silt	50-60	38-40	25	UNDEFINED
10.00	32.81	19.82	-12987.14	-65.52	1.21	undefined	UNDFND	UNDFD	UDF	UNDEFINED

Dr - All sands (Jamiolkowski et al. 1985)      PHI -      Robertson and Campanella 1983      Su: Nk= 10

\*\*\*\* Note: For interpretation purposes the PLOTTED CPT PROFILE should be used with the TABULATED OUTPUT from CPTINTR1 (v 3.04) \*\*\*\*

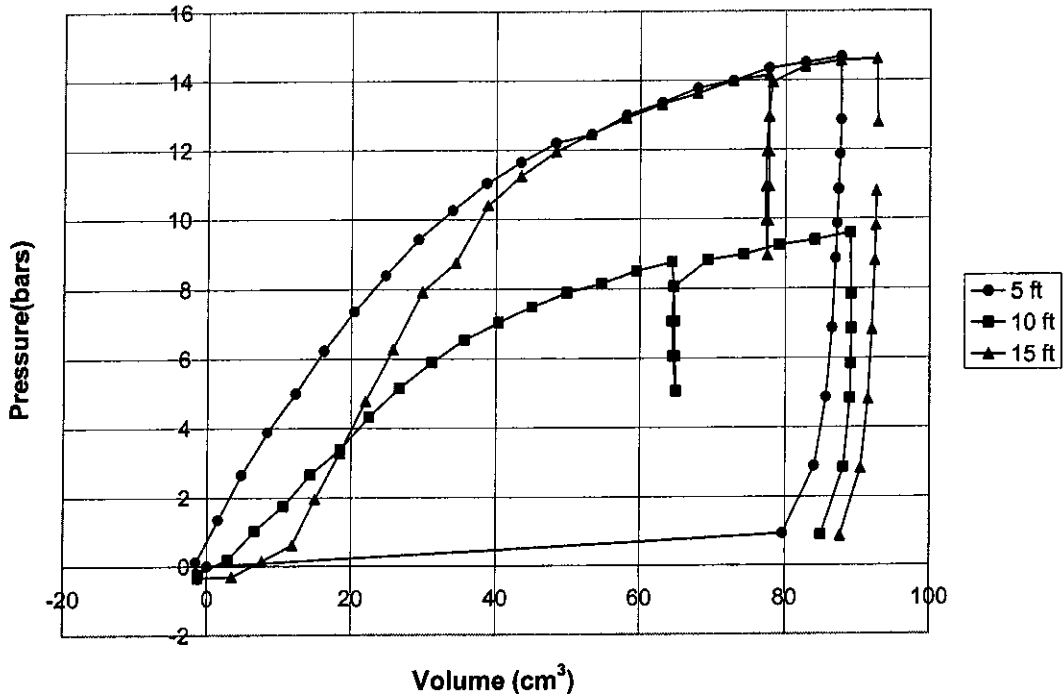


Figure 110 Corrected PENCEL Pressuremeter Test, North, Moffitt Cancer (5 – 15ft)

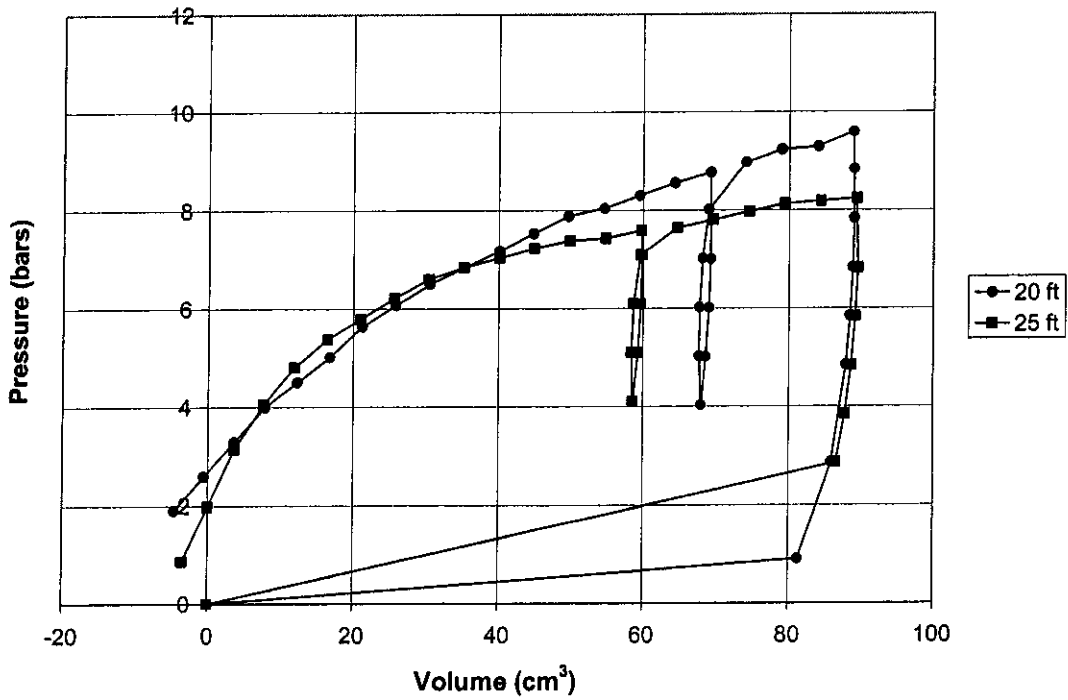


Figure 111 Corrected PENCEL Pressuremeter Test, North, Moffitt Cancer Center (20 – 25ft)

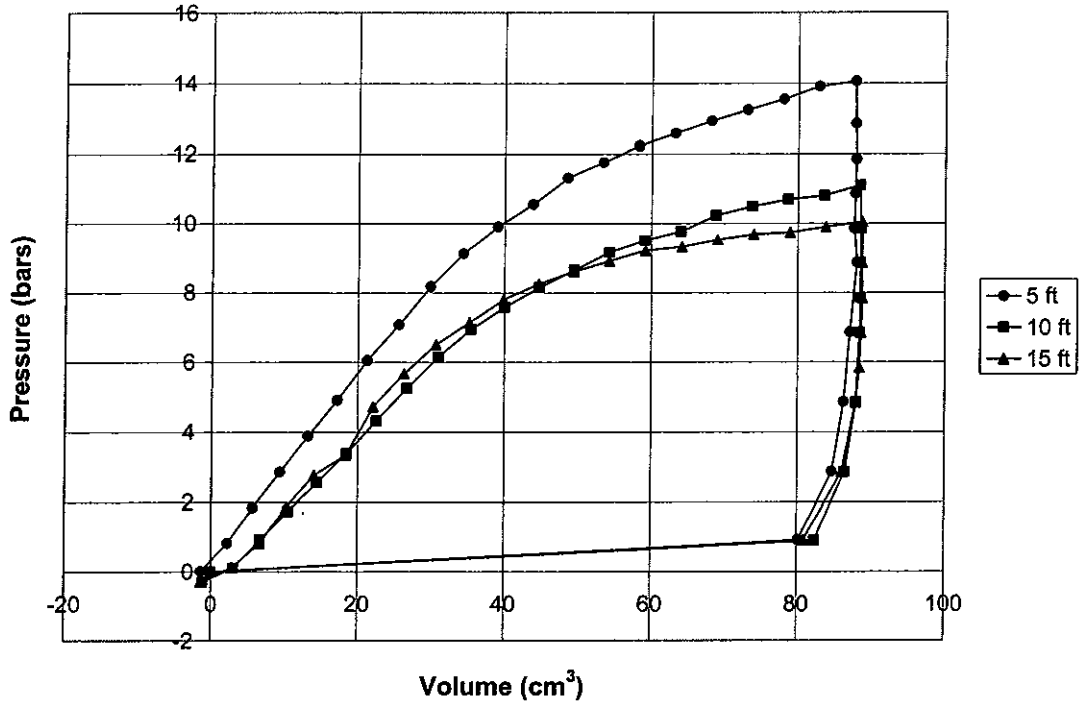


Figure 112 Corrected PENCEL Pressuremeter Test, South, Moffitt Cancer Center (5 – 15ft)

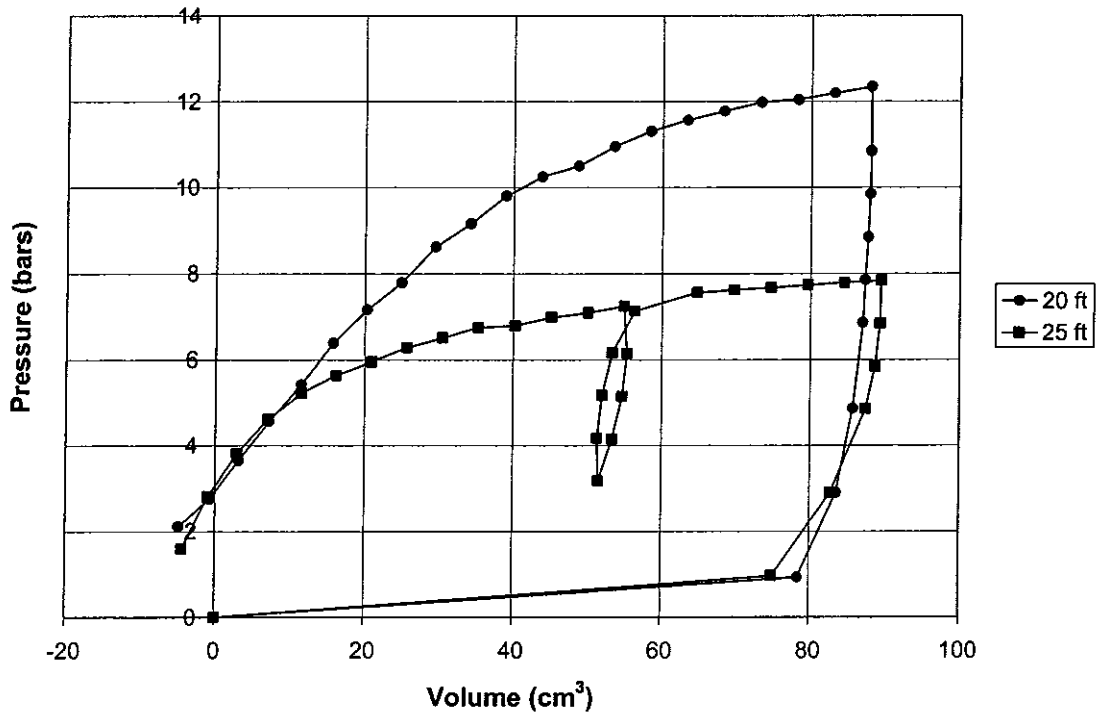
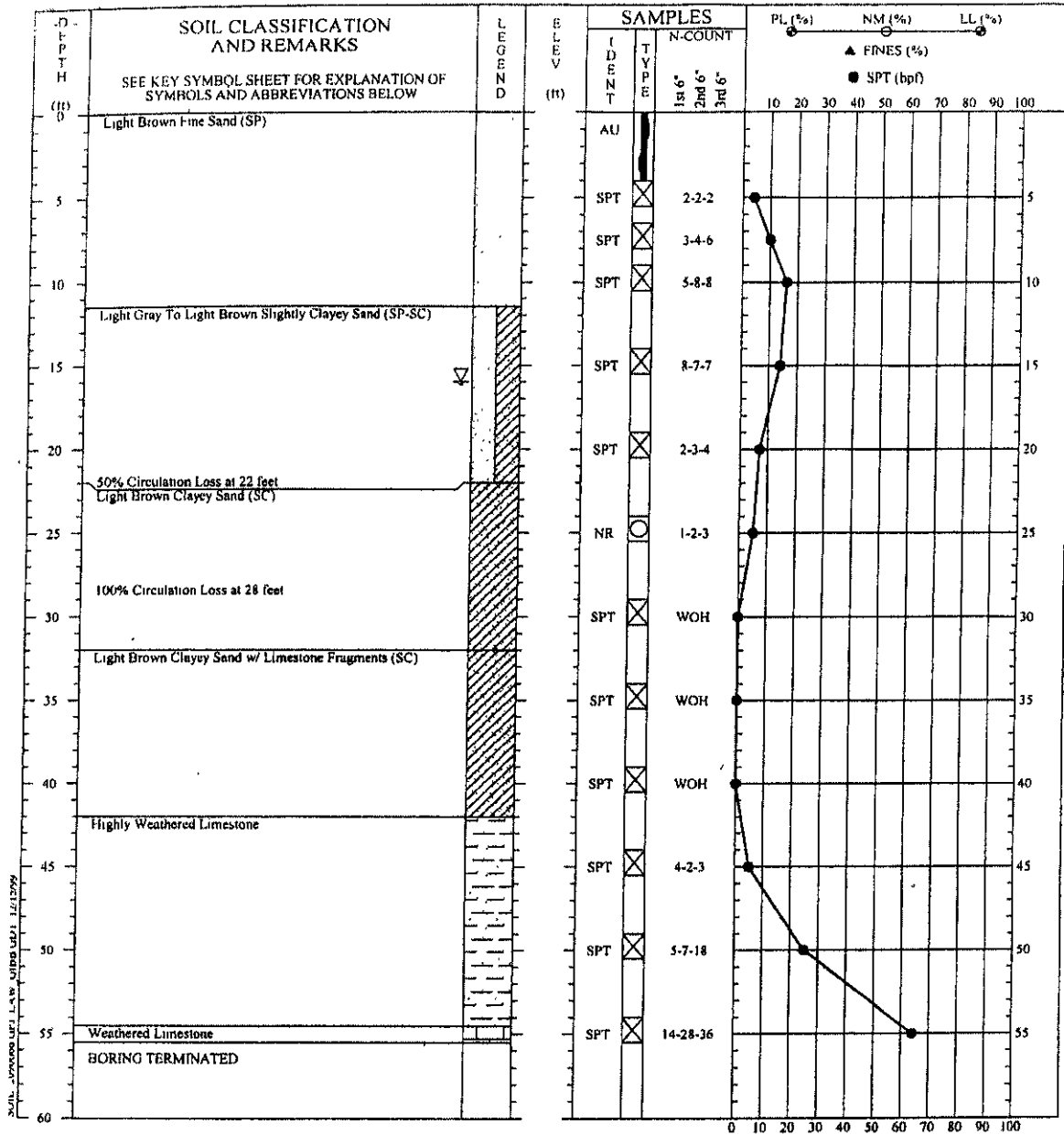


Figure 113 Corrected PENCEL Pressuremeter Test, South, Moffitt Cancer Center (20 – 25ft)



DRILLER: RH  
 EQUIPMENT: Truck-mounted rig with automatic hammer  
 METHOD: Rotary wash boring with drilling mud  
 HOLE DIA: 2-15/16"  
 REMARKS:

THIS RECORD IS A REASONABLE INTERPRETATION OF SUBSURFACE CONDITIONS AT THE EXPLORATION LOCATION. SUBSURFACE CONDITIONS AT OTHER LOCATIONS AND AT OTHER TIMES MAY DIFFER. INTERFACES BETWEEN STRATA ARE APPROXIMATE. TRANSITIONS BETWEEN STRATA MAY BE GRADUAL

SOIL TEST BORING RECORD	
PROJECT:	Moffitt Structure "G" Parking Garage
COORD N:	
COORD E:	
DRILLED:	December 2, 1999
PROJ. NO.:	40120-9-0066
BORING NO.:	G-7
PAGE	1 OF 1
 LAWGIBB Group Member	

Figure 114 Standard Penetration Test Boring G-7 at Moffitt Center

### Sheet-Pile Wall Test Section

As mentioned previously, a cantilevered sheet pile was installed to shore up the excavation of the parking garage. The sheet piles, which were driven into the ground until reaching the bottom layer of weathered limestone, are fairly stout: CZ128 sections. The piles were to be embedded approximately two feet into the weathered limestone, this results in piles tip elevations to vary between +10.00ft and +25.50ft (according to the original driving logdata sheet provided by the Ardaman and Associates, Inc.) A typical drawing of the profile with the driven wall is shown in Figure 115.

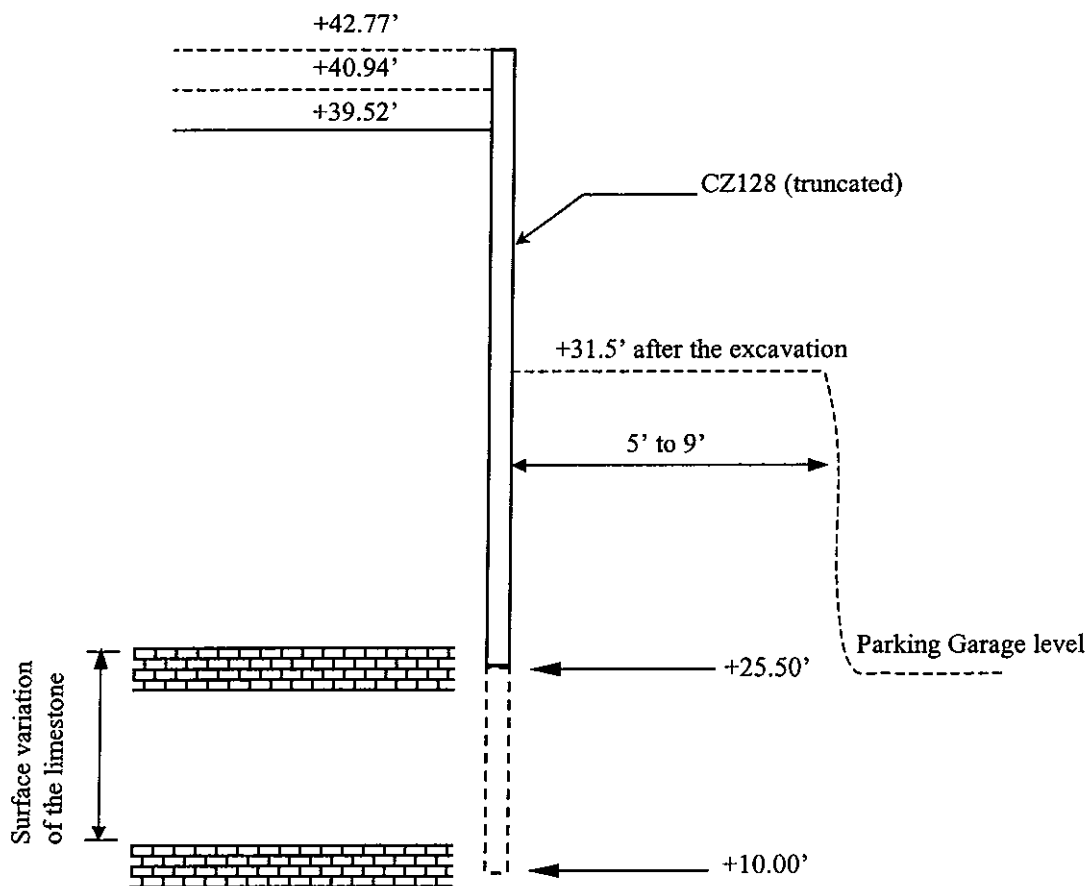


Figure 115 Typical drawing of the cantilevered sheet pile wall at Moffitt Cancer Center

In order to monitor the wall deflection depth profile, a Slope inclinometer was used. Instead of the traditional circular grooved casings, steel box sections were welded to the back of the sheet pilings at three locations along the wall. Figure 116 shows a cross section of the casing attached to the CZ128 pile. The inclinometer probe was inserted along the diagonals of the box section and reads the deflections at 45° offset to the normal to the wall. The software for inclinometer data reduction, the DMMWin Version 1.1.0, can correct the readings for the offset and provide the deflections in two directions: perpendicular to the plane of the wall and parallel to the wall (A+ and B+ directions, respectively).

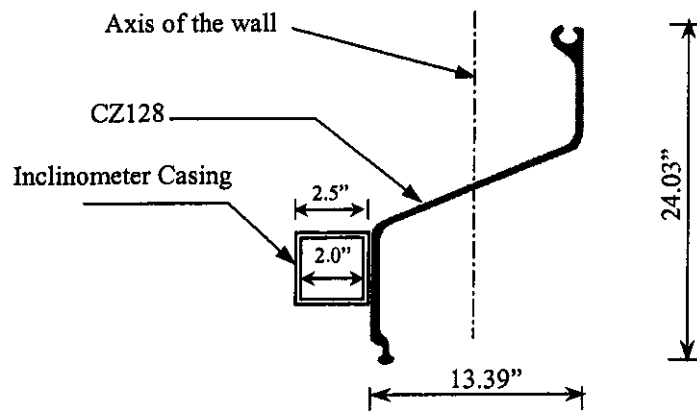
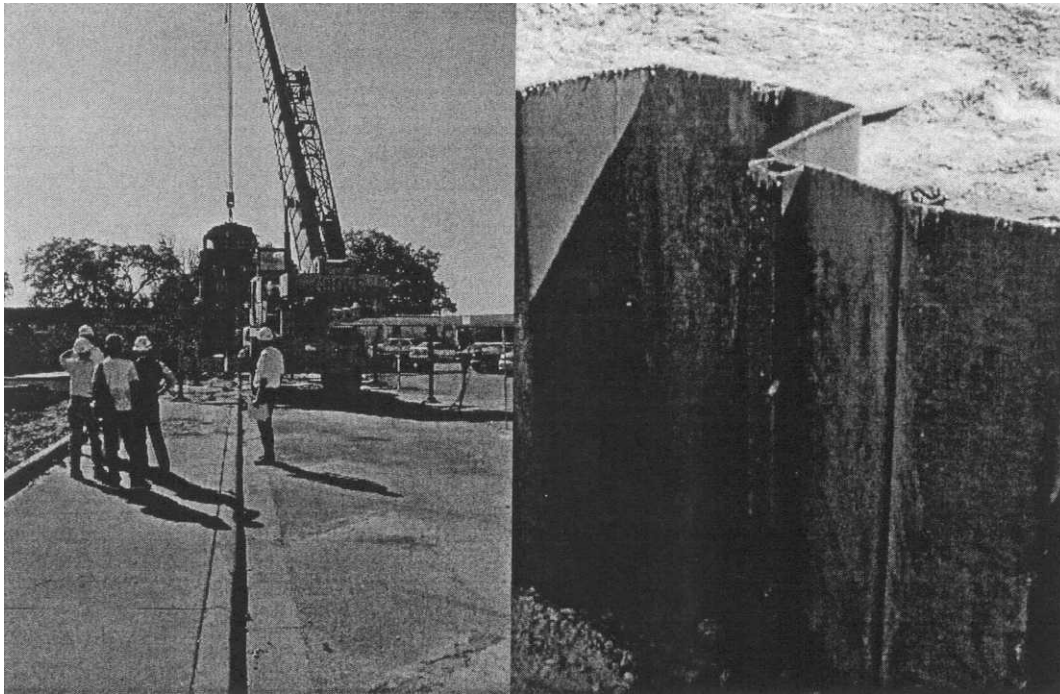


Figure 116 Schematic drawing of CZ128 with the 2.5'' by 2.5'' 1/4'' box tubing.

The photos in Figures 117 (a) and (b) were taken at the Moffitt site and show the pile driving process as well as the inclinometer casing location along the wall.



(a) (b)  
 Figure 117 CZ128 pile driving (a), and inclinometer casing attached to CZ128 (b)

The ground surface elevation behind the wall within the three inclinometer casings is rather uniform. The plan view of the concerned wall is shown in Figure 118 where the ground surface elevations at the casings are indicated: +42.77ft, +40.94ft and +39.52ft. After the excavation, the bottom of the excavation is level and is at Elevation +31.5ft for the three casings, and the elevation where the parking area is designed, at Elevation +25.5ft.

The Digitilt Inclinometer Probe and its accessories were provided by the Florida Department of Transportation (F.D.O.T.): Control Unit: Model 50309, Serial Number: S/N 26084, Probe (with Pulleys and Cable): Model 50325E. It reads the data every 1.0ft of depth along the casings.

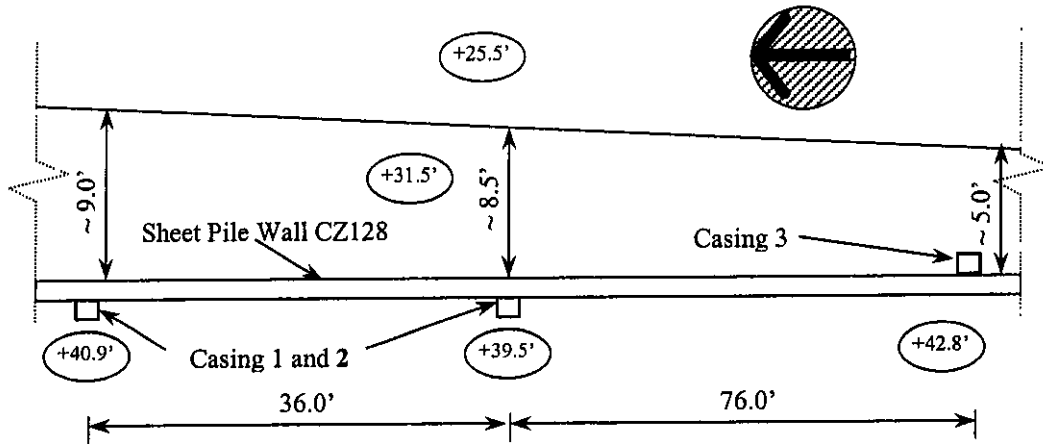


Figure 118 Plan view of inclinometer casings: 1, 2, 3 and CZ128 wall

Since the maximum top deflection of the wall was recorded at Casing 2, the predictions, for both conventional method (CWALSHT) and finite element modeling (Plaxis) were focused on the deflection of the wall at this casing. The bottom of the wall at that section is at Elevation +25.5ft, and the final soil-structure profile for the theoretical analyses is presented in Figure 119.

#### Soil Structure Profile used in CWALSHT and FEM Modeling

The modeling of the soil profile along with the wall were done for the profile corresponding to casing 2. As a remainder, the bottom of the wall is slightly embedded in the weathered limestone at the bottom of the profile. Consequently, for the numerical solution in Plaxis, a pin support is installed at the bottom of the wall in order to prevent any lateral deflection of the bottom. The total length of the wall included in the modeling is 14.0ft ( $L = 39.5 - 25.5 = 14.0$ ft). Also, three stages of the excavation, as shown in Figure 120 are simulated during the finite element computations.

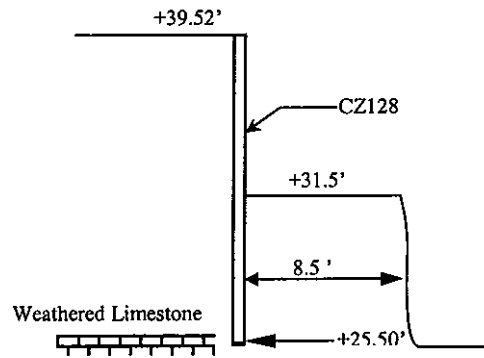


Figure 119 Soil-wall profile for CWALSHT and numerical modeling analyses-Casing 2

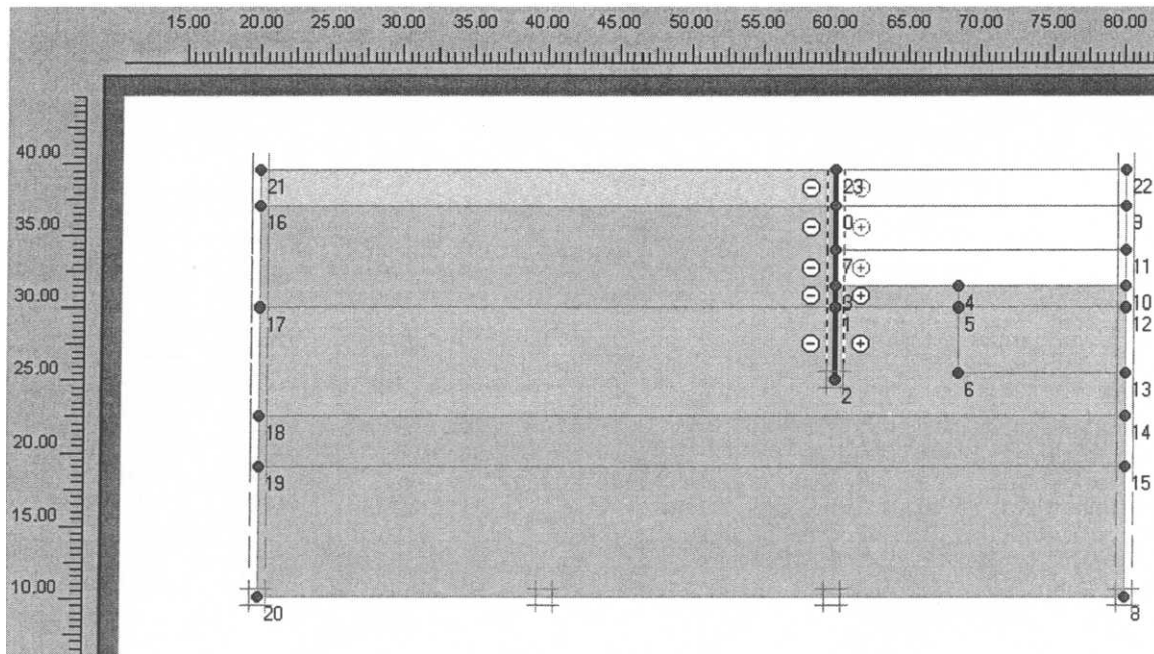


Figure 120 Soil-wall profile after 3-staged excavation – Casing 2

Slope Inclinator Data Reduction

Among the softwares for data reduction available, the Digitilt Datamate Manager for Windows was selected: (DMMWin, Version 1.1.0 manufactured by Slope Indicator Company), to reduce the data collected in the field. The data reduction is divided into two parts. The first part consists of input with the calculations presented in tables and the final cumulative deflections versus depth, table 21. The second part is the plot of the deflections in profile (versus depth) and in Plan view, Figure 121 and Figure 122. Computation on Excel spreadsheet was also prepared and summarized in Table 22 for verification. The results obtained agree.

Table 21 Tabular input and output from DMMWin Software, A Axis and B Axis – Casing 2

SITE : USF 01  
 INSTALLATION : S 01  
 DESCRIPTION : Middle Casing  
  
 CURRENT SURVEY : 5/1/01 11:15:06 AM  
 Probe Serial No : 26084  
  
 INITIAL SURVEY : 4/16/01 12:00:06 PM  
 Probe Serial No : 26084  
  
 DATE PRINTED : 7/31/01 3:31:18 PM

Data Reduction for A Axis:

Depth (ft)	Initial A0	Initial A180	Initial Incr. Dev. (in)	Current A0	Current A180	Current Incr. Dev. (in)	Incr. Disp. (in)	Cum. Disp. (in)
2	50	-34	0.0252	73	-52	0.0375	0.0123	0.1425
3	56	-39	0.0285	76	-56	0.0396	0.0111	0.1302
4	62	-42	0.0312	84	-64	0.0444	0.0132	0.1191
5	60	-44	0.0312	81	-66	0.0441	0.0129	0.1059
6	60	-40	0.0300	80	-60	0.0420	0.0120	0.0930
7	48	-28	0.0228	72	-51	0.0369	0.0141	0.0810
8	26	-10	0.0108	50	-32	0.0246	0.0138	0.0669
9	10	7	0.0009	30	-11	0.0123	0.0114	0.0531
10	-14	30	-0.0132	0	14	-0.0042	0.0090	0.0417
11	-50	70	-0.0360	-34	52	-0.0258	0.0102	0.0327
12	-92	112	-0.0612	-73	92	-0.0495	0.0117	0.0225
13	-122	140	-0.0786	-104	122	-0.0678	0.0108	0.0108
14	0	0	0.0000	0	0	0.0000	0.0000	0.0000

Table 21 Continued.

SITE : USF 01  
 INSTALLATION : S 01  
 DESCRIPTION : Middle Casing  
  
 CURRENT SURVEY : 5/1/01 11:15:06 AM  
 Probe Serial No : 26084  
  
 INITIAL SURVEY : 4/16/01 12:00:06 PM  
 Probe Serial No : 26084  
  
 DATE PRINTED : 7/31/01 3:31:19 PM

## Data Reduction for B Axis:

Depth (ft)	Initial B0	Initial B180	Initial Incr. Dev. (in)	Current B0	Current B180	Current Incr. Dev. (in)	Incr. Disp. (in)	Cum. Disp. (in)
2	-179	192	-0.1113	-161	186	-0.1041	0.0072	0.0651
3	-166	179	-0.1035	-154	176	-0.0990	0.0045	0.0579
4	-152	168	-0.0960	-140	159	-0.0897	0.0063	0.0534
5	-145	160	-0.0915	-134	152	-0.0858	0.0057	0.0471
6	-141	155	-0.0888	-132	149	-0.0843	0.0045	0.0414
7	-132	144	-0.0828	-122	138	-0.0780	0.0048	0.0369
8	-118	133	-0.0753	-106	123	-0.0687	0.0066	0.0321
9	-104	118	-0.0666	-91	108	-0.0597	0.0069	0.0255
10	-90	103	-0.0579	-78	96	-0.0522	0.0057	0.0186
11	-86	98	-0.0552	-77	90	-0.0501	0.0051	0.0129
12	-74	86	-0.0480	-63	79	-0.0426	0.0054	0.0078
13	-38	48	-0.0258	-34	44	-0.0234	0.0024	0.0024
14	0	0	0.0000	0	0	0.0000	0.0000	0.0000

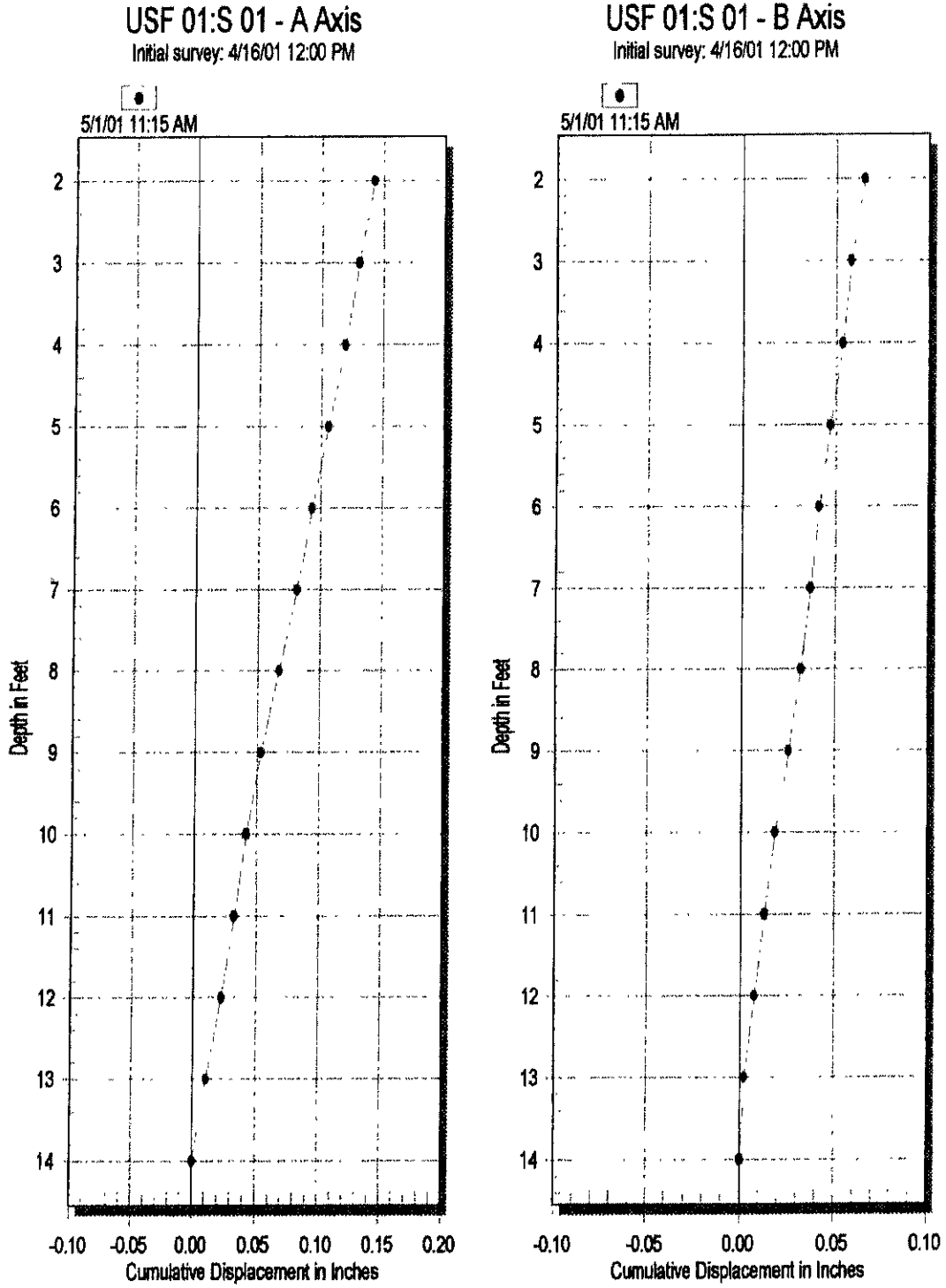


Figure 121 Deflections in A Axis (Perpendicular to wall) and B Axis (Parallel) – Casing 2

**USF 01:S 01 - A Axis vs B Axis**

Initial survey: 4/16/01 12:00 PM

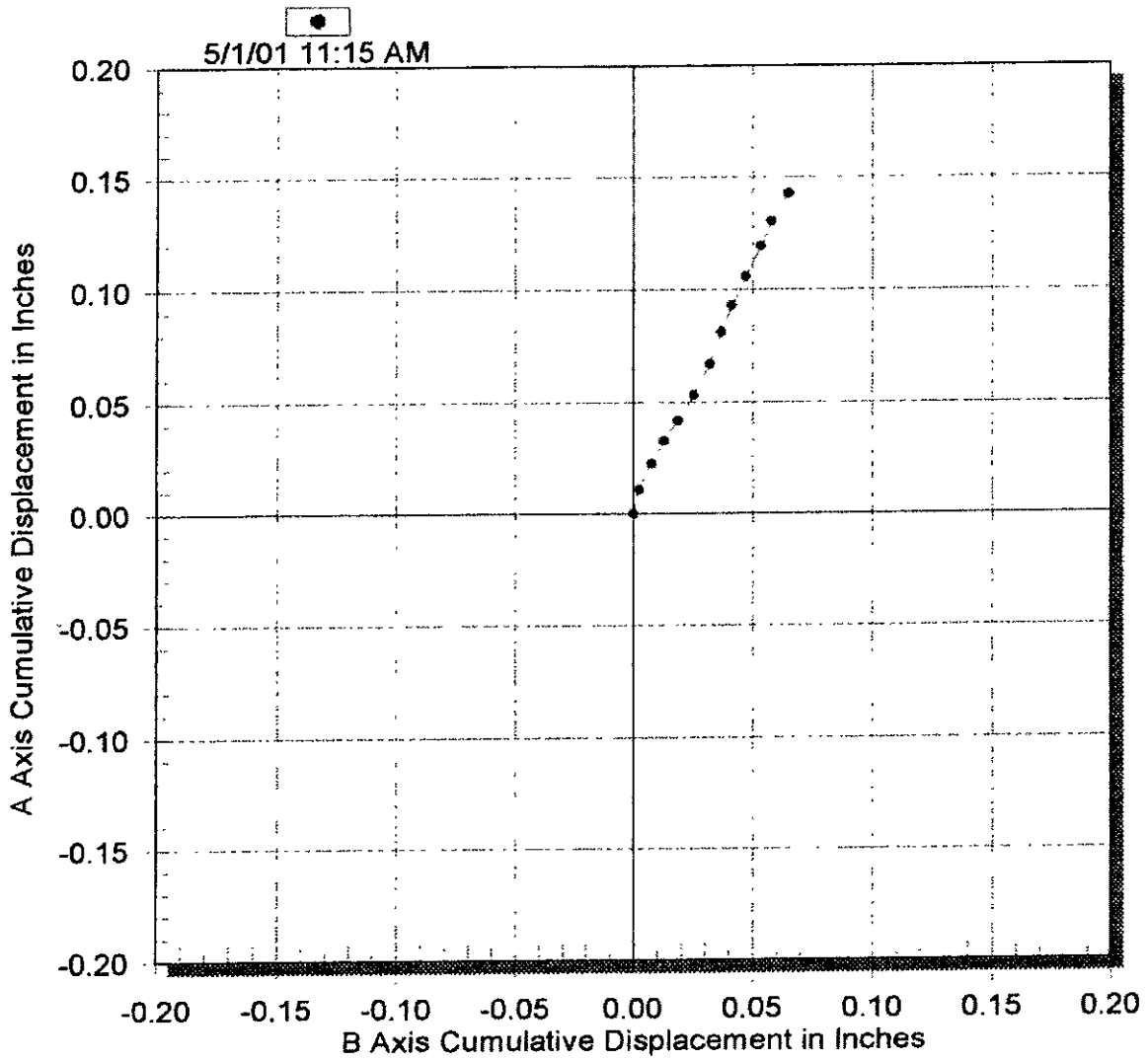


Figure 122 Plan view of wall deflection – Casing 2

Table 22 Excel spreadsheet for inclinometer deflection

## A Axis Data

## Reduction

Depth (ft)	Init. Diff.	A+	A-	Alg. Diff.	CHANGE	Deflect.	Cumul. (in)
13	-261.5	-104.5	122	-226.5	35.0	0.011	0.011
12	-203.5	-73	92.5	-165.5	38.0	0.011	0.022
11	-120.0	-34.5	52.5	-87	33.0	0.010	0.032
10	-44.5	-0.5	14.5	-15	29.5	0.009	0.041
9	3.0	30.5	-11	41.5	38.5	0.012	0.052
8	36.5	50.5	-32	82.5	46.0	0.014	0.066
7	76.5	71.5	-51	422.5	46.0	0.014	0.080
6	100.0	80.5	-60.5	141	41.0	0.012	0.092
5	103.0	81	-65.5	146.5	43.5	0.013	0.105
4	103.0	83.5	-64	147.5	44.5	0.013	0.119
3	95.0	76.5	-56	132.5	37.5	0.011	0.130
2	84.0	73	-52	125	41.0	0.012	0.142

## B Axis Data

## Reduction

Depth (ft)	Init. Diff.	B+	B-	Alg . Diff.	CHANGE	Deflect.	Cumul.(in)
13	-85.5	-33.5	43.5	-77	8.5	0.003	0.003
12	-159.5	-63	79	-142	17.5	0.005	0.008
11	-184.0	-77	90.5	-167.5	16.5	0.005	0.013
10	-193.0	-78	95.5	-173.5	19.5	0.006	0.019
9	-221.5	-91	108	-199	22.5	0.007	0.025
8	-251.5	-105.5	123	-228.5	23.0	0.007	0.032
7	-277.0	-122	138	-260	17.0	0.005	0.037
6	-296.0	-132	149	-281	15.0	0.005	0.042
5	-304.5	-134.5	151.5	-286	18.5	0.006	0.047
4	-321.0	-140.5	159	-299.5	21.5	0.006	0.054
3	-345.0	-153.5	176.5	-330	15.0	0.005	0.058
2	-371.0	-161	186	-347	24.0	0.007	0.066

### Input Parameters and Numerical Modeling:

The numerical values of the soil and wall properties input for the conventional method and the finite element methods are different. Within the finite element modeling, different constitutive models use different types of soil properties for input parameters:

1. First, for the elastic behavior of the CZ128 Wall, only the Elasticity Modulus  $E$  and the Moment of Inertia  $I$  are needed for the CWALSHT program; whereas the both the flexural rigidity  $EI$  and the normal stiffness  $EA$  are input for the finite element Modeling. These properties are presented in Table 23.
2. Second, for the soil behavior, the conventional method with CWALSHT requires the input of the following strength parameters in the program: Friction angle  $\phi$ , Cohesion  $c$  and the Dry and Total Unit Weights  $\gamma$ . Table 24 lists the input parameters used by Ardaman and Associates (Report) resulting from the Miniature Cone Penetrometer test (MCPT). The soil properties correlated from SPT are in Table 25 whereas those from CPT test and PMT test are summarized in Table 27.
3. In addition to the parameters mentioned for CWALSHT, the finite element modeling with Plaxis, the Mohr-Coulomb constitutive model requires the elastic parameters: Young's Modulus  $E^{ref}$  and the Poisson's Ratio  $\nu$ ; the Hardening model, requires the following additional parameters: Oedometer Modulus  $E_{oed}^{ref}$ , and Unload-Reload  $E_{ur}^{ref}$ . The default values are used, which are:  $E_{oed}^{ref} = E_{50}^{ref}$

and Unload-Reload  $E_{ur}^{ref}=3 \times E_{50}^{ref}$  The soil properties for the finite element modeling are listed in Table 26 for the SPT and Table 27 and Table 28 for Mohr-Coulomb and for Hardening Soil, respectively.

4. The program CWALSHT can simulate the actual surface profile of the soil as it is shown in Figure 124. The typical soil profile used for CWALSHT analysis is in Figure 18 whereas that of Numerical analysis is in Figure 126 (before the excavation). The results from the different types of computations are summarized in Table 32 and Table 31 to be compared with the measured deflections from the Slope Inclinometer test.

Table 23 CZ128 wall properties for CWALSHT and Plaxis

Program	CWALSHT	Plaxis
Wall Properties		
Cross Section Area, $A$	-	$EA = 2.227E+08$ (lb/ft)
Elastic Modulus, $E$	29,000,000 (psi)	
Moment of Inertia, $I$	236.5 (in <sup>4</sup> )	$EI = 4.763E+07$ (lb.ft <sup>2</sup> /ft)
Equivalent Thickness, $d$	-	1.602 (ft)
Weight, $w$	-	26.2 (ft/ft)

Correlations for the Input Parameters:

In addition to the actual SPT tests, blow counts were also estimated for the CPT test by using  $q_c/N$  correlations. These are indicated as CPT(N). For the SPT and the CPT based blow count, CPT (N), the friction angles were correlated from Peck et al., (1974):

$$\phi (^{\circ}) = 53.881 - 27.6034 \times \exp(-0.0147 \times N)$$

The undrained shear strength  $c$  was obtained from Terzaghi and Peck, (1948). The Young's Modulus was correlated from the following equations found in Bowles, (1996):

$$E \text{ (kPa)} = 500 \times (N+15) \quad \text{for sand}$$

$$E \text{ (tsf)} = (150 \text{ to } 200) \times c \quad \text{for clay}$$

Finally the unit weights were estimated from the FLPier Manual (FDOT, 2001). These unit weights were used for all other insitu test input of this study.

For the CPT, the friction angles were using the correlations from Robertson and Campanella (1983), based on the effective overburden pressure  $\sigma'_v$  and the cone tip resistance  $q_c$ . The undrained shear strength  $c$  is based on the following empirical correlation:

$$c = (q_c - \sigma'_v) / N_k \quad \text{where } N_k = 10 \text{ to } 15$$

The following Young's Modulus equations from Bowles, (1995) were used to correlate with  $q_c$ :

$$E = (2 \text{ to } 4) \times q_c \quad \text{for Sand and Silty Sand}$$

$$E = (3 \text{ to } 8) \times q_c \quad \text{for clay}$$

The soil properties from the PMT testing were estimated using the correlations in Baguelin et al., (1978). It is combined with the relationship between Menard pressuremeter strength and stiffness parameters with of PENCEL pressuremeter, Briaud,

(1992). Following the procedures, the friction angles turned out to be extremely high ( $\phi > 50^\circ$ ), hence the friction angles resulting from the matching of the insitu pressuremeter curves with the FEM curves were used.

The relations used for the Modulus are:

$$E_{Menard} = \frac{EP_{encel}}{2.03 \times \alpha}$$

where  $\alpha$  is a function of the ratio  $E_M / p_l$ .

The undrained cohesion is directly computed from Baguelin et al., (1978):

$$c_u = \frac{p_l - p_0}{\beta}$$

where  $\beta = 6.5$  was used from the boundary values: 5.6 and 7.4.

Table 24 Soil Properties from MCPT for CWALSHT analysis by Ardaman and Associates(Sounding C-3)

Layer Bottom (ft)	SPT $N$ (bl/ft)	Unit Weight (pcf)	$\phi$ ( $^\circ$ )	$S_u$ (psf)	Wall Friction ( $^\circ$ )	Wall Adhesion (psf)
GS*=0 12.00	8	112	33	-	14	-
15.00	20	118	36	-	14	-
20.00	15	118	36	-	14	-
26.00	25	118	36	-	14	-
30.00	10	112	33	11.0	14	-
36.00	10	110	-	1100	-	600
EOB**	-	135	-	2000	-	1000

\*GS = Ground Surface: Elev. +42.5

\*\*EOB = End of Boring

Table 25 Soil Properties from SPT Boring G-7 for CWALSHT analysis

Bottom (ft)	SPT $N$ (bl/ft)	$\gamma$ (pcf)	$\phi$ ( $^{\circ}$ )	Wall Friction ( $^{\circ}$ )
GS = 0 4.75	4	99.9	27.9	14.8
7.25	10	115.1	30.1	16.1
11.00	16	117.7	32.1	17.4
16.00	14	116.4	31.4	17.0
21.00	7	102.4	29.0	15.5
26.00	5	101.1	28.2	15.0

GS = Elevation +39.5ft

Table 26 Soil Properties from SPT for FEM analysis with Plaxis

Bottom (ft)	SPT $N$ (bl/ft)	$\gamma$ (pcf)	$\phi$ ( $^{\circ}$ )	$E_s$ (psi)	$E_{ur}=3xE_s$ (psi)
GS = 0 4.75	4	99.9	27.9	1377.5	4132.5
7.25	10	115.1	30.1	1812.5	5437.5
11.00	16	117.7	32.1	2247.5	6742.5
16.00	14	116.4	31.4	2102.5	6307.5
21.00	7	102.4	29.0	1595.0	4785.0
26.00	5	101.1	28.2	1450.0	4350.0

GS = Elevation +39.5

Table 27 Soil Properties from Soundings CPT1, PMT1 for CWALSHT

Tests →	CPT (N)						CPT					PMT											
Bottom (ft)	SPT <i>N</i> (bl/ft)	$\gamma_m$ (pcf)	$\phi$ (°)	$S_u$ (psf)	Wall Friction (°)	Adhesion (psf)	$q_c$ (psi)	$\phi$ (°)	$S_u$ (psf)	Wall Friction (°)	Adhesion (psf)	$E_M$ (psi)	$p_l$ (psi)	$\phi$ (°)	$S_u$ (psf)	Wall Friction (°)	Adhesion (psf)						
GS*=0 4.92	36	114.5	37.6	-	22.5	-	2580.1	47	-	28.2	-	2157.3	214.6	37.8	-	22.7	-						
7.51	14	111.3	31.4	-	18.8	-	857.2	43	-	25.8	-							1880.5	166.8	33.5	-	20.1	-
12.30																							
12.50																							
17.49	25	114.5	34.8	-	20.9	-	1449.9	45	-	27.0	-	1982.4	152.3	31	-	18.6	-						
18.86												1632.8	181.3	30	-	18.0	-						
19.69							326.3	-	2944	-	1472	2214.5	116.0	-	1650	-	824.8						
22.51	17	120.9	-	2610		1305	326.3	-	2944	-	1472	2214.5	116.0	-	1650	-	824.8						
22.97																							
33.36 EOB**	8	114.5	-	1044		522																	

\*GS = Ground Surface: Elevation +40.0ft

\*\*EOB = End of Boring

Table 28 Soil Properties for FEM analysis with Plaxis: Mohr-Coulomb Model

Correlated for Mohr-Coulomb												
	CPT(N)					CPT			PMT			
Layer	Bottom (ft)	$\gamma_m$ (pcf)	$\phi$ (°)	$S_u$ (psf)	$E^{ref}$ (kPa)	$\phi$ (°)	$S_u$ (psf)	$E^{ref}$ (psi)	$\phi'$ (°)	$E^{ref}$ (psi)	$c'$ (psf)	Bottom (m)
Sand	GS*=0	114.5	37.6	-	3697.5	48	-	5118.5				GS=0
Sand	4.92								37.8	3188.1	-	1.50
Sand	7.51	111.3	31.4	-	2102.5	43	-	2504.3				2.29
Sand	12.30								33.5	2779.1	-	3.75
Sand	12.50											3.81
Sand	17.49					45	-	4893.3	31	2929.7	-	5.33
Sand	18.86	114.5	34.8	-	2900.0							5.75
Sand	19.69								30	2437.5	-	6.00
Clay	22.51	120.9	-	2610	2718.8							6.86
Clay	22.96					-	2944	1794.4				7.00
Clay	33.63	114.5	-	1044	1450.0				20	1636.0	1650	10.25
	EOB**											EOB

\*GS = Ground Surface = Elev.+40.0ft  $c'$ ,  $\phi'$  : from curve matching using M-C Model

\*\*EOB = End of Boring

Table 29 Input parameters for numerical modeling with Plaxis: Hardening Soil Model

Correlated for Hardening Soil:									
$m = 0.5, \nu_{ur} = 0.2, E_{oed} = E_{50}^{ref}, E_{ur} = 3 \times E_{50}^{ref}$									
	CPT(N)			CPT			PMT		
Bottom (ft)	$E_{50}^{ref}$ (psi)	$\phi$ (°)	$S_u$ (psf)	$E_{50}^{ref}$ (psi)	$\phi$ (°)	$S_u$ (psf)	$E_{50}^{ref}$ (psi)	$\phi'$ (°)	Bottom (m)
GS*=0	3697.5	37.6	-	5118.5	48	-			GS=0
4.92							3188.1	38.0	1.50
7.51	2102.5	31.4	-	2504.3	43	-			2.29
12.30							2779.1	31.0	3.75
12.50									3.81
17.49				4893.3	45	-	2929.7	30.0	5.33
18.86	2900.0	34.8	-						5.75
19.69							2437.5	29.0	6.00
22.51	2718.8	-	2610						6.86
22.97				1794.4	-	2944.1			7.00
33.63	1450.0	-	1044				1636.0	19.0	10.25
EOB**									EOB

\*GS = Ground Surface = Elev. +40.0ft

\*\*EOB = End of Boring

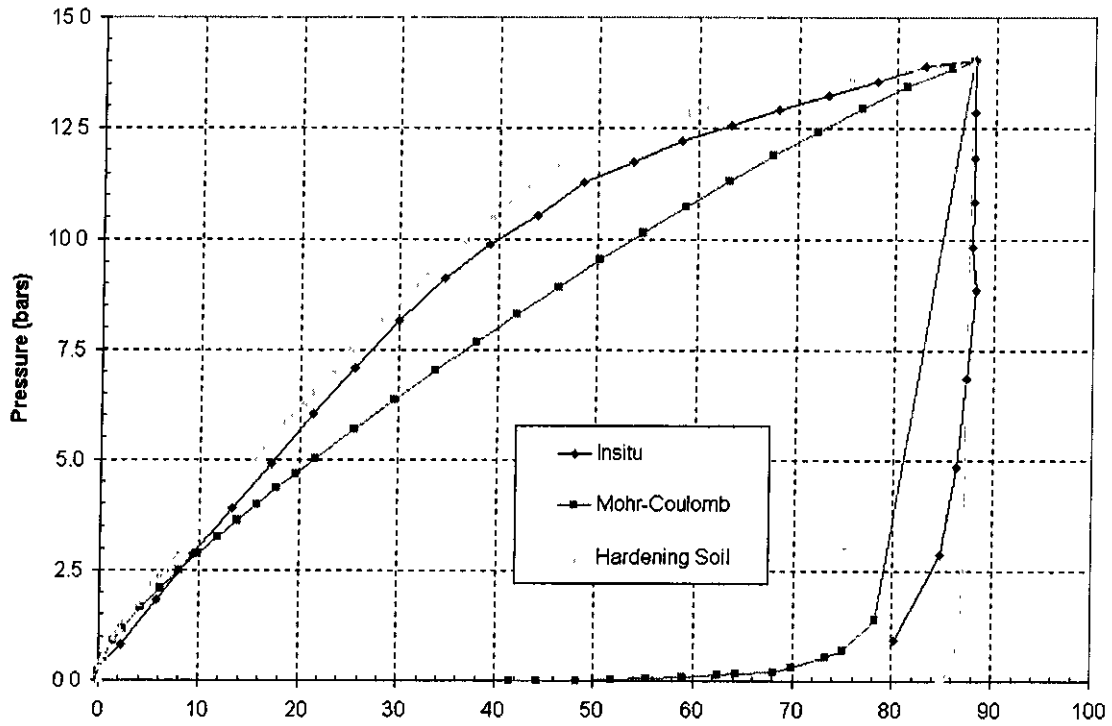


Figure 123 Matching Mohr-Coulomb and Hardening Soil Models with insitu PMT Curve (3.00ft)

Table 30 Soil properties from PMT curve matching (figure 123)

Layer Bottom (ft)	Mohr-Coulomb			Hardening Soil	
	$E^{ref}$ (psi)	$\phi'$ (°)	$c'$ (psi)	$E_{50}^{ref}$ (psi)	$\phi'$ (°)
GS=0 4.92 7.51	21895	37.8	-	42050	38.0
12.30 12.50	21025	33.5	-	29000	31.0
17.49	20155	31.0		14500	30.0
18.86 19.69 22.51	18850	30	-	10295	29.0
22.97 33.63 EOB	10585	20.0	104.4	4350	19.0



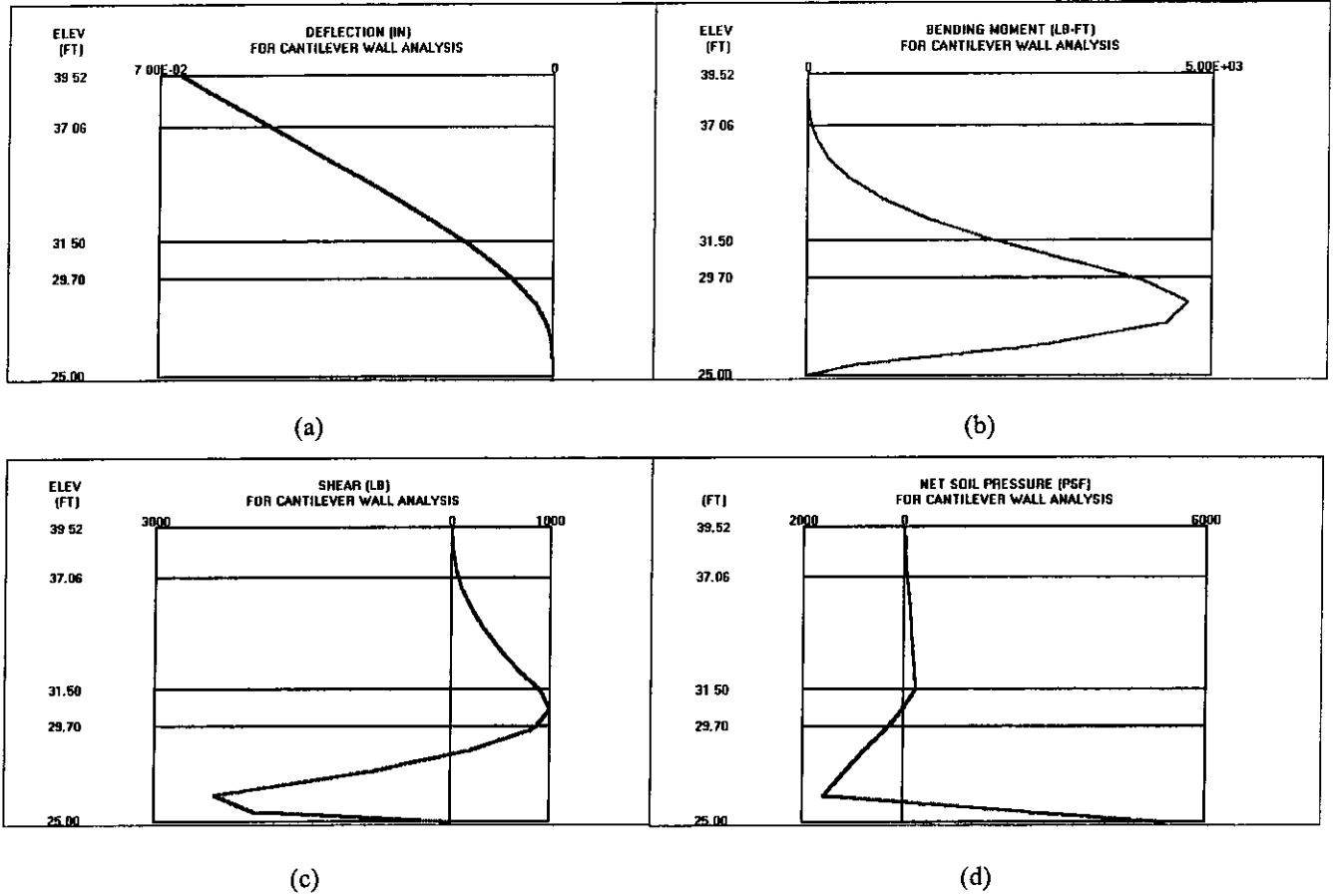


Figure 125 CWALSHT results: (a) deflected shape, (b) moment diagram, (c) shear diagram, (d) net pressure

Table 31 Comparison of results from CWALSHT

Insitu Testing	Deflection (inches)
MCPT	0.07
SPT	0.07
CPT(N)	0.06
CPT	0.04
PMT	0.06

### Finite Element Meshing and Results with Plaxis

The type of problem in the finite element modeling is Plane Strain, Plaxis uses triangular finite elements over the soil profile as shown in Figure 126. The Soil –Wall interface elements are introduced as well. The reduction factor  $R_f$  used is 0.7 for friction between Sand and Steel Wall and 0.5 between Clay and the Steel Wall. During the calculations process, excavation by steps is taken into account and performed in three stages. Among the output plots provided by Plaxis are the Deformed Mesh, lateral Deflection of the wall, Moment distribution and Shear diagram. Figure 127 shows those results. The deflections of the top of the wall predicted by finite element modeling are summarized in Table 32

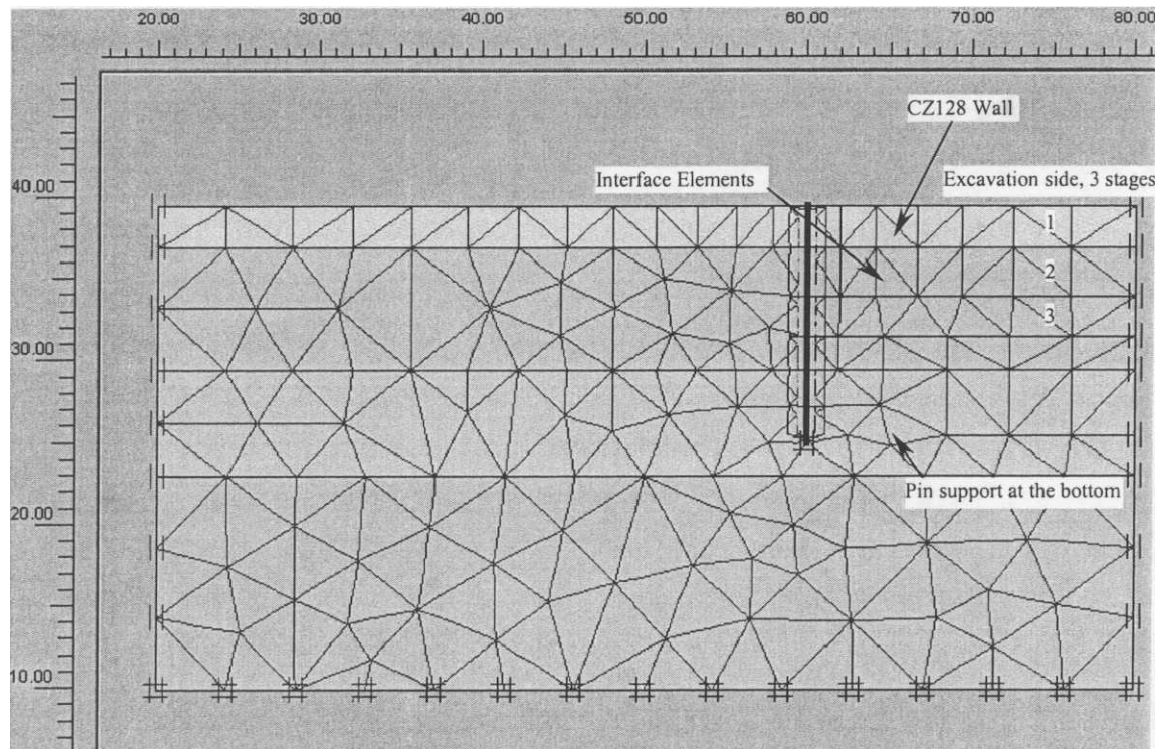


Figure 126 Finite element modeling the soil-wall structure (plane strain)

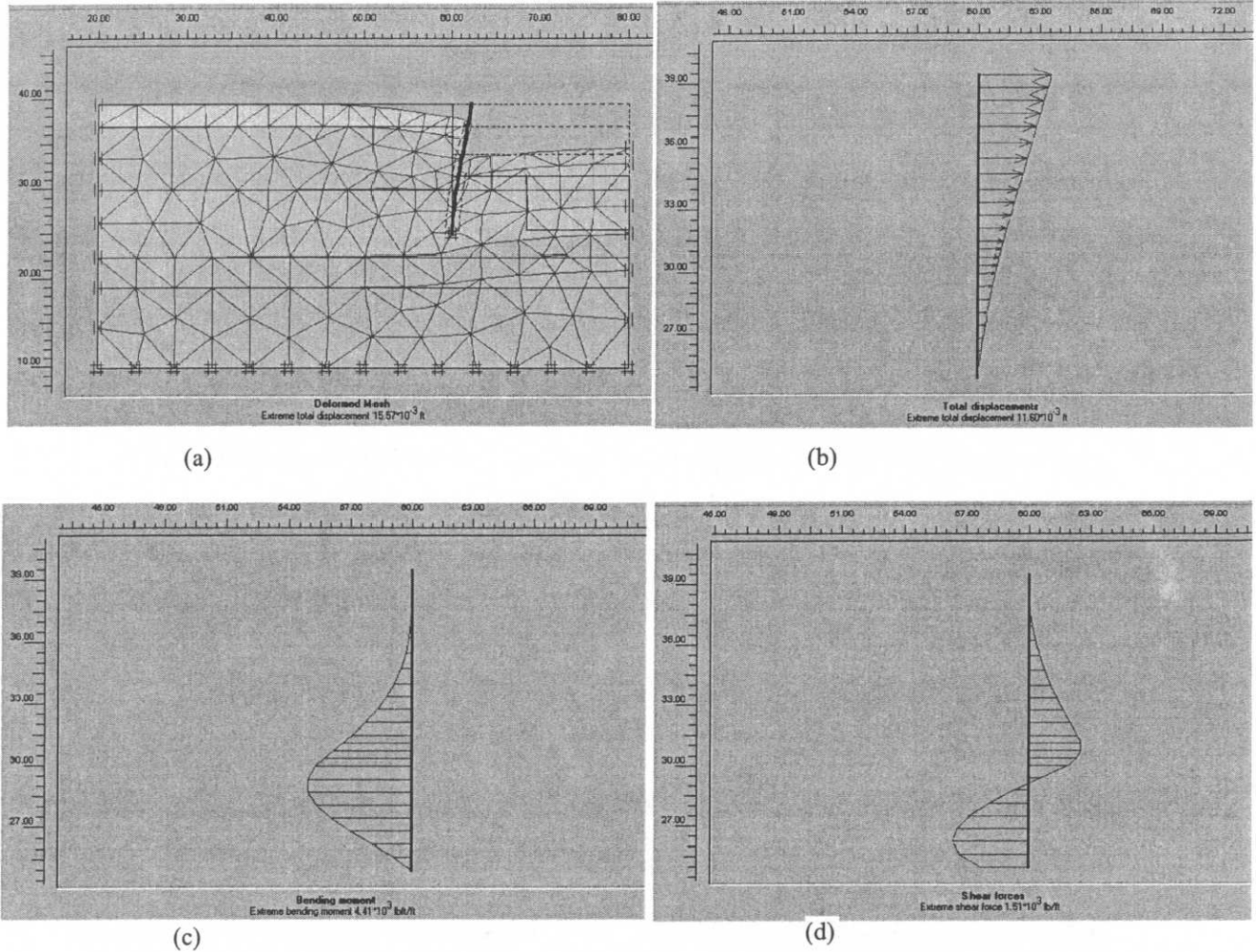


Figure 127 Results from FEM with Plaxis: (a) Deformed Mesh, (b) Wall Deflection(c) Moment Diagram, (d) Shear Diagram

Table 32 Comparison of results from FEM analysis with Plaxis

Model	Deflection (inches)	
	Mohr-Coulomb	Hardening Soil
Insitu test		
SPT	0.72	0.18
CPT(N)	0.54	0.14
CPT	0.11	0.03
PMT (Correlated)	0.56	0.13
PMT (Curve Matching)	0.10	0.05

## Discussion

### Influence of the Choice of Modulus and Constitutive Model

The different strength parameters from the various insitu tests enable us to analyze the effect of these strength parameters on the results, in particular, the friction angle  $\phi$  with the finite element modeling. The use of the elastic modulus  $E$  in the finite element program is also studied. In the Mohr-Coulomb computations above, the moduli used are the loading moduli from each insitu tests; the Hardening soil model includes the unload-reload modulus. Nevertheless, the soil around the sheet pile wall undergoes unloading conditions after the excavation: the backfill side, and the bottom of excavation tending to heave. In this section, computation using the unload-reload modulus is carried out. The unload-reload moduli  $E_{ur}$  are estimated to be three times the reference moduli as suggested in Plaxis Manual and listed in Table 29

$$E_{ur} = 3 \times E^{ref}$$

Since the Mohr-Coulomb Model is the one that does not take into account the unload reload effect, it was decided that using the unload-reload modulus was more appropriate. Consequently, a reanalysis using the unload – reload modulus in the Mohr-Coulomb model was performed. The results are plotted in Figure 129, and the resulting deflections at the top of the wall are listed in Table 34 or comparison with the measured deflections and the previous calculations. These comparisons show that the Mohr-Coulomb model using the unload – reload modulus is practically equal to the Hardening model results.

As conclusion, for these small deformations in unloading conditions, the major difference between the two models is that the Hardening model uses the unload modulus which is three times stiffer than the loading modulus used by the Mohr-Coulomb model.

### Linear Elastic Model

When constructing a structure such as a retaining wall, the designer will always want the wall to be safe with a reasonable factor of safety, say from 1.5 to 3. Thus, the soil does not undergo large deformations and hence the stiffness involved could be the elastic modulus, Young's modulus. A computation for the finite element Elastic Model of the soil was performed. This model uses as main input parameters only the moduli in Table 27. The strength parameters  $c$  and  $\phi$  were not involved in the computation.

As shown in table 33, the resulting predicted deflections are smaller than those from Mohr-Coulomb Model and Hardening Soil Model.

### Comparison and Discussion of the Measured Deflection versus Predicted Deflections

Figures 128 and 129 present the Inclinometer measured deflections and all of the theoretically predicted deflections. The top deflections of the wall from the various methods are summarized in Table 34.

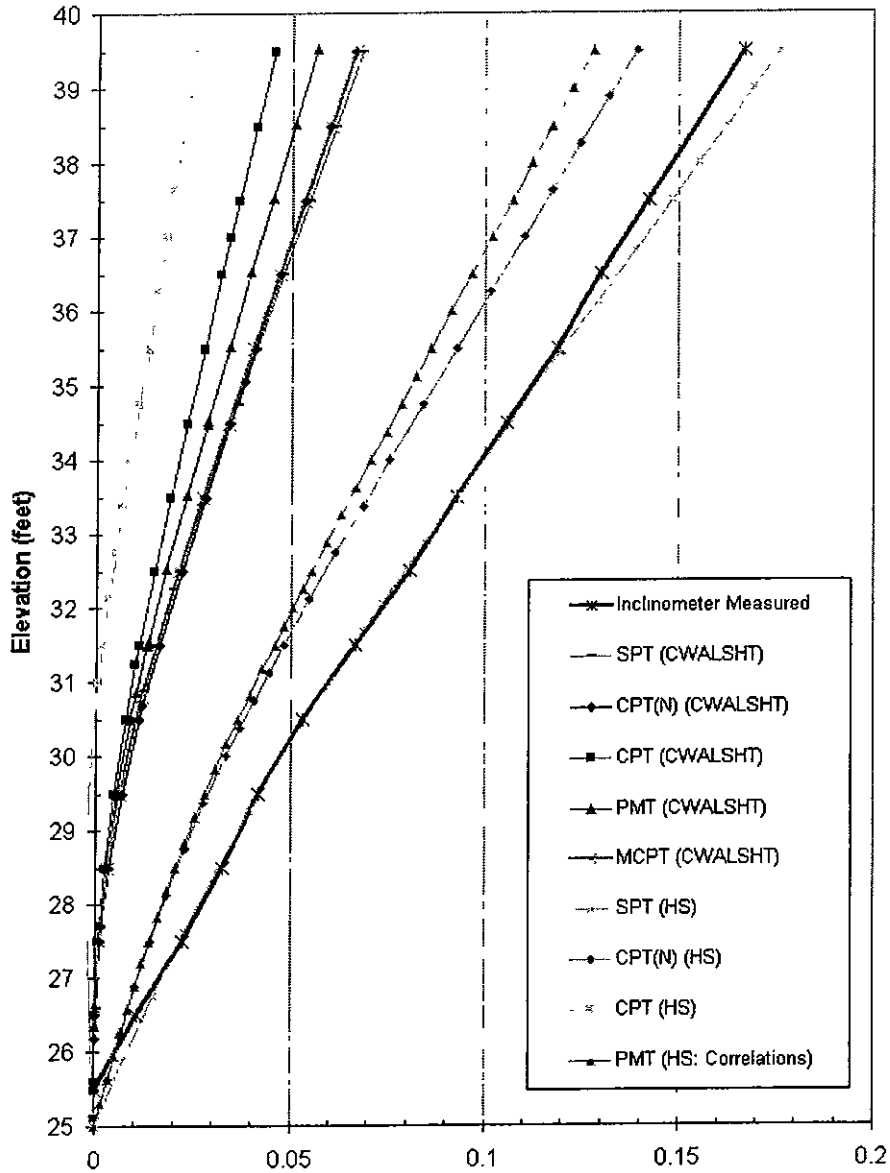


Figure 128 Comparison of results: measured vs. predicted (MC: Mohr-Coulomb, HS: Hardening Soil)

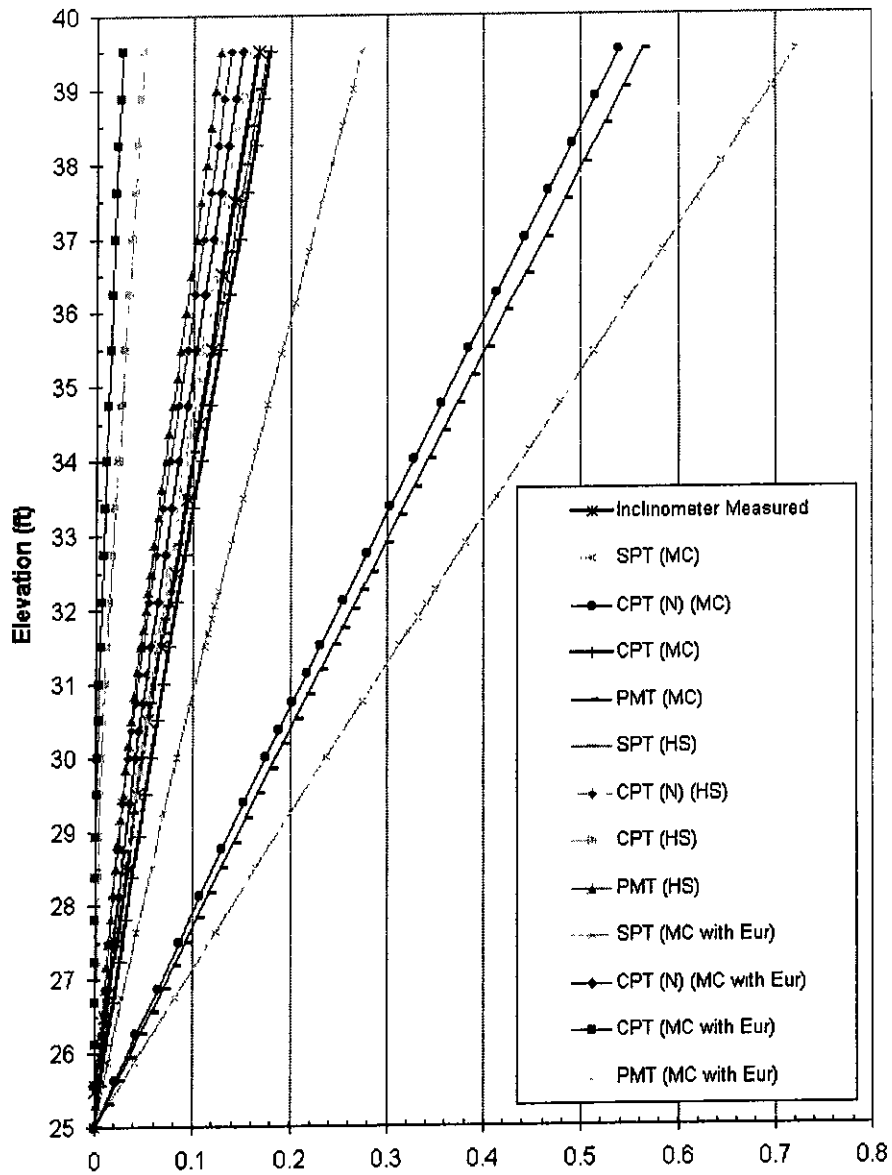


Figure 129 Constitutive models and unload-reload moduli on Plaxis modeling (MC: Mohr-Coulomb, HS: Hardening Soil)

Table 33 Deflections of top of the wall: measured versus predicted

Deflection (inches)	1. Measured with Slope Inclinator					
	0.17					
	2. Predicted: Conventional method and FEM method					
Insitu Test Methods	MCPT	SPT	CPT(N)	CPT	PMT*( $\phi$ curve-fitted)	
					Correlations	Curve Fitting
CWALSHT	0.07	0.07	0.06	0.04	0.06	
Plaxis Mohr-Coulomb	-	0.72	0.54	0.11	0.56	0.09
Plaxis Hardening Soil	-	0.18	0.14	0.03	0.13	0.05
Plaxis Linear Elastic	-	0.10	0.08	0.03	0.07	

\*Curve fitting,  $\phi$  constant,  $E$  varied

Table 34 Effect of modulus and Constitutive Models on top deflection

Deflection (inches)	1. Measured with Slope Inclinator			
	0.17			
	2. Predicted: Predicted with FEM using Plaxis			
Insitu TestModels & Moduli	SPT	CPT(N)	CPT	PMT
Mohr-Coulomb Modulus $E^{ref}$	0.72	0.54	0.11	0.56
Mohr-Coulomb Modulus $E_{ur} = 3 \times E^{ref}$	0.27	0.15	0.007	0.16
Hardening Soil Modulus $E_{50}^{ref}$	0.18	0.14	0.03	0.13

All of the wall top deflection predictions by CWALSHT (average: 0.060inches) are less than half the actual measured deflection of 0.167inches. CWALSHT is not very sensitive to the variation of the strength parameters  $c$  and  $\phi$ . For instance, despite the

large range in the friction angles between CPT ( $43^\circ$  to  $47^\circ$ ) and SPT ( $27.9^\circ$  to  $32.1^\circ$ ), the difference in deflections between using CPT and SPT derived input parameters is only about 0.02 inches. Furthermore, CWALSHT does not require any stiffness parameters of the soil as input. A review of the insitu test input shows that the friction angles from SPT, CPT ( $N$ ), PMT and MCTP are all in the neighborhood of  $32^\circ$ , with the exception of CPT, which is around  $45^\circ$ . However, the highest input value accepted by CWALSHT was  $47^\circ$ . Below Elevation +34.0ft (depth around 6.0ft), the undrained cohesion also varies significantly among the four tests: ranging from 2949psf (CPT) to 1100psf (MCPT). Another computation was performed by keeping all other parameters from the CPT the same, and just varying the cohesion values. The results showed that the effect is negligible.

The strength parameters  $c$  and  $\phi$  used for the finite element analysis are the same as those for CWALSHT except for the Hardening Soil Modeling using PMT data. However, it is observed that the Modulus of the soil  $E^{ref}$  or  $E_{50}^{ref}$  has a fairly large influence on the results for either Mohr-Coulomb or Hardening Soil models. In addition, the change in friction angle also affects the prediction of the wall deflections. For the case of Mohr-Coulomb Model, the stiffnesses were in the same order of magnitude for SPT, CPT ( $N$ ), CPT and PMT. For instance, the predicted deflection using the high friction angle values from CPT was 0.11 inches which is about 80% less than that resulting from using the average friction angles of  $33^\circ$  obtained from the PMT test (0.56 inches). This is also true for the case of the Hardening Soil model: 0.03 inches versus 0.13 inches.

For the PMT parameters, if the stiffness values obtained from the curve-fitting method, which are considerably higher (Table 30) were used, different results were

obtained. In the case of the Mohr-Coulomb Model, the top deflection was underestimated by about 50%: 0.09 inches. Thus, a change in modules from the correlated ones (Table 28) to curve-fitted ones (Table 30) in the Mohr-Coulomb Model lowered the prediction from 0.56 inches to 0.09 inches. For the case of Hardening Soil model, the curve-fitting moduli values resulted in a top deflection about half of that from Mohr-Coulomb model: 0.05 inches and 0.09 inches, respectively.

Computations with the Mohr-Coulomb model using the unload-reload moduli  $E_{ur}$  in Table 29 give good predictions using the input derived from SPT, CPT( $N$ ) and PMT. Good predictions were obtained as well by using the reference moduli  $E_{50}^{ref}$  with the Hardening Soil using parameters from SPT, CPT( $N$ ), and PMT. These results are shown in Table 34.

In summary, the plots in Figure 128 can be divided in 3 groups of predictions: (1) the smallest deflections (both CPT), (2) the more accurate predictions (6 cases mentioned above) and (3) the over predicted deflections. The underproduction results are due to the high friction angles. The unloading conditions in the problem are considered by Mohr-Coulomb only by introducing directly the unload-reload modules  $E_{ur}$ , whereas it is taken into account by Hardening Soil model through the reference modulus  $E_{50}^{ref}$ .

## Conclusions

### Conclusions from finite element modeling

1. Higher friction angle produces less deformation
2. Higher stiffness produces less deformation

3. Mohr Coulomb model results in an over-conservative higher value of the deflection than that of the Hardening Soil Model, due to the latter using a stiffer unload modulus
4.  $E_{ur}$  in the Mohr Coulomb model can be as good analysis as Hardening soil in deep excavation problems.

### Conclusions concerning Input Parameters

Referring to the measured deflection of the wall, the most accurate predictions are the SPT and CPT ( $N$ ) derived parameters using the Hardening Soil Model, followed by the CPT parameters using the Mohr Coulomb Model and the PMT (correlated) Hardening Soil Model. The common point these three scenarios have is that they all have the same order of magnitude of stiffness values; and the high friction angle from CPT over-compensated the softer Mohr Coulomb loading modules. For the other predictions, it is noted that the input parameters, which are the strength and the stiffness, and the model (Mohr Coulomb and Hardening Soil) did not compensate to obtain better results.

The results obtained from the Elastic Model for soils showed that generally the predicted deflections are smaller than in Mohr-Coulomb and Soil Hardening Model Table 33. Hence, the Linear Elastic model is too unconservative even though the measured deflection was fairly small.

The conclusions are:

1. Friction angle values ( $\phi$ ) from CPT Robertson and Campanella, Ticino Sand (Calibration Chamber Correlations) are unrealistically high.
2. SPT and CPT( $N$ ) (FL Pier) and Correlated PMT (Jezequiel and Briaud) give better results for the Hardening Soil model when  $\phi$  SPT was used.

3. It was found out that even at very small deformation of the soil, the linear elastic model for soils is not appropriate for this type of problem.
4. CWALSHT under-predicts wall deformations unconservatively and has less sensitivity of the few input parameters.
5. Plaxis has more analysis capability and parameter sensitivity over CWALSHT.
6. For unloading problems,  $E_{ur}$  can be reliably used with the Mohr-Coulomb model.

## CHAPTER 7 GREEN COVE SPRINGS CIRCULAR FOOTING PREDICTION

### Introduction

Assessment of footing settlement is critical in assuring the serviceability criterion of the structure that it supports. At present, the criterion for a satisfactory shallow foundation involves evaluating the bearing capacity of the soil underneath and the settlement caused by the applied load. Various calculations have been used to estimate the settlement of a footing, depending on various approaches, assumptions, and types of soil data available, laboratory or insitu test data. The methods can be divided into two categories, conventional methods and the finite element based methods (constitutive models). In this chapter, estimation of the settlement of a shallow concrete footing using the data from insitu testing is studied using both conventional analytical methods and finite element methods to ascertain the appropriateness of each to predict the settlement of a shallow footing.

The University of Florida conducted a static load test of a shallow concrete footing in collaboration with the Applied Foundation Testing, Inc. The site is located in Green Cove Springs, inside the headquarters of the AFT, Inc., Clay County, Florida.

### Objectives

The main objective is to predict the settlement due to static loading using a number of conventional methods in practice and finite element analysis. The calculations

are based on the soil properties obtained from the insitu tests conducted on the site by the University of Florida. The insitu tests are: Cone Penetration Test (CPT), the Dilatometer Test (DMT) and the PENCEL Pressuremeter Test (PMT). In addition to these tests, the LawGibb Group for this study also performed the Standard Penetration Test (SPT) and Sampling.

### Scope of the Work

The following tasks included in this chapter in order to attain the objectives above are:

1. Presentation of the data form the CPT, DMT, PMT, and SPT tests and identifying the input parameters for theoretical analyses;
2. Constructing a concrete footing and defining its physical and mechanical properties;
3. Instrumentation of the footing with reference beams, load cells, and LVDTs.
4. Loading process and data acquisition during the loading sequences, and measurement of the actual settlement of the concrete footing;
5. Comparison of the measured settlement with the results obtained from back-up survey measurements.
6. Predictions of the settlement using the CSANDSET for the conventional methods and the Plaxis code for the finite element analysis.
7. Comparison of the LVDTs measured settlement with the results from theoretical calculations

### Site Description and Insitu Testing

The static load test was carried out at the headquarters of the Applied Foundation Testing, Inc. in Green Cove Springs, Florida. The soundings for the insitu testing were located at a distance about 10.0ft (maximum) from the center of the projected footing as illustrated in Figure 130 (No map of the site was available).

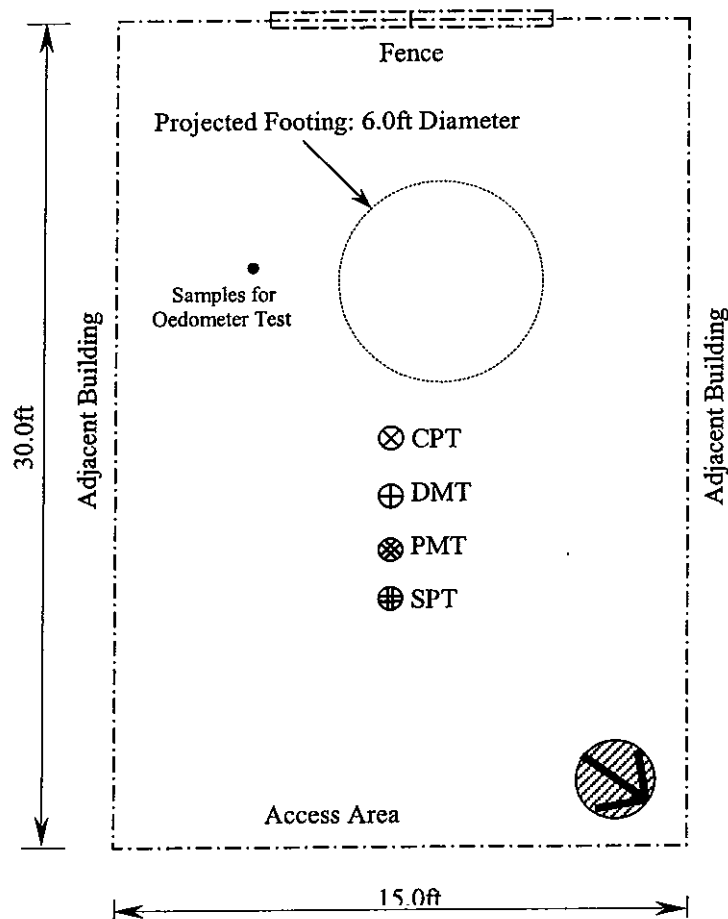


Figure 130 Insitu testing boring locations at Applied Foundation Testing Inc., site

The University of Florida cone truck was used for the CPT, DMT, and PMT tests at 6 different depths. The CPT testing was conducted to a depth 34.4ft (10.5m) below the ground surface; the DMT testing was performed to 27.6ft (8.4m); and the six depths for

the PMT testing were at 3.3ft (1.0m), 6.6ft (2.0m), 9.8ft (3.0m), 16.4ft (5.0m), 23.0ft (7.0m), and 32.8ft (10.0m). The data resulting from CPT are presented in Figure 131 and Table 35, whereas data from DMT testing are in presented in Table 36; also for the DMT, the typical presentation of DMT data versus depth is shown in Figure 132. The pore pressure readings were not included in the testing procedure for CPT and DMT. However, the ground water table could be estimated to be at depth about 5.5ft (1.68m) below the surface based on the SPT sounding and sampling carried out by Law Gibb Inc.

Figure 133 and Figure 134 show the corrected Pressuremeter pressure versus volume curves. The 3 tests (CPT, DMT, PMT) indicate that the soil profile is composed of a very stiff sand layer down to the depth of about 16.4ft (5.0m) below the ground surface, underlain by a very soft (highly compressible) clay layer below the 19.7ft (6.0m) depth. A rather dense silty sand layer is located in between the sand and clay layers. The SPT blow counts versus depth from the test performed by the Law Engineering Group are plotted in Figure 135 as well.

University of Florida  
 Operator : Brian/Landy  
 Sounding : gca012 Pg 1 / 1  
 Cone Load : 519  
 CPT Date : 04-23-01 10:22  
 Location : Green Cove Spring  
 Job No. : Project 01

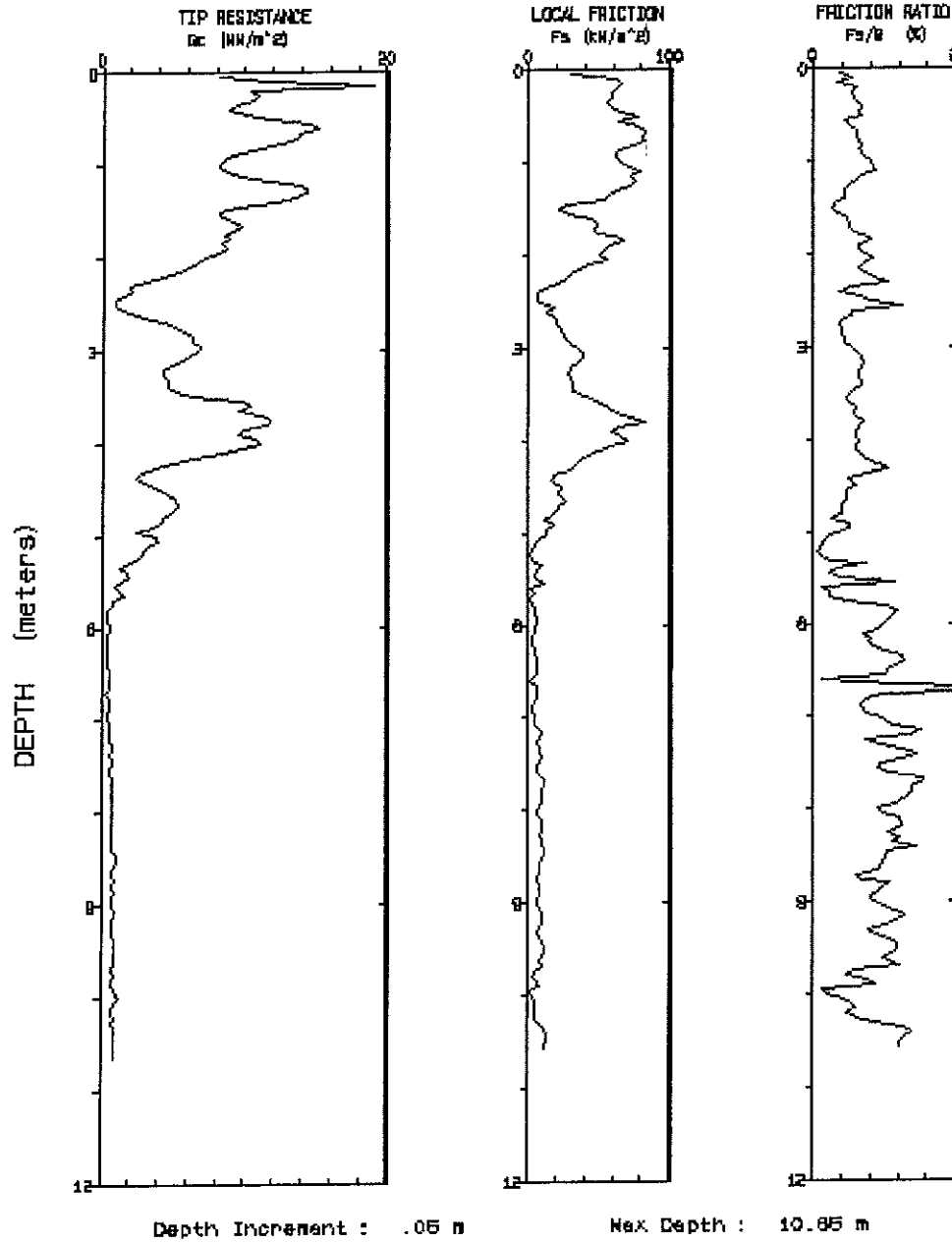


Figure 131 Cone penetration test sounding at Green Cove Springs

Table 35 Soil properties from CPT data reduction

DEPTH		Qc (avg)	Fs (avg)	Rf (avg)	SIGV'	SOIL BEHAVIOUR TYPE	Eq - Dr	PHI	SPT	Su
(meters)	(feet)	(MN/m <sup>2</sup> )	(kN/m <sup>2</sup> )	(%)	(bar)		(%)	deg.	N	bar
0.25	0.82	12.03	56.08	0.47	0.02	sand	>90	>48	24	UNDEFINED
0.50	1.64	10.12	63.04	0.62	0.07	sand to silty sand	>90	>48	25	UNDEFINED
0.75	2.46	13.96	77.20	0.55	0.11	sand	>90	>48	28	UNDEFINED
1.00	3.28	9.44	65.64	0.70	0.16	sand to silty sand	>90	>48	24	UNDEFINED
1.25	4.10	11.06	74.24	0.67	0.20	sand to silty sand	>90	>48	28	UNDEFINED
1.50	4.92	11.59	44.48	0.38	0.25	sand	>90	46-48	23	UNDEFINED
1.75	5.74	9.03	43.46	0.48	0.29	sand to silty sand	80-90	44-46	23	UNDEFINED
2.00	6.56	8.27	57.74	0.70	0.34	sand to silty sand	70-80	44-46	21	UNDEFINED
2.25	7.38	5.12	38.10	0.74	0.38	silty sand to sandy silt	60-70	42-44	17	UNDEFINED
2.50	8.20	1.52	10.38	0.68	0.43	sandy silt to clayey silt	UNDFND	UNDFD	6	.9
2.75	9.02	3.36	17.58	0.52	0.47	silty sand to sandy silt	40-50	38-40	11	UNDEFINED
3.00	9.84	6.40	27.98	0.44	0.52	sand to silty sand	60-70	40-42	16	UNDEFINED
3.25	10.66	5.14	33.98	0.66	0.56	sand to silty sand	50-60	40-42	13	UNDEFINED
3.50	11.48	5.50	32.76	0.60	0.61	sand to silty sand	50-60	40-42	14	UNDEFINED
3.75	12.30	10.51	57.42	0.55	0.65	sand	70-80	42-44	21	UNDEFINED
4.00	13.12	10.58	68.26	0.65	0.70	sand to silty sand	70-80	42-44	26	UNDEFINED
4.25	13.94	6.73	44.74	0.66	0.74	sand to silty sand	60-70	40-42	17	UNDEFINED
4.50	14.76	3.16	21.16	0.67	0.79	silty sand to sandy silt	<40	36-38	11	UNDEFINED
4.75	15.58	5.08	22.60	0.44	0.83	sand to silty sand	50-60	38-40	13	UNDEFINED
5.00	16.40	3.67	14.24	0.39	0.88	silty sand to sandy silt	40-50	36-38	12	UNDEFINED
5.25	17.22	3.10	3.76	0.12	0.92	silty sand to sandy silt	<40	34-36	10	UNDEFINED
5.50	18.04	1.67	6.04	0.36	0.97	sandy silt to clayey silt	UNDFND	UNDFD	7	1.0
5.75	18.86	1.08	4.40	0.41	1.01	sandy silt to clayey silt	UNDFND	UNDFD	4	.6
6.00	19.69	0.48	5.04	1.06	1.06	sensitive fine grained	UNDFND	UNDFD	2	.2
6.25	20.51	0.45	3.66	0.81	1.10	sensitive fine grained	UNDFND	UNDFD	2	.2
6.50	21.33	0.50	5.68	1.14	1.15	sensitive fine grained	UNDFND	UNDFD	2	.2
6.75	22.15	0.46	4.68	1.02	1.19	sensitive fine grained	UNDFND	UNDFD	2	.2
7.00	22.97	0.52	3.94	0.76	1.24	sensitive fine grained	UNDFND	UNDFD	3	.2
7.25	23.79	0.64	7.20	1.13	1.28	sensitive fine grained	UNDFND	UNDFD	3	.3
7.50	24.61	0.68	7.94	1.17	1.33	sensitive fine grained	UNDFND	UNDFD	3	.3
7.75	25.43	0.68	8.86	1.30	1.37	undefined	UNDFND	UNDFD	UDF	UNDEFINED
8.00	26.25	0.71	8.58	1.21	1.42	undefined	UNDFND	UNDFD	UDF	UNDEFINED
8.25	27.07	0.76	8.74	1.14	1.46	clayey silt to silty clay	UNDFND	UNDFD	4	.4
8.50	27.89	0.89	10.18	1.14	1.51	clayey silt to silty clay	UNDFND	UNDFD	4	.4
8.75	28.71	0.85	6.84	0.81	1.55	clayey silt to silty clay	UNDFND	UNDFD	4	.4
9.00	29.53	0.83	7.60	0.92	1.60	clayey silt to silty clay	UNDFND	UNDFD	4	.4
9.25	30.35	0.82	9.20	1.12	1.64	clayey silt to silty clay	UNDFND	UNDFD	4	.4
9.50	31.17	0.88	8.98	1.02	1.69	clayey silt to silty clay	UNDFND	UNDFD	4	.4
9.75	31.99	0.84	8.36	0.99	1.73	clayey silt to silty clay	UNDFND	UNDFD	4	.4
10.00	32.81	0.97	4.26	0.44	1.78	sandy silt to clayey silt	UNDFND	UNDFD	4	.5
10.25	33.63	0.84	4.34	0.52	1.82	sensitive fine grained	UNDFND	UNDFD	4	.4
10.50	34.45	0.91	11.02	1.21	1.87	clayey silt to silty clay	UNDFND	UNDFD	5	.4

Dr - All sands (Jamiolkowski et al. 1985)

PHI - Robertson and Campanella 1983

Su: Nk= 15

\*\*\*\* Note: For interpretation purposes the PLOTTED CPT PROFILE should be used with the TABULATED OUTPUT from CPTINTR1 (v 3.04)

Table 36 Soil properties from DMT data reduction

DILATOMETER DATA LISTING & INTERPRETATION (BASED ON THE 1988 DILATOMETER MANUAL)  
 GPE, INC.

SNDG. NO. DMT-22

JOB FILE: UNIVERSITY OF FLORIDA RESEARCH

FILE NO.: 83-500

LOCATION: GREEN COVE SPRINGS

SNDG.BY : BRIAN/CHRIS/LANDY - UF CPT TRUCK

SNDG. DATE: 12 DEC 01

ANAL.BY : LANDY R./UF - GEOTECHNICAL GROUP

ANAL. DATE: 12 DEC 01

ANALYSIS PARAMETERS:	LO RANGE =10.00 BARS	ROD DIAM. = 3.70 CM	BL.THICK. = 15.0 MM	SU FACTOR = 1.00
SURF. ELEV. = 0.00 M	LO GAGE 0 = 0.00 BARS	FR.RED.DIA. = 4.80 CM	BL.WIDTH = 96.0 MM	PHI FACTOR = 1.00
WATER DEPTH = 1.68 M	HI GAGE 0 = 0.00 BARS	LIN.ROD WT. = 6.50 KGF/M	DELTA-A = 0.20 BARS	OCR FACTOR = 1.00
SP.GR.WATER = 1.000	CAL GAGE 0 = 0.00 BARS	DELTA/PHI = 0.50	DELTA-B = 0.27 BARS	M FACTOR = 1.00
MAX SU ID = 0.60	SU OPTION = MARCHETTI	MIN PHI ID = 1.20	OCR OPTION= MARCHETTI	K0 FACTOR = 1.00

UNIT CONVERSIONS: 1 BAR = 1.019 KGF/CM2 = 100 KPA = 1.044 TSF = 14.51 PSI 1 M = 3.2808 FT

Z	ELEV	THRUST	A	B	DA	DB	ZMRNG	ZMLO	ZMHI	ZMCAL	P0	P1	U0	GAMMA	SVP	KD
(M)	(M)	(KGF)	(BAR)	(T/M3)	(BAR)											
*****	*****	*****	*****	*****	*****	*****	*****	*****	*****	*****	*****	*****	*****	*****	*****	*****
0.20	-0.20	463.	0.15	15.00	0.20	0.27	10.00	0.00	0.00	0.00	0.35X	14.73	0.000	1.80	0.038	9.21
0.40	-0.40	1399.	0.45	5.95	0.20	0.27	10.00	0.00	0.00	0.00	0.40	5.68	0.000	1.70	0.072	5.51
0.60	-0.60	1919.	2.25	15.60	0.20	0.27	10.00	0.00	0.00	0.00	1.81	15.33	0.000	1.90	0.108	16.77
0.80	-0.80	2459.	4.25	15.80	0.20	0.27	10.00	0.00	0.00	0.00	3.90	15.53	0.000	2.00	0.146	26.69
1.00	-1.00	1713.	3.45	13.80	0.20	0.27	10.00	0.00	0.00	0.00	3.16	13.53	0.000	1.90	0.184	17.13
1.20	-1.20	4136.	4.45	19.80	0.20	0.27	10.00	0.00	0.00	0.00	3.91	19.53	0.000	2.00	0.222	17.56
1.40	-1.40	6322.	6.55	24.40	0.20	0.27	10.00	0.00	0.00	0.00	5.88	24.13	0.000	2.00	0.262	22.47
1.60	-1.60	6337.	6.65	26.80	0.20	0.27	10.00	0.00	0.00	0.00	5.87	26.53	0.000	2.00	0.301	19.49
1.80	-1.80	6466.	8.25	17.40	0.20	0.27	10.00	0.00	0.00	0.00	8.02	17.13	0.012	1.95	0.328	24.40
2.00	-2.00	5211.	5.85	19.40	0.20	0.27	10.00	0.00	0.00	0.00	5.40	19.13	0.031	2.00	0.347	15.45
2.20	-2.20	4547.	4.65	18.00	0.20	0.27	10.00	0.00	0.00	0.00	4.21	17.73	0.051	2.00	0.367	11.33
2.40	-2.40	3343.	3.65	13.20	0.20	0.27	10.00	0.00	0.00	0.00	3.40	12.93	0.071	1.90	0.385	8.63
2.60	-2.60	1337.	2.60	8.85	0.20	0.27	10.00	0.00	0.00	0.00	2.51	8.58	0.090	1.90	0.403	6.01
2.80	-2.80	1538.	2.20	8.70	0.20	0.27	10.00	0.00	0.00	0.00	2.10	8.43	0.110	1.90	0.421	4.73
3.00	-3.00	1250.	1.95	8.15	0.20	0.27	10.00	0.00	0.00	0.00	1.86	7.88	0.130	1.80	0.437	3.96
3.20	-3.20	1132.	1.70	7.15	0.20	0.27	10.00	0.00	0.00	0.00	1.65	6.88	0.149	1.80	0.453	3.31
3.40	-3.40	1116.	1.60	6.80	0.20	0.27	10.00	0.00	0.00	0.00	1.56	6.53	0.169	1.80	0.469	2.97
3.60	-3.60	1996.	2.05	8.30	0.20	0.27	10.00	0.00	0.00	0.00	1.96	8.03	0.188	1.80	0.485	3.66
3.80	-3.80	3014.	3.65	13.20	0.20	0.27	10.00	0.00	0.00	0.00	3.40	12.93	0.208	1.90	0.501	6.36
4.00	-4.00	2752.	3.95	13.40	0.20	0.27	10.00	0.00	0.00	0.00	3.70	13.13	0.228	1.90	0.519	6.69
4.20	-4.20	1296.	2.30	7.90	0.20	0.27	10.00	0.00	0.00	0.00	2.24	7.63	0.247	1.80	0.536	3.73
4.40	-4.40	710.	1.30	5.75	0.20	0.27	10.00	0.00	0.00	0.00	1.30	5.48	0.267	1.80	0.551	1.88
4.60	-4.60	1235.	2.10	8.55	0.20	0.27	10.00	0.00	0.00	0.00	2.00	8.28	0.287	1.80	0.567	3.02
4.80	-4.80	1029.	1.80	7.35	0.20	0.27	10.00	0.00	0.00	0.00	1.75	7.08	0.306	1.80	0.583	2.47
5.00	-5.00	890.	1.55	6.75	0.20	0.27	10.00	0.00	0.00	0.00	1.51	6.48	0.326	1.80	0.598	1.98

Table 36 Continued

DILATOMETER DATA LISTING & INTERPRETATION (BASED ON THE 1988 DILATOMETER MANUAL)  
 GPE, INC.  
 JOB FILE: UNIVERSITY OF FLORIDA RESEARCH  
 LOCATION: GREEN COVE SPRINGS  
 SNDG.BY : BRIAN/CHRIS/LANDY - UF CPT TRUCK  
 ANAL.BY : LANDY R./UF - GEOTECHNICAL GROUP

SNDG. NO. DMT-22  
 FILE NO: 83-500  
 SNDG. DATE: 12 DEC 01  
 ANAL. DATE: 12 DEC 01

ANALYSIS PARAMETERS:      LO RANGE =10.00 BARS      ROD DIAM. = 3.70 CM      BL.THICK. = 15.0 MM      SU FACTOR = 1.00  
 SURF. ELEV. = 0.00 M      LO GAGE 0 = 0.00 BARS      FR.RED.DIA. = 4.80 CM      BL.WIDTH = 96.0 MM      PHI FACTOR = 1.00  
 WATER DEPTH = 1.68 M      HI GAGE 0 = 0.00 BARS      LIN.ROD WT. = 6.50 KGF/M      DELTA-A = 0.20 BARS      OCR FACTOR = 1.00  
 SP.GR.WATER = 1.000      CAL GAGE 0 = 0.00 BARS      DELTA/PHI = 0.50      DELTA-B = 0.27 BARS      M FACTOR = 1.00  
 MAX SU ID = 0.60      SU OPTION = MARCHETTI      MIN PHI ID = 1.20      OCR OPTION= MARCHETTI      K0 FACTOR = 1.00

UNIT CONVERSIONS:      1 BAR = 1.019 KGF/CM2 = 100 KPA = 1.044 TSF = 14.51 PSI      1 M = 3.2808 FT

Z	ELEV	THRUST	A	B	DA	DB	ZMRNG	ZMLO	ZMHI	ZMCAL	P0	P1	U0	GAMMA	SVP	KD
(M)	(M)	(KGF)	(BAR)	(T/M3)	(BAR)											
*****	*****	*****	*****	*****	*****	*****	*****	*****	*****	*****	*****	*****	*****	*****	*****	*****
5.20	-5.20	993.	1.80	8.25	0.20	0.27	10.00	0.00	0.00	0.00	1.70	7.98	0.345	1.80	0.614	2.21
5.40	-5.40	1003.	1.70	5.70	0.20	0.27	10.00	0.00	0.00	0.00	1.72	5.43	0.365	1.80	0.630	2.16
5.60	-5.60	432.	1.75	3.80	0.20	0.27	10.00	0.00	0.00	0.00	1.87	3.53	0.385	1.60	0.643	2.31
5.80	-5.80	339.	2.20	3.15	0.20	0.27	10.00	0.00	0.00	0.00	2.38	2.88	0.404	1.60	0.655	3.01
6.00	-6.00	231.	2.40	3.35	0.20	0.27	10.00	0.00	0.00	0.00	2.58	3.08	0.424	1.60	0.667	3.23
6.20	-6.20	247.	2.60	3.90	0.20	0.27	10.00	0.00	0.00	0.00	2.76	3.63	0.444	1.60	0.679	3.41
6.40	-6.40	273.	2.80	4.15	0.20	0.27	10.00	0.00	0.00	0.00	2.96	3.88	0.463	1.70	0.692	3.60
6.80	-6.80	329.	2.70	4.05	0.20	0.27	10.00	0.00	0.00	0.00	2.86	3.78	0.502	1.70	0.719	3.27
7.20	-7.20	370.	3.72	5.20	0.20	0.27	10.00	0.00	0.00	0.00	3.87	4.93	0.542	1.70	0.747	4.46
7.60	-7.60	417.	3.50	5.25	0.20	0.27	10.00	0.00	0.00	0.00	3.64	4.98	0.581	1.70	0.774	3.95
8.00	-8.00	381.	3.85	5.45	0.20	0.27	10.00	0.00	0.00	0.00	3.99	5.18	0.620	1.70	0.801	4.21
8.40	-8.40	406.	4.25	5.70	0.20	0.27	10.00	0.00	0.00	0.00	4.40	5.43	0.659	1.70	0.829	4.51

**Table A6 Continued**

DILATOMETER DATA LISTING & INTERPRETATION (BASED ON THE 1988 DILATOMETER MANUAL)  
 GPE, INC.  
 JOB FILE: UNIVERSITY OF FLORIDA RESEARCH  
 LOCATION: GREEN COVE SPRINGS  
 SNDG.BY : BRIAN/CHRIS/LANDY - UF CPT TRUCK  
 ANAL.BY : LANDY R./UF - GEOTECHNICAL GROUP

SNDG. NO. DMT-22  
 FILE NO. : 83-500  
 SNDG. DATE: 12 DEC 01  
 ANAL. DATE: 12 DEC 01

ANALYSIS PARAMETERS:      LO RANGE =10.00 BARS      ROD DIAM. = 3.70 CM      BL.THICK. = 15.0 MM      SU FACTOR = 1.00  
 SURF. ELEV. = 0.00 M      LO GAGE 0 = 0.00 BARS      FR.RED.DIA. = 4.80 CM      BL.WIDTH = 96.0 MM      PHI FACTOR = 1.00  
 WATER DEPTH = 1.68 M      HI GAGE 0 = 0.00 BARS      LIN.ROD WT. = 6.50 KGF/M      DELTA-A = 0.20 BARS      OCR FACTOR = 1.00  
 SP.GR.WATER = 1.000      CAL GAGE 0 = 0.00 BARS      DELTA/PHI = 0.50      DELTA-B = 0.27 BARS      M FACTOR = 1.00  
 MAX SU ID = 0.60      SU OPTION = MARCHETTI      MIN PHI ID = 1.20      OCR OPTION= MARCHETTI      KO FACTOR = 1.00

UNIT CONVERSIONS:      1 BAR = 1.019 KGF/CM2 = 100 KPA = 1.044 TSF = 14.51 PSI      1 M = 3.2808 FT

Z (M)	ELEV (M)	ID	ED (BAR)	K0	SU (BAR)	QD (BAR)	PHI (DEG)	SIGFF (BAR)	PHIO (DEG)	PC (BAR)	OCR	M (BAR)	SOIL TYPE
*****	*****	*****	*****	*****	*****	*****	*****	*****	*****	*****	*****	*****	*****
0.20	-0.20	41.09	499.									1212.	SAND
0.40	-0.40	13.25	183.									363.	SAND
0.60	-0.60	7.49	469.									1403.	SAND
0.80	-0.80	2.99	404.	3.10		73.4	45.2	0.25	41.9	9.67	66.2	1385.	SILTY SAND
1.00	-1.00	3.29	360.	2.07		49.7	43.1	0.31	39.9	5.59	30.3	1083.	SILTY SAND
1.20	-1.20	4.00	542.	1.80		137.1	47.5	0.39	45.1	5.31	23.9	1644.	SAND
1.40	-1.40	3.10	633.	2.37		209.6	47.7	0.46	45.5	10.39	39.7	2068.	SILTY SAND
1.60	-1.60	3.52	717.	2.04		210.6	47.5	0.52	45.4	9.04	30.0	2246.	SAND
1.80	-1.80	1.14	316.	3.11						16.24	49.5	1058.	SILT
2.00	-2.00	2.56	477.	1.66		170.9	46.3	0.60	44.4	7.05	20.3	1388.	SILTY SAND
2.20	-2.20	3.25	469.	1.15		152.4	46.5	0.63	44.6	3.74	10.2	1229.	SILTY SAND
2.40	-2.40	2.87	331.	0.92		111.4	45.2	0.66	43.3	2.51	6.5	784.	SILTY SAND
2.60	-2.60	2.51	211.	0.86		40.7	39.6	0.66	37.4	1.99	4.9	430.	SILTY SAND
2.80	-2.80	3.18	220.	0.65		50.3	41.2	0.70	39.1	1.24	2.9	406.	SILTY SAND
3.00	-3.00	3.47	209.	0.61		40.9	39.8	0.72	37.7	1.06	2.4	354.	SAND
3.20	-3.20	3.48	181.	0.55		37.6	39.3	0.74	37.2	0.87	1.9	280.	SAND
3.40	-3.40	3.56	172.	0.51		37.6	39.2	0.76	37.1	0.77	1.6	249.	SAND
3.60	-3.60	3.42	211.	0.46		69.0	42.7	0.81	41.0	0.75	1.5	343.	SAND
3.80	-3.80	2.99	331.	0.74		100.4	43.7	0.85	42.1	2.03	4.0	697.	SILTY SAND
4.00	-4.00	2.71	327.	0.83		89.1	42.7	0.87	41.0	2.57	5.0	701.	SILTY SAND
4.20	-4.20	2.70	187.	0.61		41.9	38.7	0.87	36.8	1.28	2.4	303.	SILTY SAND
4.40	-4.40	4.04	145.	0.48		24.4	35.4	0.87	33.3	0.67	1.2	152.	SAND
4.60	-4.60	3.66	218.	0.54		41.1	38.4	0.92	36.6	1.01	1.8	318.	SAND
4.80	-4.80	3.70	185.	0.50		34.7	37.3	0.94	35.5	0.86	1.5	238.	SAND
5.00	-5.00	4.18	172.	0.47		30.7	36.4	0.95	34.6	0.72	1.2	189.	SAND

**Table 36 Continued**

DILATOMETER DATA LISTING & INTERPRETATION (BASED ON THE 1988 DILATOMETER MANUAL)  
 GPE, INC.  
 JOB FILE: UNIVERSITY OF FLORIDA RESEARCH  
 LOCATION: GREEN COVE SPRINGS  
 SNDG. BY: BRIAN/CHRIS/LANDY - UF CPT TRUCK  
 ANAL. BY: LANDY R./UF - GEOTECHNICAL GROUP

SNDG. NO. DMT-22  
 FILE NO.: 83-500  
 SNDG. DATE: 12 DEC 01  
 ANAL. DATE: 12 DEC 01

ANALYSIS PARAMETERS:      LO RANGE =10.00 BARS      ROD DIAM. = 3.70 CM      BL.THICK. = 15.0 MM      SU FACTOR = 1.00  
 SURF. ELEV. = 0.00 M      LO GAGE 0 = 0.00 BARS      FR.RED.DIA. = 4.80 CM      BL.WIDTH = 96.0 MM      PHI FACTOR = 1.00  
 WATER DEPTH = 1.68 M      HI GAGE 0 = 0.00 BARS      LIN.ROD WT. = 6.50 KGF/M      DELTA-A = 0.20 BARS      OCR FACTOR = 1.00  
 SP.GR.WATER = 1.000      CAL GAGE 0 = 0.00 BARS      DELTA/PHI = 0.50      DELTA-B = 0.27 BARS      M FACTOR = 1.00  
 MAX SU ID = 0.60      SU OPTION = MARCHETTI      MIN PHI ID = 1.20      OCR OPTION= MARCHETTI      K0 FACTOR = 1.00

UNIT CONVERSIONS:      1 BAR = 1.019 KGF/CM2 = 100 KPA = 1.044 TSF = 14.51 PSI      1 M = 3.2808 FT

Z (M)	ELEV (M)	ID	ED (BAR)	K0	SU (BAR)	QD (BAR)	PHI (DEG)	SIGFF (BAR)	PHIO (DEG)	PC (BAR)	OCR	M (BAR)	SOIL TYPE
*****	*****	*****	*****	*****	*****	*****	*****	*****	*****	*****	*****	*****	*****
5.20	-5.20	4.63	218.	0.48		33.8	36.8	0.98	35.1	0.81	1.3	259.	SAND
5.40	-5.40	2.73	129.	0.48		34.3	36.8	1.01	35.0	0.82	1.3	147.	SILTY SAND
5.60	-5.60	1.12	58.	0.62						0.81	1.3	60.	SILT
5.80	-5.80	0.26	17.	0.79	0.24					1.24	1.9	22.	CLAY
6.00	-6.00	0.23	17.	0.83	0.27					1.41	2.1	23.	CLAY
6.20	-6.20	0.38	30.	0.87	0.29					1.56	2.3	42.	SILTY CLAY
6.40	-6.40	0.37	32.	0.91	0.32					1.73	2.5	47.	SILTY CLAY
6.80	-6.80	0.39	32.	0.84	0.29					1.55	2.2	43.	SILTY CLAY
7.20	-7.20	0.32	37.	1.07	0.45					2.61	3.5	62.	CLAY
7.60	-7.60	0.44	47.	0.98	0.40					2.24	2.9	72.	SILTY CLAY
8.00	-8.00	0.35	41.	1.02	0.45					2.56	3.2	66.	SILTY CLAY
8.40	-8.40	0.28	36.	1.08	0.50					2.95	3.6	60.	CLAY

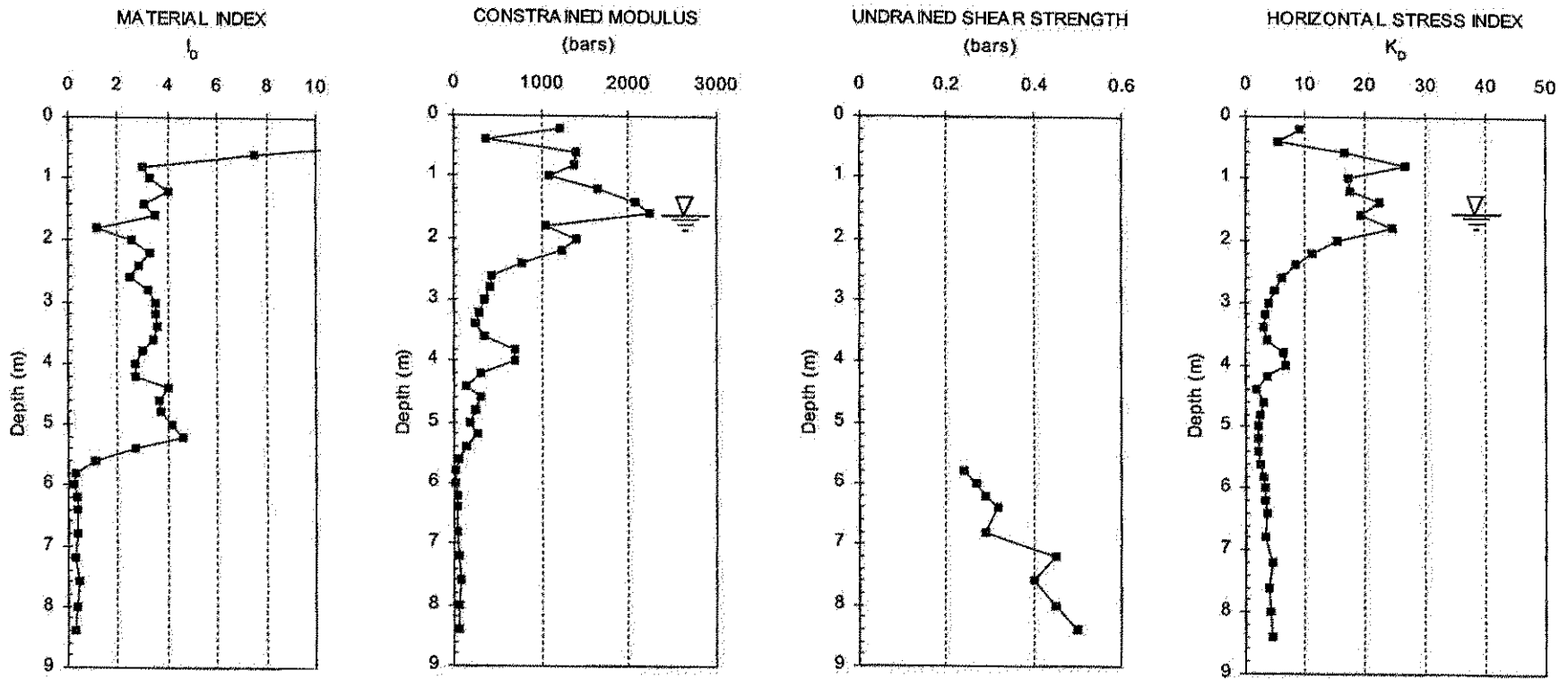


Figure 132 DMT data at Green Cove Springs

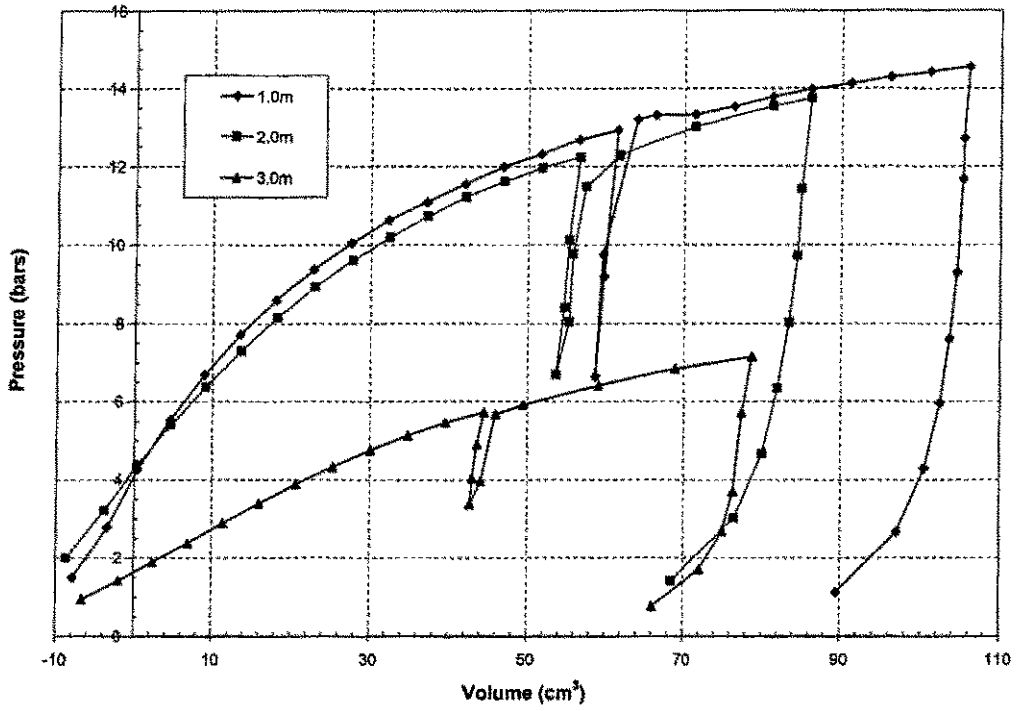


Figure 133 Corrected pressuremeter curves at depths  $z = 1.0\text{m}, 2.0\text{m}, 3.0\text{m}$

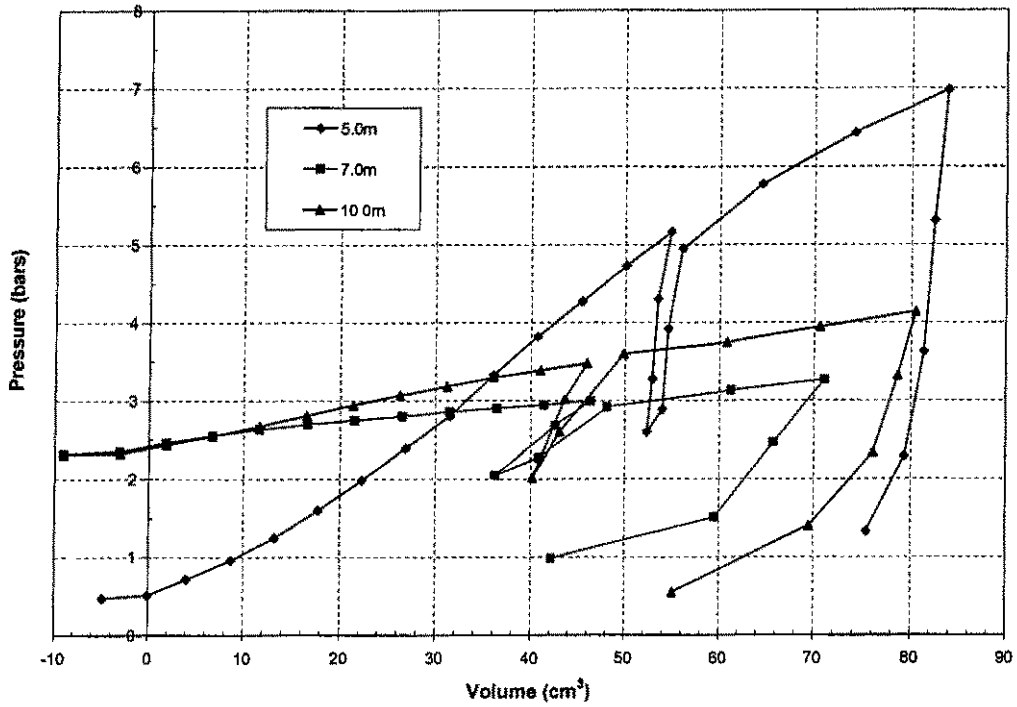


Figure 134 Corrected pressuremeter curves at depths  $z = 5.0\text{m}, 7.0\text{m}, 10.0\text{m}$

The SPT used was the Automatic Hammer type and the sampler was the Shelby tube of 3.0 inches diameter.

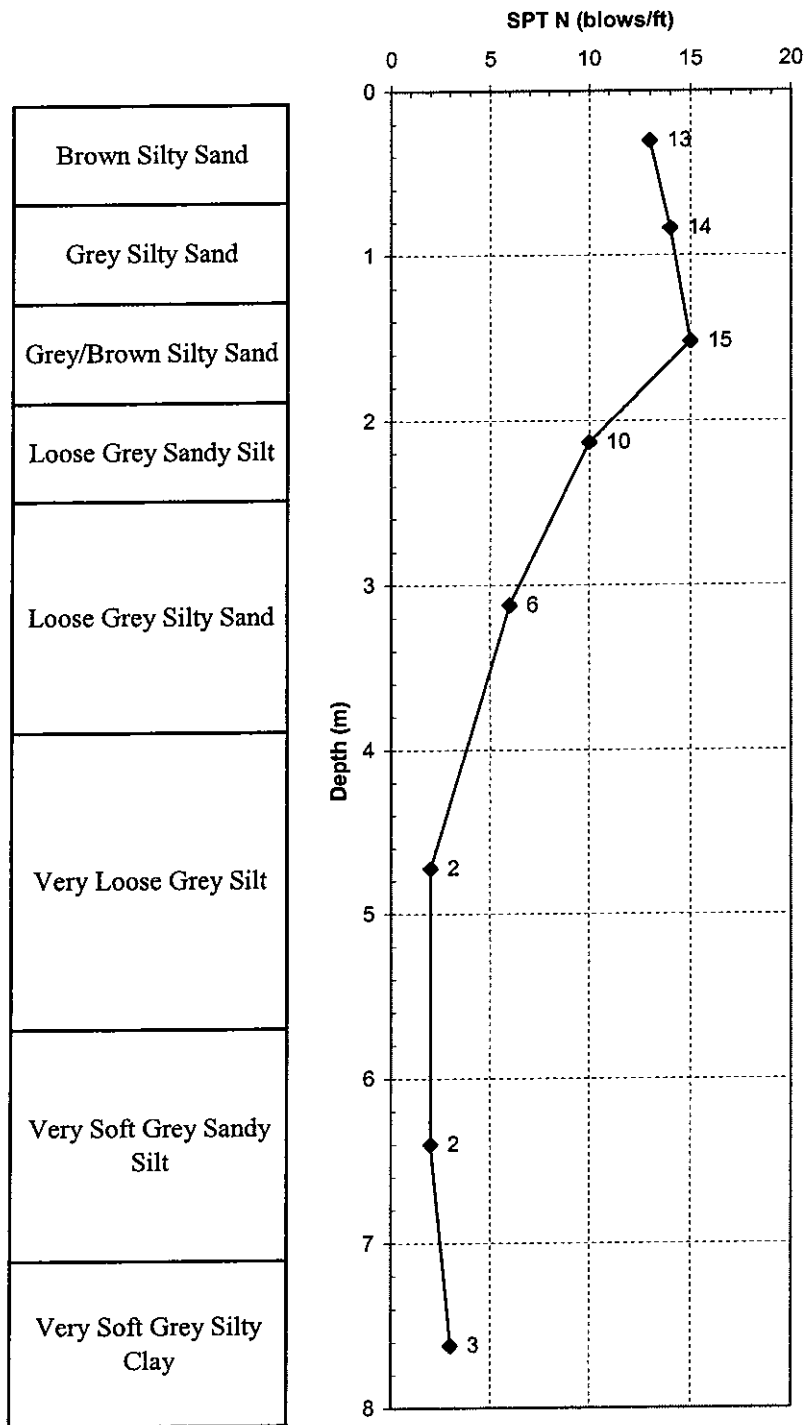


Figure 135 SPT blow counts and soil description

### Test Footing

For this study, a reinforced circular 6.0 ft (1.8m) diameter 2.0 ft (0.6m) thick concrete footing was constructed. In order to overcome the superficial thin hard layer (crust) at the site, the footing was embedded 2.0ft (0.6m) into the ground. With the ground water table being at depth 5.5ft (1.7m), the soil-structure profile for the load testing is presented in Figure 136 and Figure 137.

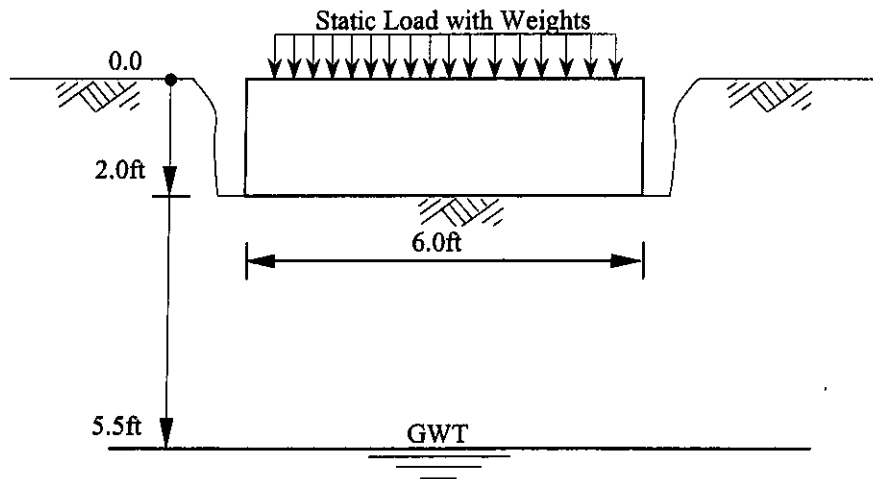


Figure 136 Soil-footing profile with ground water table

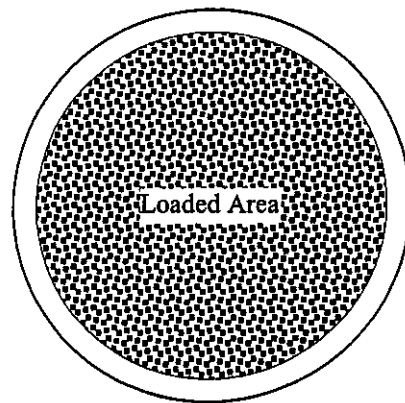


Figure 137 Plan view of concrete footing and loaded area

As no codified design was required for the load testing on the concrete footing, the following simple tasks were included in order to have an appropriate design: selecting

the mechanical strength of the concrete material; selecting the reinforcing steel: in size, in number, and spacing for reinforcement.

In the first task, the unconfined compressive strength is the property that defines the mechanical strength of the concrete. A compressive strength of about  $f'_c = 7000\text{psi}$  was targeted. During the casting of the footing, four cylindrical concrete specimens of two different sizes were taken. After nearly 80 days of age, the concrete samples were tested for the compressive strength according to the ASTM Standard C873-99: Standard Method for Compressive Strength of Concrete Cylinders Cast in Place in Cylindrical Molds. The unit weight of the cylindrical specimens were also estimated using the ASTM standard: C138: Standard Test Method for Density (Unit Weight). Figure 138 and Table 37 describe the quantitative details of the concrete tests. In Table 37, the average compressive strength for the three specimens turned out to be 6912psi, while the average unit weight for the four specimens is 141.7 pcf (22.26kN/m<sup>3</sup>).

Table 37 Compressive and unit weight tests on the concrete specimens

Concrete Specimens crushing with

TINIUS OLSEN, Model CMH 289 Controller (2000 Recorder)

Specimen No.	1	2	3	4	Average
Diameter (in.)	6.15	6.10	4.36	4.35	5.24
Height (in.)	11.88	12.00	8.00	8.00	9.97
Dry Weight (lb)	27.73	27.89	8.25	8.34	18.05
Submerged (lb)	15.40	15.64	4.62	4.68	10.08
Unit Weight (pcf)	140.4	142.0	141.7	142.3	141.6
$F_{\max}$ (lb)	220279	195634	XX	98474	171462
Stress (psi)	7415	6694	XX	6626	6912
Loading rate (lb/min)	60000	60000	26600	26600	43300
Def. Rate (in./min)	0.038	0.03	0.02	0.02	0.03
Age (days)	80	80	80	80	80

XX: Undefined

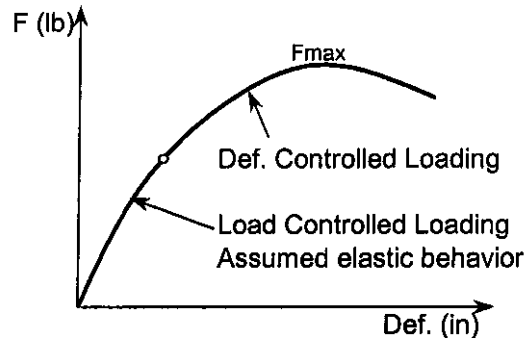


Figure 138 Loading process using TINIUS OLSEN, model CMH 289 controller

In the second task, the main requirement was determine the amount of reinforcing steel for design in flexure. The ACI code for structural slabs of uniform thickness uses the minimal amount:  $\rho_{\min} = 0.002$ . Thus, because of symmetry, for the 6.0ft (1.8m) diameter footing, 2.0ft (0.6m) thick, 6 Rebar #6 (Grade 60: Yield strength  $f_y = 60\text{ksi}$ ) were used in one direction and 6 more for the perpendicular direction. They were placed on the bottom of the footing as shown in Figure 139. Photos were taken as well during the making of the concrete footing.

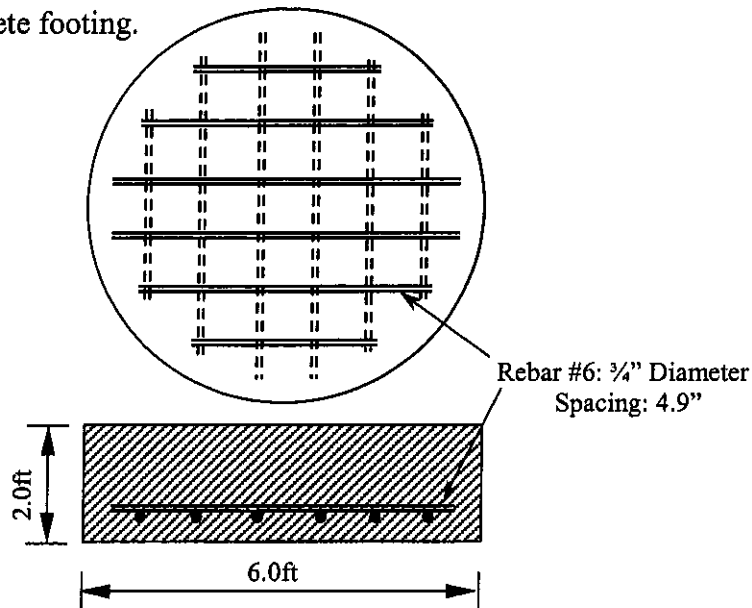


Figure 139 Steel reinforced concrete footing

Figure 140 shows the footing with the metallic culvert forming before and after the casting of the concrete.

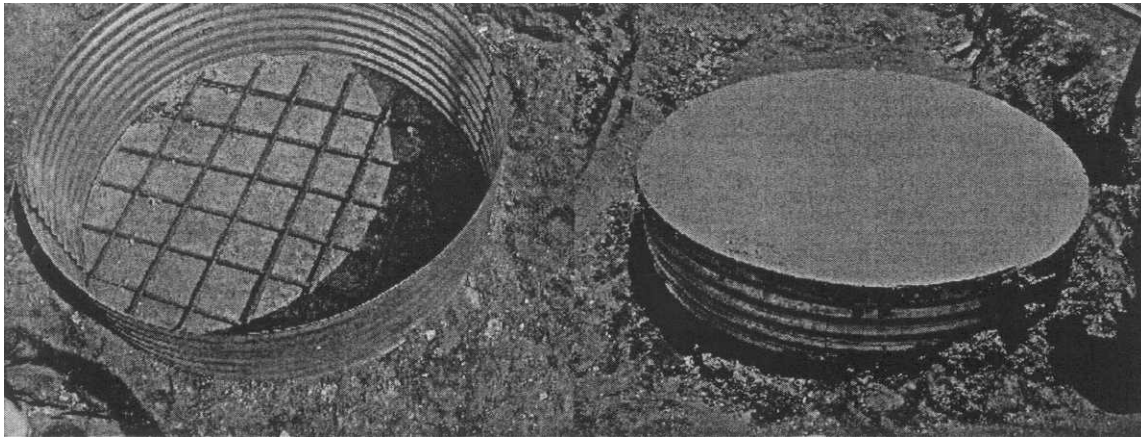


Figure 140 Footing before and after the casting of the concrete

#### Equipment:

The footing static loading was conducted by successively stacking STATNAMIC dead weights on the footing. In order to successfully monitor the progress in loading and the corresponding displacement (settlement), special devices to measure the applied load and the displacement are installed on the footing structure. In this study, load cells were used for the measuring the applied loads and LVDTs were used for the settlement. The measuring devices were connected to a computer (Megadec) where the original data were collected for future data reduction. Three identical load cells were evenly placed on a steel plate (angle  $120^\circ$  apart from each other about the center and at the same distance from the center). The steel plate of diameter 52" and thickness 6" was necessary in order to assure a leveled surface before the proper loading starts, Figure 141. The load cells were covered with another steel plate of larger diameter to accommodate the circular weights.

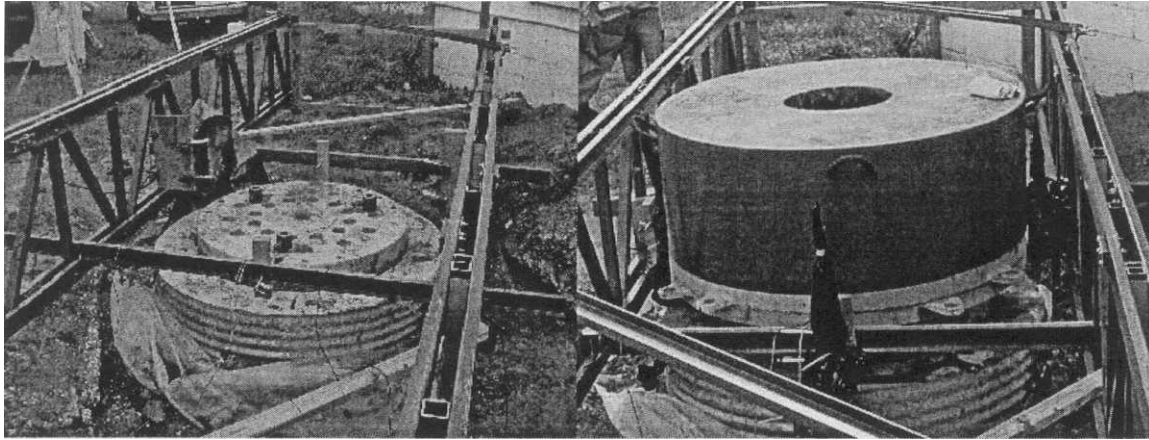


Figure 141 Load cells, LVDTs, steel plates (bottom and top), and seating weight

Figure 141 also shows the fiberglass reference beams to support the 4 LVDTs that are evenly placed on the footing after the initial seating weight of 24.08kips (Concrete footing, Bottom plate, Top plate and a 6.6kips weight) at the bottom of the footing in contact with the soil. The two reference beams are 24.0ft (7.3m) long and 3.0ft (0.9) high, and are set about 7.0ft (2.1m) apart from each other. Four posts, which were 24.0ft (7.3m) apart longitudinally and 7.0ft (2.1m) apart laterally, support the hanging reference beams. Several small cross beams were also needed in order to hold the LVDTs that are located in the centerline of the two beams and/or to laterally stiffen the two beams. Finally, a survey level was brought to the site to ensure the horizontality of the reference beams. The lay-out of the reference beams, load cells, LVDTs steel plates and the poles is presented in Figure 142. Figures 143 and 144 illustrate the connection among the data acquisition system and the footing and accessories system.

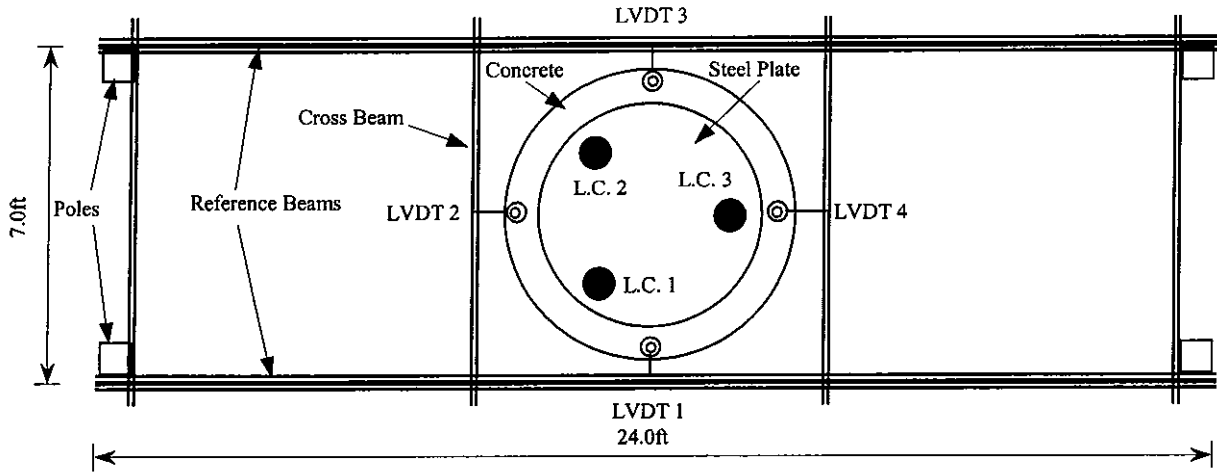


Figure 142 Layout of the load cells (L.C.), LVDTs and reference beams

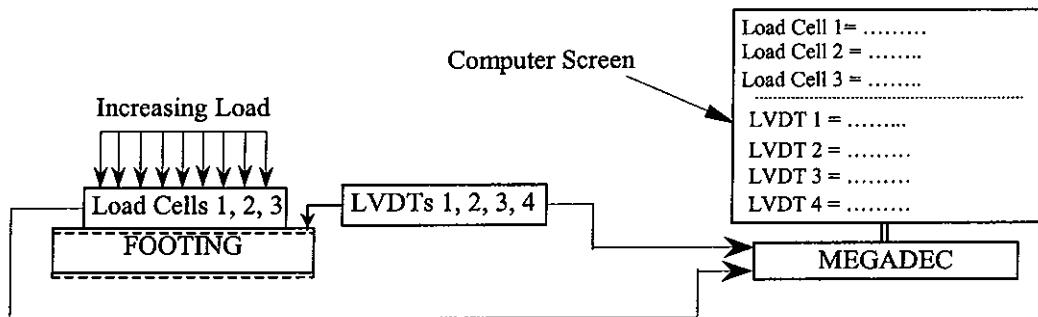


Figure 143 Data acquisition with the computer and Megadec

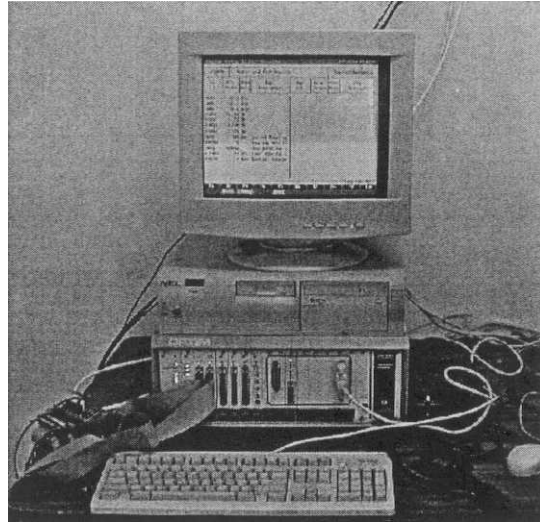


Figure 144 Data acquisition equipment used at Green Cove Springs

### Survey Measurements

For verification and redundancy of the settlements recorded from the LVDTs, an engineering survey of the load testing was undertaken simultaneously. In this study, the engineering survey consists of mounting two scaled rulers on stationary objects that serve as fixed references (back-sights) and two other scaled rulers (fore-sights) on objects that are expected to settle as a result of the loading process. The survey system is presented in Figure 145. For the stationary back-sight objects, a wall of the adjacent building and a stockpiled cylindrical weight were chosen; while two diagonally opposite reference beam posts and the seating weight on the footing were monitored for settlement during loading. The level was installed as close as possible for accurate viewing of all targets, as shown.

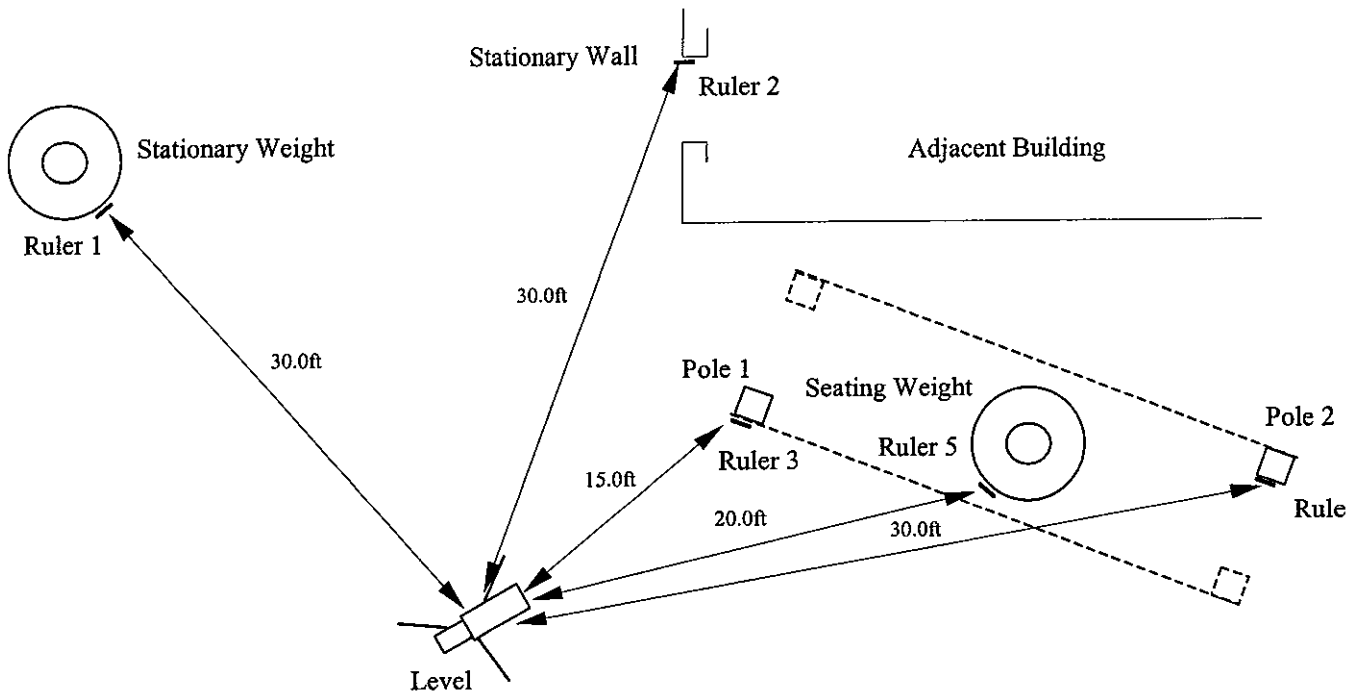


Figure 145 Survey level and ruler locations

The distances shown in Figure 145 are only indicative and not exact. Also, the height where the five rulers were placed is in the neighborhood of 5.0ft above the ground surface.

### Loading Sequence

After all of the accessory equipment (reference beams, load cells, LVDTs, level, computer and seating weights) were completely set up, the initial readings, both load and displacements, on the computer system were recorded and subsequently the loading sequence was started. Table 38 lists the schedule followed when each load increment was added so the total load and accumulating settlements were accordingly recorded. Figure 146 shows the loading process and final applied load.

Table 38 Loading schedule followed at Green Cove Springs

Date	Partial Time (sec)	Cumulative Time		Weights (kips)	Load (kips)	Pressure* (tsf)
		(sec)	(days)			
6/27/01	0	0	0.00	6.600 5.500	1.21E+01	0.43
6/28/02	71100	7.11E+04	0.82	11.000 10.800	3.86E+01	0.90
6/29/01	81900	1.53E+05	1.77	9.670 9.559 9.075	6.69E+01	1.40
7/2/01	254100	4.07E+05	4.71	10.000 10.154 10.198	9.73E+01	1.93
7/3/01	85800	4.93E+05	5.70	8.877 10.132 10.022	1.26E+02	2.45

\*Includes the weight of the lower steel plate and the Footing

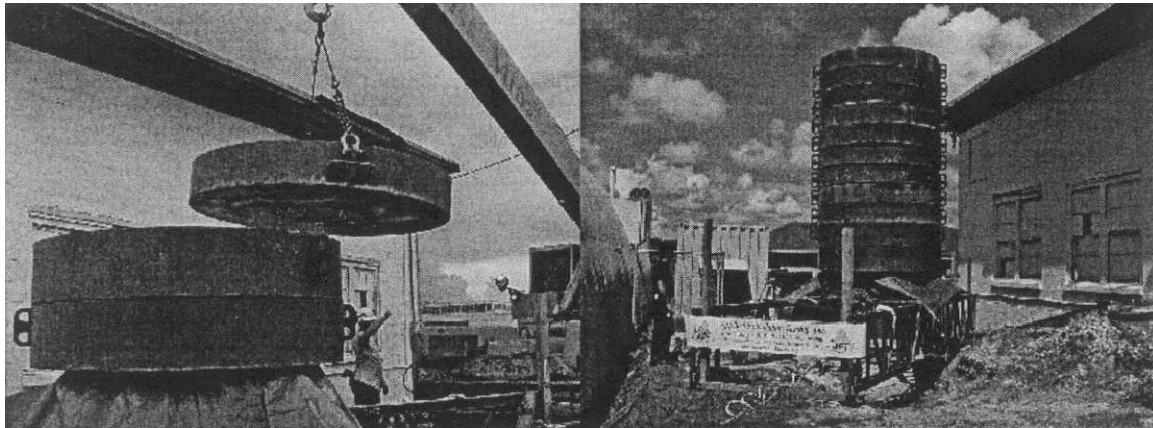


Figure 146 Loading process and final load applied

Figure 147 presents the plot of the load versus elapsed time, for several hours after each load increment was put in place:

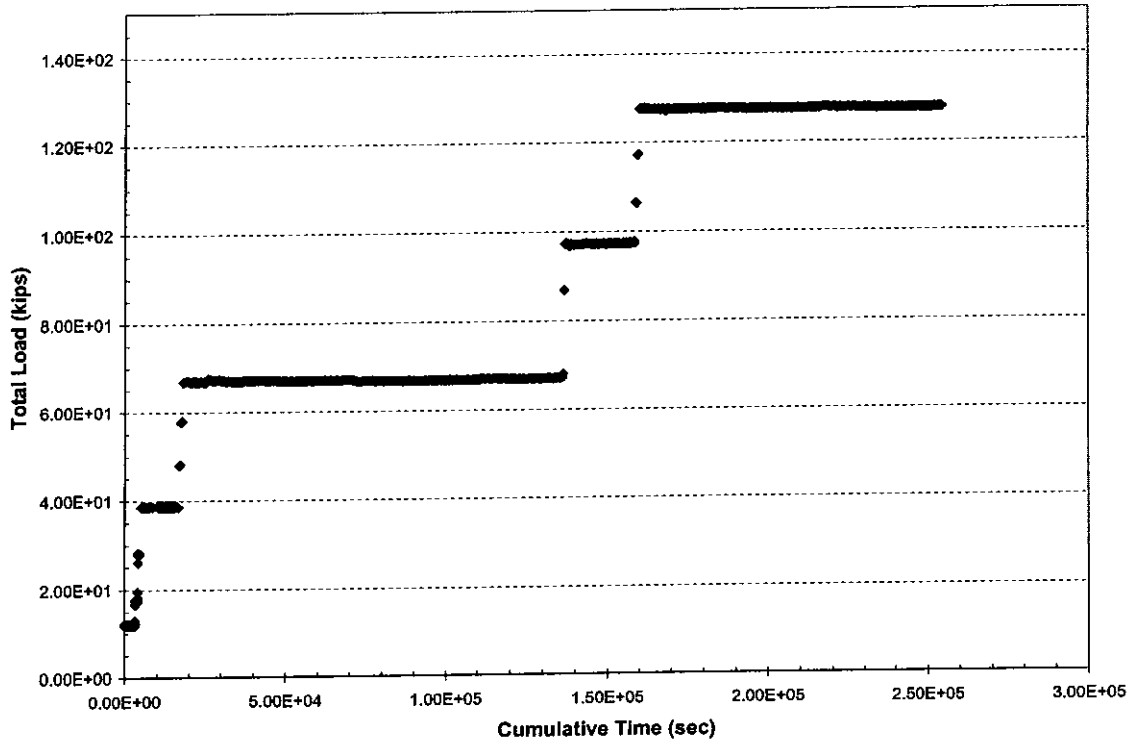


Figure 147 Plot of the load steps versus time

### Soil-Structure Profile for the Conventional and Finite Element Modeling:

#### Conventional Method:

The conventional method chosen for this study was the CSANDSET Program, which includes a number of methods of settlement calculations for a shallow rectangular footing. As the footing in Green Cove Springs is circular, the model used was a square footing having exactly the same contact area with the soil as that of the actual circular footing. Thus, the edge of the square footing becomes  $L = 5.32\text{ft}$  (1.6m). The net bearing

pressure at the base of the footing, from Table 38 was evaluated at 2.4tsf. Also, the ground water table is located at 5.5ft (1.7m) below the ground surface (el. 0.0ft). For the Oweis method and the Schmertmann method, five layers were specified before a rigid layer was encountered at depth 26.0ft (7.9m). Figure 148 shows the sketch the geometrical input for the conventional methods.

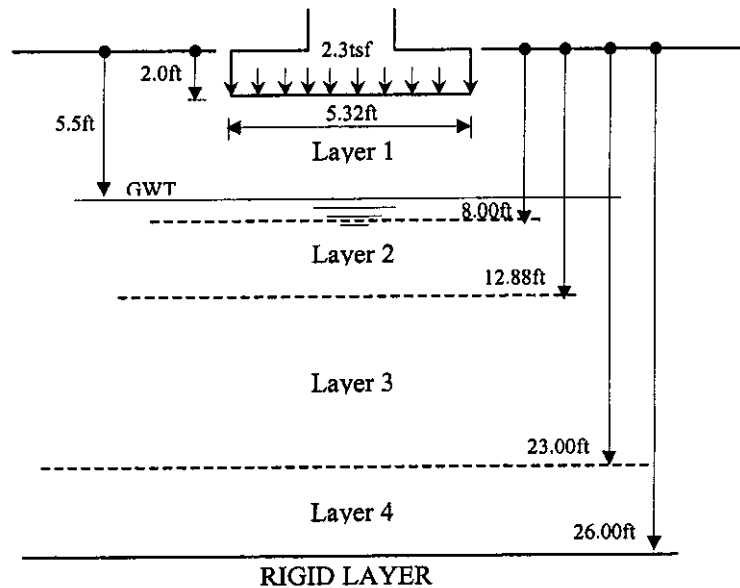


Figure 148 Soil layers for Schmertmann and Oweis methods in CSANDSET

The input parameters soil properties for the conventional methods are listed in Table 39, and the properties of the sublayers required in the Oweis and Schmertmann methods are also presented in Table 40. The  $K_0$  values are the average over the corresponding layer from the DMT testing results.

Table 39 Input of main parameters for CSANDSET

Soil Properties of Soil over B = 5.32ft below the Base	Input Values
Blow Count (Blows/ft)	13
CPT End Bearing (tsf)	102.1
Total Unit Weight (pcf)	116
Saturated Unit Weight (pcf)	120
Coefficient $K_0$ at Rest	2.16 (from DMT)
Depth of Rigid Layer (ft)	26.00
Ground Water Table (ft)	5.5
Poisson's Ratio	0.3

Table 40 Properties of layers for Oweis and Schmertmann methods

LAYER	Bottom (ft)	$\gamma_m$ (pcf)	$\gamma_{sat}$ (pcf)	SPT	$q_c$ (tsf)	$K_0$
1	8.00	116	120	13	102.1	2.16
2	12.88	110	115	6	56.4	0.63
3	23.00	100	110	2	30.1	0.66
4	26.00	100	110	3	7.0	1.04

In addition to CSANDSET, the conventional methods using DMT and PMT methods were also used.

### Finite Element Method

For the finite element modeling, the circular footing is appropriately represented using the axisymmetric model. Therefore, the geometrical configuration represents only half of the domain as it is shown in Figure 151. The edge of the footing was made as frictionless by using a zero interface. The elastic non-porous material constitutive model was used for the concrete. These properties are listed in Table 44. The domain is discretized into triangular elements each with 15 nodes and 12 stress points. The width of 12.0ft was selected based on the location of the poles, points where no settlements

occurred, according to the results from the survey operation. The height of the model, 26.0ft (8.0m) was estimated from the assumed depth of influence 4 times the diameter of the footing (6.0ft).

### Correlations for the Input Parameters

The following correlations used for the finite element modeling are assumed to be compatible with the normally consolidated properties of the soil layers. As it will be observed in the sequel, the overconsolidation property will be accounted by using a factor involving the overconsolidation ratio, OCR.

For the SPT, the friction angles were correlated from Peck et al., (1974):

$$\phi (^{\circ}) = 53.881 - 27.6034 \times \exp(-0.0147 \times N)$$

The undrained shear strength  $c$  was obtained from Terzaghi and Peck, (1948).

The Young's Modulus was correlated from the equations below:

$$E \text{ (kPa)} = 500 \times (N + 15) \quad \text{for sand}$$

$$E \text{ (tsf)} = (150 \text{ to } 200) \times c \quad \text{for clay}$$

Finally the unit weights were estimated from FLPier Manual (FDOT, 2001).

These unit weights were used for all other insitu test input parameters.

For the CPT, the friction angles were using the correlation from Robertson and Campanella, (1983), based on the effective overburden pressure  $\sigma'_v$  and the cone tip resistance,  $q_c$ ; the undrained shear strength  $c$  are based on the following empirical correlation:

$$c = (q_c - \sigma'_v) / N_k \quad \text{where } N_k = 10 \text{ to } 15$$

The following Young's Modulus equations from Bowles, (1996) were used to correlate with  $q_c$ :

$$E = (2 \text{ to } 4) \times q_c \quad \text{for Sand and Silty Sand}$$

$$E = (3 \text{ to } 8) \times q_c \quad \text{for Clay}$$

The standard correlations were used for the DMT. For convenience, the main parameters used are repeated below:

The friction angle is a function of the coefficient of lateral pressure at rest,  $K_0$  and the horizontal stress index,  $K_D$ , Marchetti, (2001):

$$\phi_{\text{safe,DMT}} = 28^\circ + 14.6^\circ \times \log K_D - 2.1^\circ \times \log^2 K_D \quad \text{for } I_D > 1.8 \text{ (Sand)}$$

The Undrained Shear Strength is given by the following equation:

$$C_{u,DMT} = 0.22 \times \sigma'_{v0} \times (0.5 \times K_D)^{1.25} \quad \text{for } I_D < 1.2 \text{ (Clay)} \quad [\text{psf}]$$

The Elastic Modulus  $E$  is calculated knowing the constrained modulus from the DMT:

$$E = \frac{(1+\nu)(1-2\nu)}{(1-\nu)} M = (1-\nu)^2 E_D \quad [\text{psf}]$$

where  $\nu$  is the Poisson's Ratio (effective), and  $E_D$  the Dilatometer Modulus.

#### Overconsolidation Ratio, OCR:

The DMT Testing is the only insitu test that provides an estimate of the stress history. Interpretation of the  $K_D$  versus depth profile (Figure 132) is a practical tool to identify whether a layer is normally consolidated or over-consolidated. In the case of cohesionless soils, the availability of CPT data from the same site helps in the estimation of the overconsolidation ratio, OCR, as is suggested by Marchetti et al. (2001). This interpretation shows in Table 41 that the sand layer through the depth 9.2ft (2.8m) is overconsolidated for uncemented sands, which is the case at Green Cove Springs Site, a

ratio of  $M_{DMT}/q_c = 12-24$  indicates overconsolidated sands. The Overconsolidation Ratio, OCR, was computed in the “Dilatometer” program as well, however the values are very inflated. Consequently, the more universal correlation established by Kulhawy and Mayne, (1982) is used in this study:

$$OCR = \left( \frac{K_0}{1 - \sin \phi} \right)^{\frac{1}{\sin \phi}}$$

$K_0$  and  $\phi$  (plane strain) being the values estimated from the dilatometer data reduction.

Laboratory consolidation tests on “undisturbed” samples were also carried out in order to confirm that the sand layer idea at the Green Cove Springs Site (Figure 149) was overconsolidated. Consolidometer ring samples were extracted from 2.5ft (0.8m) and 3.5 ft (1.1 m) depths below the ground surface. Deeper samples could not be taken as the excavated soils caved in quickly. Thus, a comparison of the Overconsolidation Ratio OCR at 2.5 and 3.0 ft. depths is presented in Table 42. The estimation of the Overconsolidation Ratios from the Laboratory Consolidation Test is presented in Figures 149 and 150 as well. Soil disturbance in sands during the hand sampling is considered to be the main cause of the difference between the estimates from the consolidation method and the Kulhawy and Mayne based analysis. The OCR values chosen for the finite element analysis are those from the Kulhawy and Mayne (1982), not only that the equation was established from many tests that cover a variety of soil (from Clay to Gravel), but also, in our comparison, the values are the closest to the average values for the depths 2.5 ft (0.8m) and 3.5 ft (1.1m), Table 42. Thus, the following correlation for

Elastic Modulus  $E_{OCR}$  was used for the constitutive model Mohr-Coulomb, Bowles (1996):

$$E_{OCR} = E_{NC} \times \sqrt{OCR}$$

$E_{NC}$  is the elastic modulus estimated from the correlations used in this study in all type of test. This correlation is particularly selected among others because the Modulus should be a function of the OCR value (here non-linear), rather than just a multiple of the  $E_{NC}$  value from a given range of multiplier. As for the Hardening Soil Model, the OCR value is taken into account in the Initial condition (input type) of the soil clusters, hence the  $E_{NC}$  values are kept as the input parameters for the Elastic Modulus.

Table 41 Stress history for sand by combining DMT and CPT data

Depth (m)	$M_{DMT}$ (bars)	$q_c$ (bars)	Ratio $M_{DMT}/q_c$
0.2	1212	120.3	10.07
0.4	363	110.75	3.28
0.6	1403	120.4	11.65
0.8	1385	139.6	9.92
1.0	1083	94.4	11.47
1.2	1644	110.6	14.86
1.4	2068	113.25	18.26
1.6	2246	103.1	21.78
1.8	1058	90.3	11.72
2.0	1388	82.7	16.78
2.2	1229	51.2	24.00
2.4	784	33.2	23.61
2.6	430	24.4	17.62
2.8	406	33.6	12.08
3.0	354	64	5.53
3.2	280	51.4	5.45
3.4	249	53.2	4.68
...	...	...	...

Table 42 Comparison of overconsolidation ratios - OCR

Depth (ft)	Laboratory Consolidation	Kulhawy and Mayne (1982)	Dilatometer Program*
2.5	12.8	28.1	66.2
3.5	5.5	15.6	30.3

\* Schmertmann, based on Kulhawy and Mayne (1982)

Theoretical and finite element computation of settlement using the soil properties resulting from the consolidation test was also performed. Because of lack of data, the properties corresponding to the depth 3.5ft was extended to 12.0ft below the base of the footing (assumed to be the depth of influence). These properties are listed in Table 43. The “Soft Soil Model” was the constitutive model selected in Plaxis under the “drained” type (as opposed to the Undrained combined with Consolidation in the Calculation process) for the foundation soils.

Table 43 Soil properties from consolidation tests

Properties	Layer 0.0 to 1.0ft	Layer 1.0ft to 12ft
Thickness (ft)	1.0	12.0
Void Ratio, $e_0$	0.726	0.722
Compression Index, $C_c$	0.0622	0.0611
Swelling Index, $C_s$	0.0149	0.0147
Past Maximum Stress (tsf)	1.8	1.1
Sublayers Thickness, $\Delta H$ (ft)	0.2 (5 layers)	0.5 (22 layers)
Permeability (ft/day)	$11.48 \times 10^{-5}$	$13.58 \times 10^{-5}$

### Oedometer 1 - Depth 2.5ft

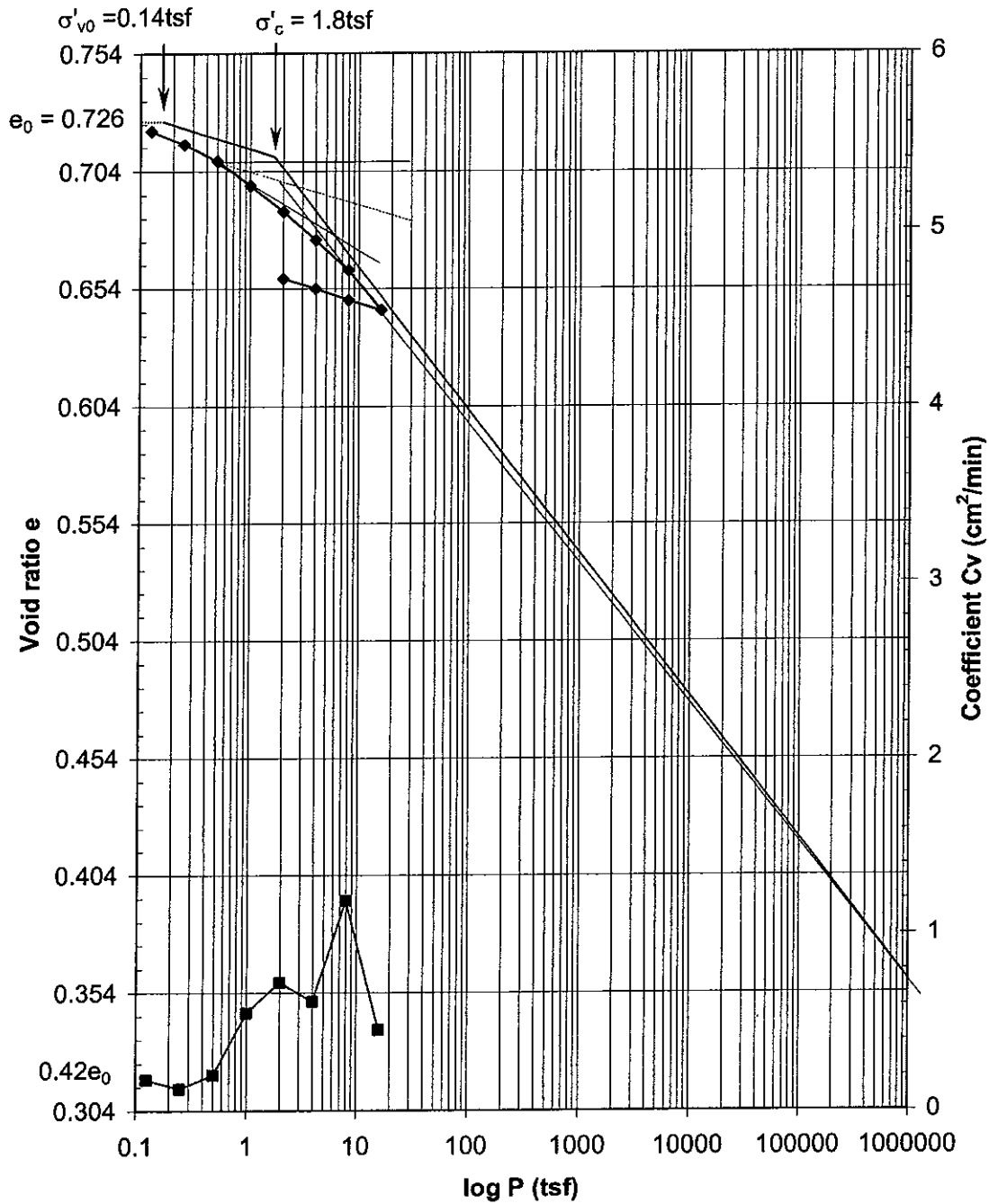


Figure 149 Overconsolidation ratio at depth 2.5ft from consolidation test, OCR  $\cong$  12.8

### Oedometer 2 - Depth 3.5ft

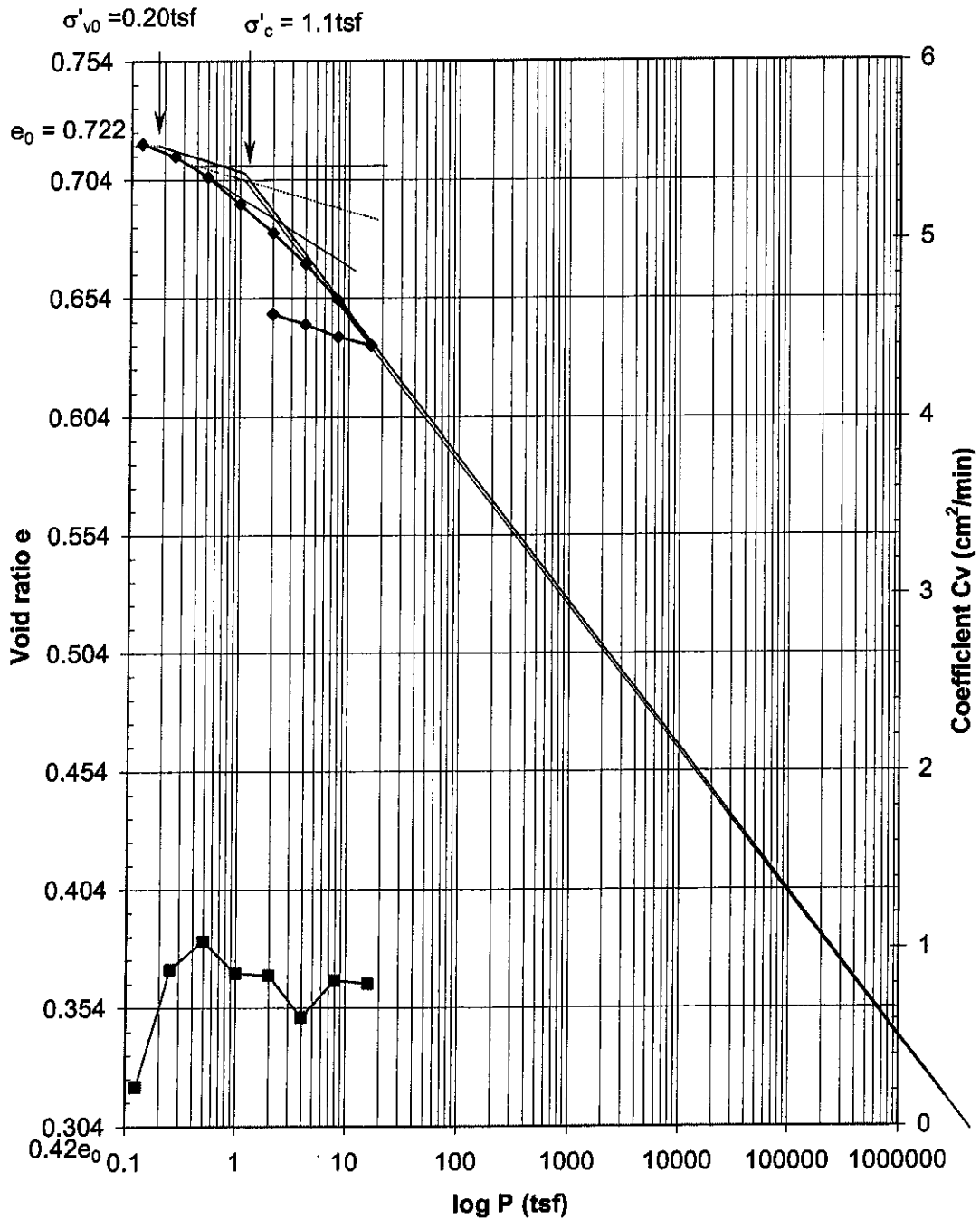


Figure 150 Overconsolidation ratio at depth 3.5ft from consolidation test,  $\text{OCR} \approx 5.5$

The input parameters for the PMT testing were estimated from the correlations in Baguelin et al., (1978), combined with the relationship between Menard pressuremeter strength and stiffness parameters with those of PENCEL pressuremeter, Briaud J-L., (1992). Following the procedures, the friction angles turned out to be extremely high ( $\phi > 50^\circ$ ), hence the friction angles resulting from the matching the insitu pressuremeter curves with the FEM curves were used. The Relations used for the Modulus are:

$$E_{Menard} = \frac{EPencil}{2.03 \times \alpha}$$

where  $\alpha$  is function of the ratio  $E_M/p_f$ .

The undrained cohesion is directly computed from:

$$c_u = \frac{p_1 - p_0}{\beta}$$

where  $\beta = 6.5$  was used from the boundary values: 5.6 and 7.4.

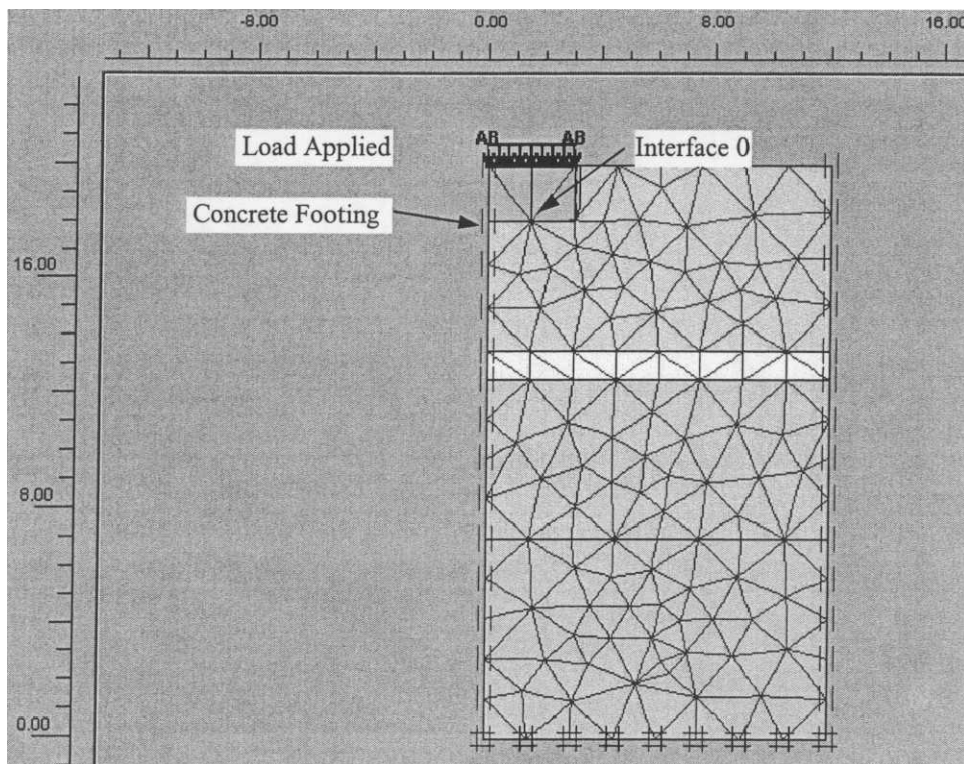


Figure 151 Model meshing for finite element analysis with Plaxis

The input parameters for the finite element modeling are presented in Table 45. These properties are the “normally consolidated properties of the soil layers, that is, the Elastic moduli are obtained from the aforementioned correlations. Thus, for the Mohr-Coulomb modeling, the modulus will be multiplied by the square root of the OCR value if the layer in question is overconsolidated.

Table 44 Properties of the Footing Concrete

Properties	Values
Unit Weight (pcf)	150
Elastic Modulus (psi)	$4.3 \times 10^6$
Material Type	Nonporous

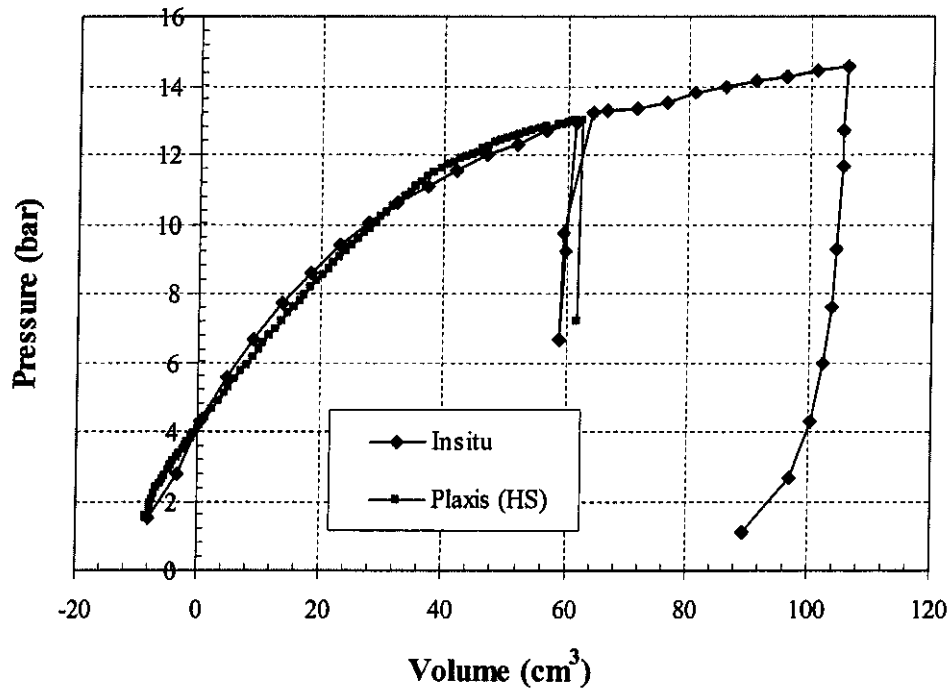


Figure 152 Curve fitting with Plaxis (Hardening Soil Model) to determine PMT  $\phi$  (depth = 1.0m)

Table 45 Soil properties from the different insitu tests for Plaxis (OCR = 1)

Bottom (m)	SPT					CPT						DMT				PMT					Bottom (m)
	N (bl/ft)	$\gamma_m$ (pcf)	$\phi$ (°)	$S_u$ (psf)	E (psi)	$q_c$ (psi)	$\phi$ (°)	$\phi$ (N) (°)	$S_u$ (psf)	E (psi)	E (N) (psi)	M (psi)	$\phi$ (°)	$S_u$ (psf)	E (psi)	$p_l$ (psi)	$E_M$ (psi)	$\phi$ (°)	$S_u$ (psf)	E (psi)	
GS=0																214.6	2414.3	37.1	-	3567.9	GS=0
4.92	14	120.0	31.4	-	2102.5	1549.7	47.5	35.8	-	4649.0	2863.8	21933.1	46.3	-	16293.1						4.92
6.23																					6.23
6.56																					6.56
7.22	10	110.0	30.1	-	1812.5											208.8	1905.3	33.4	-	2815.8	7.22
7.51																					7.51
8.20																					8.20
8.20	6	100.0	28.6	-	1522.5	594.5	42.0	32.4	-	2157.6	2138.8	5895.3	41.0	-	4379.3						9.51
9.51																					9.51
9.84																					9.84
11.81																116.0	849.1	26	-	1254.8	11.81
13.06																					13.06
13.12																					13.12
13.12						1115.3	42.8	33.7	-	3346.0	2407.0										13.45
13.45																					13.45
13.94																					13.94
17.72	2	90.0	27.1	-	1232.5							3326.7	37.1	-	2471.2	118.9	877.3	25	-	1309.5	17.72
19.69																					19.69
20.01																					20.01
25.98						104.7	-		803.8	575.5	1116.7	720.7	-	751.7	535.3	55.1	152.3	-	751.7*	227.2	25.98
27.89																					27.89
32.81																					32.81
36.09																65.3	207.5	-	867.8	204.5	36.09
EOB																					EOB

\* Value from Pressure-Volume curve fitting with Plaxis (Hardening Soil Model) – Figure 151

GWT = 5.5ft (1.68m) below the GS (Ground Surface)

Table 46 presents the OCR values resulting from the aforementioned Kulhawy and Mayne correlation.

Table 46  $K_0$  and OCR values from DMT based on Kulhawy and Mayne, (1982)

Depth (m)	$K_0$	OCR
0.2	-	-
0.4	-	-
0.6	-	-
0.8	3.10	28.133
1	2.07	15.603
1.2	1.80	13.602
1.4	2.37	19.806
1.6	2.04	16.118
1.8	3.11	-
2	1.66	11.900
2.2	1.15	7.202
2.4	0.92	5.078
2.6	0.86	3.877
2.8	0.65	2.659

Estimate of Bearing Capacity:

As a part of the geotechnical investigation for this study, the bearing capacity of the soil for our footing was also estimated using the following three methods: Vesic (1975), Meyerhof (1963), and Terzaghi (1943). The computations were performed in a spreadsheet form and presented in Table 47:

Table 47 Bearing capacity estimation

$$\begin{aligned}\gamma_m \text{ (pcf)} &= 117.7 \\ B \text{ (ft)} &= 6 \\ D_f \text{ (ft)} &= 2 \\ \text{GWT (ft)} &= 5.5 \\ \gamma_{\text{avg}} \text{ (pcf)} &= 92.65\end{aligned}$$

<b>VESIC (1975)</b>	<b>MEYERHOF (1963)</b>	<b>TERZAGHI (1943)</b>
$\phi (^{\circ}) = 31.4$	$\phi (^{\circ}) = 31.4$	$\phi (^{\circ}) = 31.4$
<b>Bearing Capacity Factors</b>		
$N_{\phi} = 3.18$	$N_{\phi} = 3.18$	
$N_q = 21.61$	$N_q = 21.61$	$N_q = 26.52$
$N_{\gamma} = 5.10$	$N_{\gamma} = 19.87$	$N_{\gamma} = 25.35$
<b>Correction Factors</b>		
$\lambda_{qs} = 1.61$	$\lambda_{qs} = 1.32$	
$\lambda_{qd} = 1.09$	$\lambda_{qd} = 1.06$	
$\lambda_{qi} = 1.00$	$\lambda_{qi} = 1.00$	
$\lambda_{\gamma s} = 1.00$	$\lambda_{\gamma s} = 1.32$	
$\lambda_{\gamma d} = 1.00$	$\lambda_{\gamma d} = 1.06$	
$\lambda_{\gamma i} = 1.00$	$\lambda_{\gamma i} = 1.00$	
<b><u>Ultimate Bearing Capacities</u></b>		
<b><math>q_{\text{ult}} \text{ (tsf)} = 4.90</math></b>	<b><math>q_{\text{ult}} \text{ (tsf)} = 7.41</math></b>	<b><math>q_{\text{ult}} \text{ (tsf)} = 5.12</math></b>

Obviously, the net bearing applied: 2.45tsf (Table 38) was safely smaller than the ultimate bearing capacities from the three methods. The maximum applied load corresponds to a factor of safety greater than 2 ( $FS > 2$ ). This also confirms that using the secant modulus  $E_{50}$  for the finite element modeling is appropriate (rather than using the initial modulus  $E_0$  or  $E_{25}, \dots$ ).

## Results

### Measured Settlements (LVDTs and Survey)

As mentioned earlier in this chapter, four LVDTs were used to measure the settlement caused by application of the static loads. The output data from the four LVDTs along with the load cells are plotted versus time. The reading was taken every

300seconds (5minutes) during the 6-day span load testing (Table 38). Consequently, only the settlements and Loads recorded few hours after application of each incremental load is presented in the output graph of Figure 153. As the readings from the four LVDTs are not exactly the same, but reasonably within the same range, the average value was used for the analysis.

The settlement observed from the survey operation is consistent with the average values from the LVDTs. Table 48 shows the results from LVDTs and Survey for comparison. It can be stated that the precision on the survey was satisfactory and the LVDTs measurements were carried out appropriately without any technical problems. The rest of the results are presented in Table 49 and Table 50.

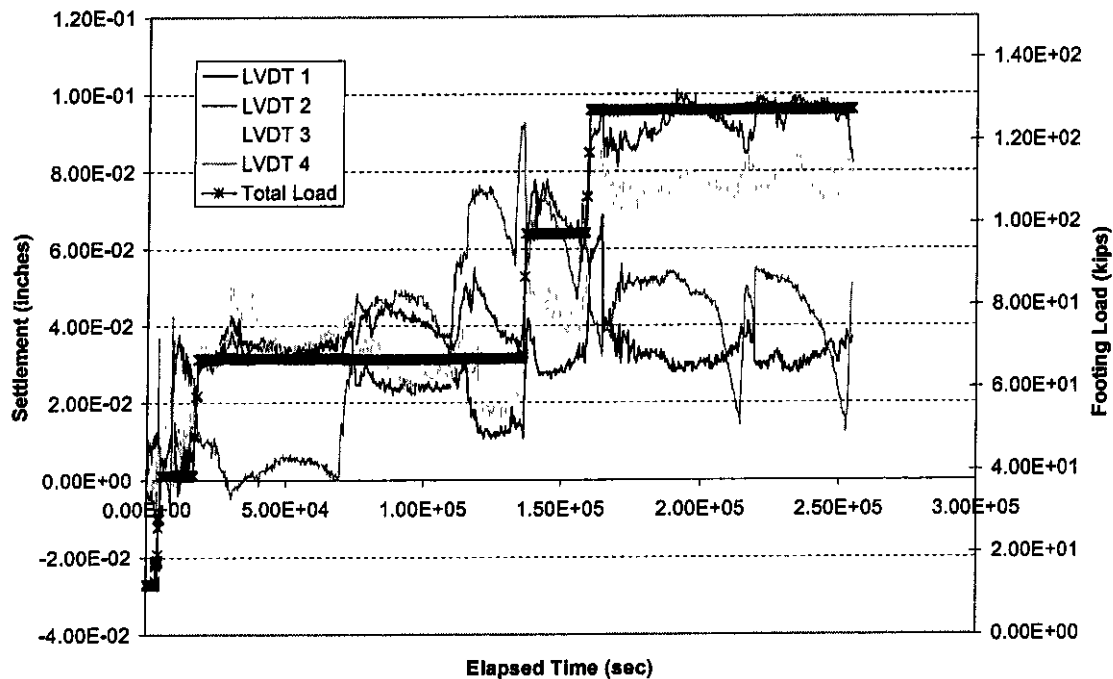


Figure 153 LVDTs settlements and load versus time

Table 48 Settlements measured with LVDTs and survey versus loads

Settlement (inches)	Loading Sequence (tsf)					
	0	0.276	0.746	1.247	1.783	2.318
LVDT Measurement (average)	0	0.00	0.02	0.04	0.05	0.10
SURVEY Measured	0	-	-	0.06	0.12	0.20

Table 49 Settlements from LVDTs versus conventional methods

Settlements (inches)	Loading Sequence (tsf)				
	0.276	0.746	1.247	1.783	2.318
LVDT Measured	0.00	0.02	0.04	0.05	0.10
Conventional Oedometer Test	0.29	0.49	0.65	0.85	1.10
PMT	0.04	0.13	0.24	0.35	0.46
DMT	0.04	0.11	0.19	0.26	0.34
Terzaghi <sup>a)</sup>	0.16	0.44	0.74	1.06	1.37
Teng	0.04	0.12	0.2	0.28	0.37
Elastic Theory <sup>b)</sup> : Rigid	0.09	0.24	0.4	0.57	0.74
Center	0.09	0.26	0.43	0.61	0.80
D'Appolonia (1970) <sup>a)</sup>	0.03	0.09	0.16	0.22	0.29
Peck and Bazaraa <sup>a)</sup>	0.05	0.15	0.25	0.37	0.49
Schmertmann (1970) <sup>c)</sup>	0.05	0.18	0.32	0.47	0.62
Schmertmann (1978) <sup>c)</sup>	0.04	0.16	0.31	0.47	0.65
Schultz & Sherif <sup>a)</sup>	0.07	0.14	0.23	0.32	0.41
Meyerhof <sup>a)</sup>	0.08	0.21	0.35	0.50	0.65
Peck, Hanson, Thornburn <sup>a)</sup>	0.15	0.42	0.7	1.00	1.30
Bowles <sup>b)</sup>	0.13	0.36	0.6	0.86	1.12
NAVFAC DM 7.1 <sup>a), c)</sup>	0.1	0.26	0.44	0.63	0.82
Oweis <sup>a), b)</sup> : Rigid	0.02	0.12	0.34	0.69	1.15
Center	0.03	0.23	0.64	1.28	2.08

a) SPT based Method

b) Electic Theory based Method

c) CPT based Method

Table 50 Settlements from LVDTs versus finite element analysis with Plaxis using insitu data

Settlements (inches)		Loading Sequence (tsf)				
		0.276	0.746	1.247	1.783	2.318
LVDT Measured		0.00	0.02	0.04	0.05	0.10
Soft Soil Model with Plaxis		0.27	0.49	0.84	1.36	2.05
MOHR-COULOMB	SPT	0.04	0.13	0.28	0.50	0.81
	CPT (using correlated SPT N)	0.04	0.11	0.21	0.35	0.52
	CPT	0.04	0.12	0.21	0.31	0.41
	DMT	0.04	0.12	0.22	0.32	0.43
	PMT	0.08	0.24	0.45	0.71	1.04
HARDENING SOIL	SPT	0.08	0.22	0.36	0.53	0.73
	CPT (using correlated SPT N)	0.06	0.17	0.28	0.42	0.61
	CPT	0.07	0.19	0.34	0.52	0.72
	DMT	0.06	0.17	0.29	0.42	0.57
	PMT	0.11	0.29	0.51	0.80	1.24

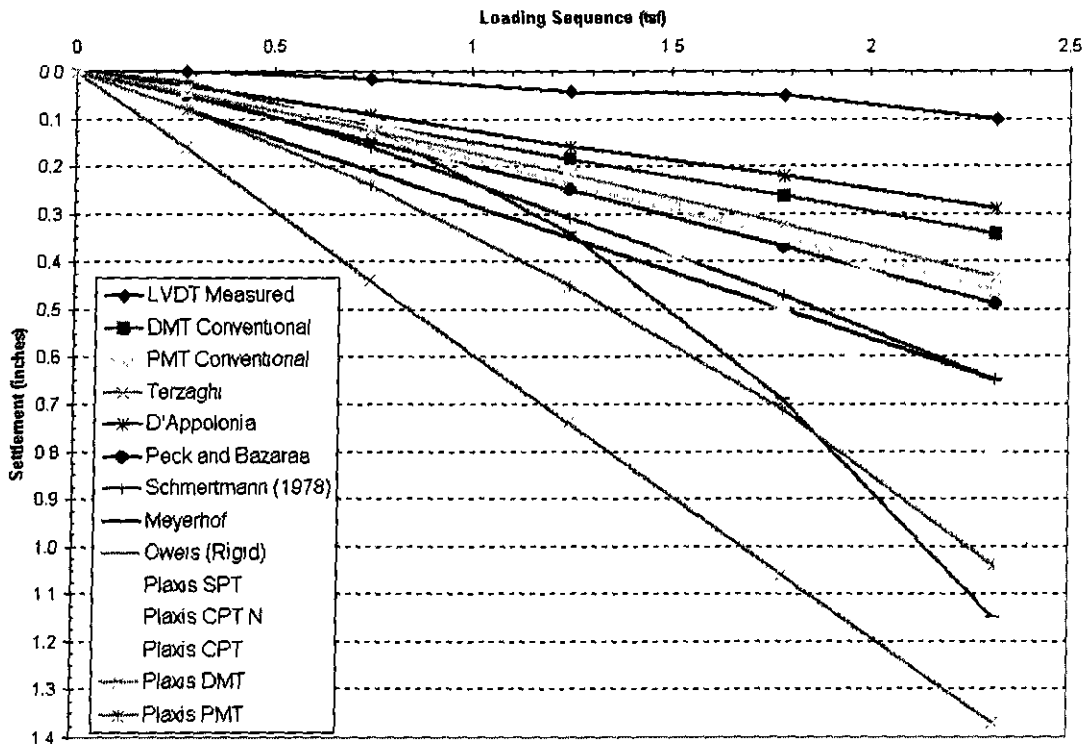


Figure 154 Graphical representation of the settlement: predicted and measured (Plaxis: Mohr-Coulomb Model).

Given that the settlements estimated using the Hardening Soil Model are generally greater than those from the Mohr-Coulomb Model, they are not included in Figure 154.

### Discussion of Results

At first glance, all of the calculation methods, conventional and finite element, overpredict the settlement of the footing throughout the load testing. As shown earlier, the conventional methods are primarily based on the SPT blow counts or the CPT tip resistance; and in this study, the CPT correlated blow counts were used and they are generally greater than the SPT blow counts. The most accurate settlement was estimated with the D'Appolonia method (1970), 0.29 inches; this method evaluates the modulus of compressibility of the sand from the SPT blow counts, with some correction factors introduced in the computation. The next most accurate calculation method is the Schulz and Sherif method, with the final settlement of 0.41 inches. The actual settlement is so small that even a relatively small overprediction appears to be excessive. In fact the two most accurate calculation methods above are at least twice as much as the final measured settlement, nevertheless, the best predicted settlement is still within 0.2 inches.

On the other hand, the Oweis method is the least accurate with 2.08 inches of total settlement at the center. This method is considered to be among the most conservative methods in calculating settlement in sands. Following the Oweis method is Terzaghi method with a total settlement of 1.37 inches. Oweis method, which is also based on the elastic theory, uses the SPT blow count in the calculation. The other methods are situated in the middle, among those methods are the Meyerhof and NAVFAC DM 7.1 methods.

The conventional methods based on the DMT and PMT also give relatively promising results. The PMT method that uses the pressuremeter strength and stiffness parameters ( $p_L$  and  $E_M$ ) is in fairly good accuracy with 0.46 inches. The DMT, which uses the constrained modulus in the calculation, results in closer estimation with 0.34 inches. The reason the difference between the actual settlement and the computed settlements could be attributed to various factors. First, it is realized that the overconsolidation ratio of the superficial layer is a critical parameter for input. However, the sole insitu testing that permits to evaluate the OCR value of a soil is the DMT Testing. The DMT testing proves that the overlying sand is overconsolidated but the estimated OCR values from the data reduction (Dilatometer Program, which uses Schmertmann correlation) are unrealistically high.

As for the finite element analysis, the input data that results in best accuracy of the calculation are those from the CPT and the DMT testing using the Mohr-Coulomb Model. In the case of DMT, the elastic modulus of the overconsolidated layers are directly obtained from the values of the constrained modulus  $M_{DMT}$ , whereas that for the CPT input data follows the procedure developed earlier in this study (product of the square root of the OCR value and the normally consolidated modulus). The settlement predicted from the CPT was slightly smaller as the CPT estimated friction angles are slightly higher. The other insitu tests estimates, using CPT correlated blow counts  $N$ , the SPT and the PMT, did not give good settlement predictions. Besides the oedometer settlements (Laboratory Test rather than Insitu Test, which is the focus of this study), the settlement predicted from the PMT input parameters is the least accurate, followed by the SPT, 1.04 inches and 0.81 inches respectively. The SPT blow count  $N$  values are too low

considering that the first sand layer is overconsolidated, which is substantiated in that the CPT correlated N values are significantly larger. The operator and equipment sensitivity (energy) factor of the SPT testing could be a factor to the disagreement of the blow counts. The input parameters from the CPT correlated N has a reasonably accurate settlement result, 0.52 inches. This prediction is again about 5 times the actual settlement, the latter is too small to make a more meaningful comparison. The Hardening Soil model in Plaxis did not give better settlement predictions than the Mohr-Coulomb Model. This constitutive model, although it takes into account directly the OCR values of an overconsolidated layer (alternatively the past maximum pressure, POP) overpredicted the settlements with a minimum of 0.57 inches for DMT and a maximum of 1.24 inches for PMT. Nevertheless, the Hardening Soil model seems to provide less discrepancy among the results with the different insitu testing input parameters (omitting the PMT result).

### Conclusion and Recommendations

The methods of settlement predictions are based on different assumptions and approaches, empirical, theoretical, and semi-empirical or finite element. Variety of the cases (different bearing pressure, geometry of footing, ...) is not included in the analysis as only one shallow footing is considered. Therefore, the conclusions that follow this study may not be guaranteed to be generally true and more cases are needed in order to reach more pertinent statements. However, what results from this study is a very useful preliminary understanding of when to use conventional methods, as opposed to finite element methods, and what model to use in the finite element analysis as far as settlement prediction of footings on sand is concerned. The presence of an overconsolidated sand layer within the zone of influence of the footing leads to a realization that a careful

evaluation of the stress history of a site is critical. The parameters involved for accounting for stress history are the coefficient of lateral pressure  $K_0$  or the overconsolidation ratio OCR as they are related to one another. It is rather difficult to estimate from the laboratory consolidation test the OCR value (or past maximum stress) of sand as sand curves do not follow the classical clay curves. As the main purpose of this study is the usefulness of insitu testing in prediction problems, the DMT is the only insitu testing that provides for the stress history of a soil profile without resorting to correlation. However, the OCR seems to be unrealistically large with the Schmertmann (1982) relation for sand in the dilatometer program. It has been realized as well that the CPT testing data (in combination of the DMT data, Marchetti et al., (2001)) help for a better understanding of the stress history of a soil profile.

1. It is fundamental to know the best interpretation of the stress history of a soil profile, in this case sand, for the settlement prediction either using conventional methods or finite element methods.
2. The conventional methods, especially D'Appolonia, Schultz & Sherif, DMT provide more accurate estimations in case of an overconsolidated sandy layer within the zone of influence of the shallow footing.
3. The finite element method using DMT with Mohr-Coulomb Model is fairly accurate and no correlation involving the OCR value is required as this latter is already built in the elastic modulus, via the constrained modulus.
4. The CPT testing is also a good method for the case of a shallow footing settlement prediction.

5. The blow count correlated from the CPT data is more consistent with the other insitu testing data than the SPT blow count taken at the site in both conventional methods and finite element method.
6. The PMT and the SPT do not provide good settlement predictions in case where the sand layer within the zone of influence is overconsolidated.
7. The hardening soil model in finite element model overpredicts the settlement in overconsolidated sand using any type insitu input parameters.

The following recommendations can also be stated:

1. The DMT and CPT insitu tests are mandatory in evaluating settlement of a shallow footing on sands. Not only do they give better predictions but also help define the stress history of the soil profile load testing on a shallow footing.
2. The SPT and PMT tests are not reliable in predictions of settlements either for conventional methods or for finite element methods
3. It is less tedious and more accurate to predict the settlement using the conventional methods than using finite element methods
4. If finite element method is the choice in settlement prediction, the Mohr-Coulomb Model provides better results when used with the OCR value taken into account.

These statements should be validated by analyzing more case histories in shallow footing static load testing with sufficient variety of input parameters from various insitu tests.

## CHAPTER 8 CONCLUSION

### Conclusions

1. A input parameter sensitivity analysis of the FEM models shows that  $\phi$  is the most sensitive parameter.  $E_{50}$ ,  $E_{oed}$ , and  $m$  had little effect on modeling a triaxial test.
2.  $\phi$  values from triaxial laboratory tests agreed with estimates from DMT, but not CPT for Saunder's creek. However,  $\phi$  values from triaxial tests were much lower than those estimated from CPT and DMT tests at the SW Recreation Center. Similarly, triaxial  $\phi$  values were much lower than those estimated from CPT and DMT tests for the Archer Landfill site.
3. Modulus values ( $E_{50}$ ) determined from triaxial tests agreed well with those estimated from DMT, and unloading PMT at Saunder's Creek. However, at the SW Recreation Center, the triaxial  $E_{50}$  values were much lower than those estimated from DMT and PMT tests. The  $E_{50}$  triaxial test modulus values at the Archer Landfill site agreed with those estimated from DMT and PMT unloading tests.
4. FEM simulations of triaxial test stress-strain curves produced excellent results. The hardening models ( PLAXIS – Hardening Soil and PlasFEM – Sandler Dimaggio) simulated the non-linear behavior better than the Mohr-Coulomb or Drucker-Prager models.

5. FEM simulations of field PMT curves using triaxial test based parameters were unsuccessful. It was necessary to increase the triaxial  $E_{50}$  values by  $\Omega = 1.3078e^{0.0164p_l}$   $R^2 = 0.8515$ , where  $\Omega$  is the triaxial  $E_{50}$  modulus multiplier and  $p_l$  is the PENCEL limit pressure.
6. For the sheet-pile wall, conventional analyses (CWALSHT) using parameters from SPT, CPT, and PMT under-predicted wall deformations unconservatively.
7. The FEM Hardening Soil Model more accurately predicted sheet-pile wall deflections than the Mohr-Coulomb Model. This is due to the Hardening Soil Model using a stiffer unload modulus.
8. Even at very small deflections (less than 25mm), the Linear Elastic FEM Model unconservatively underpredicts wall deflections.
9. Wall deflections were accurately predicted using the Hardening Soil Model with input parameters estimated from SPT correlations and “curved matched” PMT values. CPT based parameters under-predicted wall deformations due to too high  $\phi$  value estimates.
10. Fundamentally, the stress history of a soil profile, i.e., OCR or preconsolidation pressure, must be known for any settlement prediction either using conventional or finite element methods.
11. Surprisingly, of the conventional methods for estimating settlements (CSANDSET), only the SPT based D’Appolonia, and Peck and Bazaraa methods provided reasonable estimates of the observed settlement.
12. The conventional DMT method, which correlates OCR values slightly overestimated measured settlements.

13. None of the insitu test derived input parameters (SPT,CPT, DMT, and PMT) coupled with FEM Mohr-Coulomb or Hardening Soil models, accurately predicted the shallow footing settlements.

### Recommendations

Fundamentally, the FEM constitutive models require knowledge of the insitu state of stress (OCR, preconsolidation stress, or  $K_0$ ), and pore pressure. Unless an accurate estimate of these values is known, design predictions will be limited. For design problems involving driven structural elements (piles, sheet-piles) the state of stress due to driving is unknown. However, inserted insitu devices (CPT,DMT, and PMT) perhaps create similar stress states and thus lead to better predictions. It is our opinion that FEM analyses for this boundary value problem are superior to conventional analyses, and the hardening soil model is recommended. For settlement design problems, insertion of the insitu probe alters the stress state. Consequently, only the DMT provides accurate estimations of OCR and is recommended. For settlements, conventional methods were more accurate than FEM.

As a first approximation for conventional or FEM input parameters, the correlations listed in Chapter 3 are recommended. Alternatively, “curve matching” PMT results can provide valid input parameters.

APPENDIX  
ADDITIONAL INSITU TEST DATA

University of Florida	
Operator : BLANTON	CPT Date : 06-15-99 11:48
Sounding : CORE30 Pg 1 / 1	Location : STA-380+22 6'LCL
Cone Used : 0274	Job No. : B7040-1598 SR.20

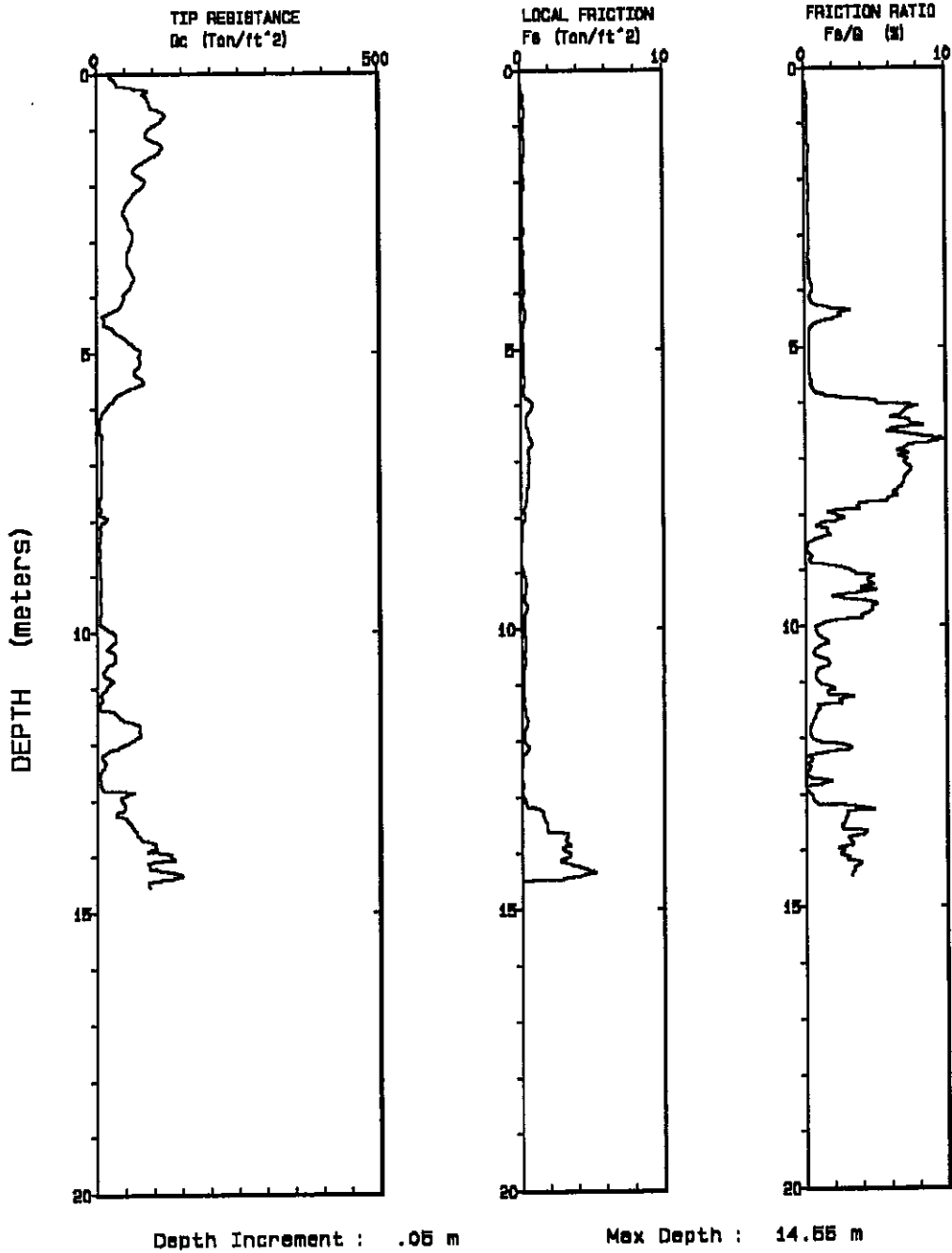


Figure A1 Cone penetration test at SR 20 Swift/Sanders Creek

Table A1 Summary of cone penetration test at State Road 20 Swift/Sanders Creek

University of Florida

Operator :BLANTON CPT Date :06-15-99 10:58  
 On Site Loc:STA-380+45 6'LCL Cone Used :0274  
 Job No. :57040-1538 SR.20 Water table (meters) : 10  
 Tot. Unit Wt. (avg) : 110 pcf

DEPTH		Qc (avg)	Fs (avg)	Rf (avg)	SIGV'	SOIL BEHAVIOUR TYPE	Eq - Dr	PHI	SPT	Su
(meters)	(feet)	(tsf)	(tsf)	(%)	(tsf)		(%)	deg.	N	tsf
0.25	0.82	102.22	0.39	0.38	0.02	sand	>90	>48	20	UNDEFINED
0.50	1.64	217.91	1.09	0.50	0.07	sand	>90	>48	42	UNDEFINED
0.75	2.46	154.46	0.83	0.54	0.11	sand	>90	>48	30	UNDEFINED
1.00	3.28	91.01	0.47	0.51	0.16	sand to silty sand	>90	>48	22	UNDEFINED
1.25	4.10	43.39	0.22	0.52	0.20	silty sand to sandy silt	60-70	44-46	14	UNDEFINED
1.50	4.92	55.23	0.28	0.50	0.25	sand to silty sand	60-70	44-46	13	UNDEFINED
1.75	5.74	147.99	0.95	0.64	0.29	sand	>90	46-48	28	UNDEFINED
2.00	6.56	100.10	0.83	0.83	0.34	sand to silty sand	80-90	44-46	24	UNDEFINED
2.25	7.38	74.62	0.51	0.68	0.38	sand to silty sand	70-80	42-44	18	UNDEFINED
2.50	8.20	49.29	0.46	0.93	0.43	silty sand to sandy silt	50-60	40-42	16	UNDEFINED
2.75	9.02	47.11	0.27	0.57	0.47	silty sand to sandy silt	50-60	40-42	15	UNDEFINED
3.00	9.84	39.45	0.42	1.07	0.52	silty sand to sandy silt	40-50	38-40	13	UNDEFINED
3.25	10.66	45.04	0.38	0.83	0.56	silty sand to sandy silt	50-60	40-42	14	UNDEFINED
3.50	11.48	45.02	0.40	0.88	0.61	silty sand to sandy silt	50-60	38-40	14	UNDEFINED
3.75	12.30	50.05	0.26	0.51	0.65	sand to silty sand	50-60	38-40	12	UNDEFINED
4.00	13.12	60.71	0.26	0.42	0.70	sand to silty sand	50-60	40-42	15	UNDEFINED
4.25	13.94	51.51	0.25	0.49	0.74	sand to silty sand	50-60	38-40	12	UNDEFINED
4.50	14.76	40.11	0.20	0.49	0.79	silty sand to sandy silt	40-50	36-38	13	UNDEFINED
4.75	15.58	50.59	0.18	0.36	0.83	sand to silty sand	40-50	38-40	12	UNDEFINED
5.00	16.40	43.48	0.16	0.38	0.88	sand to silty sand	40-50	36-38	10	UNDEFINED
5.25	17.22	52.81	0.20	0.38	0.92	sand to silty sand	40-50	38-40	13	UNDEFINED
5.50	18.04	48.45	0.28	0.59	0.97	sand to silty sand	40-50	36-38	12	UNDEFINED
5.75	18.86	30.59	0.82	2.69	1.01	sandy silt to clayey silt	UNDFND	UNDFD	12	2.9
6.00	19.69	45.49	1.27	2.79	1.06	sandy silt to clayey silt	UNDFND	UNDFD	17	4.4
6.25	20.51	55.56	1.14	2.06	1.11	sandy silt to clayey silt	UNDFND	UNDFD	21	5.4
6.50	21.33	52.85	1.04	1.96	1.15	silty sand to sandy silt	40-50	36-38	17	UNDEFINED
6.75	22.15	38.93	0.77	1.97	1.20	sandy silt to clayey silt	UNDFND	UNDFD	15	3.7
7.00	22.97	7.97	0.67	8.41	1.24	undefined	UNDFND	UNDFD	UDF	UNDEFINED
7.25	23.79	7.86	0.66	8.41	1.29	undefined	UNDFND	UNDFD	UDF	UNDEFINED

Table A1 Continued

University of Florida

Operator :BLANTON

CPT Date :06-15-99 10:58

On Site Loc:STA-380+45 6'LCL

Cone Used :0274

Job No. :57040-1538 SR.20

Water table (meters) : 10

Tot. Unit Wt. (avg) : 110 pcf

DEPTH (meters)	DEPTH (feet)	Qc (avg) (tsf)	Fs (avg) (tsf)	Rf (avg) (%)	SIGV' (tsf)	SOIL BEHAVIOUR TYPE	Eq - Dr (%)	PHI deg.	SPT N	Su tsf
7.50	24.61	8.23	0.62	7.50	1.33	clay	UNDFND	UNDFD	8	.6
7.75	25.43	8.66	0.20	2.35	1.38	silty clay to clay	UNDFND	UNDFD	6	.7
8.00	26.25	5.88	0.06	0.99	1.42	sensitive fine grained	UNDFND	UNDFD	3	.4
8.25	27.07	5.20	0.07	1.40	1.47	sensitive fine grained	UNDFND	UNDFD	2	.3
8.50	27.89	5.12	0.02	0.42	1.51	sensitive fine grained	UNDFND	UNDFD	2	.3
8.75	28.71	6.89	0.09	1.32	1.56	sensitive fine grained	UNDFND	UNDFD	3	.5
9.00	29.53	8.96	0.22	2.41	1.60	silty clay to clay	UNDFND	UNDFD	6	.7
9.25	30.35	11.74	0.29	2.49	1.65	clayey silt to silty clay	UNDFND	UNDFD	6	1.0
9.50	31.17	22.44	0.22	0.97	1.69	sandy silt to clayey silt	UNDFND	UNDFD	9	2.0
9.75	31.99	17.83	0.27	1.49	1.74	sandy silt to clayey silt	UNDFND	UNDFD	7	1.6
10.00	32.81	19.81	0.32	1.62	1.78	sandy silt to clayey silt	UNDFND	UNDFD	8	1.8
10.25	33.63	35.08	0.30	0.86	1.81	silty sand to sandy silt	<40	30-32	11	UNDEFINED
10.50	34.45	35.02	0.26	0.75	1.83	silty sand to sandy silt	<40	30-32	11	UNDEFINED
10.75	35.27	69.09	0.43	0.62	1.85	sand to silty sand	40-50	36-38	17	UNDEFINED
11.00	36.09	73.35	0.40	0.54	1.87	sand to silty sand	40-50	36-38	18	UNDEFINED
11.25	36.91	73.20	0.45	0.62	1.89	sand to silty sand	40-50	36-38	18	UNDEFINED
11.50	37.73	46.56	0.34	0.74	1.91	silty sand to sandy silt	<40	32-34	15	UNDEFINED
11.75	38.55	12.36	0.11	0.86	1.93	sandy silt to clayey silt	UNDFND	UNDFD	5	1.0
12.00	39.37	9.87	0.08	0.77	1.95	sandy silt to clayey silt	UNDFND	UNDFD	4	.7
12.25	40.19	9.79	0.11	1.11	1.97	clayey silt to silty clay	UNDFND	UNDFD	5	.7
12.50	41.01	10.07	0.21	2.11	1.99	clayey silt to silty clay	UNDFND	UNDFD	5	.7
12.75	41.83	7.26	0.07	0.97	2.01	sensitive fine grained	UNDFND	UNDFD	3	.4
13.00	42.65	5.59	0.01	0.22	2.03	sensitive fine grained	UNDFND	UNDFD	3	.3
13.25	43.47	6.93	0.07	0.94	2.05	sensitive fine grained	UNDFND	UNDFD	3	.4
13.50	44.29	72.24	0.49	0.68	2.07	sand to silty sand	40-50	34-36	17	UNDEFINED
13.75	45.11	69.56	1.64	2.36	2.09	sandy silt to clayey silt	UNDFND	UNDFD	27	6.7
14.00	45.93	67.98	1.56	2.30	2.11	sandy silt to clayey silt	UNDFND	UNDFD	26	6.5
14.25	46.75	73.86	1.47	1.99	2.13	silty sand to sandy silt	40-50	34-36	24	UNDEFINED
14.50	47.57	105.79	2.83	2.67	2.15	sandy silt to clayey silt	UNDFND	UNDFD	41	10.3
14.75	48.39	112.89	2.96	2.63	2.16	silty sand to sandy silt	50-60	36-38	36	UNDEFINED

Dr - All sands (Jamiolkowski et al. 1985)

PHI -

Robertson and Campanella 1983

Su: Nk= 10

Table A2 Summary of dilatometer test at State Road 20 Swift/Sanders Creek

DILATOMETER DATA LISTING & INTERPRETATION (BASED ON THE 1988 DILATOMETER MANUAL)

SNDG. NO. SR20W1

University of Florida

JOB FILE: State Road 20

FILE NO. : UF 2000-1

LOCATION: Sta 380+25

SNDG.BY: PUSH USING FDOT CPT TRUCK

SNDG. DATE: 22 FEB 2000

ANAL.BY: Brian Anderson, Timmy Blanton, Ronnie, Henry

ANAL. DATE: 22 FEB 2000

ANALYSIS PARAMETERS:      LO RANGE = 0.00 BARS              ROD DIAM. = 3.70 CM              BL.THICK. = 13.7 MM              SU FACTOR = 1.00  
 SURF. ELEV. = 0.00 M      LO GAGE 0 = 0.00 BARS              FR.RED.DIA. = 4.80 CM              BL.WIDTH = 94.0 MM              PHI FACTOR = 1.00  
 WATER DEPTH = 1.22 M      HI GAGE 0 = 0.00 BARS              LIN.ROD WT. = 6.50 KGF/M              DELTA-A = 0.12 BARS              OCR FACTOR = 1.00  
 SP.GR.WATER = 1.000      CAL GAGE 0 = 0.00 BARS              DELTA/PHI = 0.50              DELTA-B = 0.68 BARS              M FACTOR = 1.00  
 MAX SU ID = 0.60              SU OPTION = MARCHETTI              MIN PHI ID = 1.20              OCR OPTION= MARCHETTI              K0 FACTOR = 1.00

UNIT CONVERSIONS:      1 BAR = 1.019 KGF/CM2 = 1.044 TSF = 14.51 PSI      1 M = 3.2808 FT

Z	THRUST	A	B	C	DA	DB	ZMRNG	ZMLO	ZMHI	ZMCAL	P0	P1	P2	U0	GAMMA	SVP	KD
(M)	(KGF)	(BAR)	(T/M3)	(BAR)													
*****	*****	*****	*****	*****	*****	*****	*****	*****	*****	*****	*****	*****	*****	*****	*****	*****	*****
3.00	2295.	2.80	11.80		0.12	0.68	0.00	0.00	0.00	0.00	2.51	11.12		0.175	1.90	0.365	6.40
3.50	1607.	4.20	15.20		0.12	0.68	0.00	0.00	0.00	0.00	3.81	14.52		0.224	1.90	0.409	8.76
4.00	1428.	3.50	13.00		0.12	0.68	0.00	0.00	0.00	0.00	3.18	12.32		0.273	1.90	0.453	6.42
4.50	1183.	3.40	11.40		0.12	0.68	0.00	0.00	0.00	0.00	3.16	10.72		0.322	1.90	0.497	5.70
5.00	1173.	2.60	9.40		0.12	0.68	0.00	0.00	0.00	0.00	2.42	8.72		0.371	1.90	0.542	3.78
5.50	1117.	2.50	9.20		0.12	0.68	0.00	0.00	0.00	0.00	2.32	8.52		0.420	1.90	0.586	3.25
6.00	510.	3.50	4.60		0.12	0.68	0.00	0.00	0.00	0.00	3.60	3.92		0.469	1.50	0.620	5.06
6.50	1571.	2.50	6.20		0.12	0.68	0.00	0.00	0.00	0.00	2.47	5.52		0.518	1.70	0.650	3.01
7.00	709.	4.00	6.20		0.12	0.68	0.00	0.00	0.00	0.00	4.05	5.52		0.567	1.70	0.684	5.09
7.50	867.	4.00	6.40		0.12	0.68	0.00	0.00	0.00	0.00	4.04	5.72		0.616	1.70	0.718	4.77
8.00	964.	2.60	4.20		0.12	0.68	0.00	0.00	0.00	0.00	2.68	3.52		0.665	1.60	0.750	2.69
8.50	821.	2.20	4.20		0.12	0.68	0.00	0.00	0.00	0.00	2.26	3.52		0.714	1.60	0.780	1.98
9.00	903.	2.50	5.60		0.12	0.68	0.00	0.00	0.00	0.00	2.50	4.92		0.763	1.70	0.812	2.15
9.50	1372.	3.00	9.00		0.12	0.68	0.00	0.00	0.00	0.00	2.86	8.32		0.813	1.80	0.848	2.41
10.00	1459.	3.80	9.20		0.12	0.68	0.00	0.00	0.00	0.00	3.69	8.52		0.862	1.80	0.888	3.19
10.50	2280.	5.20	14.20		0.12	0.68	0.00	0.00	0.00	0.00	4.91	13.52		0.911	1.90	0.929	4.30
11.00	1535.	5.00	13.20		0.12	0.68	0.00	0.00	0.00	0.00	4.75	12.52		0.960	1.90	0.973	3.89
11.50	1607.	3.80	11.80		0.12	0.68	0.00	0.00	0.00	0.00	3.56	11.12		1.009	1.90	1.018	2.51
12.00	1091.	3.80	5.40		0.12	0.68	0.00	0.00	0.00	0.00	3.88	4.72		1.058	1.70	1.057	2.67
12.50	1015.	3.50	5.60		0.12	0.68	0.00	0.00	0.00	0.00	3.55	4.92		1.107	1.70	1.091	2.24
13.00	949.	4.40	5.80		0.12	0.68	0.00	0.00	0.00	0.00	4.49	5.12		1.156	1.70	1.126	2.96
13.50	1499.	4.20	9.40		0.12	0.68	0.00	0.00	0.00	0.00	4.10	8.72		1.205	1.80	1.162	2.49
14.00	3264.	14.60	29.00		0.12	0.68	0.00	0.00	0.00	0.00	14.04	28.32		1.254	2.10	1.209	10.58

Table A2 Ccontinued

University of Florida  
 JOB FILE: State Road 20  
 LOCATION: Sta 380+25  
 SNDG.BY: PUSH USING FDOT CPT TRUCK  
 ANAL.BY: Brian Anderson, Timmy Blanton, Ronnie, Henry

FILE NO. : UF 2000-1  
 SNDG.DATE: 22 FEB 2000  
 ANAL.DATE: 22 FEB 2000

ANALYSIS PARAMETERS:      LO RANGE = 0.00 BARS      ROD DIAM. = 3.70 CM      BL.THICK. = 13.7 MM      SU FACTOR = 1.00  
 SURF.ELEV. = 0.00 M      LO GAGE 0 = 0.00 BARS      FR.RED.DIA. = 4.80 CM      BL.WIDTH = 94.0 MM      PHI FACTOR = 1.00  
 WATER DEPTH = 1.22 M      HI GAGE 0 = 0.00 BARS      LIN.ROD WT. = 6.50 KGF/M      DELTA-A = 0.12 BARS      OCR FACTOR = 1.00  
 SP.GR.WATER = 1.000      CAL GAGE 0 = 0.00 BARS      DELTA/PHI = 0.50      DELTA-B = 0.68 BARS      M FACTOR = 1.00  
 MAX SU ID = 0.60      SU OPTION = MARCHETTI      MIN PHI ID = 1.20      OCR OPTION= MARCHETTI      K0 FACTOR = 1.00

UNIT CONVERSIONS:      1 BAR = 1.019 KGF/CM2 = 1.044 TSF = 14.51 PSI      1 M = 3.2808 FT

Z (M)	ID	UD	ED (BAR)	K0	SU (BAR)	QD (BAR)	PHI (DEG)	SIGFF (BAR)	PHIO (DEG)	PC (BAR)	OCR	M (BAR)	SOIL TYPE
*****	*****	*****	*****	*****	*****	*****	*****	*****	*****	*****	*****	*****	*****
3.00	3.69	0.00	299.	0.71		79.7	44.3	0.62	42.2	1.40	3.8	631.	SAND
3.50	2.99	0.00	372.	1.19		47.2	39.6	0.67	37.3	3.99	9.8	886.	SILTY SAND
4.00	3.14	0.00	317.	0.92		43.8	39.2	0.74	37.1	2.58	5.7	671.	SILTY SAND
4.50	2.66	0.00	262.	0.89		35.2	37.4	0.80	35.3	2.51	5.0	525.	SILTY SAND
5.00	3.07	0.00	219.	0.64		38.6	38.0	0.88	36.1	1.38	2.5	362.	SILTY SAND
5.50	3.25	0.00	215.	0.59		37.3	37.5	0.94	35.7	1.24	2.1	328.	SILTY SAND
6.00	0.10	0.00	11.	1.17	0.43					2.64	4.3	20.	MUD
6.50	1.56	0.00	106.	0.50		55.0	39.5	1.06	38.0	1.06	1.6	142.	SANDY SILT
7.00	0.42	0.00	51.	1.18	0.48					2.94	4.3	92.	SILTY CLAY
7.50	0.49	0.00	58.	1.12	0.47					2.78	3.9	101.	SILTY CLAY
8.00	0.42	0.00	29.	0.71	0.24					1.19	1.6	34.	SILTY CLAY
8.50	0.82	0.00	44.	0.54						0.77	1.0	38.	CLAYEY SILT
9.00	1.39	0.00	84.	0.54		31.1	34.2	1.27	32.8	1.22	1.5	84.	SANDY SILT
9.50	2.67	0.00	189.	0.50		47.9	36.9	1.36	35.7	1.25	1.5	234.	SILTY SAND
10.00	1.71	0.00	168.	0.61		47.9	36.3	1.41	35.2	1.94	2.2	236.	SANDY SILT
10.50	2.15	0.00	299.	0.69		74.2	38.6	1.51	37.6	2.79	3.0	514.	SILTY SAND
11.00	2.05	0.00	270.	0.72		47.2	35.3	1.54	34.3	2.95	3.0	437.	SILTY SAND
11.50	2.96	0.00	262.	0.52		55.4	36.6	1.62		1.60	1.6	340.	SILTY SAND
12.00	0.30	0.00	29.	0.71	0.33					1.66	1.6	33.	CLAY
12.50	0.56	0.00	47.	0.61	0.28					1.31	1.2	46.	SILTY CLAY
13.00	0.19	0.00	22.	0.78	0.40					2.08	1.8	27.	CLAY
13.50	1.60	0.00	160.	0.56		50.6	35.0	1.83	34.3	1.98	1.7	187.	SANDY SILT
14.00	1.12	0.00	496.	1.90						16.25	13.4	1265.	SILT

University of Florida	
Operator : Brian1/Brian2	CPT Date : 02-17-00 14: 47
Sounding : awrec2 Pg 1 / 1	Location : SW Rec Center
Cone Used : 619	Job No. : Insitu 2000

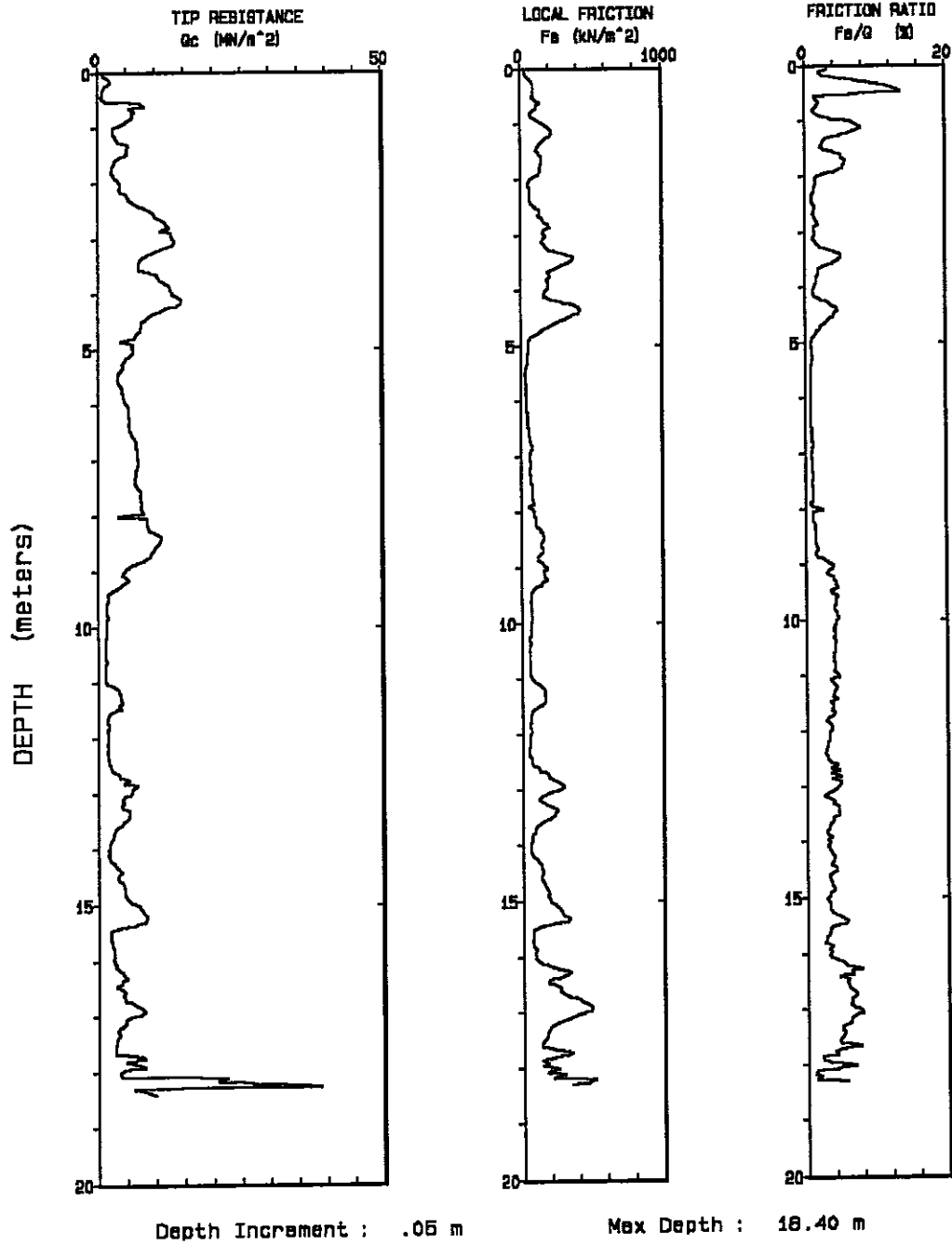


Figure A2 Cone penetration test at Southwest Recreation Center

Table A3 Summary of cone penetration test at Southwest Recreation Center

Hogentogler & Co. Inc.

Operator :Brian1/Brian2

On Site Loc :SW Rec Center

CPT Date :02-17-00 14:47

Job No. :Insitu 2000

Cone Used :619

Tot. Unit Wt. (avg) : 18 kN/m^3

Water table (meters) : 1.8

DEPTH (meters)	DEPTH (feet)	Qc (avg) (MN/m^2)	Fs (avg) (kN/m^2)	Rf (avg) (%)	SIGV' (MPa)	SOIL BEHAVIOR TYPE	Eq - Dr (%)	PHI deg.	SPT N	Su MPa
0.25	0.82	1.70	60.86	3.57	2249.12	silty clay to clay	UNDFND	UNDFD	11	.1
0.50	1.64	0.89	90.26	10.12	6747.35	undefined	UNDFND	UNDFD	UDF	UNDEFINED
0.75	2.46	6.76	113.38	1.68	11245.59	silty sand to sandy silt	80-90	>48	23	UNDEFINED
1.00	3.28	4.56	113.26	2.48	15743.82	sandy silt to clayey silt	UNDFND	UNDFD	18	.3
1.25	4.10	3.11	206.00	6.62	20242.06	clay	UNDFND	UNDFD	31	.2
1.50	4.92	5.08	130.14	2.56	24740.29	sandy silt to clayey silt	UNDFND	UNDFD	20	.3
1.75	5.74	2.83	143.32	5.07	29238.53	clay	UNDFND	UNDFD	28	.1
2.00	6.56	3.08	111.10	3.61	33001.30	clayey silt to silty clay	UNDFND	UNDFD	15	.2
2.25	7.38	4.42	59.16	1.34	35048.00	silty sand to sandy silt	50-60	42-44	15	UNDEFINED
2.50	8.20	7.26	78.00	1.07	37094.70	sand to silty sand	70-80	42-44	18	UNDEFINED
2.75	9.02	10.92	141.56	1.30	39141.40	sand to silty sand	80-90	44-46	27	UNDEFINED
3.00	9.84	12.53	180.48	1.44	41188.09	sand to silty sand	80-90	44-46	31	UNDEFINED
3.25	10.66	11.76	170.56	1.45	43234.79	sand to silty sand	80-90	44-46	29	UNDEFINED
3.50	11.48	7.57	333.64	4.41	45281.48	clayey silt to silty clay	UNDFND	UNDFD	38	.5
3.75	12.30	9.60	220.00	2.29	47328.18	silty sand to sandy silt	70-80	44-46	32	UNDEFINED
4.00	13.12	12.62	186.14	1.47	49374.88	sand to silty sand	80-90	44-46	32	UNDEFINED
4.25	13.94	13.79	243.12	1.76	51421.57	silty sand to sandy silt	80-90	44-46	46	UNDEFINED
4.50	14.76	9.23	386.64	4.19	53468.27	clayey silt to silty clay	UNDFND	UNDFD	46	.6
4.75	15.58	7.25	193.14	2.66	55514.97	sandy silt to clayey silt	UNDFND	UNDFD	29	.4
5.00	16.40	5.79	64.12	1.11	57561.66	silty sand to sandy silt	50-60	40-42	19	UNDEFINED
5.25	17.22	5.12	48.72	0.95	59608.36	silty sand to sandy silt	50-60	40-42	17	UNDEFINED
5.50	18.04	3.87	33.72	0.87	61655.06	silty sand to sandy silt	40-50	38-40	13	UNDEFINED
5.75	18.86	3.99	32.30	0.81	63701.75	silty sand to sandy silt	40-50	38-40	13	UNDEFINED
6.00	19.69	4.73	38.66	0.82	65748.45	silty sand to sandy silt	50-60	38-40	16	UNDEFINED
6.25	20.51	5.46	44.32	0.81	67795.15	silty sand to sandy silt	50-60	40-42	18	UNDEFINED
6.50	21.33	5.59	47.86	0.86	69841.84	silty sand to sandy silt	50-60	40-42	19	UNDEFINED
6.75	22.15	6.50	60.84	0.94	71888.55	sand to silty sand	50-60	40-42	16	UNDEFINED
7.00	22.97	6.97	68.72	0.99	73935.24	sand to silty sand	60-70	40-42	17	UNDEFINED
7.25	23.79	6.88	64.52	0.94	75981.95	sand to silty sand	60-70	40-42	17	UNDEFINED
7.50	24.61	6.74	69.40	1.03	78028.63	sand to silty sand	50-60	40-42	17	UNDEFINED
7.75	25.43	7.55	78.40	1.04	80075.33	sand to silty sand	60-70	40-42	19	UNDEFINED
8.00	26.25	6.95	80.12	1.15	82122.02	silty sand to sandy silt	50-60	40-42	23	UNDEFINED
8.25	27.07	8.80	101.74	1.16	84168.72	sand to silty sand	60-70	40-42	22	UNDEFINED
8.50	27.89	10.72	150.32	1.40	86215.45	sand to silty sand	70-80	40-42	27	UNDEFINED

Table A3 Continued

Hogentogler & Co. Inc.

Operator :Brian1/Brian2

On Site Loc :SW Rec Center

Job No. :Insitu 2000

Tot. Unit Wt. (avg) : 18 kN/m^3

CPT Date :02-17-00 14:47

Cone Used :619

Water table (meters) : 1.8

DEPTH (meters)	(feet)	Qc (avg) (MN/m^2)	Fs (avg) (kN/m^2)	Rf (avg) (%)	SIGV' (Mpa)	SOIL BEHAVIOR TYPE	Eq - Dr (%)	PHI deg.	SPT N	Su MPa
8.75	28.71	9.57	145.74	1.52	88262.12	silty sand to sandy silt	60-70	40-42	32	UNDEFINED
9.00	29.53	5.96	143.32	2.40	90308.82	sandy silt to clayey silt	UNDFND	UNDFD	24	.3
9.25	30.35	4.69	164.68	3.51	92355.51	clayey silt to silty clay	UNDFND	UNDFD	23	.3
9.50	31.17	2.28	92.22	4.05	94402.21	silty clay to clay	UNDFND	UNDFD	15	.1
9.75	31.99	1.61	67.88	4.23	96448.90	clay	UNDFND	UNDFD	16	9.5
10.00	32.81	1.64	70.00	4.27	98495.59	clay	UNDFND	UNDFD	16	9.7
10.25	33.63	1.50	60.52	4.03	100542.29	clay	UNDFND	UNDFD	15	.0
10.50	34.45	1.42	57.38	4.04	102589.00	clay	UNDFND	UNDFD	14	8.2
10.75	35.27	1.44	56.42	3.93	104635.70	silty clay to clay	UNDFND	UNDFD	10	8.2
11.00	36.09	1.46	61.00	4.18	106682.39	clay	UNDFND	UNDFD	15	.0
11.25	36.91	3.51	138.42	3.95	108729.09	clayey silt to silty clay	UNDFND	UNDFD	18	.2
11.50	37.73	3.83	145.52	3.80	110775.78	clayey silt to silty clay	UNDFND	UNDFD	19	.2
11.75	38.55	1.77	64.16	3.63	112822.47	silty clay to clay	UNDFND	UNDFD	12	.1
12.00	39.37	1.78	58.38	3.29	114869.18	clayey silt to silty clay	UNDFND	UNDFD	9	.1
12.25	40.19	1.72	53.30	3.10	116915.88	clayey silt to silty clay	UNDFND	UNDFD	9	9.9
12.50	41.01	1.96	54.96	2.81	118962.57	clayey silt to silty clay	UNDFND	UNDFD	10	.1
12.75	41.83	3.57	136.32	3.82	121009.27	clayey silt to silty clay	UNDFND	UNDFD	18	.2
13.00	42.65	5.82	258.48	4.44	123055.96	silty clay to clay	UNDFND	UNDFD	39	.3
13.25	43.47	4.34	145.50	3.35	125102.66	clayey silt to silty clay	UNDFND	UNDFD	22	.2
13.50	44.29	5.11	220.72	4.32	127149.35	clayey silt to silty clay	UNDFND	UNDFD	26	.3
13.75	45.11	3.12	108.30	3.47	129196.06	clayey silt to silty clay	UNDFND	UNDFD	16	.1
14.00	45.93	2.06	63.42	3.08	131242.75	clayey silt to silty clay	UNDFND	UNDFD	10	.1
16.75	54.95	4.80	306.48	6.38	153756.41	clay	UNDFND	UNDFD	48	.3
17.00	55.77	7.12	461.90	6.49	155803.09	very stiff fine grained (*)	UNDFND	UNDFD	>50	UNDEFINED
17.25	56.59	4.17	275.50	6.61	157849.81	clay	UNDFND	UNDFD	42	.2
17.50	57.41	3.26	160.06	4.90	159896.50	clay	UNDFND	UNDFD	33	.1
17.75	58.23	4.87	228.14	4.68	161943.20	silty clay to clay	UNDFND	UNDFD	32	.3
18.00	59.06	5.50	179.24	3.26	163989.88	sandy silt to clayey silt	UNDFND	UNDFD	22	.3
18.25	59.88	22.47	330.44	1.47	166036.58	sand to silty sand	80-90	42-44	>50	UNDEFINED

Dr - All sands (Jamiołkowski et al. 1985) PHI - Robertson and Campanella 1983 Su: Nk= 15

Table A4 Summary of dilatometer test at Southwest Recreation Center

DILATOMETER DATA LISTING & INTERPRETATION (BASED ON THE 1988 DILATOMETER MANUAL)  
 University of Florida  
 JOB FILE : INSITU CLASS  
 LOCATION : Boring #12  
 SNDG BY : PUSH USING UF CPT TRUCK  
 ANAL BY : Insitu Class

SNDG. NO. SWREC1  
 FILE NO. : UF 2000-3  
 SNDG.DATE: 16 March 2000

ANAL.DATE: 16 March 2000

ANALYSIS PARAMETERS:      LO RANGE = 0.00 BARS      ROD DIAM. = 3.70 CM      BL.THICK. = 13.7 MM      SU FACTOR = 1.00  
 SURF. ELEV. = 0.00 M      LO GAGE 0 = 0.17 BARS      FR.RED.DIA. = 4.80 CM      BL.WIDTH = 94.0 MM      PHI FACTOR = 1.00  
 WATER DEPTH = 0.00 M      HI GAGE 0 = 0.00 BARS      LIN.ROD WT. = 6.50 KGF/M      DELTA-A = 0.17 BARS      OCR FACTOR = 1.00  
 SP.GR.WATER = 1.000      CAL GAGE 0 = 0.00 BARS      DELTA/PHI = 0.50      DELTA-B = 0.50 BARS      M FACTOR = 1.00  
 MAX SU ID = 0.60      SU OPTION = MARCHETTI      MIN PHI ID = 1.20      OCR OPTION= MARCHETTI      K0 FACTOR = 1.00  
 UNIT CONVERSIONS:      1 BAR = 1.019 KGF/CM2 = 1.044 TSF = 14.51 PSI      1 M = 3.2808 FT

Z (M)	THRUST (KGF)	A (BAR)	B (BAR)	C (BAR)	DA (BAR)	DB (BAR)	ZMRNG (BAR)	ZMLO (BAR)	ZMHI (BAR)	ZMCAL (BAR)	P0 (BAR)	P1 (BAR)	P2 (BAR)	U0 (BAR)	GAMMA (T/M3)	SVP (BAR)	KD
0.20	4491.	5.70	20.10		0.17	0.50	0.00	0.17	0.00	0.00	5.19	19.60		0.020	2.00	0.036	143.59
0.40	5353.	8.40	22.20		0.17	0.50	0.00	0.17	0.00	0.00	7.92	21.70		0.039	1.95	0.055	142.91
0.60	4400.	6.90	18.90		0.17	0.50	0.00	0.17	0.00	0.00	6.51	18.40		0.059	2.00	0.074	86.84
0.80	3810.	4.40	10.80		0.17	0.50	0.00	0.17	0.00	0.00	4.29	10.30		0.079	1.80	0.092	45.79
1.00	3674.	3.00	9.40		0.17	0.50	0.00	0.17	0.00	0.00	2.89	8.90		0.098	1.90	0.109	25.69
1.20	3992.	5.80	13.20		0.17	0.50	0.00	0.17	0.00	0.00	5.64	12.70		0.118	1.95	0.127	43.55
1.40	4128.	9.00	18.80		0.17	0.50	0.00	0.17	0.00	0.00	8.72	18.30		0.137	1.95	0.145	59.01
1.60	3538.	6.00	10.60		0.17	0.50	0.00	0.17	0.00	0.00	5.98	10.10		0.157	1.80	0.163	35.81
2.20	2994.	6.50	12.80		0.20	0.72	0.00	0.17	0.00	0.00	6.43	12.08		0.216	1.95	0.214	29.03
2.40	3583.	6.20	12.00		0.20	0.72	0.00	0.17	0.00	0.00	6.16	11.28		0.236	1.95	0.233	25.44
2.60	2994.	7.00	14.80		0.20	0.72	0.00	0.17	0.00	0.00	6.86	14.08		0.255	1.95	0.251	26.26
2.80	2994.	6.80	13.20		0.20	0.72	0.00	0.17	0.00	0.00	6.73	12.48		0.275	1.95	0.270	23.89
3.00	2994.	7.40	13.50		0.20	0.72	0.00	0.17	0.00	0.00	7.34	12.78		0.294	1.95	0.289	24.41
3.20	3130.	8.20	14.50		0.20	0.72	0.00	0.17	0.00	0.00	8.13	13.78		0.314	1.95	0.307	25.43
3.40	4128.	9.50	18.60		0.20	0.72	0.00	0.17	0.00	0.00	9.29	17.88		0.334	1.95	0.326	27.48
3.60	5262.	10.40	32.50		0.20	0.72	0.00	0.17	0.00	0.00	9.54	31.78		0.353	2.15	0.347	26.51
3.80	5489.	9.40	31.40		0.20	0.72	0.00	0.17	0.00	0.00	8.55	30.68		0.373	2.15	0.369	22.14
4.00	4763.	10.00	16.00		0.20	0.72	0.00	0.17	0.00	0.00	9.95	15.28		0.393	1.90	0.389	24.54
4.20	4990.	13.00	32.30		0.20	0.72	0.00	0.17	0.00	0.00	12.28	31.58		0.412	2.10	0.409	29.03
4.40	5443.	11.00	20.60		0.20	0.72	0.00	0.17	0.00	0.00	10.77	19.88		0.432	1.95	0.429	24.09
4.60	4581.	11.00	21.20		0.20	0.72	0.00	0.17	0.00	0.00	10.74	20.48		0.451	1.95	0.448	22.97
4.80	4717.	15.40	27.10		0.20	0.72	0.00	0.17	0.00	0.00	15.06	26.38		0.471	2.10	0.468	31.19
5.00	6033.	13.00	32.10		0.20	0.72	0.00	0.17	0.00	0.00	12.29	31.38		0.491	2.10	0.489	24.11
5.20	6895.	8.80	29.10		0.20	0.72	0.00	0.17	0.00	0.00	8.03	28.38		0.510	2.00	0.510	14.75
5.40	8936.	10.20	33.50		0.20	0.72	0.00	0.17	0.00	0.00	9.28	32.78		0.530	2.15	0.531	16.48
5.60	9662.	12.20	34.80		0.20	0.72	0.00	0.17	0.00	0.00	11.32	34.08		0.550	2.15	0.554	19.45
5.80	9934.	12.20	34.80		0.20	0.72	0.00	0.17	0.00	0.00	11.32	34.08		0.569	2.15	0.576	18.65

Table A4 Continued

DILATOMETER DATA LISTING & INTERPRETATION (BASED ON THE 1988 DILATOMETER MANUAL)

SNDG. NO. SWREC1

University of Florida

JOB FILE: INSITU CLASS

FILE NO : UF 2000-3

LOCATION: Boring #12

SNDG.BY : PUSH USING UF CPT TRUCK

SNDG.DATE: 16 March 2000

ANAL.BY : Insitu Class

ANAL.DATE: 16 March 2000

ANALYSIS PARAMETERS:	LO RANGE = 0.00 BARS	ROD DIAM. = 3.70 CM	BL.THICK. = 13.7 MM	SU FACTOR = 1.00
SURF.ELEV. = 0.00 M	LO GAGE 0 = 0.17 BARS	FR.RED.DIA. = 4.80 CM	BL.WIDTH = 94.0 MM	PHI FACTOR = 1.00
WATER DEPTH = 0.00 M	HI GAGE 0 = 0.00 BARS	LIN.ROD WT. = 6.50 KGF/M	DELTA-A = 0.17 BARS	OCR FACTOR = 1.00
SP.GR.WATER = 1.000	CAL GAGE 0 = 0.00 BARS	DELTA/PHI = 0.50	DELTA-B = 0.50 BARS	M FACTOR = 1.00
MAX SU ID = 0.60	SU OPTION = MARCHETTI	MIN PHI ID = 1.20	OCR OPTION= MARCHETTI	K0 FACTOR = 1.00
UNIT CONVERSIONS:	1 BAR = 1.019 KGF/CM2 = 1.044 TSF = 14.51 PSI		1 M = 3.2808 FT	

Z (M)	THRUST (KGF)	A (BAR)	B (BAR)	C (BAR)	DA (BAR)	DB (BAR)	ZMRNG (BAR)	ZMLO (BAR)	ZMHI (BAR)	ZMCAL (BAR)	P0 (BAR)	P1 (BAR)	P2 (BAR)	U0 (BAR)	GAMMA (T/M3)	SVP (BAR)	KD
6.00	9707.	11.80	34.70		0.20	0.72	0.00	0.17	0.00	0.00	10.90	33.98		0.589	2.15	0.599	17.22
6.20	8346.	10.20	30.40		0.20	0.72	0.00	0.17	0.00	0.00	9.44	29.88		0.608	2.15	0.621	14.21
6.40	6940.	15.80	35.40		0.20	0.72	0.00	0.17	0.00	0.00	15.07	34.68		0.628	2.10	0.643	22.44
6.60	5157.	8.40	26.90		0.20	0.72	0.00	0.17	0.00	0.00	7.72	26.18		0.648	2.00	0.664	10.65
6.80	7049.	6.80	32.90		0.20	0.72	0.00	0.17	0.00	0.00	5.74	32.18		0.667	2.00	0.684	7.42
7.00	8165.	10.40	32.30		0.20	0.72	0.00	0.17	0.00	0.00	9.55	31.58		0.687	2.15	0.705	12.58
7.20	7847.	11.40	27.80		0.20	0.72	0.00	0.17	0.00	0.00	10.83	27.08		0.707	2.10	0.727	13.92
7.40	8165.	9.10	29.00		0.20	0.72	0.00	0.17	0.00	0.00	8.35	28.28		0.726	2.00	0.747	10.20
7.60	6849.	8.60	25.40		0.20	0.72	0.00	0.17	0.00	0.00	8.01	24.68		0.746	2.00	0.767	9.46
7.80	5579.	7.20	17.00		0.20	0.72	0.00	0.17	0.00	0.00	6.96	16.28		0.765	1.95	0.786	7.87
8.00	4944.	8.10	21.80		0.20	0.72	0.00	0.17	0.00	0.00	7.66	21.08		0.785	2.00	0.805	8.54
8.20	4581.	7.50	21.40		0.20	0.72	0.00	0.17	0.00	0.00	7.05	20.68		0.805	2.00	0.825	7.57
8.40	4219.	10.20	19.10		0.20	0.72	0.00	0.17	0.00	0.00	10.00	18.38		0.824	1.95	0.844	10.87
8.60	3883.	10.60	18.00		0.20	0.72	0.00	0.17	0.00	0.00	10.48	17.28		0.844	1.95	0.863	11.16
8.80	3593.	9.30	16.40		0.20	0.72	0.00	0.17	0.00	0.00	9.19	15.68		0.864	1.95	0.881	9.45
9.00	3583.	8.00	22.80		0.20	0.72	0.00	0.17	0.00	0.00	7.51	22.08		0.883	2.00	0.901	7.35
9.20	4137.	6.80	20.80		0.20	0.72	0.00	0.17	0.00	0.00	6.35	20.08		0.903	2.00	0.920	5.92
9.40	4359.	6.80	14.80		0.20	0.72	0.00	0.17	0.00	0.00	6.65	14.08		0.922	1.95	0.939	6.09
9.60	3915.	7.80	15.60		0.20	0.72	0.00	0.17	0.00	0.00	7.66	14.88		0.942	1.95	0.958	7.01
9.80	4631.	10.00	21.80		0.20	0.72	0.00	0.17	0.00	0.00	9.66	21.08		0.962	1.95	0.977	8.90
10.00	5802.	8.80	27.80		0.20	0.72	0.00	0.17	0.00	0.00	8.10	27.08		0.981	2.00	0.996	7.14
10.20	4781.	11.20	24.80		0.20	0.72	0.00	0.17	0.00	0.00	10.77	24.08		1.001	2.10	1.016	9.61
10.40	3574.	9.20	15.40		0.20	0.72	0.00	0.17	0.00	0.00	9.14	14.68		1.021	1.95	1.036	7.83
10.60	2944.	9.80	16.00		0.20	0.72	0.00	0.17	0.00	0.00	9.74	15.28		1.040	1.95	1.055	8.24
10.80	2889.	11.00	17.10		0.20	0.72	0.00	0.17	0.00	0.00	10.94	16.28		1.060	1.90	1.073	9.21
11.00	2885.	12.40	19.60		0.20	0.72	0.00	0.17	0.00	0.00	12.29	18.88		1.079	1.90	1.091	10.27
11.20	3311.	11.80	31.80		0.20	0.72	0.00	0.17	0.00	0.00	11.05	31.08		1.099	2.15	1.111	8.95

Table A4 Continued

DILATOMETER DATA LISTING & INTERPRETATION (BASED ON THE 1988 DILATOMETER MANUAL)

University of Florida  
 JOB FILE: INSITU CLASS  
 LOCATION: Boring #12  
 SNDG BY : PUSH USING UF CPT TRUCK  
 ANAL BY : Insitu Class

SNDG. NO. SWREC1

FILE NO. : UF 2000-3

SNDG.DATE: 16 March 2000  
 ANAL.DATE: 16 March 2000

ANALYSIS PARAMETERS:      LO RANGE = 0.00 BARS      ROD DIAM. = 3.70 CM      BL.THICK. = 13.7 MM      SU FACTOR = 1.00  
 SURF. ELEV. = 0.00 M      LO GAGE 0 = 0.17 BARS      FR.RED.DIA. = 4.80 CM      BL.WIDTH = 94.0 MM      PHI FACTOR = 1.00  
 WATER DEPTH = 0.00 M      HI GAGE 0 = 0.00 BARS      LIN.ROD WT. = 6.50 KGF/M      DELTA-A = 0.17 BARS      OCR FACTOR = 1.00  
 SP.GR.WATER = 1.000      CAL GAGE 0 = 0.00 BARS      DELTA/PTI = 0.50      DELTA-B = 0.50 BARS      M FACTOR = 1.00  
 MAX SU ID = 0.60      SU OPTION = MARCHETTI      MIN PHI ID = 1.20      OCR OPTION= MARCHETTI      K0 FACTOR = 1.00

UNIT CONVERSIONS:      1 BAR = 1.019 KGF/CM2 = 1.044 TSF = 14.51 PSI      1 M = 3.2808 FT

Z (M)	ID	UD	ED (BAR)	K0	SU (BAR)	QD (BAR)	PHI (DEG)	SIGFF (BAR)	PHIO (DEG)	PC (BAR)	OCR	M (BAR)	SOIL TYPE
*****	*****	*****	*****	*****	*****	*****	*****	*****	*****	*****	*****	*****	*****
0.20	2.79	0.00	500.									2512.	SILTY SAND
0.40	1.75	0.00	478.									2400.	SANDY SILT
0.60	1.84	0.00	413.	10.16		136.3	47.5	0.13	43.6	43.87	590.6	1876.	SILTY SAND
0.80	1.43	0.00	209.	5.13		126.3	48.2	0.16	44.7	15.19	164.1	822.	SANDY SILT
1.00	2.15	0.00	209.	2.40		129.6	49.9	0.19	46.9	4.43	40.8	708.	SILTY SAND
1.20	1.28	0.00	245.	5.07		127.1	46.1	0.22	42.8	21.06	166.1	954.	SANDY SILT
1.40	1.12	0.00	332.	5.02						28.55	196.4	1390.	SILT
1.60	0.71	0.00	143.	3.84						14.64	90.1	530.	CLAYEY SILT
2.20	0.91	0.00	196.	3.42						13.90	64.9	688.	SILT
2.40	0.87	0.00	178.	3.18						12.30	52.8	602.	CLAYEY SILT
2.60	1.09	0.00	251.	3.24						13.96	55.5	856.	SILT
2.80	0.89	0.00	200.	3.07						12.94	47.9	664.	CLAYEY SILT
3.00	0.77	0.00	189.	3.11						14.30	49.5	631.	CLAYEY SILT
3.20	0.72	0.00	196.	3.18						16.24	52.8	663.	CLAYEY SILT
3.40	0.96	0.00	298.	3.32						19.43	59.6	1030.	SILT
3.60	2.42	0.00	772.	3.16		159.3	43.7	0.59	41.6	24.13	69.6	2641.	SILTY SAND
3.80	2.71	0.00	768.	2.59		173.5	44.5	0.63	42.5	17.41	47.2	2498.	SILTY SAND
4.00	0.56	0.00	185.	3.12	1.97					19.45	50.0	620.	SILTY SAND
4.20	1.63	0.00	670.	3.55		136.2	41.8	0.68	39.7	36.88	90.2	2350.	SANDY SILT
4.40	0.88	0.00	316.	3.09						20.82	48.5	1054.	CLAYEY SILT
4.60	0.95	0.00	338.	3.01						20.18	45.1	1112.	SILT
4.80	0.78	0.00	393.	3.56						33.97	72.6	1405.	CLAYEY SILT
5.00	1.62	0.00	662.	2.92		176.9	42.8	0.82	41.1	29.37	60.0	2208.	SANDY SILT
5.20	2.71	0.00	706.	1.62		232.8	45.8	0.88	44.3	9.81	19.2	2025.	SILTY SAND
5.40	2.69	0.00	815.	1.77		306.4	46.6	0.92	45.2	12.09	22.8	2424.	SILTY SAND
5.60	2.11	0.00	790.	2.17		323.8	46.0	0.95	44.6	18.52	33.5	2472.	SILTY SAND
5.80	2.12	0.00	790.	2.06		334.8	46.1	0.99	44.8	17.56	30.5	2441.	SILTY SAND

Table A4 Continued

DILATOMETER DATA LISTING & INTERPRETATION (BASED ON THE 1988 DILATOMETER MANUAL)  
 University of Florida  
 JOB FILE: INSITU CLASS  
 LOCATION: Boring #12  
 SNDG BY : PUSH USING UF CPT TRUCK  
 ANAL BY : Insitu Class

SNDG. NO. SWREC1  
 FILE NO. : UF 2000-3  
 SNDG.DATE: 16 March 2000  
 ANAL.DATE: 16 March 2000

ANALYSIS PARAMETERS:      LO RANGE = 0.00 BARS      ROD DIAM. = 3.70 CM      BL.THICK. = 13.7 MM      SU FACTOR = 1.00  
 SURF.ELEV. = 0.00 M      LO GAGE 0 = 0.17 BARS      FR.RED.DIA. = 4.80 CM      BL.WIDTH = 94.0 MM      PHI FACTOR = 1.00  
 WATER DEPTH = 0.00 M      HI GAGE 0 = 0.00 BARS      LIN.ROD WT. = 6.50 KGF/M      DELTA-A = 0.17 BARS      OCR FACTOR = 1.00  
 SP.GR.WATER = 1.000      CAL GAGE 0 = 0.00 BARS      DELTA/PI = 0.50      DELTA-B = 0.50 BARS      M FACTOR = 1.00  
 MAX SU ID = 0.60      SU OPTION = MARCHETTI      MIN PHI ID = 1.20      OCR OPTION= MARCHETTI      K0 FACTOR = 1.00  
 UNIT CONVERSIONS:      1 BAR = 1.019 KGF/CM2 = 1.044 TSF = 14.51 PSI      1 M = 3.2808 FT

Z (M)	ID	UD	ED (BAR)	K0	SU (BAR)	QD (BAR)	PHI (DEG)	SIGFF (BAR)	PHIO (DEG)	PC (BAR)	OCR	M (BAR)	SOIL TYPE
*****	*****	*****	*****	*****	*****	*****	*****	*****	*****	*****	*****	*****	*****
6.00	2.24	0.00	801.	1.89		328.3	46.1	1.03	44.9	15.48	25.8	2414.	SILTY SAND
6.20	2.29	0.00	702.	1.55		283.2	45.9	1.07	44.6	10.97	17.7	1990.	SILTY SAND
6.40	1.36	0.00	681.	2.74		199.8	42.3	1.08	40.9	34.26	53.2	2222.	SANDY SILT
6.60	2.61	0.00	641.	1.26		168.3	43.6	1.12	42.4	7.65	11.5	1640.	SILTY SAND
6.80	5.21	0.00	917.	0.63		253.4	47.0	1.18	46.0	2.28	3.3	2056.	SAND
7.00	2.49	0.00	764.	1.38		276.4	45.5	1.21	44.4	9.96	14.1	2077.	SILTY SAND
7.20	1.61	0.00	564.	1.60		257.4	44.6	1.24	43.5	13.49	18.6	1587.	SANDY SILT
7.40	2.61	0.00	692.	1.06		283.4	46.0	1.29	45.0	6.39	8.6	1742.	SILTY SAND
7.60	2.30	0.00	579.	1.04		233.9	45.0	1.31	44.0	6.22	8.1	1417.	SILTY SAND
7.80	1.51	0.00	324.	0.89		190.1	44.2	1.33	43.2	4.69	6.0	734.	SANDY SILT
8.00	1.95	0.00	466.	1.04		161.9	42.9	1.35	41.9	6.28	7.8	1095.	SILTY SAND
8.20	2.18	0.00	473.	0.93		151.1	42.7	1.38	41.7	5.18	6.3	1061.	SILTY SAND
8.40	0.91	0.00	291.	1.94						11.84	14.0	750.	SILT
8.60	0.71	0.00	236.	1.97						12.61	14.6	615.	CLAYEY SILT
8.80	0.78	0.00	225.	1.77						9.93	11.3	550.	CLAYEY SILT
9.00	2.20	0.00	506.	1.00		111.2	40.4	1.48	39.4	6.16	6.8	1121.	SILTY SAND
9.20	2.52	0.00	477.	0.76		138.5	42.1	1.54	41.2	3.78	4.1	966.	SILTY SAND
9.40	1.30	0.00	258.	0.78		145.8	42.2	1.57	41.4	4.04	4.3	520.	SANDY SILT
9.60	1.08	0.00	251.	1.46						6.78	7.1	538.	SILT
9.80	1.31	0.00	396.	1.16		141.8	40.9	1.62	40.1	9.26	9.5	946.	SANDY SILT
10.00	2.67	0.00	659.	0.86		195.0	43.2	1.68	42.5	5.35	5.4	1450.	SILTY SAND
10.20	1.36	0.00	462.	1.26		142.7	40.5	1.68	39.7	11.32	11.1	1137.	SANDY SILT
10.40	0.68	0.00	192.	1.57						8.71	8.4	433.	CLAYEY SILT
10.60	0.64	0.00	192.	1.63						9.61	9.1	443.	CLAYEY SILT
10.80	0.55	0.00	189.	1.75	1.59					11.62	10.8	456.	SILTY CLAY
11.00	0.59	0.00	229.	1.87	1.86					14.01	12.8	578.	SILTY CLAY
11.20	2.01	0.00	695.	1.28		87.6	37.1	1.78	36.4	12.36	11.1	1666.	SILTY SAND

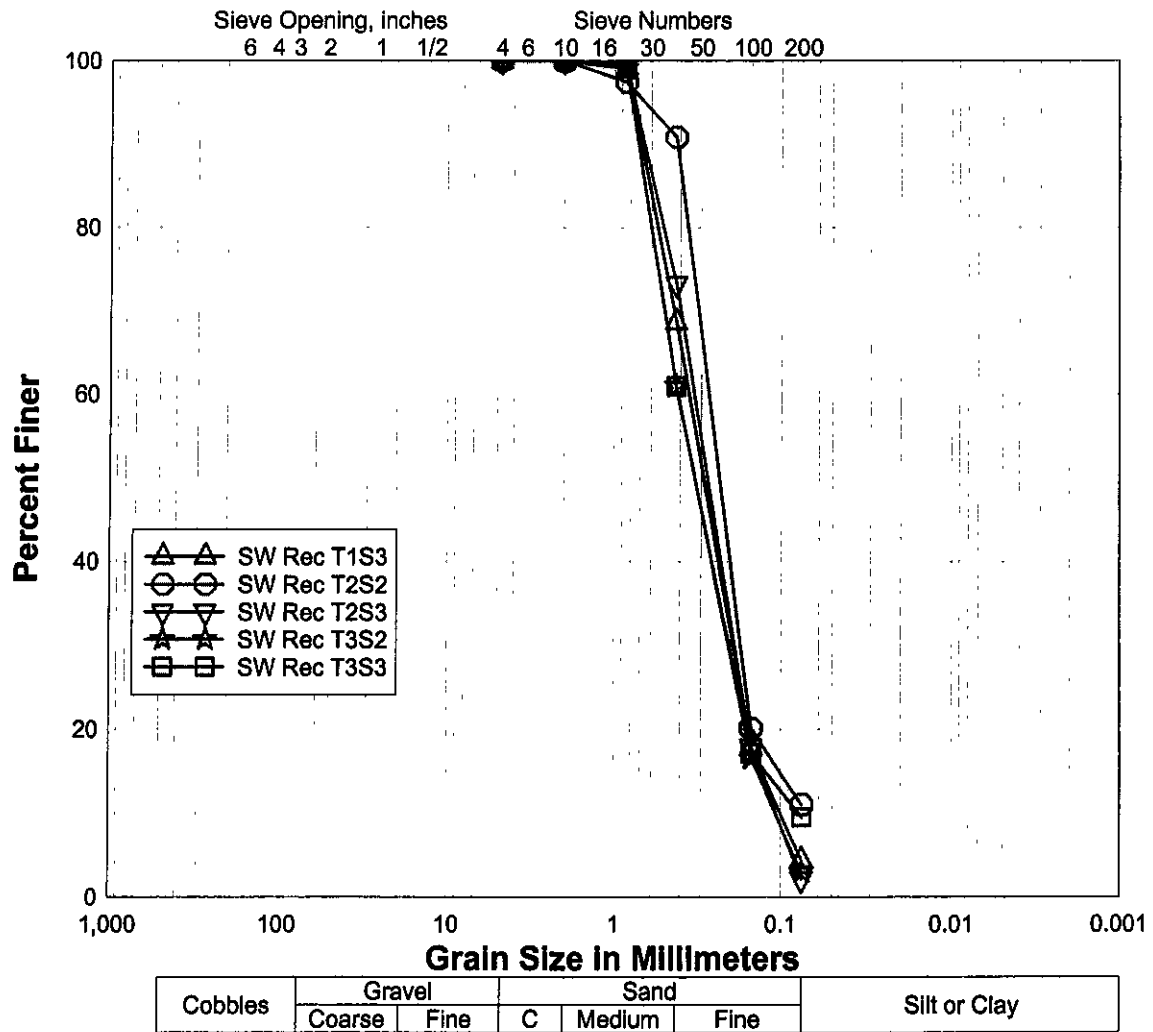


Figure A3 Grain size distributions for tubes tested from Southwest Recreation Center

University of Florida	
Operator : Steve	CPT Date : 08-15-00 11:35
Sounding : swref2 Pg 1 / 1	Location : Archer Landfill
Cone Used : B19	Job No. : AL-4

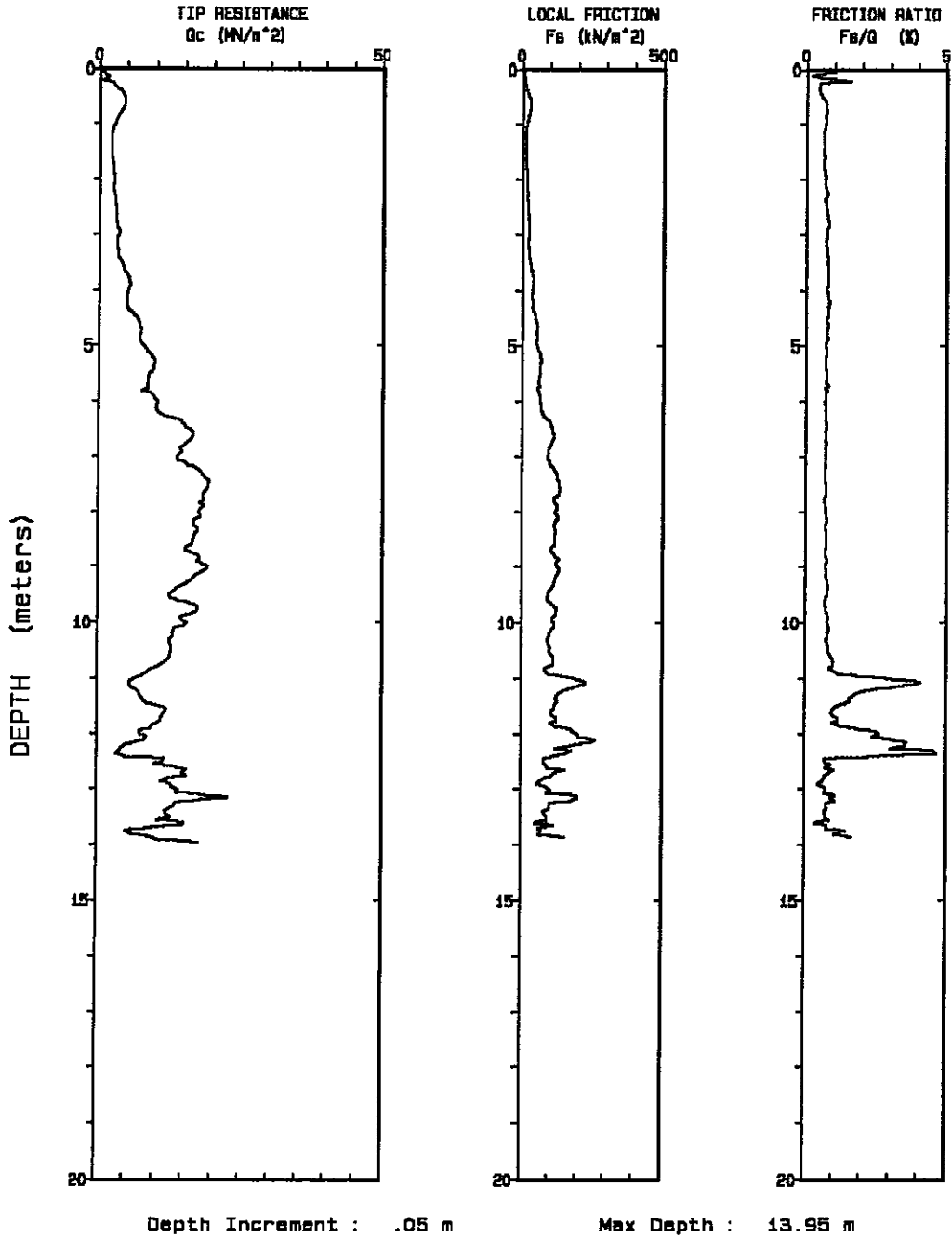


Figure A4 Cone penetration test at Archer Landfill

**Table A5 Summary of cone penetration test at Archer Landfill**

University of Florida

Operator :Steve CPT Date :08-15-00 11:35  
 On Site Loc:Archer Landfill Cone Used :619  
 Job No. :AL-4 Water table (meters) : 15  
 Tot. Unit Wt. (avg) : 18 kN/m<sup>3</sup>

DEPTH (meters)	QC (avg) (feet)	Fs (avg) (MN/m <sup>2</sup> )	Rf (avg) (kN/m <sup>2</sup> )	SIGV' (%)	SIGV' (bar)	SOIL BEHAVIOUR TYPE	Eq - Dr (%)	PHI (deg.)	SPT N	Su bar
0.25	0.82	1.16	6.70	0.58	0.02	sandy silt to clayey silt	UNDFND	UNDFD	5	1.1
0.50	1.64	3.64	17.72	0.49	0.07	silty sand to sandy silt	70-80	>48	12	UNDEFINED
0.75	2.46	4.19	28.50	0.68	0.11	silty sand to sandy silt	70-80	46-48	14	UNDEFINED
1.00	3.28	3.02	19.94	0.66	0.16	silty sand to sandy silt	50-60	42-44	10	UNDEFINED
1.25	4.10	2.17	13.40	0.62	0.20	silty sand to sandy silt	40-50	40-42	7	UNDEFINED
1.50	4.92	2.02	12.22	0.60	0.25	sandy silt to clayey silt	UNDFND	UNDFD	8	1.9
1.75	5.74	2.21	13.66	0.62	0.29	silty sand to sandy silt	40-50	38-40	7	UNDEFINED
2.00	6.56	2.50	16.04	0.64	0.34	silty sand to sandy silt	40-50	38-40	8	UNDEFINED
2.25	7.38	2.49	17.06	0.68	0.38	silty sand to sandy silt	40-50	38-40	8	UNDEFINED
2.50	8.20	2.82	18.94	0.67	0.43	silty sand to sandy silt	40-50	38-40	9	UNDEFINED
2.75	9.02	3.02	22.22	0.73	0.47	silty sand to sandy silt	40-50	38-40	10	UNDEFINED
3.00	9.84	3.37	24.88	0.74	0.52	silty sand to sandy silt	40-50	38-40	11	UNDEFINED
3.25	10.66	3.20	22.44	0.70	0.56	silty sand to sandy silt	40-50	38-40	11	UNDEFINED
3.50	11.48	3.55	26.02	0.73	0.61	silty sand to sandy silt	40-50	38-40	12	UNDEFINED
3.75	12.30	4.63	34.70	0.75	0.65	silty sand to sandy silt	50-60	38-40	15	UNDEFINED
4.00	13.12	5.30	39.54	0.75	0.70	sand to silty sand	50-60	38-40	13	UNDEFINED
4.25	13.94	4.94	38.34	0.78	0.74	silty sand to sandy silt	50-60	38-40	16	UNDEFINED
4.50	14.76	5.78	43.46	0.75	0.79	sand to silty sand	50-60	38-40	14	UNDEFINED
4.75	15.58	7.27	53.26	0.73	0.83	sand to silty sand	60-70	40-42	18	UNDEFINED
5.00	16.40	7.44	53.68	0.72	0.88	sand to silty sand	60-70	40-42	19	UNDEFINED
5.25	17.22	9.15	64.86	0.71	0.92	sand to silty sand	60-70	40-42	23	UNDEFINED
5.50	18.04	9.55	66.92	0.70	0.97	sand to silty sand	60-70	40-42	24	UNDEFINED
5.75	18.86	8.70	61.46	0.71	1.01	sand to silty sand	60-70	40-42	22	UNDEFINED
6.00	19.69	9.38	63.70	0.68	1.06	sand to silty sand	60-70	40-42	23	UNDEFINED
6.25	20.51	10.54	72.96	0.69	1.10	sand to silty sand	60-70	40-42	26	UNDEFINED
6.50	21.33	14.75	103.20	0.70	1.15	sand	70-80	42-44	30	UNDEFINED
6.75	22.15	16.19	113.02	0.70	1.19	sand	70-80	42-44	32	UNDEFINED
7.00	22.97	14.36	97.32	0.68	1.24	sand	70-80	40-42	29	UNDEFINED

Table A5 Continued

University of Florida

Operator : Steve CPT Date : 08-15-00 11:35  
 On Site Loc: Archer Landfill Cone Used : 619  
 Job No. : AL-4 Water table (meters) : 15  
 Tot. Unit Wt. (avg) : 18 kN/m<sup>3</sup>

DEPTH (meters)	DEPTH (feet)	Qc (avg) (MN/m <sup>2</sup> )	Fs (avg) (kN/m <sup>2</sup> )	Rf (avg) (%)	SIGV <sup>1</sup> (bar)	SOIL BEHAVIOUR TYPE	Eq - Dr (%)	PHI deg.	SPT N	Su bar
7.25	23.79	15.82	107.66	0.68	1.28	sand	70-80	40-42	32	UNDEFINED
7.50	24.61	18.72	130.24	0.70	1.33	sand	80-90	42-44	37	UNDEFINED
7.75	25.43	18.67	132.42	0.71	1.37	sand	80-90	42-44	37	UNDEFINED
8.00	26.25	18.04	123.26	0.68	1.42	sand	70-80	42-44	36	UNDEFINED
8.25	27.07	17.24	125.42	0.73	1.46	sand	70-80	40-42	34	UNDEFINED
8.50	27.89	17.01	121.50	0.71	1.51	sand	70-80	40-42	34	UNDEFINED
8.75	28.71	16.01	114.28	0.71	1.55	sand	70-80	40-42	32	UNDEFINED
9.00	29.53	18.07	128.14	0.71	1.60	sand	70-80	40-42	36	UNDEFINED
9.25	30.35	17.35	126.92	0.73	1.64	sand	70-80	40-42	35	UNDEFINED
9.50	31.17	13.82	105.32	0.76	1.69	sand	60-70	40-42	28	UNDEFINED
9.75	31.99	15.56	109.46	0.70	1.73	sand	70-80	40-42	31	UNDEFINED
10.00	32.81	15.67	118.44	0.76	1.78	sand	70-80	40-42	31	UNDEFINED
10.25	33.63	13.58	106.94	0.79	1.82	sand	60-70	38-40	27	UNDEFINED
10.50	34.45	12.83	99.24	0.77	1.87	sand	60-70	38-40	26	UNDEFINED
10.75	35.27	12.21	113.88	0.93	1.91	sand to silty sand	60-70	38-40	31	UNDEFINED
11.00	36.09	8.37	121.74	1.45	1.96	silty sand to sandy silt	50-60	36-48	28	UNDEFINED
11.25	36.91	6.32	188.10	2.98	2.00	sandy silt to clayey silt	UNDFND	UNDFD	25	6.1
11.50	37.73	8.71	125.12	1.44	2.05	silty sand to sandy silt	50-60	36-38	29	UNDEFINED
11.75	38.55	11.55	119.24	1.03	2.09	sand to silty sand	60-70	38-40	29	UNDEFINED
12.00	39.37	8.96	158.76	1.77	2.14	silty sand to sandy silt	50-60	36-38	30	UNDEFINED
12.25	40.19	6.58	204.88	3.11	2.18	sandy silt to clayey silt	UNDFND	UNDFD	26	6.3
12.50	41.01	7.10	122.90	1.73	2.23	silty sand to sandy silt	40-50	34-36	24	UNDEFINED
12.75	41.83	14.02	115.36	0.82	2.27	sand	60-70	38-40	28	UNDEFINED
13.00	42.65	12.85	81.98	0.64	2.32	sand	60-70	38-40	26	UNDEFINED
13.25	43.47	17.29	155.84	0.90	2.36	sand	70-80	38-40	35	UNDEFINED
13.50	44.29	12.65	94.28	0.75	2.41	sand	60-70	36-38	25	UNDEFINED
13.75	45.11	10.89	80.50	0.74	2.45	sand to silty sand	50-60	36-38	27	UNDEFINED

Dr - All sands (Jamiolkowski et al. 1985) PHI - Robertson and Campanella 1983 SU: Nk= 10

Table A6 Summary of dilatometer test at Archer Landfill

DILATOMETER DATA LISTING & INTERPRETATION (BASED ON THE 1988 DILATOMETER MANUAL)

SNDG. NO. ALF 1

University of Florida

JOB FILE: Archer Landfill - Research

FILE NO. : UF 2001-1

LOCATION: ALF 1

SNDG BY : PUSH USING UF CPT TRUCK

SNDG.DATE: 07 February 2001

ANAL BY : J. Brian Anderson

ANAL.DATE: 07 March 2001

ANALYSIS PARAMETERS:      LO RANGE    =40.00 BARS      ROD DIAM.    = 3.57 CM      BL.THICK.    = 13.7 MM      SU FACTOR = 1.00  
 SURF.ELEV.    = 0.00 M      LO GAGE 0    = 0.10 BARS      FR.RED.DIA. = 4.80 CM      BL.WIDTH    = 94.0 MM      PHI FACTOR = 1.00  
 WATER DEPTH = 10.00 M      HI GAGE 0    = 0.00 BARS      LIN.ROD WT. = 6.50 KGF/M      DELTA-A     = 0.20 BARS      OCR FACTOR = 1.00  
 SP.GR.WATER = 1.000      CAL GAGE 0   = 0.00 BARS      DELTA/PHI    = 0.50      DELTA-B     = 0.55 BARS      M FACTOR = 1.00  
 MAX SU ID    = 0.60      SU OPTION    = MARCHETTI      MIN PHI ID    = 1.20      OCR OPTION= MARCHETTI      K0 FACTOR = 1.00  
 UNIT CONVERSIONS:      1 BAR = 1.019 KGF/CM2 = 1.044 TSF = 14.51 PSI      1 M = 3.2808 FT

Z	THRUST	A	B	C	DA	DB	ZMRNG	ZMLO	ZMHI	ZMCAL	P0	P1	P2	U0	GAMMA	SVP	KD
(M)	(KGF)	(BAR)	(T/M3)	(BAR)													
*****	*****	*****	*****	*****	*****	*****	*****	*****	*****	*****	*****	*****	*****	*****	*****	*****	*****
0.40	2250.	1.00	5.80		0.20	0.55	40.00	0.10	0.00	0.00	0.90	5.15		0.000	1.80	0.031	28.58
0.60	2182.	1.00	5.00		0.20	0.55	40.00	0.10	0.00	0.00	0.94	4.35		0.000	1.80	0.067	14.05
0.80	2009.	1.00	4.60		0.20	0.55	40.00	0.10	0.00	0.00	0.96	3.95		0.000	1.70	0.101	9.47
1.00	1850.	0.80	4.20		0.20	0.55	40.00	0.10	0.00	0.00	0.77	3.55		0.000	1.70	0.134	5.71
1.20	1796.	0.80	3.50		0.20	0.55	40.00	0.10	0.00	0.00	0.80	2.85		0.000	1.70	0.168	4.78
1.40	1750.	0.80	3.80		0.20	0.55	40.00	0.10	0.00	0.00	0.79	3.15		0.000	1.70	0.201	3.91
1.60	1786.	1.20	4.80		0.20	0.55	40.00	0.10	0.00	0.00	1.16	4.15		0.000	1.80	0.236	4.91
1.80	1827.	0.80	4.00		0.20	0.55	40.00	0.10	0.00	0.00	0.78	3.35		0.000	1.70	0.270	2.88
2.00	1977.	0.80	4.00		0.20	0.55	40.00	0.10	0.00	0.00	0.78	3.35		0.000	1.70	0.303	2.56
2.20	2036.	0.90	4.50		0.20	0.55	40.00	0.10	0.00	0.00	0.86	3.85		0.000	1.70	0.337	2.55
2.40	2032.	1.00	4.80		0.20	0.55	40.00	0.10	0.00	0.00	0.95	4.15		0.000	1.70	0.370	2.56
2.60	2132.	1.00	5.10		0.20	0.55	40.00	0.10	0.00	0.00	0.93	4.45		0.000	1.80	0.404	2.31
2.80	2214.	1.00	5.20		0.20	0.55	40.00	0.10	0.00	0.00	0.93	4.55		0.000	1.80	0.440	2.11
3.00	2309.	1.10	5.40		0.20	0.55	40.00	0.10	0.00	0.00	1.02	4.75		0.000	1.80	0.475	2.15
3.20	2341.	1.10	5.40		0.20	0.55	40.00	0.10	0.00	0.00	1.02	4.75		0.000	1.80	0.510	2.00
3.40	2314.	1.10	5.40		0.20	0.55	40.00	0.10	0.00	0.00	1.02	4.75		0.000	1.80	0.546	1.87
3.60	2477.	1.10	5.80		0.20	0.55	40.00	0.10	0.00	0.00	1.00	5.15		0.000	1.80	0.581	1.73
3.80	2705.	1.40	6.70		0.20	0.55	40.00	0.10	0.00	0.00	1.27	6.05		0.000	1.80	0.616	2.06
4.00	2855.	1.50	7.20		0.20	0.55	40.00	0.10	0.00	0.00	1.35	6.55		0.000	1.80	0.652	2.08

Table A6 Continued

DILATOMETER DATA LISTING & INTERPRETATION (BASED ON THE 1988 DILATOMETER MANUAL)  
 University of Florida  
 JOB FILE : Archer Landfill - Research  
 LOCATION : ALF 1  
 SNDG.BY : PUSH USING UF CPT TRUCK  
 ANAL.BY : J. Brian Anderson

SNDG. NO. ALF 1  
 FILE NO. : UF 2001-1  
 SNDG.DATE: 07 February 2001  
 ANAL.DATE: 07 March 2001

ANALYSIS PARAMETERS:      LO RANGE =40.00 BARS      ROD DIAM. = 3.57 CM      BL.THICK. = 13.7 MM      SU FACTOR = 1.00  
 SURF. ELEV. = 0.00 M      LO GAGE 0 = 0.10 BARS      FR.RED.DIA. = 4.80 CM      BL.WIDTH = 94.0 MM      PHI FACTOR = 1.00  
 WATER DEPTH = 10.00 M      HI GAGE 0 = 0.00 BARS      LIN.ROD WT. = 6.50 KGF/M      DELTA-A = 0.20 BARS      OCR FACTOR = 1.00  
 SP.GR.WATER = 1.000      CAL GAGE 0 = 0.00 BARS      DELTA/PHI = 0.50      DELTA-B = 0.55 BARS      M FACTOR = 1.00  
 MAX SU ID = 0.60      SU OPTION = MARCHETTI      MIN PHI ID = 1.20      OCR OPTION= MARCHETTI      K0 FACTOR = 1.00  
 UNIT CONVERSIONS:      1 BAR = 1.019 KGF/CM2 = 1.044 TSF = 14.51 PSI      1 M = 3.2808 FT

Z	THRUST	A	B	C	DA	DB	ZMRNG	ZMLO	ZMHI	ZMCAL	P0	P1	P2	U0	GAMMA	SVP	KD
(M)	(KGF)	(BAR)	(T/M3)	(BAR)													
*****	*****	*****	*****	*****	*****	*****	*****	*****	*****	*****	*****	*****	*****	*****	*****	*****	*****
4.20	3023.	1.70	7.80		0.20	0.55	40.00	0.10	0.00	0.00	1.53	7.15		0.000	1.80	0.687	2.23
4.40	3150.	1.70	7.80		0.20	0.55	40.00	0.10	0.00	0.00	1.53	7.15		0.000	1.80	0.722	2.12
4.60	3296.	1.80	8.60		0.20	0.55	40.00	0.10	0.00	0.00	1.60	7.95		0.000	1.80	0.758	2.11
4.80	3414.	2.00	9.00		0.20	0.55	40.00	0.10	0.00	0.00	1.79	8.35		0.000	1.80	0.793	2.25
5.00	3477.	2.10	9.00		0.20	0.55	40.00	0.10	0.00	0.00	1.89	8.35		0.000	1.90	0.829	2.28
5.20	3459.	2.20	9.20		0.20	0.55	40.00	0.10	0.00	0.00	1.99	8.55		0.000	1.90	0.867	2.29
5.40	3486.	2.20	9.30		0.20	0.55	40.00	0.10	0.00	0.00	1.98	8.65		0.000	1.90	0.904	2.19
5.60	3709.	2.20	9.80		0.20	0.55	40.00	0.10	0.00	0.00	1.96	9.15		0.000	1.90	0.941	2.08
5.80	3964.	2.30	10.40		0.20	0.55	40.00	0.10	0.00	0.00	2.03	9.75		0.000	1.90	0.978	2.08
6.00	4136.	2.40	10.70		0.20	0.55	40.00	0.10	0.00	0.00	2.12	10.05		0.000	1.90	1.016	2.09
6.20	4432.	2.50	11.30		0.20	0.55	40.00	0.10	0.00	0.00	2.20	10.65		0.000	1.90	1.053	2.09
6.40	4932.	2.40	12.30		0.20	0.55	40.00	0.10	0.00	0.00	2.04	11.65		0.000	1.90	1.090	1.87
6.60	5446.	3.60	16.00		0.20	0.55	40.00	0.10	0.00	0.00	3.12	15.35		0.000	1.90	1.128	2.76
6.80	5000.	3.20	13.70		0.20	0.55	40.00	0.10	0.00	0.00	2.81	13.05		0.000	1.90	1.165	2.41
7.00	5182.	2.40	14.40		0.20	0.55	40.00	0.10	0.00	0.00	1.94	13.75		0.000	1.90	1.202	1.61
7.20	5205.	2.80	14.70		0.20	0.55	40.00	0.10	0.00	0.00	2.34	14.05		0.000	1.90	1.239	1.89
7.40	5050.	2.40	14.10		0.20	0.55	40.00	0.10	0.00	0.00	1.95	13.45		0.000	1.90	1.277	1.53
7.60	5291.	2.50	14.80		0.20	0.55	40.00	0.10	0.00	0.00	2.02	14.15		0.000	1.90	1.314	1.54
7.80	5859.	4.30	16.70		0.20	0.55	40.00	0.10	0.00	0.00	3.82	16.05		0.000	2.00	1.352	2.82
8.00	6236.	5.00	17.70		0.20	0.55	40.00	0.10	0.00	0.00	4.50	17.05		0.000	2.00	1.392	3.24

**Table A6      Continued**

DILATOMETER DATA LISTING & INTERPRETATION (BASED ON THE 1988 DILATOMETER MANUAL)  
 University of Florida  
 JOB FILE : Archer Landfill - Research  
 LOCATION : ALF 1  
 SNDG.BY : PUSH USING UF CPT TRUCK  
 ANAL.BY : J. Brian Anderson

SNDG. NO. ALF 1  
 FILE NO. : UF 2001-1  
 SNDG.DATE: 07 February 2001  
 ANAL.DATE: 07 March 2001

ANALYSIS PARAMETERS:      LO RANGE =40.00 BARS      ROD DIAM. = 3.57 CM      BL.THICK. = 13.7 MM      SU FACTOR = 1.00  
 SURF. ELEV. = 0.00 M      LO GAGE 0 = 0.10 BARS      FR.RED.DIA. = 4.80 CM      BL.WIDTH = 94.0 MM      PHI FACTOR = 1.00  
 WATER DEPTH = 10.00 M      HI GAGE 0 = 0.00 BARS      LIN.ROD WT. = 6.50 KGF/M      DELTA-A = 0.20 BARS      OCR FACTOR = 1.00  
 SP.GR.WATER = 1.000      CAL GAGE 0 = 0.00 BARS      DELTA/PHI = 0.50      DELTA-B = 0.55 BARS      M FACTOR = 1.00  
 MAX SU ID = 0.60      SU OPTION = MARCHETTI      MIN PHI ID = 1.20      OCR OPTION= MARCHETTI      K0 FACTOR = 1.00  
 UNIT CONVERSIONS:      1 BAR = 1.019 KGF/CM2 = 1.044 TSF = 14.51 PSI      1 M = 3.2808 FT

Z (M)	ID	UD	ED (BAR)	K0	SU (BAR)	QD (BAR)	PHI (DEG)	SIGFF (BAR)	PHIO (DEG)	PC (BAR)	OCR	M (BAR)	SOIL TYPE
*****	*****	*****	*****	*****	*****	*****	*****	*****	*****	*****	*****	*****	*****
0.40	4.74	0.00	148.									516.	SAND
0.60	3.64	0.00	118.									334.	SAND
0.80	3.13	0.00	104.									255.	SILTY SAND
1.00	3.63	0.00	97.									194.	SAND
1.20	2.55	0.00	71.									131.	SILTY SAND
1.40	3.00	0.00	82.									138.	SILTY SAND
1.60	2.59	0.00	104.	0.34		65.5	47.0	0.41	44.5	0.24	1.0	194.	SILTY SAND
1.80	3.31	0.00	89.									127.	SAND
2.00	3.31	0.00	89.									118.	SAND
2.20	3.49	0.00	104.									136.	SAND
2.40	3.38	0.00	111.	0.11		77.0	46.3	0.64	44.4	0.05	0.1	146.	SAND
2.60	3.77	0.00	122.	0.09		81.2	46.2	0.70	44.4	0.03	0.1	150.	SAND
2.80	3.91	0.00	126.	0.08		84.6	46.0	0.76	44.3	0.03	0.1	144.	SAND
3.00	3.65	0.00	129.	0.12		87.9	45.6	0.81	44.0	0.06	0.1	151.	SAND
3.20	3.65	0.00	129.	0.12		89.3	45.2	0.87	43.7	0.07	0.1	143.	SAND
3.40	3.65	0.00	129.	0.14		88.3	44.7	0.93	43.2	0.09	0.2	135.	SAND
3.60	4.14	0.00	144.	0.11		95.1	44.9	0.99	43.5	0.06	0.1	140.	SAND
3.80	3.75	0.00	166.	0.16		102.7	44.8	1.05	43.5	0.14	0.2	187.	SAND
4.00	3.84	0.00	180.	0.16		108.3	44.7	1.11	43.5	0.15	0.2	205.	SAND

Table A6 Continued

DILATOMETER DATA LISTING & INTERPRETATION (BASED ON THE 1988 DILATOMETER MANUAL)

SNDG. NO. ALF 1

University of Florida

JOB FILE : Archer Landfill - Research

FILE NO. : UF 2001-1

LOCATION : ALF 1

SNDG.BY : PUSH USING UF CPT TRUCK

SNDG.DATE: 07 February 2001

ANAL.BY : J. Brian Anderson

ANAL.DATE: 07 March 2001

ANALYSIS PARAMETERS:	LO RANGE = 40.00 BARS	ROD DIAM. = 3.57 CM	BL.THICK. = 13.7 MM	SU FACTOR = 1.00
SURF. ELEV. = 0.00 M	LO GAGE 0 = 0.10 BARS	FR.RED.DIA. = 4.80 CM	BL.WIDTH = 94.0 MM	PHI FACTOR = 1.00
WATER DEPTH = 10.00 M	HI GAGE 0 = 0.00 BARS	LIN.ROD WT. = 6.50 KGF/M	DELTA-A = 0.20 BARS	OCR FACTOR = 1.00
SP.GR.WATER = 1.000	CAL GAGE 0 = 0.00 BARS	DELTA/PHI = 0.50	DELTA-B = 0.55 BARS	M FACTOR = 1.00
MAX SU ID = 0.60	SU OPTION = MARCHETTI	MIN PHI ID = 1.20	OCR OPTION= MARCHETTI	K0 FACTOR = 1.00
UNIT CONVERSIONS:	1 BAR = 1.019 KGF/CM2 = 1.044 TSF = 14.51 PSI		1 M = 3.2808 FT	

Z (M)	ID	UD	ED (BAR)	K0	SU (BAR)	QD (BAR)	PHI (DEG)	SIGFF (BAR)	PHIO (DEG)	PC (BAR)	OCR	M (BAR)	SOIL TYPE
*****	*****	*****	*****	*****	*****	*****	*****	*****	*****	*****	*****	*****	*****
4.20	3.67	0.00	195.	0.19		114.1	44.6	1.17	43.5	0.21	0.3	233.	SAND
4.40	3.67	0.00	195.	0.17		119.2	44.6	1.23	43.6	0.19	0.3	225.	SAND
4.60	3.98	0.00	220.	0.17		124.7	44.6	1.29	43.6	0.20	0.3	253.	SAND
4.80	3.67	0.00	228.	0.21		128.5	44.4	1.35	43.4	0.28	0.3	275.	SAND
5.00	3.41	0.00	224.	0.22		130.5	44.2	1.41	43.2	0.33	0.4	273.	SAND
5.20	3.30	0.00	228.	0.25		129.4	43.8	1.47	42.9	0.41	0.5	278.	SAND
5.40	3.36	0.00	231.	0.24		130.6	43.6	1.53	42.8	0.41	0.5	274.	SAND
5.60	3.67	0.00	250.	0.21		139.7	43.9	1.59	43.1	0.35	0.4	284.	SAND
5.80	3.80	0.00	268.	0.20		149.5	44.1	1.66	43.4	0.33	0.3	304.	SAND
6.00	3.73	0.00	275.	0.20		156.0	44.1	1.72	43.5	0.34	0.3	314.	SAND
6.20	3.85	0.00	293.	0.19		167.4	44.4	1.79	43.8	0.31	0.3	334.	SAND
6.40	4.70	0.00	333.	0.11		188.2	45.2	1.86	44.7	0.12	0.1	348.	SAND
6.60	3.92	0.00	424.	0.24		202.6	44.8	1.92	44.3	0.56	0.5	587.	SAND
6.80	3.64	0.00	355.	0.24		186.8	44.2	1.98	43.7	0.53	0.5	450.	SAND
7.00	6.10	0.00	410.	0.09		199.1	45.1	2.05	44.7	0.09	0.1	375.	SAND
7.20	5.00	0.00	406.	0.15		197.8	44.5	2.11	44.2	0.25	0.2	428.	SAND
7.40	5.89	0.00	399.									347.	SAND
7.60	6.00	0.00	421.	0.11		203.3	44.5	2.24	44.3	0.14	0.1	368.	SAND
7.80	3.20	0.00	424.	0.30		215.9	43.9	2.29	43.6	0.97	0.7	595.	SILTY SAND
8.00	2.79	0.00	435.	0.36		227.1	43.8	2.35	43.6	1.37	1.0	655.	SILTY SAND

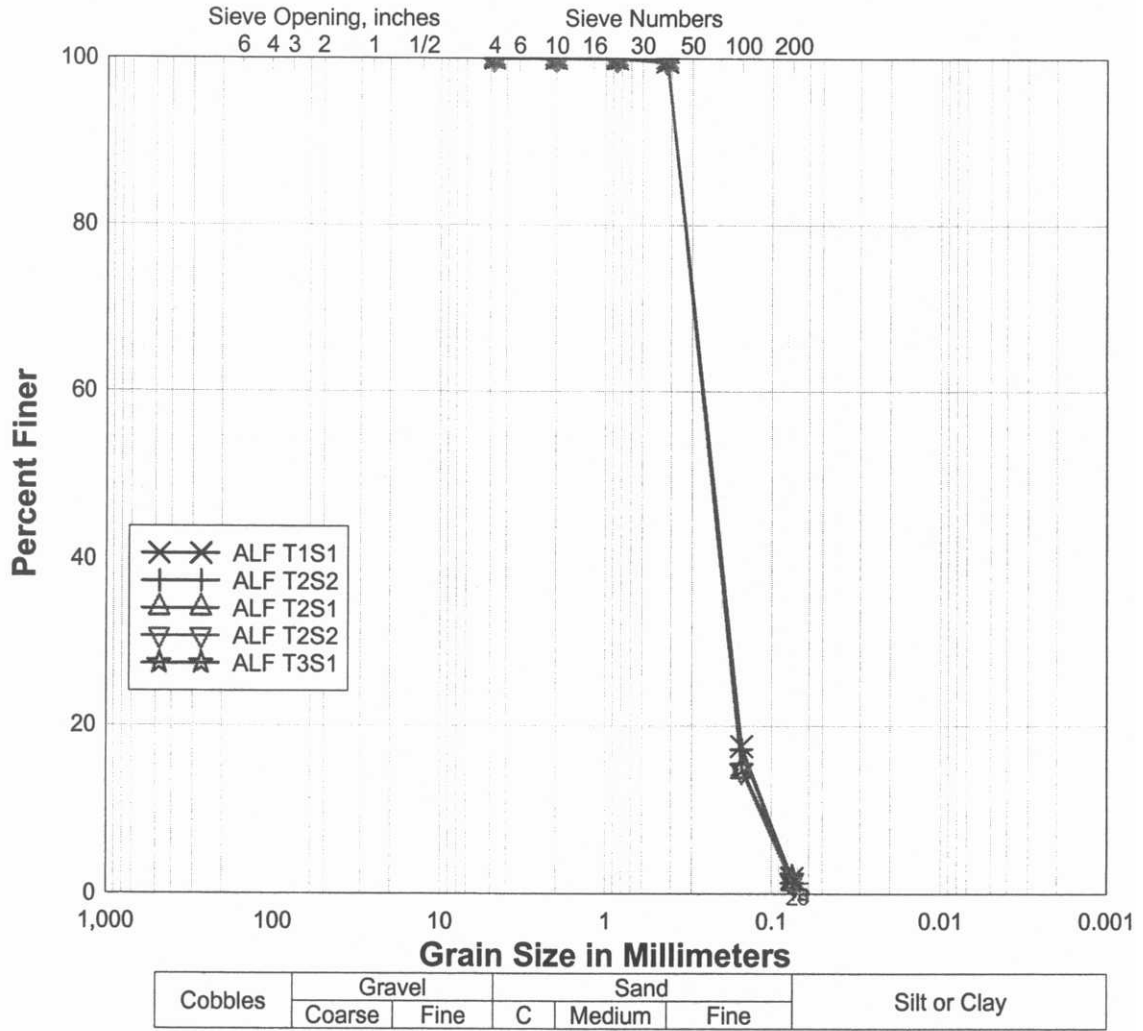


Figure A5 Grain size distributions for tubes tested Archer Landfill

## LIST OF REFERENCES

- Baguelin, F., Jézéquel, J. F., and Shields, D. H., The Pressuremeter and Foundation Engineering, Trans Tech Publications, Clausthal Germany, 1978.
- Briaud, J. -L., The Pressuremeter, A.A. Balkema, Brookfield, 1992.
- Briaud, J. -L. and Shields, D. H., “A Special Pressuremeter and Pressuremeter Test for Pavement Evaluation and Design”, Geotechnical Testing Journal, ASTM, Vol. 2, No. 3, pp 143-151, 1979.
- Briaud, J. -L., and Shields, D. H., “Pressuremeter Tests at Shallow Depth”, Journal of the Geotechnical Engineering Division, ASCE, Vol. 107, GT8, 1981a.
- Briaud, J. -L. and Shields, D. H., “Use of a Pressuremeter to Predict the Modulus and Strength of Pavement Layers”, Transportation Research Record, No. 810, 1981b.
- Bowles, J. E., Foundation Analysis and Design, 5<sup>th</sup> Edition, McGraw Hill, New York, 1996.
- Cambridge Insitu, “SELF-BORING PRESSUREMETERS—AN INTRODUCTION” [http://www.cambridge-insitu.com/csbp\\_leaflet2.htm](http://www.cambridge-insitu.com/csbp_leaflet2.htm) (2/26/2001).
- Cambridge Insitu, “CPM equipment description” <http://www.cambridge-insitu.com/specs/Instruments/CPM.html> (2/26/2001).
- Coduto, D., Foundation Design: Principles and Practices, Prentice Hall, Englewood Cliffs, 1994.
- Davidson, J. L., and Bloomquist, D. G., “A Modern Cone Penetration Testing Vehicle”, Proceedings of Use of Insitu Tests in Geotechnical Engineering, ASCE, New York, 1986.
- Drucker, D. C., and Prager, W., “Soil Mechanics and Plastic or Limit Design”, Journal of Applied Mathematics, Vol. 10, pp 157-165, 1952.
- Fahey, M. and Jewel, R.J., “Effect of Pressuremeter Compliance on Measurement of Shear Modulus”, Proceedings of the Third International Symposium on Pressuremeters, British Geotechnical Society, Oxford, pp 115-124, 1990.

- Florida Department of Transportation, FloridaPier Users Manual, FDOT, Tallahassee, <http://www.dot.state.fl.us/stuctures/proglib.htm>.
- Fyffe, S., Reid, W. M., and Summers, J. B., “The Push-In Pressuremeter: 5 Years of Offshore Experience”, The Pressuremeter and Its Marine Applications (2nd Int. Symp.), ASTM STP 950, pp 22-37. 1985.
- Houlsby, G.T. and Schnaid, F., “Interpretation of Shear Moduli from Cone-Pressuremeter Tests in Sand”, Géotechnique, Vol. 44, No. 1, pp 147-164, 1994.
- Houlsby, G.T. and Yu, H.S., “Finite Element Analysis of the Cone-Pressuremeter Test”, Proceedings of the 3rd International Symposium on Pressuremeters, ISP3 Oxford, April 2-6, pp 221-230, 1990.
- Hughes, J. M. O. and Robertson, P. K., “Full-Displacement Pressuremeter Testing in Sand”, Canadian Geotechnical Journal, Vol. 22, No.3, pp 298-307. 1985.
- Marchetti, S., Monaco, P., Totani, G., and Calabrese, M., “The Flat Dilatometer Test (DMT) in Soil Investigations”, A Report by the ISSMGE Committee TC16, Proceedings IN SITU 2001, International Conference on In Situ Measurement of Soil Properties, Bali, Indonesia, 2001.
- Mayne, P. W. and Kulhawy, F. H., “ $K_0$  – OCR Relationships in Soil”, Journal of the Geotechnical Division, ASCE, Vol. 108, No. GT6, pp 851-872, 1982.
- McVay, M. C., unpublished course notes, 1999.
- Peck, R.B., Hanson, W.E., Thornburn, T.H., Foundation Engineering, John Wiley and Sons, New York, 1974.
- Pile Buck, Steel Sheet Piling Specifications Chart, Pile Buck, Inc., 1995.
- Pinto, P. L., Coupled Finite Element Formulations for Dynamic Soil Structure Interaction, Ph.D. Dissertation, University of Florida, 1998.
- Plaxis Version 7 Users Guide, Eds. Brinkgreve, R. B. J., and Vermeer, P. A., A.A., Balkema, Rotterdam, 1998.
- Reid, W. M., St. John, H. D., Fyffe, S., and Rigden, W. J., “The Push-In Pressuremeter”, Proceedings of the Symposium on the Pressuremeter and its Marine Applications, Editions Technip, Paris, 1982.
- Roctest, Inc., “PRESSUREMETER Model G-Am MENARD” [http://www.roctest.com/roctelemac/product/product/g-am\\_menard.html](http://www.roctest.com/roctelemac/product/product/g-am_menard.html) (2/26/2001).

Robertson, P. K. and Campanella, R. G., "Interpretation of Cone Penetration Tests: Parts 1 and 2," Canadian Geotechnical Journal, Vol. 20, pp 718-745, 1983.

Sandler, I. S., and Dimaggio, F. L., "Material Model for Granular Soils", Journal of the Engineering Mechanics Division, ASCE, Vol. 97, No. EM3, pp 935-950, 1971.

Sandler I. S., Dimaggio, F. L., and Baladi, G. Y., Generalized Cap Model for Geological Materials," Journal of the Geotechnical Engineering Division, ASCE, Vol. 102, No. GT7, pp 683-698, 1976.

Schmertmann, J. H., "Suggested Method for Performing the Flat Dilatometer Test", Geotechnical Testing Journal, ASTM, Vol. 9, No. 2, pp 93-101, 1986.

Schnaid, F. and Houlsby, G.T. "An Assessment of Chamber Size Effects in the Calibration of Insitu Tests in Sand", Géotechnique, Vol. 41, No. 3, pp 437-445, 1991.

Schnaid, F. and Houlsby, G.T. "Measurement of the Properties of Sand in a Calibration Chamber by the Cone Pressuremeter Test", Géotechnique, Vol. 42, No. 4, pp 587-601, 1992.

Terzaghi, K., Peck, R.B., Soil Mechanics in Engineering Practice, John Wiley and Sons, New York, 1968.

Voyiadjis, G. Z., Tumay, M. T., Panos, D. K., "Finite Strain Analysis of Pressuremeter Test," Journal of Geotechnical Engineering, ASCE, Vol. 116, No. 6, pp 1002-1007, 1990.

Withers, N. J., Howie, J., Hughes, J. M. O. and Robertson, P. K., "Performance and Analysis of Cone Pressuremeter Tests in Sands", Géotechnique, Vol. 39, No. 3, pp 433-454, 1989.

Withers, N. J., Schaap, L. H. J. and Dalton, J. C. P., "The Development of a Full Displacement Pressuremeter", Proceedings of the Second International Symposium on the Pressuremeter and its Marine Applications, ASTM STP 950, pp 38-56, 1986.

## ACKNOWLEDGEMENTS

The authors would like to acknowledge the following individuals and organizations for their assistance with field projects:

State Road 20 Ronnie Lewis, Ben Watson and David Horhota – FDOT.

Southwest Recreation Center Chuck Hogan- UF Physical Plant, Howie Ferguson  
UF Campus Planning, Eric Drummond - PPI, Mike Garau – UF and Universal  
Engineering Sciences.

Archer Landfill Ron Bishop- Alachua County Geologist, and Universal  
Engineering Sciences.

Moffitt Cancer Center Mark Miller- Moffitt Foundation Project Manager and  
Mark Peronto- FDOT.

Green Cove Springs Mike Muchard and Don Robertson – Applied Foundation  
Testing, Brian Hathaway- Law Engineering, Danny Brown, Scott Jacobs, Josh  
Logan, Paul Bullock, Jason Gowland and Bob Konz – UF.

The authors would also like to acknowledge the project coordinator Peter Lai for  
his support and technical assistance.

